THE MECHANICAL BEHAVIOUR OF CYLINDRICAL GRP PANELS

ROBERT THOMAS HARTSHORN

Doctor of Philosophy

THE UNIVERSITY OF ASTON IN BIRMINGHAM

May 1987

THE UNIVERSITY OF ASTON IN BIRMINGHAM

TITLE : THE MECHANICAL BEHAVIOUR OF CYLINDRICAL GRP PANELS
NAME : ROBERT THOMAS HARTSHORN
DEGREE : DOCTOR OF PHILOSOPHY
YEAR : 1987

Thesis Summary

Glass reinforced plastic (GRP) is now an established material for the fabrication of sonar windows. Its good mechanical strength, light weight, resistance to corrosion and acoustic transparency, are all properties which fit it for this application.

This thesis describes a study, undertaken at the Royal Naval Engineering College, Plymouth, into the mechanical behaviour of a circular cylindrical sonar panel. This particular type of panel would be used to cover a flank array sonar in a ship or submarine. The case considered is that of a panel with all of its edges mechanically clamped and subject to pressure loading on its convex surface.

A comprehensive program of testing, to determine the orthotropic elastic properties of the laminated composite panel material is described, together with a series of pressure tests on 1:5 scale sonar panels. These pressure tests were carried out in a purpose designed test rig, using air pressure to provide simulated hydrostatic and hydrodynamic loading. Details of all instrumentation used in the experimental work are given in the thesis.

The experimental results from the panel testing are compared with predictions of panel behaviour obtained from both a Galerkin solution of Flügge's cylindrical shell equations (orthotropic case), and finite element modelling of the panels using PAFEC. A variety of appropriate panel boundary conditions are considered in each case.

A parametric study, intended to be of use as a preliminary design tool, and based on the above Galerkin solution, is also presented. This parametric study considers cases of boundary conditions, material properties, and panel geometry, outside of those investigated in the experimental work.

Finally conclusions are drawn and recommendations made regarding possible improvements to the procedures for design, manufacture and fixing of sonar panels in the Royal Navy.

Keywords:

CYLINDRICAL - PANELS
ORTHOTROPIC - MATERIAL
SONAR - WINDOWS

To Jeanette James and Sophia

ACKNOWLEDGEMENTS

The work reported in this thesis was carried out with the support of the Royal Naval Engineering College (RNEC), Plymouth, and the Admiralty Research Establishment (ARE), Portland. I am indebted to both of these organisations.

I am also indebted to the many individuals, within these and other organisations, with whom I have discussed this work, either formally or informally. Their ideas and viewpoints are inevitably woven into the text. Particular thanks are due to my Supervisor at Aston University, Dr Tom RICHARDS, for his continued support, patience and advice throughout; and to Professor K CHANDRASHEKHARA of the Indian Institute of Science for his invaluable contribution to the Galerkin numerical analysis.

I am grateful to my colleagues at RNEC, particularly to Lieutenant Commander Ben DOBSON who brought the problems of sonar domes to my attention in the first place; and to Dr John SUMMERSCALES for his advice on composite testing techniques. I must also express my thanks to Miss Polly DAWES, Assistant Librarian, and to Mr Terry DAVIS of the Computer Section; for their assistance with literature searching and computer programming respectively.

I must also express my most sincere thanks to Mr Jon CARPENTER of RNEC and also of Western Approach Consultants Ltd. Jon has offered unstinting help and advice throughout the course of this work, and has been willing to apply the same degree of enthusiasm to wielding a heavy torque wrench, as he has to sorting out temperamental instrumentation problems.

Finally I must thank Miss Pam HUSON for struggling through the typing of this epic, in its many iterations, without the aid of a word processor.

CONTENTS

LIST OF TABLES

LIST OF FIGURES

NOTATION

$[C_{ij}]$	Material stiffness matrix.
$[S_{ij}]$	Material compliance matrix
E, G, ν, D	Material elastic properties (Young's modulus, shear modulus, Poisson's ratio, Plate Stiffness.)
Subscript 1,2,3	Refer to lamina co-ordinate directions.
Subscript x,y,z	Refer to laminate co-ordinate directions.
*Subscript x,ϕ,z	Refer to cylindrical panel co-ordinate directions.
M_x, M_ϕ, $M_{x\phi}$	Bending and twisting moments in x and ϕ directions per unit length of shell.
N_x, N_ϕ, $N_{x\phi}$	Membrane forces (direct and shear) in x and ϕ directions per unit length of shell.
Q_x Q_ϕ	Shear forces in x and ϕ directions per unit length of shell.
u, v, w	Displacements in x, ϕ and z directions.
σ_x^d, σ_ϕ^d	Direct (membrane) stresses in x and ϕ directions.
σ_x^b, σ_ϕ^b	Bending stresses in x and ϕ directions.
p	Pressure load on shell.
R	Radius of cylindrical panel (to middle surface)
L	Semi length of cylindrical panel.
α	Semi central angle of cylindrical panel.
h,t	Semi thickness and thickness of panel ($h = t/2$)

*Note: Laminate directions x,y,z correspond to panel direction x,ϕ,z for all panels in this study.

CHAPTER 1

INTRODUCTION

1.1 Introduction

Sonar domes and sonar panels used in the ships and submarines of the Royal Navy are now manufactured exclusively of glass reinforced plastic (GRP). Sonar domes, as well as providing mechanical protection for the underlying sonar arrays, also act as acoustic windows for the sonar signals. The performance of a sonar system is therefore dependent on optimum mechanical design of the dome; an overdesigned dome for example, will result in unnecessary attenuation of sonar signals. In practice the difficulties of achieving an optimum dome design, will be aggravated by any lack of agreement between predicted behaviour of the dome on the one hand, and experimentally measured behaviour of the dome, or of a model of the dome, on the other. Unfortunately such lack of agreement has proved common with GRP domes. Problems of lack of agreement have often been severe enough to cast doubts on the whole design process and in such cases design has become largely a process of experiment.

The need to reconcile theoretically predicted behaviour, normally from finite element modelling, with what real domes are observed to do, has become increasingly important as sonar performance itself has improved. To date, disagreements between predictions and practice have been attributed variously, to the theoretical model, the experimental model and the properties of the dome material.

1.2 This Study

This thesis describes a study into the mechanical behaviour of a particular sonar dome type, namely a cylindrical panel of

rectangular planform. Such a panel would be entirely appropriate to a side or flank array sonar on a ship or submarine. The aim of the study is to resolve some of the design difficulties mentioned above. Because of the nature of the design difficulties the approach to the problem has been made along three distinct lines; experimental panel testing using a purpose designed test rig, theoretical panel analysis using both finite element methods and a Galerkin type procedure, and investigation of material properties with a comprehensive series of material tests.

A test rig was designed and manufactured for use in conjunction with the existing structural testing facility at the Royal Naval Engineering College (RNEC), Manadon, Plymouth. This rig was designed so that open cylindrical shell panels of dimensions appropriate to a 1:5 scale sonar, could be subjected to pressure loads to simulate the hydrodynamic loads experienced by real sonar panels. The design of the test rig is described in Chapter 9. Five panels were produced and tested in this rig. Two of the panels were of aluminium alloy and the remaining three of a GRP sonar dome laminate. Test samples of material were cut from these five panels (the panels were produced oversize to allow for this) so that the composition of the test samples was identical to that of the complete panels. These test samples were subjected to a comprehensive series of tests to determine, with as much certainty as possible, the elastic properties of the material. Test methods and material testing are described in Chapters 6 to 8.

The results of the panel testing, for both the aluminium and GRP panels were compared with both predictions from a Galerkin type solution and with predictions from finite element analysis. The Galerkin analysis is detailed in Chapter 12 and the finite element

analysis in Chapter 14. The Galerkin solution was also used to obtain parametric information outside of that directly applicable to the tested panels and this is given in Chapter 13.

From the results of the experimental testing and of the analysis, conclusions are drawn and design recommendations made in Chapter 15. These recommendations are intended to be directly applicable to cylindrical GRP sonar panels for use in the ships and submarines of the Royal Navy, but they also have relevance to the design of composite shells in general and to open cylindrical shells in particular in many other applications.

CHAPTER 2

HISTORICAL BACKGROUND

2.1 Introduction

Reinforced plastics are now well established as marine structural materials. Glass reinforced plastic (GRP) in particular, possesses an extraordinary combination of properties making it uniquely suitable for such applications. High strength and low weight can be combined with corrosion resistance, good dielectric and non-magnetic properties and its overall maintenance requirements are generally lower than those of traditional materials.

During the last ten or twenty years GRP has become, in most circumstances, the first choice material for small and medium sized pleasure craft; in these applications the low maintenance and resistance to rot and corrosion makes the material an attractive alternative to wood. These useful properties are desirable in any application, but it is the other attributes of the material, particularly its non-magnetic properties that have led to the recent use of GRP for the much larger structures of complete warship hulls particularly those of mine-countermeasure vessels. These larger hulls include:

Royal Navy 'Hunt' class (15) and Wilton (1)

'Tripartite' class : Belgium (15), France (15), Netherlands (15), Taiwan (6)

'Lerici' class : Italy (10), Indonesia (6), Nigeria (2)

Swedish Defence Authority 'Landsort' class (6) and Coast Guard Cutters (2)

Soviet Navy 'Zhenya' class (3) and 'Andryusha' class (3)

The numbers in brackets indicate the numbers of hulls in service, or known to be on order, as of early 1987. These are all very large structures, the smallest of the above vessels having an overall length in excess of 40 metres.

The design of a complete ship's hull in GRP presents problems of many kinds. Some of these are due to the scale of the structure and involve consideration of manufacturing techniques, Others are due to the structural difficulties of designing an adequately stiff hull to be built with a relatively low modulus material. A hull is basically a thin walled structure and many aspects of plate and shell theory are applicable to its design; the ability to stiffen the structure with internal frames and bulkheads and to stiffen individual areas with sandwich construction or ribbing is vital in allowing the designer to overcome the problems of the material's inherent flexibility. Structural weight is not usually a problem in warships and since the lay up cost/ton of stiffeners can be typically five times the cost/ton of unstiffened laminate it is often economic simply to add extra thickness, or more laminations, to the basic shell.

The durability of GRP when exposed to sea-water has been the subject of some debate and there is no doubt that the material does suffer more degradation in service than was expected in some early optimistic predictions. In spite of this, one of the earliest large GRP substructures for marine use, the fairwater fitted to USS HALFBEAK, entered service in 1954 and was found to be still within specification when replaced by a more modern design eleven years later.

2.2 Sonar Domes

One marine application of GRP that is not confined to mine-countermeasure vessels is its use for sonar domes and sonar windows. Sonar domes are not popular with marine designers. Sonar engineers dislike them because they attenuate acoustic signals and Naval architects dislike them because they tend to mar the otherwise clean lines of a hull. The ideal sonar dome should be fair enough to promote good flow with minimum drag, should give minimum transmission loss and beam distortion and should be strong enough to withstand all hydrodynamic and mechanical loadings. It should also generate a minimum of self noise.

Of the large variety of structural materials that could possibly be used for sonar domes and panels there are at present three serious candidates:

(1) Steel

(2) Cord Reinforced Rubbers

(3) Glass Reinforced Plastics

2.3 Steel

Until well after World War II, domes of thin steel plating over steel support frameworks met most needs. The advantages of steel are that it lends itself to simple manufacturing processes, it is reasonably strong and stiff and it is easy to maintain. Double curvature presents some fabrication problems but these can be largely overcome with intelligent design of the support frame.

With significant improvements in sonar technology during the 1950s the obvious discontinuities of a framed structure began to cause serious loss of sonar performance and the need then arose for a single unstiffened shell type design. In these high performance situations other disadvantages of steel become more serious.

Protection from corrosion is always a problem, and steel domes, particularly thin ones, can generate considerable self noise.

2.4 Cord Reinforced Rubbers

The second group of materials that have been used in this application are cord reinforced rubbers. These materials are considered because of their excellent acoustic properties, very low self noise generation and good resistance to damage. The main problem with rubber is its inherent flexibility. To maintain form, a rubber dome normally needs to be internally pressurised to combat external hydrodynamic loadings. At the higher speeds of modern vessels maintaining the shape of the dome in this way becomes difficult. Other disadvantages of rubber are that manufacturing costs are high and although the material is very durable, if it does become damaged repair is difficult and special facilities are required. The US Navy, for a number of years, favoured rubber domes on the grounds of their acoustic properties, but the fundamental mechanical problems have not been overcome.

2.5 Glass Reinforced Plastics

The Royal Navy has adopted glass reinforced plastic, more specifically glass reinforced polyester as its preferred material for sonar domes. Experimental domes in this material were first produced by the Admiralty Underwater Weapons Establishment (AUWE) at Portland - since renamed Admiralty Research Establishment (ARE Portland). This establishment is responsible for all of the RN's sonar research. The initial GRP dome tests were carried out in 1955 and the early results although good were variable with respect to acoustic transmission. A subsequent development and testing programme in collaboration with the Weymouth based firm W & J TOD plc, over the next few years, established a type of GRP lay up which would

give repeatable acoustic transmission properties together with reasonable mechanical strength. This lay up was a combination of Woven Roving (WR) and Chopped Strand Mat (CSM) glass fibre, both 'E' type glass, in a matrix of unfilled polyester resin.

During the 1960s more than 300 GRP domes were produced and fitted to RN ships. Most of these early domes were built with metal frameworks and were directly interchangeable with their steel counterparts. By the late 1960s, however, experience of GRP in service was such that unreinforced domes could be constructed with reasonable confidence enabling the full advantages of the material to be realised. Unframed GRP domes are now the norm in the RN for both surface ships and submarines and similar domes have been supplied by W & J TOD to many overseas navies.

2.6 Design Strategy for GRP Domes

Although GRP is now the RN's established material for sonar domes and windows, continuing improvement in sonar performance demands ever more critical design of the GRP structures. For maximum acoustic efficiency a sonar window must be as thin as possible but structurally it must be able to resist the external loadings - for some recent lightweight sonar systems it must also be as light as possible. The main loading of interest is the hydrodynamic pressure due to speed through the water and the manoeuvring of the ship or boat; hydrostatic loadings are not normally considered since sonar arrays are free flooding and are therefore not subject to the same hydrostatic loadings as say a submarine pressure hull. Foreign object impact is of course always a possibility with any marine structure, and for warships particularly an ability to withstand shock loadings from underwater explosions is also important. Whilst GRP meets the strength and toughness criteria very well, the desire for the best possible acoustic

performance inevitably produces conflict between structural considerations on the one hand and acoustic performance on the other.

Current practice for the design of GRP domes and panels consists of a combination of finite element analysis and the testing of large scale models. The finite element package used for most of the RN's sonar dome analysis is the PAFEC system and the model testing is usually carried out at one fifth full size.

The PAFEC finite element package provides a number of element types suitable for GRP shells and is available both to ARE (Portland) and to the Royal Naval Engineering College (RNEC) at Manadon, Plymouth. Formal collaborative agreements exist between ARE (Portland) and RNEC and these agreements provide the basis for a variety of themes of research; the analysis of GRP structures is one of these themes.

2.7 Structural Testing

In 1978 a structural testing facility was set up at RNEC to undertake testing of marine structures in liaison with ARE (Portland) and whilst ARE (Portland) has been the principal user of this facility, a number of other organisations connected with the defence industries have also become involved. These include; Plessey Marine Research Unit, Strachen and Henshaw, Devonport Dockyard, ARE (Portsdown), Vickers and Imperial College. The test facility has been most extensively used for sonar dome testing and a number of 1:5 scale domes and panels have been tested with simulated loadings.

The size of sonar arrays in modern vessels means that even a 1:5 scale model is still a formidable and expensive structure, however, experience with GRP suggests that smaller scale models are not really practical because they do not accurately reflect the behaviour of the real structure.

Scaling down a shell structure involves making the shell thinner and with a laminated structure the only realistic way to achieve this is by using fewer laminations. Laminates made thinner in this way do not generally have the same properties as the original. Sonar dome laminates are laid up with many layers and the macro-properties of the material reflect this; a very thin laminate of only a few layers will have very different properties. A scale of 1:5 is a compromise, at this scale a typical laminate will have sufficient layers to be broadly representative of the real material and the structure will be large enough to allow its lay up to be carried out under realistic workshop conditions. Material properties are then fairly uniform and reproducible. Simulated loadings can be provided in the laboratory by a number of means. Uniform pressure loads can be simulated with air pressure, an appropriate test rig being required to suit the particular pattern of dome. Point loads can be simulated by means of hydraulic rams, and more complex hydrodynamic loading profiles can be built up by a combination of rams and pneumatic pressure bags which can be placed in a suitable array between the dome and a reaction structure.

2.8 Limitations of the Design Strategy

2.8.1 General Limitation

Clearly almost any load case can be simulated on a model but a design strategy which depends too heavily on the 'try it and see' approach can become very expensive. This is particularly true when the real loading on the structure can take many forms, as is the case with marine structures, and where a performance premium is placed on achieving an optimum solution.

In principle finite element modelling should provide the means to carry out most of these simulations quickly, cheaply and reliably, removing the need for model testing entirely or at least allowing a great reduction in the testing programme.

Unfortunately for the development of GRP sonar domes any real movement towards reliance on finite element modelling has been elusive. Agreement between model testing and finite element analysis has never been good and has often been very poor indeed. Even on the occasions when experimental results have been in reasonable agreement with the analysis the experimental results have then been difficult to reproduce. There are a number of possible reasons for these disagreements between finite element analysis and experimental work including, deficiencies in the modelling, deficiencies in the experimental testing, and lack of understanding of the behaviour of the material. It has now become clear that there is some room for improvement in both analysis and testing. So far as finite element analysis or any other analytical modelling techniques are concerned, results will depend upon accurate knowledge of the mechanical behaviour of structural material, the geometry of the structure itself, the support boundary conditions, and the external loadings on the structure. GRP sonar domes present problems in all of these areas.

2.8.2 Material Limitations

The laminate is a hand lay up material and its properties are influenced by factors beyond the control of the designer. Furthermore, even where the material is laid up under controlled conditions with adequate quality control

and with uniform properties, these properties are difficult to characterise.

Until recently, no real attempt was made to take account of the anisotropic nature of the material. Finite element analysis has often been based on the assumption that the material is isotropic and homogeneous which is clearly not the case. In reality the material is anisotropic and hetrogeneous and although no realistic analysis can be expected to account for all aspects of behaviour, an analysis based on orthotropic assumptions might be expected to produce improved results. This type of laminate can be shown to be broadly orthotropic so far as its major properties are concerned. However, in reality, more recent finite element results using orthotropic elements have been disappointing. This is almost certainly because little attempt has been made experimentally to verify the assumed values of the orthotropic elastic constants.

Accurate control of laminate thickness also presents problems with hand lay up GRP. Mean thickness can be controlled approximately by specification of the number of laminae, and more accurately if the quantity of resin used to wet out each layer is also specified. Unfortunately with a hand lay up process it is unlikely that the mean thickness will be exactly as specified and the thickness will inevitably vary somewhat about the mean, from point to point on the dome. How, if at all, should this variation be allowed for? Because the thickness variation is almost exclusively due to resin rich areas in the laminate - it is relatively easy to control the number of layers and weight of the glass mat - the thick areas of the lam-

inate will generally contain no more glass than the thin areas. Since the amount of glass is the predominant factor influencing the material's stiffness and strength, then the thick areas are not necessarily very much stiffer than the thin ones.

This is true at least as far as membrane stiffness is concerned. The story may not be true for bending stiffness. Bending stiffness will of course be greatly influenced by where in the laminate the excess resin lies. If it is in the central laminations then the bending stiffness may be substantially increased. If it is near the surface of the laminate then its effect on bending stiffness will be very much less.

2.8.3 Boundary Conditions

Boundary conditions for sonar domes have always presented problems. The GRP domes are fixed to the hull of the ship or casing of the submarine with bolted joints. The design of these joints is a separate, if related, issue but since the hull structures are generally steel and very much stiffer than the GRP structures the edge conditions of the latter have generally been assumed clamped. The assumption of clamped edge conditions, as opposed to partial clamping, simplifies the finite element analysis and seems justified on the grounds that even if the fully clamped condition cannot be realised in practice, any practical departure from full clamping may be small and have an insignificant effect on the behaviour of the panel. The present work has shown this assumption to be fallacious as will be shown later. Very small departures from full clamping can have very significant effects on the behaviour of shell structures and although this has long been understood in a qualitative way, the degree to which it can apply in

particular circumstances is often not appreciated.

One way of avoiding the problem of imperfect clamping is to add elastic supports to the finite element model. The problem with this approach is that selection of spring constants becomes, at best, uncertain. At worst, dockyard assembly can render the real situation totally indeterminate.

2.9 Types of Discrepancy Encountered To Date

It is interesting to examine the several ways in which experimental results for GRP domes and panels tend to be at variance with finite element predictions. These variations have been found, to a greater or lesser extent, with all of the domes tested to date, and represent the main reason for the continuation of extensive large scale model testing.

First, all models tested show deflections, measured perpendicular to the surface, far greater than those predicted by finite element analysis. Deflections several hundred percent higher than predicted values are not uncommon.

Second, symmetrical structures, subjected to symmetrical loading patterns, often exhibit serious levels of asymmetry in their deflection behaviour. This has usually been assumed to be a material lay up problem, but in cases where quality control has revealed no obvious material problems, suggestions of structural instability or buckling have been made.

Third, measured deflections have generally shown significant non-linearity with load, even when loads and deflections have been small, and in cases where classical shell theory would predict almost perfect linear behaviour. This non-linearity is obviously not predictable by a linear finite element model. PAFEC however, also has a non-linear capability, and this too has failed to predict the type

of non-linear behaviour found in practice. Various reasons have been suggested to explain this last problem, including material non-linearity, early onset of large displacement behaviour, (unpredicted because of the limitations of thin shell theory applied to laminates), and also the onset of some modes of instability or buckling.

Whilst the reasons for the discrepancies between finite element analysis and experimental results have been the subject of conjecture, the fact that the discrepancies exist indicates that some improvement in the design strategy for sonar domes is required. Considerable financial savings could be made if the extensive and expensive testing of model domes could be reduced.

2.10 This Investigation

The work reported here is an attempt to improve the design procedure for GRP sonar domes, through a better understanding of the causes of some of the discrepancies mentioned above. The work is directly applicable to the design of GRP sonar domes for the RN but it also has application to other pressure loaded shell structures, and in particular to cylindrical shell panels of any material.

The particular structure considered is a cylindrical shell panel made of GRP. The panel has all of its edges clamped and it is subjected to a uniform pressure loading on its convex side. This panel corresponds directly to a sonar panel for a side or flank array sonar system. The uniform loading is considered to be a reasonable representation of the hydrodynamic loading a real panel might experience in service. This is because the sonar panel occupies a relatively small proportion of the side of the vessel so that the loading can be considered reasonably uniform over the panel. The loading would not of course be constant with time.

As well as representing a perfectly valid sonar dome type in its own right, the cylindrical shell panel is ideal for this investigation for a number of other reasons. These are:

(1) The cylindrical geometry is the simplest geometry that will exhibit true shell behaviour, involving combination of membrane and bending action as found in shells of more general form. This relatively simple geometry allows the possibility of a theoretical analysis which can be quite independent of the finite element analysis; for a shell of more general form, finite element analysis might well be the only practical procedure. With an alternative theoretical analysis, as used here, more confident comparisons can be made between the theoretical models and the experimental observations.

(2) The cylindrical shape is developable. The choice of a developable shell shape means that a metal shell of similar geometry can be readily manufactured, a doubly curved shell would be very difficult to fabricate in metal. A metal shell can be assumed isotropic and its material properties can be found with more certainty than can the material properties of GRP. As an experimental model, the use of a metal shell allows the effects of material properties on the shell behaviour to be investigated independently.

(3) An open cylindrical shell is generally a very inefficient shell shape because it depends for its integrity on its edge supports. An unsupported cylindrical shell panel will tend to flatten out under load in a way that a doubly curved shell or dome will not. This inefficiency, or sensitivity to edge conditions, can be valuable in an experimental model, where the effects of edge conditions are to be investigated.

The cylindrical panel investigated here offers an opportunity to make comparisons between predicted and experimental behaviour which would not be possible with a shell of more general shape. The results presented here, although they refer to, and are directly applicable, only to GRP sonar panels of cylindrical form, also have relevance to shells of more general shape and to cylindrical shell panels in many other applications.

NOTE. Much of the experimental and theoretical analysis which has been previously carried out on sonar domes, is either unpublished or classified.

A number of general references (unclassified or declassified) are given in the bibliography.

CHAPTER 3

PLATE AND SHELL THEORIES WITH APPLICATION TO COMPOSITE SHELLS

3.1 Introduction

The most prolific designer of thin shell structures, designs shells without the aid of classical shell theories, finite element analysis or digital computation. Nature has been successfully designing shell structures for millions of years and natural shells are everywhere. The most obvious examples of natural shells are egg shells, snail shells and the thin walled stems of grasses, but on a microscopic level every living cell is a thin walled structure and on a global scale even the earth itself behaves very much like a thin spherical shell.

If nature has something of a head start, men too have been designing shells for a very long time; doubtless the ancient artisans who produced the vases, urns and shell structure of lost civilisations had methods of experiment and analysis to aid them in their work. However, despite man's use of shell structures for thousands of years, modern experimental and theoretical studies of plates and shells for engineering applications, began only about 150 years ago, and only in the last 50 years or so, has sophisticated shell design permeated to all fields of industrial technology. Today the utilisation of shell structures in engineering is vast, especially in the aerospace, nuclear, petrochemical and marine industries.

In recent years, laminated composite materials have become widely used in many applications, and particularly in plate and shell structures where they have significant advantages over conventional materials. The two main advantages of laminated composites in shell

applications are their high stiffness to weight ratios compared with metals and their anisotropic properties. Anisotropy can be an advantage because it allows the properties to be tailored, (through variation of fibre orientation and lamina stacking sequence) and thus increases design flexibility.

This recent wide usage of composites for plate and shell structures has engendered a vast range of experimental and theoretical research not only on the stress-strain, strength and dynamic properties of the materials, but also on sophisticated shell theories to analyse the structures.

For many practical design purposes with 'common', rather than 'advanced' composites, the most extensively used theories remain those based on either the isotropic assumption (where the composite is treated as just another engineering material with its own global elastic constants) or else the orthotropic assumption where the entire multiple sandwich of a laminated composite is treated as a whole. The widespread availability of powerful finite element packages has made possible the use of more refined theories but ignorance of material properties often renders such sophistication ineffective for design purposes. Added to the difficulties of reviewing this literature is the difficulty that in contrast to the situation with plates, where at least for the isotropic case, there exists one generally accepted classical thin plate theory, the literature contains a variety of shell theories.

3.2 Classical Plate Theory

Classical Plate Theory (CPT) is based mainly on the work of KIRCHHOFF [1]. The assumptions for CPT and for most so called classical shell theories may be summarised as:

(1) The plate or shell is thin.

(2) The deflections are small.

(3) The material is linearly elastic (Hooke's Law applies).

(4) Transverse normal stresses are negligible.

(5) Normals to the middle surface of the plate or shell remain normal to it and undergo no change in length during the deformation process.

Particularly important in these assumptions is the normalcy condition, condition (5). This is usually referred to as the LOVE-KIRCHHOFF condition or the KIRCHHOFF-LOVE hypothesis [2]. This condition implies neglect of transverse shear strain and together with condition (4) means that the total strain energy of a shell can be expressed as the sum of the membrane and bending energies only.

For thin shells of isotropic material, the effect of neglecting transverse shear strain is slight and the assumption is certainly justified, but recent developments in the analysis of laminated shells indicate that thickness has a more pronounced effect on the behaviour of these shells than it does on isotropic ones. For any isotropic shell the transverse deflections predicted by CPT will be less than those predicted by a theory which allows for shear deformation (in dynamic situations, CPT predicted natural frequencies will be higher). Provided that the shell thickness is small compared with its other dimensions, or compared with the wavelength of any vibration mode, then the difference is normally small. However, due to the often very low transverse shear stiffness of composite laminates, shear deformation effects with these materials will be more pronounced. Reliable prediction of the deflection behaviour of laminated structures may therefore require the use of a shear deformable theory (SDT) or else if a non-shear deformable or classical type theory is used then some other allowance for additional transverse deflections may need to be made. The criterion

of thinness which, if applied to an isotropic shell might yield reasonable accuracy, may well be insufficient for a laminated shell.

In as much as the KIRCHHOFF-LOVE hypothesis is not in any position to allow for transverse shear deformation, all shear deformable theories are based on improved assumptions. The conceptual origins of these stem from the model proposed by TIMOSHENKO for problems in the dynamics of beams [3].

3.3 Shear Deformable Theories

3.3.1 REISSNER-MINDLIN Plate Theory

Probably the first significant paper in which transverse shear effects on plates were addressed was REISSNER's paper in 1945 [4]. This generated considerable interest from a number of authors, many of whom had been working in the aircraft industry during the war years and had been unable to publish their work at the time. Comments by GOODIER [5] were probably partly responsible for the second version of REISSNER's paper two years later [6]. In 1951 MINDLIN[7] published a plate theory which he acknowledged to be very similar to REISSNER's theory and developing more or less the same equations but with slightly different constants.

The basis of this REISSNER-MINDLIN Plate Theory, which can be applied equally well to shells, is the retention of the first four assumptions of CPT discussed earlier but rejection of the normalcy condition (5); this condition is replaced by the less constricting assumption that normals to the reference surface remain straight during deformation, but not necessarily normal to the middle surface.
(This assumption too may be discarded for some higher order theories - see later).

Consider the plate element Figure 3.1 with the right handed coordinate system shown, u, v and w are the displacement components in the x, y and z directions respectively of any point on the plate. The plate surfaces are represented by the planes $z \pm t/2$.

In REISSNER-MINDLIN plate theory the displacement components are expressed:

$$\left.\begin{aligned} u &= z\psi_x(x, y) \\ v &= z\psi_y(x, y) \\ w &= w(x, y) \end{aligned}\right\} \qquad (3.1)$$

The quantities ψ_x and ψ_y can be considered to be the average rotation of the cross section in the x and y directions and are expressed in terms of the slopes in these directions of the deformed middle surface of the plate, $\partial w/\partial x$, $\partial w/\partial y$ and the average transverse shear strains γ_x and γ_y.

$$\left.\begin{aligned} \psi_x &= \gamma_x - \frac{\partial w}{\partial x} \\ \psi_y &= \gamma_y - \frac{\partial w}{\partial y} \end{aligned}\right\} \qquad (3.2)$$

In CPT the transverse shear strains γ_x and γ_y would not appear.

The strain energy per unit surface area of a plate can now be considered as a summation of the strain energy due to bending and that due to shear and in REISSNER-MINDLIN plate theory is expressed:

$$\Delta U = \frac{D}{2}\left[\left(\frac{\partial \psi_x}{\partial x}\right)^2 + \left(\frac{\partial \psi_y}{dy}\right)^2 + 2\,\frac{\nu \partial \psi_x}{\partial x} \cdot \frac{\partial \psi_y}{\partial y} + \frac{1-\nu}{2}\left(\frac{\partial \psi_x}{\partial y} + \frac{\partial \psi_y}{\partial x}\right)^2\right] + k^2 \frac{Gt}{2}\left[\left(\frac{\partial w}{\partial x} + \psi_x\right)^2 + \left(\frac{\partial w}{\partial y} + \psi_y\right)^2\right] \qquad (3.3)$$

The constant k^2 is the shear factor or shear correction factor and is introduced to allow for the non-uniformity of the transverse shear strain through the plate thickness. Using a slightly different approach REISSNER gave k^2 a value of 5/6 for an isotropic plate compared with MINDLIN's value of $\pi^2/12$.

Of particular interest in REISSNER-MINDLIN theory is that 3 boundary conditions must be specified at a plate edge rather than the two KIRCHHOFF conditions of CPT.

For a free edge:

$$M_x = 0, \quad M_{yx} = 0, \quad Q_x = 0 \cdot \qquad (3.4)$$

For a simply supported edge:

$$w = 0, \quad M_{yx} = 0, \quad M_x = 0 \qquad (3.5)$$

or $$w = 0, \quad \psi_y = 0, \quad M_x = 0 \qquad (3.6)$$

For a clamped edge:

$$w = 0, \quad \psi_x = 0, \quad \psi_y = 0 \qquad (3.7$$

It is also instructive to note that considering the terms of equation (3.1) as the first terms of a power series in the coordinate z then CPT is seen to be just a special case

of REISSNER-MINDLIN theory where the transverse elastic shear modulus is assumed to be infinite and transverse shear strain is therefore zero.

3.3.2 Higher Order Plate Theories

A number of authors have proposed higher-order theories; the description "higher order" referring not to the order of the final system of differential equations but rather to the number and order of terms in the displacement equations. By utilising assumed displacement expressions of the type:

$$
\begin{aligned}
u &= z\psi_x(x, y) \\
v &= z\psi_y(x, y) \\
w &= w(x, y) + z\psi_z(x, y) + z^2\zeta_z(x, y) \ .
\end{aligned}
\tag{3.8}
$$

The effect of transverse normal strain can be included and because there is now an implied variation of transverse shear through the thickness of the plate there exists also the possibility of satisfying top and bottom boundary conditions, ie zero shear at the free surfaces.

NAGHDI [8] used displacement assumptions of this order to derive a general theory of shells in 1957 and ESSENBURG [9] demonstrated the advantages of these assumptions over lower order theories when applied to specific types of contact problems.

It should be noted at this stage that any number of plate theories can be developed and in principle any required degree of accuracy can be obtained by simply including a sufficient number of terms in the assumed displacement power series.

In practice a law of diminishing returns soon begins to operate and for most applications the complexity of the resulting analysis is not justifiable. Certainly for isotropic plates, even comparatively thick ones, it would be difficult for design purposes to justify any plate theory of higher order than that of REISSNER or MINDLIN

With laminated plates the situation is not quite so clear and most higher order theories have taken the application to laminates as their main justification. WHITNEY and SUN [10] developed a theory based on assumptions of the level of (3.8) which they applied to the case of laminated cylindrical shells [11]. NELSON and LORCH [12] gave a theory in 1974 for laminated plates based on the next highest order of assumed displacements, ie:

$$\begin{aligned} u &= z\psi_x(x, y) + z^2\zeta_x(x, y) \\ v &= z\psi_y(x, y) + z^2\zeta_y(x, y) \\ w &= w(x, y) + z\psi_z(x, y) + z^2\zeta_z(x, y) \end{aligned} \tag{3.9}$$

and REISSNER [13] has shown that a theory involving displacement assumptions:

$$\begin{aligned} u &= z\psi_x(x, y) + z^3\phi_x(x, y) \\ v &= z\psi_y(x, y) + z^3\phi_y(x, y) \\ w &= w(x, y) + z^2\zeta_z(x, y) \end{aligned} \tag{3.10}$$

although ignoring the contribution of in-plane deformation, gives very satisfactory results for the case of bending of

a plate with a circular hole. This was then compared with an exact elasticity solution.

Probably the highest order theory using this approach is that of LO, CHRISTENSEN and WU who in 1977 produced two papers [14] and [15] for the isotropic and laminated cases respectively and using displacement assumptions of the form:

$$u = z\psi_x(x, y) + z^2\zeta_x(x, y) + z^3\phi_x(x, y)$$

$$v = z\psi_y(x - y) + z^2\zeta_y(x, y) + z^3\phi_y(x, y) \qquad (3.11)$$

$$w = w(x, y) + z\psi_z(x, y) + z^2\zeta_z(x, y)$$

This is strictly speaking of the same overall order as the REISSNER theory [13] but with the addition of the quadratic terms in-plane deformation effects are included. The authors claim that this is the lowest order theory which can account for transverse shear deformation, transverse normal strain and a non-linear distribution of the in-plane displacements but they admit that it is overly complicated for most applications and very inconvenient to apply. They suggest that its application be limited to cases involving high frequency vibration modes where wavelength is of the order of plate thickness.

LO, CHRISTENSEN and WU make no use of the shear correction factors which are inherent in MINDLIN theory and are there to account for the non-uniformity of transverse shear. They claim that such correction factors are inappropriate to all higher order theories and are critical of their inclusion in [11] and [12].

This criticism is not altogether fair since low order polynomials can only imperfectly represent the true

transverse shear distribution in a laminate and if the purpose of the shear correction factors is to improve the modelling capability of the theory, then their inclusion is surely justified.

The higher order theories are not justified for most practical applications and even for thick plates a theory of the order of MINDLIN theory but generalised to either the orthotropic case or laminated anisotropic case is normally adequate. The first theory for laminated isotropic plates is due to STAVSKY [16]; this has been generalised to the laminated anisotropic case by YOUNG, NORRIS and STAVSKY [17] and represents a generalisation of REISSNER-MINDLIN plate theory to the case of arbitrarily laminated anisotropic plates and includes shear-deformation and rotary inertia effects. It has been shown by a number of authors [18], [19] and [20] that this YOUNG, NORRIS, STAVSKY (YNS) theory is quite adequate for predicting overall plate behaviour, for example, transverse deflections in the first few vibration modes. Problems only arise with a YNS type theory when accurate prediction of stress singularities or higher order vibration modes are required.

Any plate or shell theory which makes use of correction factors immediately presents the problem of what the factors should be and how they should be applied. This is a particular difficulty with anisotropic materials since it is perfectly reasonable to take the view that a correction factor should be applied to every non-zero term in the stiffness or compliance matrix of the material. For an orthotropic plate NELSON and

LORCH [12] used 9 correction factors which they determined by comparing the approximate theory response of an infinite plate to the exact solution response given by KULKARNI and PAGANO [21].

Practical laminates often consist of many plies with fibre directions varying from layer to layer and often not precisely known. In such cases it is desirable to take a less exacting approach, applying correction factors only to the predominant response modes.

For an orthotropic laminate of symmetric construction having an axis of symmetry parallel to the x axis of the plate, CHOW [22] applied two correction factors k_1^2 and k_2^2, the values of which he determined using an approach similar to that of REISSNER. WHITNEY [23] extended this to unsymmetrical laminates, showing that the numerical values of k_1^2 and k_2^2 depended on detailed laminate construction. In these papers the two correction factors are derived for the cylindrical bending mode in each of the two principal orthotropic plate directions. More recently BERT and GORDANINEJAD [24] in 1983 derived the same two correction factors, but with the assumption that the laminate material was bimodular (different elastic moduli in tension and compression).

The approach of using arbitrary correction factors, although widely accepted, is regarded as rather inelegant by some, and several attempts have been made to avoid it without recourse to increasing the order of the displacement assumptions. COHEN [25] had produced a theory replacing the usual assumptions, of either constant transverse shear stress or constant transverse shear strain, with TAYLOR series expansions

for stress resultants and couples which satisfy the plate equilibrium equations. Unfortunately, although this avoids the use of arbitrary constants, it produces results which are not substantially better, and are in some cases marginally worse, than CPT. MURPHY [26] in 1981 published a theory making use of a cubic displacement assumption for u and v similar to those used by LO et al and as in equation (3.11). However, rather than allowing ψ_x, ζ_x, ϕ_x etc to be independent, they are selected so that the 4 boundary conditions:

$$\tau_{xy} = \tau_{yz} = 0 \text{ at } z = \pm h/2$$

are satisfied. This reduces the number of independent unknowns to the number in MINDLIN type theories and this, according to MURPHY, qualifies it as a low order theory, which, even if a little less straightforward to apply, gives better results.

3.4 Shell Theories

3.4.1 Essential Features of a Shell

Up to this point we have been able to discuss plate and shell theories almost interchangeably because transverse shear, which has been the main area of discussion, affects plates and shells in similar ways. The essential feature of a shell, of course, is its curvature and in general a shell will carry its loads by a combination of membrane and bending behaviour. In the limit of flat geometry the shell becomes a plate, with combined bending and plane stress behaviour, but for general curved geometry the development of shell theory is very much more complicated than plate theory.

3.4.2 Genealogy of Shell Theories

The literature on shells is vast and growing and a comprehensive review that would be of use to practising engineers is badly needed. There are many good historical reviews, for example SECHLER [27] but these generally do not attempt to be comprehensive.

A genealogy of shell theories has been given by BERT [28], in order of increasing sophistication and potential accuracy they are:

(a) Membrane theories - only extensional effects are considered, bending stiffness ignored.

(b) Very shallow-shell theories (DONNEL-MARQUERRE).

(c) Other shallow shell theories (MORLEY-CHERNYK-KORDA).

(d) First approximation theories (LOVE's first theory - SANDERS theory).

(e) Second approximation theories (LOVE's second approximation theory - also FLUGGE - NOVOZHILOV).

(f) Exact theories within the KIRCHHOFF-LOVE hypothesis (LANGHARR-BORESI).

(g) Theories including thickness normal and thickness shear flexibility.

(h) Three dimensional elasticity theory (developed for some special cases but no general theory of this type).

All of the shell theories mentioned above have been applied or are potentially applicable to composite materials; however, because of the additional complexities of anisotropy and bend/stretch and bend/twist coupling, most of the emphasis has

been on the simpler, less exact theories. The selection of an appropriate theory depends partly on the proposed method of solution.

If a whole-shell analytical method is used for a general shell then the shallow shell theories (b) and (c) above may be insufficiently accurate. On the other hand if the shell is discretised into elements each of which is very shallow, or if the shell has a specific shallow geometry, then the MORLEY or DONNEL theories may be entirely adequate. Indeed for some internally pressurised shells the membrane theory (a) may be quite satisfactory and even simpler analysis may be appropriate in some cases. Filament-wound tubes, for example can be modelled quite effectively by a "netting analysis". In this type of analysis only the fibres are considered and are assumed to carry only tensile membrane loads. The contribution of the matrix material to the stiffness of the shell is completely ignored.

3.5 Cylindrical Shells

Of the various shell geometries of interest to engineers, cylindrical shells are by far the most common and governing equations for cylindrical shells have been available since the last century. The earliest solution for a cylinder subjected to axial compression was that due to LORENZ [29] in 1911 and solutions for buckling of complete cylinders under external pressure were given by SOUTHWELL [30] in 1913 and VON MISES [31] in 1914.

For circular cylindrical shells, the equations of DONNEL [32] suggested in 1933, form the basis of more non-linear and stability analyses than any other set of cylindrical shell equations.

The DONNEL equations can be derived in a manner somewhat similar to that used for the plate equations by considering a summation of forces and moments on a cylindrical shell element in a

slightly deformed state. Using the coordinate system and loadings shown in Figure 3.2 the equilibrium equations can be expressed in the form:

$$\frac{\partial^2 u}{\partial x^2} + \frac{1-\nu}{2}\frac{\partial^2 u}{\partial y^2} + \frac{1+\nu}{2}\frac{\partial^2 v}{\partial x \partial y} + \frac{\nu}{R}\frac{\partial w}{\partial x} = 0 \tag{3.12}$$

$$\frac{\partial^2 v}{\partial y^2} + \frac{1-\nu}{2}\frac{\partial^2 v}{\partial x^2} + \frac{1+\nu}{2}\frac{\partial^2 u}{\partial x \partial y} + \frac{1}{R}\frac{\partial w}{\partial y} = 0 \tag{3.13}$$

$$D\nabla^4 w + Nx\frac{\partial^2 w}{\partial x^2} + 2Nxy\frac{\partial^2 w}{\partial x \partial y} + Ny\frac{\partial^2 w}{\partial y^2} + \frac{Ny}{R} + \frac{Et}{(1-\nu^2)R}\left(\nu\frac{\partial u}{\partial x} + \frac{\partial v}{\partial y} + \frac{w}{R}\right) = 0 \tag{3.14}$$

These three non-linear differential equations are clearly coupled, in that they all contain derivatives of the three displacements u, v and w. DONNEL partially uncoupled these equations mathematically to give equations of the form:

$$-R\nabla^4 v = (2+\nu)\frac{\partial^3 w}{\partial x^2 \partial y} + \frac{\partial^3 w}{\partial y^3} \tag{3.15}$$

$$-R\nabla^4 u = \nu\frac{\partial^3 w}{\partial x^3} - \frac{\partial^3 w}{\partial x \partial y} \tag{3.16}$$

$$D\nabla^8 w + \frac{Et}{R^2}\frac{\partial^4 w}{\partial x^4} + \nabla^4\left(Nx\frac{\partial^2 w}{\partial x^2} + 2Nxy\frac{\partial^2 w}{\partial x \partial y} + Ny\frac{\partial^2 w}{\partial y^2}\right) = 0 \tag{3.17}$$

Equations 3.15 to 3.17 are called the DONNEL stability equations in uncoupled form, equation 3.17 can be seen to be an eighth-order differential equation in w alone.

The simplifying assumptions made in the development of the DONNEL equations limit their applicability to shallow cylindrical panels or to complete cylinders whose displacement components are

rapidly varying functions of the circumferential coordinate, ie several buckle wavelengths around the cylinder. For non-shallow shells, other authors have developed various sets of cylindrical shell equations, notably VON KARMAN and TSIEN [33] who used their equations to examine the buckling of complete cylinders under various types of loading, including axial compression and bending. FLUGGE [34] also gives cylindrical shell equations both for linear analysis and for buckling. These equations are more general than the DONNEL equations and can be applied to shallow, moderately shallow and deep cylindrical shells.

3.6 Applicability of shell theories and shell equations to Cylindrical Sonar Panels

3.6.1 Shell Theories

The cylindrical panels of interest in this study have an approximately square planform and a radius of curvature slightly less than their side length. If the ratio of smallest linear dimension to thickness is taken as radius:thickness then this ratio for the GRP panels falls in the range 70 to 140.

The lower limit of this ratio for which a thin shell analysis is acceptable depends upon the degree of accuracy required of the analysis and upon the material properties. For shells of isotropic materials a lower limit of the ratio between 20 and 40 is normally considered acceptable for all practical purposes and using this criterion the panels of this study can clearly be considered 'thin'. Since the GRP material is a laminate however, and since laminates tend to have reduced transverse shear stiffness, it is necessary to re-examine the thinness criterion. Were the transverse

shear modulus only for example, one tenth of the in-plane shear modulus then the 'effective' radius to thickness ratio of the panels would be not 70 to 140 but 7 to 14 and in such a case the panels ought properly to be considered 'thick' for the purposes of analysis.

Shear modulus tests reported later in this work indicate the values of transverse shear moduli for the GRP panel material to be approximately 50% of the value for its in-plane modulus.

This implies that the effective radius to thickness ratios for the panels are in the range 35 to 70 and under these circumstances the panels can be considered thin. All numerical and finite element analysis is thus based on the assumption that transverse shear effects can be neglected.

3.6.2 Shell equations

The geometry of the panels considered here falls into an intermediate category of cylindrical shell both from the point of view of depth and of aspect ratio. The shells are not shallow enough for the DONNEL equations to be applicable but neither are they deep. Shell equations applicable to long shells or short shells are similarly inappropriate. The shell equations used for the analysis presented later are those due to FLÜGGE. These equations are of quite general form and are applicable to any cylindrical shell.

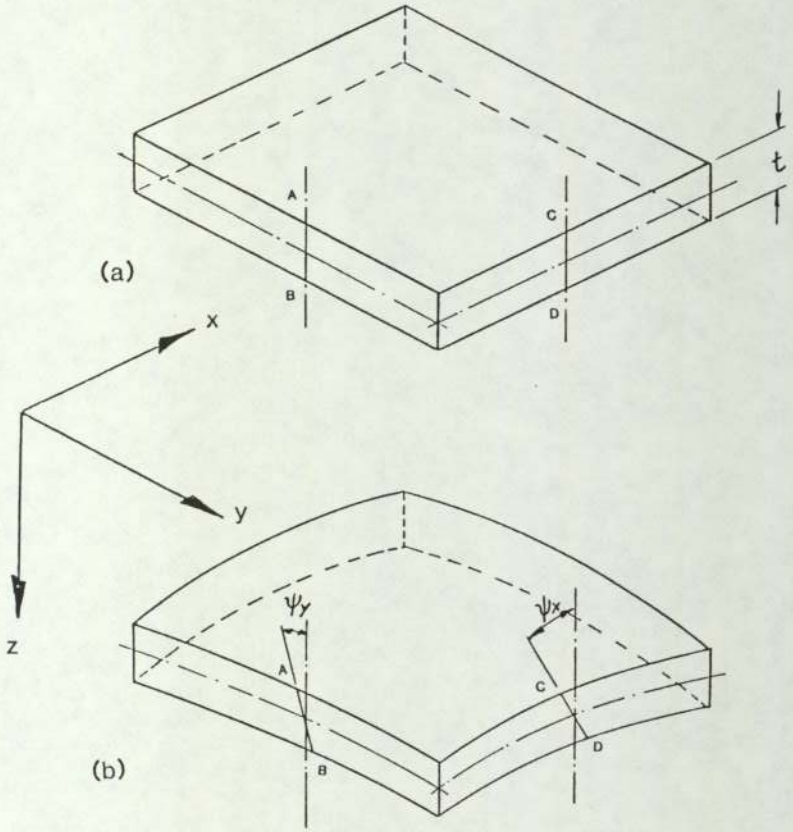

Fig. 3.1 Reissner - Mindlin plate element

a) Undeformed
b) Deformed

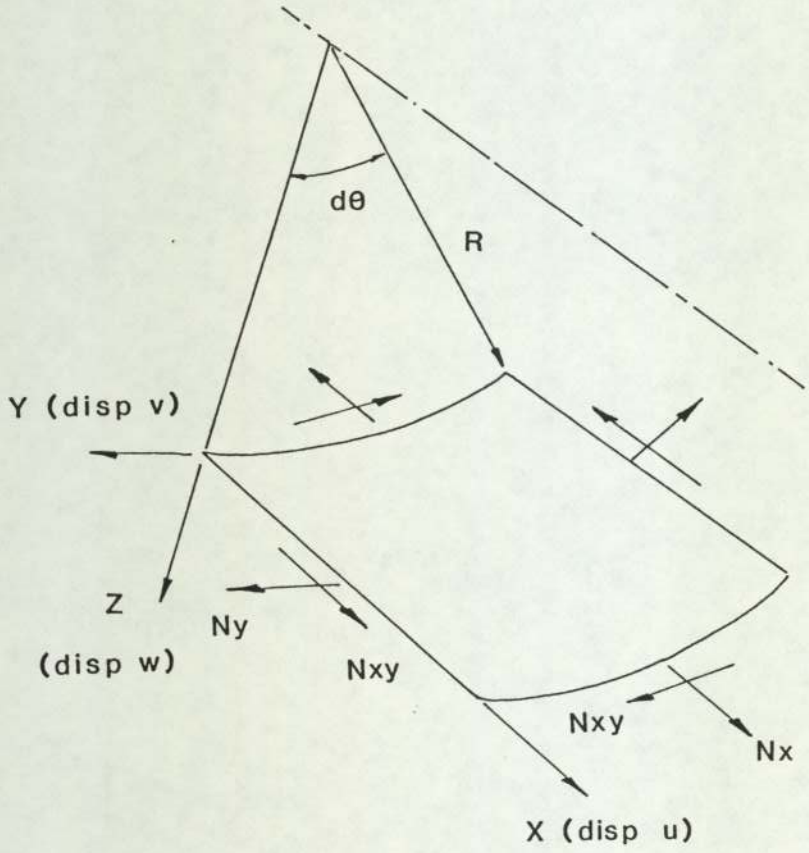

Fig 3.2 Element of a Thin Cylindrical Shell.

CHAPTER 4

REVIEW OF NUMERICAL AND EXPERIMENTAL STUDIES OF LATERALLY LOADED SHELL PANELS

4.1 Introduction

It has been shown in Chapter 3 that adequate plate and shell theories exist, and that at least for some classes of shells (shallow shells, cylindrical shells), governing equations are available. All shell theories and all governing equations are, of course, approximate to some degree in their representation of real shells, but as conceptual models of shells, within their limitations and assumptions, they are perfectly acceptable for design purposes.

The most general shell problem, or any other elasticity problem for that matter, consists of estimating the distribution of stresses, strains and displacements at all points within the loaded shell when certain boundary conditions are imposed. 'Classical' or closed form solutions are obviously to be preferred but only in the rarest of cases is it possible to solve this type of boundary value problem in an exact and direct manner. Studies of particular cases have generally been undertaken using approximate and numerical methods. In this chapter some of the reported investigations of cylindrical panels are considered, together with other shell investigations that are considered relevant to the current work. It is clear that a variety of methods of solution including Levy's method, Raleigh-Ritz, Galerkin and Finite Difference have been employed for these related problems. Finite element studies are not considered here, despite their obvious importance, because the finite element approach has become so

broad that it would not be sensible or representative to select just a few finite element studies from the enormous range of available literature. Instead finite element methods and packages are considered separately in Chapter 5.

The references included here are obviously not exhaustive and it is recognised that many important studies, particularly Russian ones have been omitted. Nevertheless, these studies are representative of the various approaches to shell problems, particularly those approaches relevant to cylindrical shells.

4.2 Particular Shell Studies including Non-Linear Behaviour and Snap Buckling

Generally speaking the problem of laterally loaded cylindrical shell panels, of interest here, has received less attention in the literature than either complete cylinders subject to pressure loading (internal and external) or cylinders and shell panels subject to axial compressive loads. However, the related 'Barn roof' problem of interest to civil engineers, has been fairly extensively studied. In fact the simply supported cylindrical shell roof (simply supported at its ends) is often used as a test to compare the performance of shell finite elements. A rigorous solution based on Levy's method for the simply supported shell roof can be found in the literature [34] as can a number of approximate solutions based on consideration of the shell as a beam, LUNDGREN [35], or as a folded plate RAMASWAMY et al [36]. A solution using Levy's method for cylindrical shells with other than simple supports was given by MORICE [37] in 1957 but this was based on the very sweeping SCHORER assumptions [38], the most important of which are:

(1) Poisson's ratio is ignored.

(2) The bending resultants M_x, $M_{x\phi}$ and $M_{\phi x}$ are small and may be neglected.

(3) The dominant strain is that in the longitudinal direction ε_1. The strains ε_2 and ε_{12} may be neglected.

The use of these assumptions, of widespread use in civil engineering, limits the validity of the analysis to that of an approximate method for long shells only.

The particular case of a cylindrical shell panel with all of its edges clamped and subject to a lateral pressure loading on the convex side does not appear to have been investigated other than by finite element methods. Related problems including cylindrical panels with other edge conditions or other loadings, and initially curved panels (not cylindrical) with clamped edges, have been the subject of a number of investigations mostly numerical and some of these studies, though very much the minority, have also involved some experimental work. Some of these studies are discussed here.

One of the first attempts to examine a clamped edge cylindrical panel was that of SINGER MEER and BARUCH [39]. In their work the stability of a laterally loaded cylindrical panel was investigated using linear theory and a Raleigh-Ritz technique. First the case of classical simple supports was analysed using the eighth order Donnel stability equation and then compared with the case where circumferential restraint was applied to the straight edges of the panel. The coupled Donnel equations were reduced to a set of algebraic equations and solved by an iterative technique. Various numerical results were presented in non-dimensional form to show that the restraint of the straight edges produces considerable stiffening of the panel.

This is a not unexpected result. However the curved edges of the cylindrical panel were not axially constrained so the panel could not be considered truly clamped.

Axial restraint has been shown to be a particularly important consideration both for complete cylindrical shells and for open cylindrical panels. ALMROTH and BROGAN [40] have shown that if the ends of a laterally loaded cylindrical panel are restrained in the longitudinal or axial direction then tensile membrane stresses will be induced in the longitudinal direction, and the predicted bifurcation type collapse, will not occur at all (Figure 4.1).

In 1970 RUSHTON [41] published a paper on the large deflection of plates with initial curvature. In this paper the dynamic relaxation method was used to solve the finite difference form of the large deflection equation. Large deflections of square plates with small initial curvature, laterally loaded on the concave side and with both simply supported and clamped edges were considered.

RUSHTON concluded from this work that for both edge conditions a considerable reduction of maximum stress resulted from the introduction of the initial curvature. Since the panel was loaded on the concave side there was, of course, no prospect of instability, although the second part of the same paper examined the post-buckling behaviour of similar initially curved plates, when subjected to edge loads in the axial direction.

A second paper by RUSHTON [42] in 1972 and along the same lines also considered lateral loading of initially curved plates but this time on the convex side. In this case the deflections due to the loading are of opposite sign to the initial deflections

and the in-plane membrane stresses are negative. Due to the presence of these compressive membrane stresses the plate is now liable to buckle. The dynamic relaxation method was used as before to investigate the pre-buckling and post-buckling behaviour of the panels. To determine the unknown buckling load the lateral load was increased in steps until a sudden change in shape occurred, then a further analysis of the critical region was undertaken with the load increasing in smaller steps. Simply supported plates of aspect ratios (where aspect ratio is defined as width/length) from square, 1:1, to 6:1 were investigated.

The author states that the staight portion of each load/defln. curve joining the pre-buckling and post-buckling regions does not necessarily represent the equilibrium path during the snap-through a load based analysis will not predict this path. The author claims to show that the buckling load of the plate decreases as the aspect ratio increases. Unfortunately this conclusion only applies to the particular case studied ie non-constant initial curvature - the trigonometric series form of the initial deflection will not represent constant curvature unless summed to infinity. Any broader interpretation of the results is also difficult since in considering the various aspect ratios the author maintains the central rise of the panels as a constant. Each change in aspect ratio must therefore imply a corresponding change in initial curvature.

RUSHTON also considered plates with clamped edges and found such plates "less likely to undergo snap-through buckling", however sudden changes in the deflected shape did still occur. The

paper also included an examination of the "probable" waveform taken by the plates during the buckling process but only symmetrical deflected shapes were considered.

HUDSON [43] submitted his PhD thesis in 1970 on the Non-Linear Behaviour of Thin Curved Panels. The problem considered was that of a doubly curved laterally loaded isotropic panel. The lateral loadings took two forms; uniform pressure and central point loading and both clamped and simply supported boundary conditions were investigated.

For the analysis of the clamped edge case the edges were fully restrained against rotational, tangential and lateral displacements with the lateral deflection of the plate described in terms of a double trigonometric Fourier series of the form:

$$w = \sum_{m}^{\infty} \sum_{n}^{\infty} w_{mn} \left[(-1)^{m+1} + \cos 2\alpha_m x\right] \left[(-1)^{n+1} + \cos 2\beta_n y\right] \quad (4.1)$$

$$m, n = 1, 3, 5 \ldots\ldots$$

where: $\alpha_m = \frac{m\pi}{a}$

and: $\beta_n = \frac{n\pi}{b}$

This was then substituted into the Von Karman compatibility equation - suitably modified to allow for the initial curvature of the panel. Using a direct comparison technique the stress function was obtained in terms of the Fourier series deflection function, a method exact in the limit but dependent on the number of terms taken in the deflection series. Both series, deflection and stress function, were then substituted into equations describing the total energy of the system. To satisfy equilibrium

and stress function, were then substituted into equations describing the total energy of the system. To satisfy equilibrium requirements the total energy was minimised and since the first four non-zero deflection coefficients were selected, a set of four non-linear algebraic simultaneous equations in terms of these coefficients was obtained.

One of the most interesting aspects of HUDSON's work is that he produced experimental results to compare with his theoretical work. He tested aluminium panels of three thicknesses, and three aspect ratios subject to point and uniform loading and with both clamped and simply supported edges. Although the panels were small and the boundary conditions in the experimental work were slightly imperfect the results are probably the first ones recorded for laterally loaded initially curved panels. Reasonably good agreement was obtained for the pressure loading case. For various reasons including plastic deformation in the vicinity of the load, the results for the point loaded case did not show such good agreement.

The non-linear behaviour of orthotropic, curved panels under lateral loading was investigated by MARSHALL [44]. His PhD thesis in 1976 was followed by several papers [45] to [47], produced in association with his co-workers, RHODES and BANKS, at the University of Strathclyde.

MARSHALL investigated panels with a spherical curvature and supported his theoretical analysis with some experimental work. Rectangular planform panels were considered and as in the earlier work of HUDSON, uniform lateral pressure loading and central point loading were considered in combination with clamped and simply supported edge conditions.

The test panels were manufactured from a unidirectional glass fibre cloth laminated in CRYSTIC 272, polyester resin. Two or three laminations were used to produce a unidirectional laminate, the method of lay up described by MARSHALL as 'crude' was actually

a rather sophisticated hand lay up method and the resulting panels as described showed good dimensional accuracy. As with HUDSON's work the main behaviour phenomenon was snap-buckling. The snap buckling effect is best described by reference to Figure 4.2 this shows the type of load-deflection relationship typical of shallow curved panels; the exact form of the relationship depending on type of loading, panel geometry and boundary conditions.

As the lateral load on the panel is increased the panel deflection follows the stable portion of the curve from O to C, at which point any further increase in load will cause the panel to snap-through to point D. Beyond point D the panel will stiffen and continue on a new stable equilibrium path. As the load is incrementally reduced the curve will again pass through point D but will now continue on to point E when any further reduction in load will result in a second snap from point E to point A. Any tendency to unsymmetrical behaviour of the panel, due to imperfections or asymmetry of loading will result in a reduction of the critical load with bifurcation of the equilibrium path at some point B.

MARSHALL's analysis followed closely the method used by HUDSON for isotropic panels. Lateral deflection and membrane stresses were expressed as Fourier series, a comparative technique was used to express stress function coefficients in terms of deflection coefficients for the clamped case and the Galerkin method was used for the simply supported case. The major difference being the constitutive relationships for the orthotropic material. MARSHALL obtained values for the principal elastic constants experimentally from flat panels laid up specially for the purpose and of the same specification as the curved panels. The elastic constants measured were E_x, E_y, ν_{xy}. G_{xy}. A 45° off-axis test was used to estimate G_{xy}. Since the laminate

was unidirectional the Young's Modulus in the fibre direction E_x was approximately three times the value of E_y.

Only the central deflection was reported by MARSHALL. This was measured using a single dial gauge in the centre of the test rig for both the point and pressure loaded cases.

Although extra dial gauges were used for some tests they were only to detect asymmetric behaviour not to determine the deflected shape of the panels; in fact for the panels tested asymmetric behaviour was not found.

Quite good agreement was reported between theory and experiment particularly for the pressure loaded case of aspect ratio = 1. Results for other aspect ratios were less good. MARSHALL et al also carried out some investigations on the asymmetrical buckling of similar plates. Initial imperfections due to lay up and reinforcement variations may tend to produce this behaviour with laminates. References [48] and [49] give useful insight into this.

4.3 Studies Specific to Laterally Loaded Cylindrical Panels

The references [41] to [49] address the problem of buckling of shells with double curvature. A cylindrical shell with single curvature may also buckle under lateral loads particularly if its curved edges are not adequately restrained in the longitudinal direction; a number of studies of such behaviour may be found in the literature. These studies have generally been directed towards the problem of the cylindrical shell roof mentioned earlier and usually to the case without edge beams. The absence of edge beams means that the straight edges of the shell or the edges running in the longitudinal direction are unsupported. The curved edges are usually assumed simply supported. Apart from approximate

approaches, where a long shell may be assumed to behave in a manner similar to a long panel in axial compression, and a short shell similar to a cylindrical tube under radial load, few studies of this case have been made. One solution has been given by CHU and TURULA [50] using a finite difference technique and the results of this have been verified experimentally by YANG and GURALNICK [51]. The work of YANG and GURALNICK is notable because it is one of the few instances of experimental studies of open cylindrical shells reported anywhere. Interestingly they concluded that small initial imperfections of the cylindrical shell geometry did not exercise a significant influence on buckling behaviour for the case of transverse loading. This confirms the earlier assertions of DONNEL and others that imperfections of cylindrical shells are less serious under transverse or lateral loading than under axial loading. Unfortunately YANG and GURALNICK gave no details of the magnitude of the initial imperfections in their panels.

The fully clamped cylindrical shell panel has received the attention of several authors, again in the Civil Engineering field and with application to roof problems. Here, buckling has not been a prime consideration and attention has been directed to linear solutions complicated by the nature of the edge conditions. PICKET and GOPALACHAYULA [52] and [53] outlined two possible approaches [52] by Fourier series and [53] by strain energy methods but gave little detail. ALLEN and HOLMAN [54] published a solution using a second order finite difference technique but this solution is of questionable value for two reasons. Firstly the differential equation used is a variation of FLÜGGE's approximate equation but with Poisson's ratio taken as zero and secondly the second order finite difference

technique which ALLEN and HOLMAN used has been shown to produce very unreliable results when applied to shell problems, resulting in some, but not all, of the computed stresses being in serious error.

CHANDRASHEKHARA and CHANDRASHEKHARA [55] and [56] working in the Civil Engineering Department of the Indian Institute of Science at Bangalore produced two separate solutions to the fully clamped roof panel subject to dead loading. The first of these [55] published in 1972 was a solution using Basic Functions or Beam Eigen functions. In this solution the displacements of the shell are expressed in terms of a series of beam functions with undetermined constants, selected so as to satisfy the desired boundary conditions of the shell. Use is made of tabulated Eigen functions for uniform vibrating beams having the same boundary conditions as the shell. This form of the displacement is substituted into the simplified governing differential equations given by FLUGGE and a Galerkin type procedure is then used for the solution. This results in a set of infinite simultaneous equations. Since only a finite number of terms can be taken, the solution can only be approximate, but it is exact in the limit, and convergence is numerically demonstrated. This is a very elegant method of solution which requires no extra approximation of the governing equations, and subject only to the number of terms taken, and the computational power available, can give any required degree of accuracy. Only the fully clamped case was considered by the authors but other boundary conditions can be treated in exactly the same way; beam functions being selected for the particular edge condition required. The main limitation of the method is that since the beam functions must satisfy the boundary conditions, only boundary conditions for

which the functions are available; clamped, simply supported, hinged etc can be used. For intermediate boundary conditions suitable 'trial' functions will not be available.

The second paper [56] published in 1973 gives a solution of the same problem using a different but complementary approach. In this approach the starting point is again FLÜGGE's simplified differential equations, but with the three equations reduced to a single eighth order equation in the displacement w alone. A Multiple Fourier Series technique is then employed resulting again in a set of infinite simultaneous equations. This time the governing equation is exactly satisfied but the boundary conditions are only satisfied approximately, again depending on the number of terms taken in the series. This second approach to the problem has the one advantage over the former one that in principle more types of boundary conditions can be accommodated. From a practical point of view however, being a far less elegant form of solution it is probably not as useful as a design aid. Extensions of this solution to slightly more general cases of loading or material properties rapidly increase the algebraic complexity of the method to a point where it becomes too tedious to be practical.

4.4 Summary

Clearly, for design purposes, any solution, numerical or analytical, which depends upon specific geometry, boundary conditions and loading can only be applied to a limited range of problems. All of the cases discussed in this chapter may have practical applications but the applications of each are very specific. Despite this limitation these methods do have advantages in some circumstances over the completely general geometry, boundary conditions and loading available with finite element

methods. For the cases with which they deal, they allow a far easier route to parametric information than do finite elements. Finite elements can of course provide parametric information, but only with tedious remeshing at each change of parameter.

These numerical methods also provide a useful check on the validity of finite element models and on the suitability of particular formulations to particular classes of problem.

For the present study with the comparatively simple cylindrical geometry and comparatively simple loading and boundary conditions (at least for the ideal case) a numerical solution offers the opportunity to obtain an independent check on the PAFEC finite element results. It also makes practical a parametric study which would be outside the scope of the experimental work.

The analysis used is detailed in Chapter 12 but is essentially the Galerkin method as used by CHANDRASHEKHARA and CHANDRASHEKHARA in reference [55]. The method of solution is as described in the reference with the important new feature of orthotropy in the material properties. The loading is also slightly different being in this case radial pressure rather than dead load. Additional boundary conditions are also included.

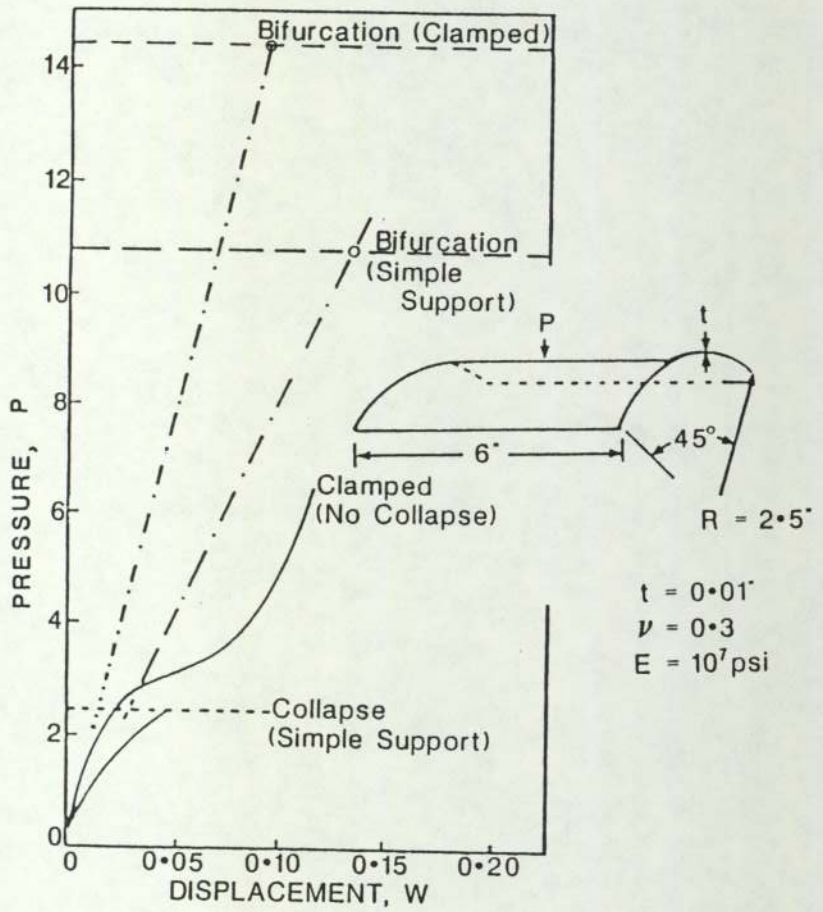

Fig. 4.1 Stable load/displacement behaviour of an axially restrained cylindrical panel. (ALMROTH & BROGAN [40])

Note: compare with classical snap-buckle effect Fig. 4.2

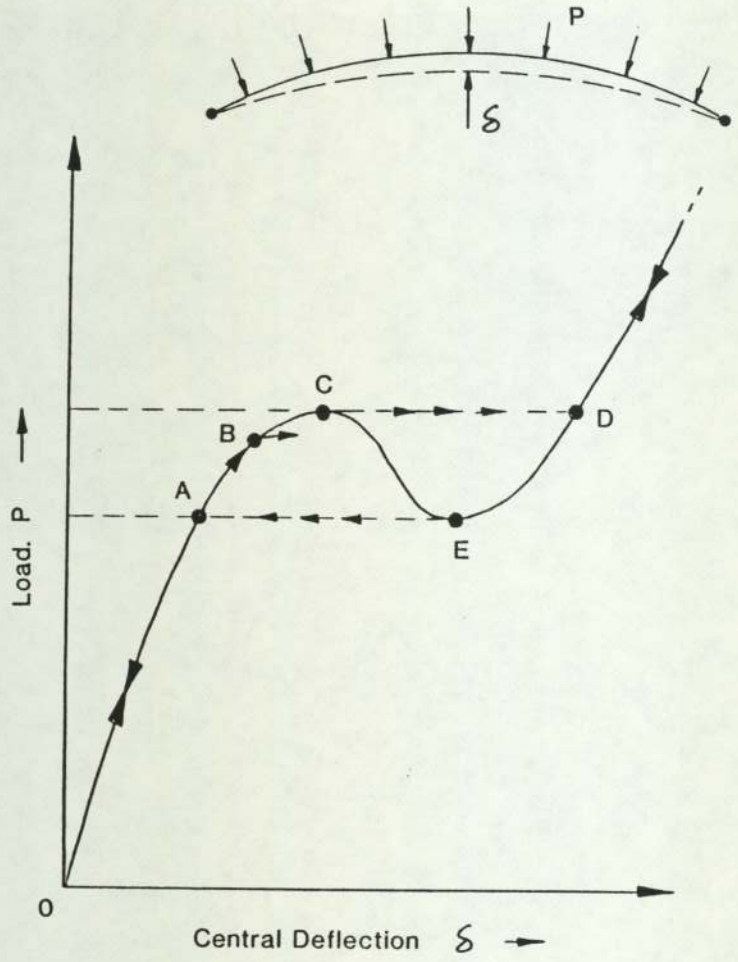

Fig. 4.2 Classical snap-buckle effect.

O to C - stable loading
C to D - snap-buckle
D to E - stable unloading
E to A - snap-buckle

CHAPTER 5

FINITE ELEMENT SYSTEMS AND PAFEC

5.1 Introduction

In spite of the attention paid up to the nineteen sixties to the development of accurate and sophisticated shell theories, there is a marked shortage in the literature of numerical examples of any of them except when applied to cases of very simple geometry.

This observation becomes understandable when it is realised that for any but the most simple cases, the algebraic complexity for a classical solution, or for a rigorous numerical solution, rapidly builds up to become quite overwhelming. For design purposes, resort has traditionally been taken in approximate methods, but even here, only in the cases of cylindrical shells and shallow panels is the foundation of the approximate methods at all secure. For these cases, at least within the basic assumptions of first-order shell theory, simplified but adequate governing equations are available. The practical and efficient analysis of shells of more general form is still often far from realised.

Given that almost all design of shells must be by numerical means, the Finite Element method is now almost invariably the preferred design tool.

Modern Finite Element Analysis is the logical extension of the Matrix Displacement Method, first seriously used in the aircraft industry in the early nineteen fifties, since then the rapidly developing capacity for cheap, fast, digital computation has made it the premier tool of engineering analysis.

The basis of the finite element method rests in subdividing a complex structure (the theoretical model of the actual structure) into a number of discrete regions or 'elements'.

In the matrix analysis of skeletal structures the division of the structure into individual elements is physically obvious but the finite element method takes the process further in its application to continuum structures in which there may or may not exist any physical boundaries between the regions or elements.

Probably the first piece of work on the finite element method was produced by TURNER et al [57] in 1956 when they introduced what were in effect plane stress and plane strain elements for static analysis. Subsequently similar elements have been applied with great success to a very large range of problems.

Following the successful development of the plane stress element a great deal of research effort in the early nineteen sixties was devoted to the development of satisfactory plate bending elements. Plate bending elements present far more of a challenge than plane stress or three-dimensional stress elements due to the nature of CPT. Because CPT is governed by a fourth order differential equation the strains are second derivatives of displacement; rather than first derivatives as in plane-stress or three-dimensional theory. This leads to increased difficulty in satisfying the requirements of inter-element displacement continuity and at the same time producing an element with good convergence characteristics.

In the early work on plate bending elements, both rectangular and triangular elements were developed. References [58] to [60] are typical of this early work. Most of the work carried out in this period was based on the strictly mechanical structural reasoning of the matrix displacement method. Finite Element analysis only came to be based on firm variational principles as a result of the convergence studies undertaken by a number of workers at this time.

A paper by MELOSH [61] in 1963 based the finite element development on the principle of minimum potential energy and the following year FRAEJS DE VEUBEKE [62] introduced the alternative possibility of defining stress and equilibrium elements based on the principle of minimum complementary energy. The establishment of finite elements on variational principles led to a number of advances. It was no longer necessary for the elements to be solid physical blocks, but rather small regions of space were defined, in which the unknown functions could be prescribed. The effect of this was to allow an expansion of the method from its solid mechanics base into fluid and thermal problems and indeed into any other area where a property shows variation from point to point in a continuum. All of these ideas and others were first brought together and usefully presented as a whole by the publication in 1967 of ZIENKIEWICZ and CHEUNG's text [63] this book provided the first comprehensive 'state of the art' treatment of finite element analysis and has since been republished in revised and very expanded editions.

5.2 Finite Element Packages

Papers on finite element analysis appear in the literature on a regular basis and new element formulations are not infrequent. Special elements are continually being formulated with claims that they perform better than existing elements in specific situations; new composite constructions, hybrid materials, sandwich plates and so on. Some of these elements never find practical application and certainly many are never subjected to rigorous testing in a variety of situations. This is not to say that useful elements are not being developed, but rather that the theoretical development is capable of far outstripping the comparatively slow process of element validation. Useful elements that do have application beyond very specific cases, normally reach a wider usership through

incorporation into commercial FE packages. These packages, run on mainframe, mini and more recently micro computers are available now to all but the smallest organisation, either through subscription or outright purchase. There exists a vast choice of such packages. In 1982 a less than exhaustive list gave over 500 major code titles, the majority of these being of United States origin.

5.3 Integration of Finite Element Analysis with CAD and CAM

FE analysis is a Computer Aided Design (CAD) tool. It may be integrated in many commercial packages with Computer Aided Draughting (also confusingly CAD) and Computer Aided Manufacture (CAM). The process illustrated in Figure 5.1(a) can be modified into a truly interactive one, Figure 5.1 (b) with the development of extra analysis packages within the pre and post processor stages.

Using modern approaches such as this it becomes possible, at least in the case of fairly routine designs, to complete the whole modelling-solution-evaluation process at one sitting. This seems to be the way in which commercial packages are developing and there is much to recommend it. Most packages offer a bewildering variety of element types and selection of elements and mesh design are pitfalls for the inexperienced operator. Unsuitable modelling at this stage may go completely undetected. Even if the selected elements are the most suitable ones, little may be known of their efficiency or of their limitations.

5.4 Evaluation of Finite Element Codes

Independent evaluations of commercial elements and element packages are rare and the process of evaluation has been described as like shooting at a moving target; not easy even for an expert marksman. Perhaps the most critical evalu-

ations of some of the elements of the more popular packages are those given by Robinson Ford Associates. This consultancy has evaluated plate bending elements [64] and membrane elements [65] from the MSC/NASTRAN, ASAS, PAFEC, ANSYS and SAP4 packages.

The results of their tests are given without specific conclusions and are open to interpretation as to their significance in particular cases. It should be noted however that of the fourteen plate bending elements tested in Reference [64] twelve failed to pass the patch test.

There have been other independent evaluations but by no means as many as one would like to see. This is probably because evaluation is an expensive business and needs the sponsorship of a large organisation, and also because results of evaluation are usually controversial anyway and out of date before fully resolved.

So far as the pre- and post-processing packages that are now becoming available are concerned, there does not appear to be any objective independent evaluation at all. Totally different evaluation criteria would be required for this, and it is difficult to see any way in which evaluation could be both detailed, and up to date.

5.5 Selection of Finite Element Packages

Of the multitude of FE packages, the choice of code for a particular organisation will depend to a great extent on the type of analysis most often required.

In Ministry of Defence (Navy) MOD(N) research establishments the PAFEC finite element package has become the standard FE system. Some MOD(N) establishments also make limited use of other systems including MSC/NASTRAN and FESDEC but PAFEC is the standard system.

5.6 The PAFEC Finite Element System

PAFEC is an acronym for Program for Automatic Finite Element Calculations and is a large program system with the ability to deal with a wide range of static, dynamic, heat transfer, acoustic, elastohydrodynamic and non-linear problems. The system is fully upwards compatible between new versions and additional programs have been added including a Design Office Graphics System, DOGS and a 3D version, DOGS 3D which are interactive with the basic PAFEC program. PIGS is the basic PAFEC Interactive Graphics program.

The main concern here is the finite element program PAFEC and this should be regarded as a general purpose system. Over one hundred element types are available with the later versions of the program and many of these are available with orthotropic as well as isotropic properties. Elements are also available for multi-layer laminates.

PAFEC is available to operate on most mainframe and some super mini computers as of 1985 for a reasonably full implementation the processor must have a minimum word length of 32 bits and utilise a virtual memory operating system. A minimum main memory of 2 Mbytes is required together with a working disc space of at least 30 Mbytes.

5.7 Finite Element Analysis of Cylindrical Sonar Panels

For the finite element analysis of the cylindrical panels of this study the PAFEC finite element program was used throughout. The program was implemented on the RNEC mainframe computer. During the course of this project the mainframe computer was changed. The original computer was a Xerox SIGMA 6 operating CP5 operating system and with a main memory of 128 k words, word length 32 bits. The replacement machine is a Control Data Ltd CYBER 840, NOS/VE operating system and a main memory of 4 M words, 64 bit word length. The PAFEC implementation was changed from level 3 (a very limited implementation) on the SIGMA 6 machine to a fully up to date implementation of level 5.1 on the CYBER 840.

A number of elements from the PAFEC library are suitable for sonar dome shell analysis. Some of these, including those used in this study, are described in the following sections. Only minimal detail of element formulations is given to support the selection of the elements. Full details of the formulations may be found in the PAFEC 'Theory and Results' Manual [66] which itself contains a comprehensive bibliography of nearly six hundred references.

5.8 PAFEC Facet Shell Elements

5.8.1 Three Node Triangular Facet Shell Element 41320

Other than the simple membrane elements this is probably the simplest element for general thin shell analysis and carries both membrane and bending loads. It is a facet element and is therefore flat.

The element has five degrees of freedom at each node u_x, u_y, u_z, ϕ_x, ϕ_y in terms of its own axis set.

After transformation into a general three dimensional mesh there are six degrees of freedom at each node u_x, u_y, u_z, ϕ_x, ϕ_y, ϕ_z. u_x, u_y are membrane displacements in element coordinates and the stiffness matrix for the membrane action is based on a constant state of stress over the element.

The hybrid method is used to find the bending stiffnesses - the variational principle used is that the complementary potential energy is a minimum. The stress assumptions for this element in terms of moments are of the form:

$$M_x = F_1 + F_2x + F_3y$$

$$M_y = F_4 + F_5x + F_6y$$

$$M_{xy} = F_7 + F_8x + F_9y$$

where M_x, M_y and M_{xy} are the internal moments per unit length and F_1 to F_9 are independent force variables.

Distributed loads on this element are simulated by distributing the total load on the element equally between the three nodes. The output stresses are calculated for the top, middle, and bottom surfaces of each element at its centroid.

Use of this element is limited to thin isotropic shells with radii of curvature large in comparison to thickness of shell.

5.8.2 Eight Node Facet Shell Element 44210

This facet element is based on an isoparametric transformation, as are most commonly used quadrilateral elements. In general isoparametric elements may have curved sides for 2 dimensional elements or curved edges and faces for 3 dimensional elements. So that the stiffness and other element matrices can be derived, the elements are transformed into very simple shapes in a co-ordinate system referred to as the $\zeta\eta$ domain, see Figure 5.3. The eight noded quadrilateral facet 44210 for example has four corner nodes and 4 side nodes. The side nodes can be positioned anywhere along the length of the side. On transformation into the $\zeta\eta$ domain the element becomes square with the side nodes at the mid point of each straight side.

For this element each node has five degrees of freedom at the element level but transforming to six at mesh level as for 41320.

The matrices relating to u_x and u_y displacements are exactly as for related plane stress elements. Bending analysis is based on thin plate theory. The element is slightly more difficult of use than the triangular facet because of the requirement that the element be flat. If side nodes are positioned out of the plane of the element errors or at least warnings will be given. Modelling of a general shell is also more difficult with quadrilaterals than with triangles. Related triangular elements are available but these should generally be avoided since they tend to give less accurate results. In general one eight noded quadrilateral can be expected to give results equivalent to

four six noded triangles.

Elements related to this element in the PAFEC scheme are 44100, 44110, 44200 and 44220.

44100 and 44110 are triangular elements with 3 and 6 nodes respectively. These elements are not recommended for general use as they are not particularly accurate. 44200 is a 4 node element (without the mid side nodes of 44210) and 44220 is a 12 node element with 2 mid side nodes per side.

5.8.3 Eight Node Facet Shell Element 44215

This element is exactly equivalent to element 44210 section 5.8.2 but with orthotropic capability.

The only matrix affected by the inclusion of orthotropic material properties is the stress strain matrix [D]. This is obtained by inversion of the compliance matrix [S] (see Chapter 6).

PAFEC data preparation requires input of material data in compliance form and all 9 compliances are normally entered for an orthotropic material. For all PAFEC orthotropic elements stress output is in terms of the principal material directions. 44215 and other orthotropic elements may in general be used with the PAFEC 'orthotropic material' module alone so that the result is a single layer homogenous material, or together with the 'laminates' module for a multiple layer material where the principal material directions of each layer can be specified.

5.8.4 Eight Node Thick Facet Shell Element 45210

This element is identical with element 44210 with respect to geometry, membrane behaviour and bending behaviour

but has the additional capability of transverse shear deformation.

It is in effect a 'MINDLIN' type plate bending element and as such offers an intermediate stage between thin facet elements and full 3D brick elements.

Although this element and its related elements would appear to be superior to thin elements, there are certain limitations which must be considered. Rounding errors become quite severe when the ratio of typical plate length to plate thickness is 10 or more for isotropic materials and there are geometric compatibility problems at element boundaries if elements are not coplanar. The elements are also of course much more expensive to use than thin elements; sixteen of the twenty one degrees of freedom used to describe bending distortion become redundant if the element is thin.

Probably the most appropriate use for these elements is in analysis of sandwich plates. For such analysis both facings should be isotropic and the core should be significantly more flexible than the facings.

Related elements in the PAFEC scheme are: 45220 twelve node quadrilateral, 45110 six node triangle and 45120 nine node triangle.

5.9 General Observations on Facet Elements for Shell Analysis

The modelling of a curved shell using facet finite elements is naturally a compromise in which some of the difficulties of a curved shell element formulation are avoided, at the expense of introducing a physical approximation to the shell geometry.

Since in the facet approach the actual curved shell is replaced by an assemblage of flat elements, located so that their nodes lie in the middle surface of the actual shell, the most useful element shape is a triangle. For shells of arbitrary or general form triangles must be used and it is unfortunate that triangular facets are generally less efficient than quadrilaterals. For shells of more restricted form such as the cylindrical shells considered here however, quadrilateral or rectangular elements are quite suitable.

A facet element which supports both plate bending and membrane (plane stress) behaviour is simply a combination of a plate bending element and a plane stress element and this uncoupling of bending and membrane behaviour at element level greatly simplifies the formulation. In any case the coupling will occur at the nodal points and it is generally assumed that as more and more facet elements are used, with compatability satisfied at more and more discrete points, the behaviour of the substitute structure will approach closer and closer to that of the actual shell. This assumption is difficult to justify mathematically but it does seem to be borne out in practice for a large range of structures with a variety of facet elements.

Facet elements are thus, in practice, very successful for shell analysis and objections to their use on asthetic grounds or on the grounds of disregard for the accepted rules of interelement compatibility would not seem to be justified for design applications. Certainly facet elements may be superior to low order curved shell elements in many applications. Some of the finite element analysis carried out during the course of this study has been done using facet elements.

5.10 Semi-Loof Curved Shell Elements 43210 and 43215

Notwithstanding the comments made above concerning the relative merits of facet and curved shell elements, the PAFEC scheme does contain a group of sophisticated curved elements of the semi-Loof type.

The quadrilateral semi-Loof elements 43210 and 43215 have eight proper nodes (4 corner and 4 midside) at each of which there are three translatory freedoms u_x, u_y, u_z. Between these eight nodes there are eight additional 'Loof nodes' or Gauss points each with a rotational freedom on an axis tangential to the element side. There are in fact a total of 43 degrees of freedom for this element reduced to 32 by various constraints on the motion.

The analytical development of the semi-Loof element is complex but it is not a 'shell theory element', rather it occupies a middle ground between a simple facet - made by combining a membrane element with a plate bending element - and a curved element formulated from shell theory.

Semi-Loof elements do have certain advantages, the shell is modelled in a more realistic fashion and good results can often be obtained with comparatively few elements with consequent reductions in cost for both mesh generation and processing. The elements do have disadvantages however. In some instances semi-Loof elements can give rise to some unusual effects including spurious mechanistic behaviour; deformation modes which store little or no strain energy. The elements are also subject to quite rigorous limitation of geometry and compatibility with other element types, and are also far more difficult to use than facet elements even when incorporated into a package such as PAFEC.

Overall these elements are useful but need to be treated with care. They are not as forgiving as simpler elements and it is probably not prudent to use them in a untried application without some independent checking.

Element 43215 is an orthotropic semi-loof quadrilateral, but a six noded 'triangular' element is available for modelling shells of general form. The six noded element is however very inferior to the quadrilateral and is never a first choice element. All of the semi-Loof elements are thin shell elements.

5.11 Element types selected for the present work

The preliminary finite element analysis reported here was carried out using PAFEC facet shell element 44210 and its orthotropic equivalent 44215. At the outset of the work these were considered the most suitable elements from those then available. The thick shell element 45210 was initially considered as a possible choice but was dismissed once it became clear that the panel geometry and material properties did not justify a thick shell approach (see Section 3.6).

During the course the work with the update of the RNEC mainframe computer, the semi-Loof elements 43210 and 43215 became available. Further FE analysis was then carried out using these elements. Results of this analysis and discussion of the relative merits of the facet and semi-loof approaches in their application to sonar panels is given in Chapter 14.

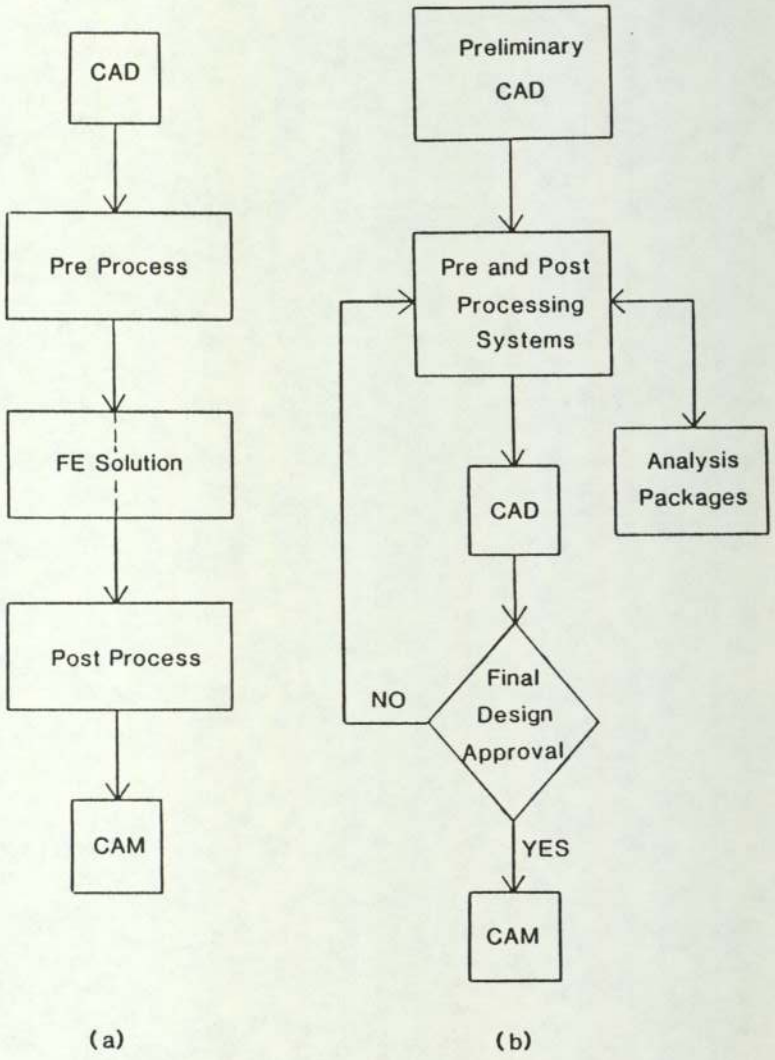

Fig. 5.1 a) Basic CAD/CAM system
b) Fully Interactive CAD/CAM system

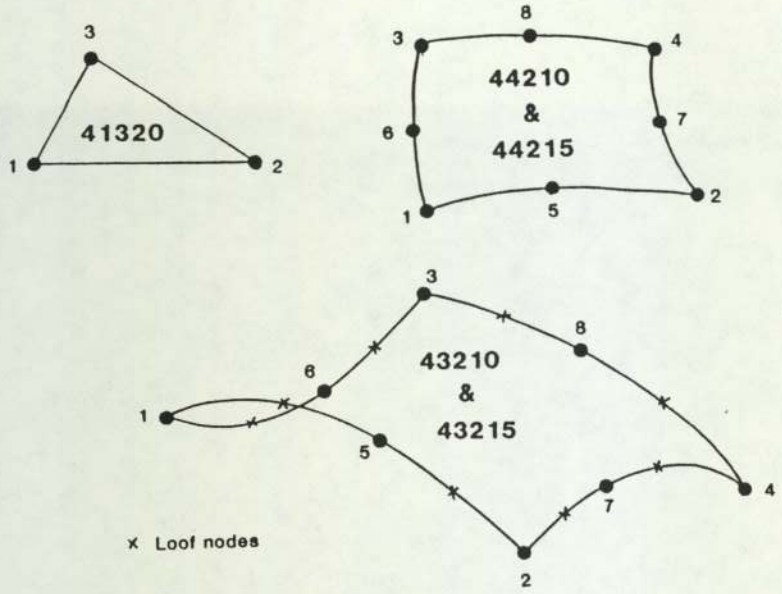

Fig. 5.2 PAFEC thin shell elements

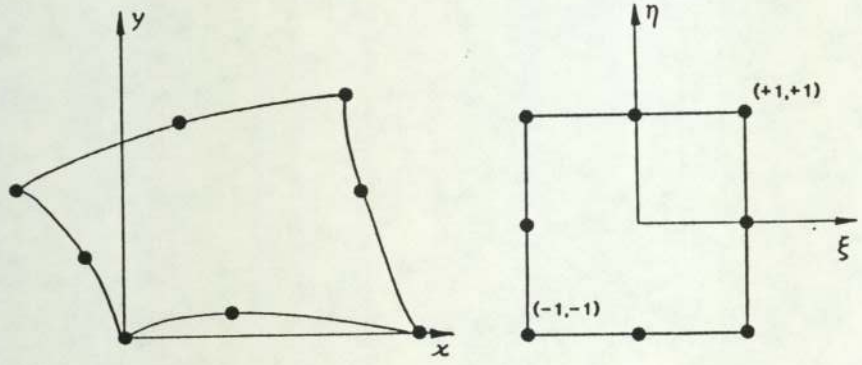

Fig. 5.3 Isoparametric transformation into $\xi\eta$ domain

CHAPTER 6

MECHANICAL BEHAVIOUR OF THE SONAR DOME LAMINATE AND SURVEY OF COMPOSITE TESTING METHODS

6.1 Material Properties

6.1.1 Composite Materials

However good the analytical models may be, without proper knowledge of the material behaviour, structural analysis cannot lead to optimal design. Traditional engineering materials, by which one normally means metals, are generally assumed to be homogeneous and isotropic, at least to a degree adequate for design purposes. The elastic properties of such materials can be completely defined by two simple constants, Young's Modulus (E) and Poisson's Ratio (ν), and both of these can be found reliably from one simple tensile test. Tests on different samples of the same material will generally give similar results to within a few percent, as will repeated tests on the same sample. Test results will also be relatively insensitive to specimen design and not much influenced by rates of loading.

In contrast to metals, composite materials are generally anisotropic and heterogeneous and their behaviour is far more complex. No sensible analysis can be undertaken based on such properties, so simplifying idealisations are normally made. For example on a macroscopic scale composites are usually considered to be homogeneous. It is possible in principle to take account of general anisotropy but few, if any, materials exhibit no symmetry in their properties and in practice many composite materials may be assumed orthotropic to some degree. The sonar dome laminate

considered in this study is such a material. It is therefore necessary to determine the mechanical properties of this material before any useful analysis of the sonar panels can be undertaken.

6.1.2 Anisotropic Materials

In general, as with isotropic materials, there exist six independent stresses and six independent strains. Using normal engineering notation for direct and shear stresses and direct and shear strains and the subscripts 1, 2 and 3 to denote the coordinate directions x, y and z, the stress strain relationships can be expressed in the form:

$$\begin{pmatrix} \sigma_1 \\ \sigma_2 \\ \sigma_3 \\ \tau_{23} \\ \tau_{31} \\ \tau_{12} \end{pmatrix} = \begin{pmatrix} C_{11} & C_{12} & C_{13} & C_{14} & C_{15} & C_{16} \\ C_{12} & C_{22} & C_{23} & C_{24} & C_{25} & C_{26} \\ C_{13} & C_{23} & C_{33} & C_{34} & C_{35} & C_{36} \\ C_{14} & C_{24} & C_{34} & C_{44} & C_{45} & C_{46} \\ C_{15} & C_{25} & C_{35} & C_{45} & C_{55} & C_{56} \\ C_{16} & C_{26} & C_{36} & C_{46} & C_{56} & C_{66} \end{pmatrix} \begin{pmatrix} \varepsilon_1 \\ \varepsilon_2 \\ \varepsilon_3 \\ \gamma_{23} \\ \gamma_{31} \\ \gamma_{12} \end{pmatrix} \quad (6.1)$$

The $[C_{ij}]$ matrix is the stiffness matrix.

An inverse relationship involving a compliance matrix $[S_{ij}]$ may be determined as:

$$\begin{pmatrix} \varepsilon_1 \\ \varepsilon_2 \\ \varepsilon_3 \\ \gamma_{23} \\ \gamma_{31} \\ \gamma_{12} \end{pmatrix} = \begin{pmatrix} S_{11} & S_{12} & S_{13} & S_{14} & S_{15} & S_{16} \\ S_{12} & S_{22} & S_{23} & S_{24} & S_{25} & S_{26} \\ S_{13} & S_{23} & S_{33} & S_{34} & S_{35} & S_{36} \\ S_{14} & S_{24} & S_{34} & S_{44} & S_{45} & S_{46} \\ S_{15} & S_{25} & S_{35} & S_{45} & S_{55} & S_{56} \\ S_{16} & S_{26} & S_{36} & S_{46} & S_{56} & S_{66} \end{pmatrix} \begin{pmatrix} \sigma_1 \\ \sigma_2 \\ \sigma_3 \\ \tau_{23} \\ \tau_{31} \\ \tau_{12} \end{pmatrix} \quad (6.2)$$

It may be shown that $C_{ij} = C_{ji}$ and $S_{ij} = S_{ji}$ so that both of these matrices $[C_{ij}]$ and $[S_{ij}]$ are symmetric. Then of the 36 terms in the matrix only 21 are independent.

6.1.3 Generally Orthotropic Materials

For the case of an orthotropic composite material for example a fibre reinforced lamina with orthogonal planes of symmetry, it is normal to refer the C_{ij} and S_{ij} matrices to these planes of symmetry. When this is done there is no longer any interaction between the direct stresses σ_1, σ_2 and σ_3 and the shear strains γ_{23}, γ_{31} and γ_{12} or between the shear stresses and the direct strains. The corresponding terms in the stiffness or compliance matrix therefore disappear resulting in, for the case of the compliance matrix,

$$\left[S_{ij}\right] = \begin{bmatrix} S_{11} & S_{12} & S_{13} & 0 & 0 & 0 \\ & S_{22} & S_{23} & 0 & 0 & 0 \\ & & S_{33} & 0 & 0 & 0 \\ & & & S_{44} & 0 & 0 \\ \text{Symmetric} & & & & S_{55} & 0 \\ & & & & & S_{66} \end{bmatrix} \quad (6.3)$$

This is for the case of a generally orthotropic material with three planes of symmetry and it can be seen that nine independent non-zero coefficients are required to complete the compliance matrix.

This matrix, expressed in terms of the 'engineering constants' E, G and ν becomes:

$$\left[S_{ij}\right] = \begin{bmatrix} \frac{1}{E_1} & \frac{-\nu_{12}}{E_1} & \frac{-\nu_{13}}{E_1} & 0 & 0 & 0 \\ & \frac{1}{E_2} & \frac{-\nu_{23}}{E_2} & 0 & 0 & 0 \\ & & \frac{1}{E_3} & 0 & 0 & 0 \\ & & & \frac{1}{G_{23}} & 0 & 0 \\ \text{Symmetric} & & & & \frac{1}{G_{31}} & 0 \\ & & & & & \frac{1}{G_{12}} \end{bmatrix} \qquad (6.4)$$

Thus, completely to characterise the elastic properties of a generally orthotropic material, nine independent elastic constants must be measured, or otherwise determined. In terms of the familiar engineering constants these are; three values of Young's Modulus (E), three values of Shear Modulus (G) and three values of Poisson's Ratio (ν). Many practical composite materials exhibit higher orders of symmetry than the general orthotropic case and for these materials fewer elastic constants may be sufficient.

6.1.4 Square Symmetric Materials

A square symmetric material is one in which there are similar properties in two mutually perpendicular directions. An example of a square symmetric composite material would be a laminate with equal amounts of reinforcement in two mutually perpendicular directions, say a bi-directional tape laminate. In this case, the

compliance matrix referred to the material symmetry axes would still retain the same number of non-zero terms but only six of the terms would be independent. If the reinforcement is to lie in the 1, 2 plane then:

$$S_{11} = S_{22},\ S_{44} = S_{55},\ S_{13} = S_{23}$$

For this case the compliance matrix becomes:

$$\left[S_{ij}\right] = \begin{bmatrix} S_{11} & S_{12} & S_{13} & 0 & 0 & 0 \\ & S_{11} & S_{13} & 0 & 0 & 0 \\ & & S_{33} & 0 & 0 & 0 \\ & & & S_{44} & 0 & 0 \\ \text{Symmetric} & & & & S_{44} & 0 \\ & & & & & S_{66} \end{bmatrix} \qquad (6.5)$$

6.1.5 Transversely Isotropic Materials

If a composite is made up so that it is isotropic in one plane, then the material is said to be transversely isotropic. There are a number of ways in which such a state can occur. Unidirectional composites are often isotropic in the plane perpendicular to the fibre direction and laminae made up of random fibres will be isotropic in the plane of the lamina. This condition, particularly the random fibre lamina case is often confused with square symmetry but the conditions are not the same. In this case, referring to the terms of the compliance matrix and assuming the symmetry is about the 3 axis:

$$S_{11} = S_{22},\ S_{44} = S_{55},\ S_{13} = S_{23} \text{ as before.}$$

In this case we also have $S_{66} = 2(S_{11} - S_{12})$.

The full matrix then becomes:

$$\left(S_{ij}\right) = \begin{pmatrix} S_{11} & S_{12} & S_{13} & 0 & 0 & 0 \\ & S_{11} & S_{13} & 0 & 0 & 0 \\ & & S_{33} & 0 & 0 & 0 \\ & & & S_{44} & 0 & 0 \\ \text{Symmetric} & & & & S_{44} & 0 \\ & & & & & 2(S_{11} - S_{12}) \end{pmatrix} \quad (6.6)$$

For this case the number of independent constants is reduced to 5.

6.2 Laminates

Strictly speaking the foregoing observations apply to homogeneous composites or to a single lamina of material. Practical laminates are made up of two or more laminae bonded together to act as an integral structural material. Each lamina in a laminate will have its own orthotropic properties with respect to its own principal material directions and any number of similar or dissimilar laminae may be stacked in any sequence to form the laminate. As a consequence of the arbitrary orientations, the laminate may not have definable principal directions of its own.

The stiffness of such a composite material may be obtained from Classical Lamination Theory (CLT). Details of CLT are given in most authoritative texts on composite materials, and will not be given here. Instead a few general observations of the effects of multiple layers on this study, will be made.

6.3 The Sonar Dome Laminate

As has been stated earlier, the type of laminated GRP material used for Royal Navy Sonar domes is designed as much for its acoustic properties as for its mechanical strength. Full details of the specification are given in Appendix A but essentially the material is a multi layer laminate of 'E' type glass fibre in an unfilled resin matrix. Laminations are alternately of woven roving and chopped strand mat and as a general rule of thumb each separate lamina contributes approximately one millimetre to the final laminate thickness.

A layer of woven roving with the warp and weft fibres at 90° will produce a generally orthotropic lamina. If the roving also has equal numbers of fibres in warp and weft directions then we might expect the lamina to exhibit square symmetry. A layer of chopped strand mat may be considered on the macroscopic scale to have random fibre directions in the plane of the mat, tending to produce a transversely isotropic lamina with its axis of symmetry normal to the fibres. The final laminate will reflect the properties of these two types of layer. Alternate layer stacking is the regime likely to produce the most nearly 'balanced' laminate and ideally an odd number of layers should be used; particularly if the number of layers is relatively small. If the final laminate is unbalanced then bend-stretch coupling will occur with the laminate curving towards its stiffer side under direct tensile loading. In this material the woven roving lamina will be stiffer than the chopped strand lamina in its principal fibre directions but less stiff in the 45° off axis directions.

All laminates considered in this study are specified to have an odd number of layers, and the woven rovings are specified to have equal weight of fibres in the warp and weft directions. With this lay up bend-stretch coupling should not occur and the overall behaviour should be square symmetric orthotropic. Also the principal axes of the material - the warp and weft directions of the rovings - are designed to be aligned with the axes of symmetry of the test panels in principle eliminating other coupling effects namely bend-twist and stretch-twist with respect to axes parallel to the sides.

In practice because the material is hand made and of variable quality, no guarantee can be given that the coupling effects are eliminated entirely. None of the panel specimens tested in this study was found to be entirely square symmetric. In view of these quality problems it would seem to be unreasonable to assume any higher order of symmetry than the general orthotropic one for the sonar dome laminate.

Left with the assumptions that the laminate is balanced and generally orthotropic, nine independent elastic constants are needed to completely define its elastic behaviour.

6.4 Possible approaches for determining Elastic Constants

Two distinct approaches are possible to determine the nine elastic constants of a generally orthotropic material. These are:

(1) Analytical methods - Micromechanics.

(2) Experimental methods.

Analytical methods are based on detailed knowledge of the composite constituents and the fibre directions and volume fractions. In essence if the elastic properties of the bulk fibre and of the bulk matrix are known - these materials are of themselves

usually isotropic - then the elastic properties of the composite can be calculated. The problem becomes one of micromechanics and can be approached in a number of ways. CHAMIS and SENDECKYJ [67] list: netting analyses, mechanics of materials approaches, self-consistent models, variational energy methods, exact solutions, statistical approaches, discrete element methods, semi-empirical approaches and microstructure theories. All of these approaches have the common objective of the prediction of the composite stiffness from the known properties of the constituents, their relative proportions, and the way in which they are assembled together. The first two may be considered mechanics of materials approaches and the others, theory of elasticity approaches.

It would be inappropriate here to examine in much detail the various aspects of composite micromechanics, several references are given in the bibliography and these cover the subject in detail. So far as fibre reinforced composites are concerned and with the present state of micromechanical analysis there is, in nearly all cases, a considerable difference between predicted stiffnesses and strengths, and stiffnesses and strengths achieved in practice. Within this limitation the value of micromechanics for design is twofold. Firstly a study of micromechanics enables the designer better to understand how composite materials function and secondly it provides a rationale for material design. If we are to design a structure, we might wish to have the freedom to design the material as well; micromechanics enables us to do this, at least approximately.

However once the material has been standardised we must concentrate on how to use the standardised material to best advantage. To do this we must use measured, not predicted material properties, and these we must obtain from mechanical testing of the real material. It would be unwise to use unsubstantiated micromechanics predictions, which might be seriously in error.

In this study the material is standardised and its properties are therefore best determined by mechanical testing methods.

6.5 Experimental Characterisation of Composites

The experimental characterisation for composite materials is generally more complicated than for ordinary homogeneous, isotropic materials because composites behave in a much more complicated fashion, as previously discussed.

In the testing of composites not only is it necessary to obtain more and different kinds of data (because there are more independent material properties), but also it is usually necessary to design the test specimens and the tests, much more carefully. In fact TSAI [68] has indicated that it may be necessary to expend as much effort on the design of suitable test specimens as on the design of the final structural component.

For the sonar dome laminate, Table 6.1 gives the engineering constants necessary for a minimal elastic characterisation of 'in plane' properties.

Property	Symbol
Young's modulus in 1 direction	E_1
Young's modulus in 2 direction	E_2
In-plane shear modulus	G_{12}
In-plane Poisson's ratio for 1 direction loading	ν_{12}

Table 6.1 In - plane elastic properties

In this table it is assumed that the reciprocal relationship between Young's Moduli and Poisson's ratios holds good:

$$\frac{\nu_{12}}{E_1} = \frac{\nu_{21}}{E_2}$$

This will be so for generally orthotropic materials, though there is some experimental evidence that it does not hold for all composites. It is also assumed that the material is not bimodular ie that the Young's moduli and Poisson's ratios are the same for tensile and compressive loading. Tests indicate that this second assumption is approximately true for reinforced plastics such as the sonar dome laminate. Additional properties which may be required for a shear deformable shell analysis are given in Table 6.2. These properties are of secondary importance in a thin shell analysis but their relative magnitudes are a measure of the relevance, or otherwise, of the thin shell approach, to any particular problem as previously discussed in Chapter 3.

Property	Symbol
Young's modulus in (3) thickness direction	E_3
Poisson's ratio associated with (1) direction loading and (3) direction response.	ν_{13}
Poisson's ratio associated with (2) direction loading and (3) direction response.	ν_{23}
(1) direction/(3) direction Shear modulus	G_{13}
(2) direction/(3) direction Shear modulus	G_{23}

Table 6.2 Through - plane elastic properties

All of the elastic properties in Tables 6.1 and 6.2 can be measured using appropriate methods. These are discussed in the following sections.

6.6 Tensile Testing of Composites

In principal the elastic constants E_1, E_2 and ν_{12} are the easiest constants to measure. As with isotropic materials they are normally measured using a simple uniaxial tension test. However, for composite materials, there are certain special problems which must be overcome.

The first and probably most important consideration for uniaxial tensile testing of fibre composites is to ensure that the loading direction coincides with an axis of material symmetry.

In a conventional tensile test on an isotropic material loading is achieved by clamping the ends and applying a prescribed elongation. There results only coincidently a prescribed stress, due to the symmetry of the isotropic material. If the same procedure is followed for an anisotropic material, or for an orthotropic material but off axis, then although the prescribed

elongation occurs, shearing stresses will occur in addition to the normal stresses and furthermore the specimen will tend to bend. The effect of this off axis loading will be greatly to reduce the apparent stiffness of the material and for a unidirectional material even one degree off axis loading may be unacceptable. A less severely orthotropic material will obviously be less severely affected but nevertheless care must be taken when setting up the test and when interpreting the results.

The basic requirements for the uniaxial tensile test are some means of applying and measuring load - usually a load cell in the loading chain of a universal testing machine - and a means of measuring the longitudinal strain. Additionally if Poisson's ratio is to be found a further means of measuring the lateral strain will be required. Strain measurements are normally made with either extensometers or electrical resistance strain gauges and it is generally believed that strain gauges give more accurate results. In practice there are a number of problems associated with the use of strain gauges on composite materials. These problems are discussed in detail in Appendix B. Also, modern strain gauge extensometers are generally far more sensitive than the traditional mechanical devices. When a large number of tests are required these instruments offer the advantages of reusability and easy calibration. Preference, therefore, accepting that there are situations where strain gauging is the only practical method, should be always to use extensometers as a first choice for the measuring of surface strains on composites.

For the uniaxial tensile test, specimen design is a most

important factor if accurate and consistent results are to be achieved. There is, unfortunately, no universably accepted standard either for specimen shape or specimen dimensions.

Various specimen shapes combined with various end connections have been proposed and used with fibre reinforced composites. Some of these are illustrated in Figures 6.1 and 6.2.

The dog-bone specimen Figure 6.1(a) is now almost totally discredited. Specimens of this shape can be made to give some useful information as regards modulus but are totally unsuitable if strength information is required. Tested to destruction, dog-bone specimens invariably fail outside the gauge length, which is clearly unsatisfactory. It is possible that longer, more gradually tapering, variations of this waisted specimen might be useful for some materials, but the expense of manufacturing the specimens would still exist, and this itself might preclude their use for routine testing.

The straight sided specimen with slight confluences, Figure 6.1(b), tends to fail at the confluences as intended, but the disturbed state of stress in the centre of the specimen makes it unsuitable for measurement of modulus. The confluences also have the effect of reducing the apparent tensile strength somewhat. Nevertheless, this is a useful specimen for routine strength testing.

Of the end connections illustrated, the single pin type, Figure 6.2(a), tends to produce a premature shear failure and the multipin type, Figure 6.2(c), is considered too complicated for use in a comprehensive testing program. The specimen

type with least disadvantages is Figure 6.1(b); a parallel sided specimen held by serrated jaw clamping. This specimen may, or may not, need reinforcement with end tabs, depending on the ability of the material to withstand the jaw clamping forces without matrix cracking. This type of specimen is recommended in BS 2782 (1976) Method 320 specimen type E, and also ISO/R527 Specimen type 1.

After some initial experimental investigations using specimens of various shapes, all of the uniaxial tensile tests carried out during the course of this project, and reported later, were carried out with tensile specimens of this parallel type. The specimens were slightly modified from the BS standard, and were considerably longer than the minimum recommended length. All specimens were tested without end tabs.

6.7 Flexural Testing

The flexure test, where a composite beam specimen is subjected to 3 point loading, is an alternative to the uniaxial tensile test, for the determination of E. The modulus obtained from this test is usually referred to as the 'Flexural modulus'.

The test is very simple and the test set up recommended by STURGEON [69] for carbon fibre reinforced plastics is illustrated in Figure 6.3. Two simple precautions are necessary if reliable results are to be obtained from this test:

(1) The deflection under the central roller should be measured by a means which is independent of the machine cross-head movement.

(2) The span/depth ratio of the specimen should be large enough so that shear deflection can be neglected. (In the suggested specimen span/depth = 100).

The flexural modulus can then be found from:

$$E_F = \frac{KL^3}{4bd^3} \qquad (6.8)$$

where: L is the test span

d is the specimen depth

b is the specimen width

K is the initial slope of the load/deflection curve

Although this test is simple to carry out there are a number of quite serious limitations which make it unsuitable for general material characterisation.

(1) The simple formula given above assumes that the material has the same modulus in tension and compression. If the material is only slightly bimodular serious errors will result.

(2) The method puts a large volume of material under a non-uniform state of stress consequently any small local imperfections in the material can have a significant effect on the result. This is in contrast to the tensile test where only imperfections in the gauge length influence the result and then only in proportion to the imperfection.

(3) Some fibre/resin systems may suffer quite large indentations by the rollers which may produce a significant error (this can be eliminated but only at the cost of complicating the test procedure).

(4) Since the result is dependent on d^3, accurate determination and control of d is essential. This may prove difficult with hand lay up materials.

In view of these limitations the 3 point flexure test is considered unsuitable for general characterisation work with composites. The main value of the test is as a general quality control method only.

The above comments apply equally to the less common 4 point bending flexural test. This test has not been extensively reported, probably because it is more difficult to set up than the 3 point test.

In the present work some initial 3 point flexure test studies were carried out on samples of the sonar dome laminates. The results were not good and are not reported here. In general flexural modulus measured by a flexure test will be found to be considerably lower than the modulus of the same sample measured in tension. This, and the nature of the thickness variation encountered in the sonar dome laminate, precludes the use of flexure testing for this project.

6.8 Shear Testing of Composites

If the uniaxial tensile testing of composites is complicated by considerations of specimen type and coupling effects, the complications encountered in shear testing are very much worse. With isotropic materials there is no need to perform any test to determine the shear modulus G. G is not an independent constant and is readily found from the relationship:

$$G = \frac{E}{2(1 + \nu)} \qquad (6.9)$$

In general for orthotropic materials this relationship does not hold good and the shear modulus must be regarded as an independent elastic constant, to be determined in its own right. In fact for generally orthotropic cases three values of shear modulus

must be determined. It may be possible, if only approximate values are required, to ignore the independence of the constants and assume some arbitrary relationship. HUBER [70] modified the above relationship for the orthotropic case to:

$$G_{12} = \frac{\sqrt{E_1 E_2}}{2(1 + \sqrt{\nu_{12} \nu_{21}})} \qquad (6.10)$$

It is difficult to see any real justification for this and it seems to be only a slight improvement on assuming the material to be isotropic with average elastic properties.

Many test methods and specimen types have been proposed for shear testing, all of which have some disadvantages for sheet materials. Filament-wound tubular specimens are satisfactory since they can be subjected to torsion testing but this is not a practical method for flat laminated materials. The main problem with all shear tests is that of achieving a reasonably uniform state of shear in the specimen. A pure shear state is not attainable in the specimen in any practical tests but the need to measure the shear modulus remains. The following sections describe some of the more common methods with their limitations.

6.9 In Plane Shear Tests

6.9.1 Rail Shear Test

The rail shear test is perhaps the most obvious means of applying a more or less uniform simple shear state to a sample of sheet material. In this test a square or rectangular sample of material is bolted between two pairs of parallel rails, the remaining two edges being left free. Upon application of loading to the rails stresses are transmitted to the specimen by the displacement

of one pair of rails relative to the other. The test is illustrated schematically in Figure 6.4.

Rail shear tests have been in use for some time as shear strength tests, but the first suggestion that they might be used to determine in-plane shear modulus seems to have been made by HENNESSEY, WHITNEY and RILEY [71] in 1965. The first reported use of the method seems to have been by HADCOCK and WHITESIDE [72] who used it to determine the shear properties of a boron-epoxy composite, and the first use on GRP would seem to be by BALABAN and JACKSON [73] (1971). The validity of this test rests on the work of WHITNEY, STANSBARGER and HOWELL [74] who presented a detailed stress analysis of the test using a Fourier series solution. They concluded that the method is valid provided that the material does not have a Poisson's ratio greater than unity and provided also that the aspect ratio of the specimen (length of specimen/width between rails) is at least 10. Photoelastic work seems to confirm that a short distance from the free edges the stress state is fairly uniform, but the narrow gauge section necessary to achieve the large length/width ratio creates problems near the clamped edges.

GARCIA, WEISSHAAR and McWITHEY [75] have used finite element analysis to investigate the feasibility of tailoring the specimen aspect ratio to a particular material. They conclude that for laminates an aspect ratio as low as 6 will yield better results than the more usual 10 or 12.

6.9.2 Double Rail Shear Test

A logical extension of the rail shear test is the double rail shear test. In this test a symmetric rail shear

fixture is used which effectively gives two single rail shear tests back to back. The fixture proposed by SIMMS [76] for use with a symmetric cross-ply laminate is shown in Figure 6.5.

This is clearly a better arrangement than the single rail test because the problems associated with off-axis loading are eliminated and the specimen has less of a tendency to twist during the test (some undesirable coupling effects will cancel) but the basic limitations on aspect ratio and Poisson's ratio still apply.

In both the single and double rail shear tests, even if the test rig configuration can be made to produce a reasonably uniform state of shear stress in the centre of the test sample, in order to determine the modulus the corresponding strains in the material must also be measured. This is normally done by strain gauges on the specimen and apart from the problems associated with this - mentioned previously, the inconvenience and cost of bonding gauges to large numbers of specimens makes the method unattractive. Attempts to overcome the need for strain gauges with rail shear tests, by measuring relative rail displacements, reduce the reliability of the test. Published results from rail tests have been very inconsistent even with strain gauged samples so that although the method might seem to be the most obvious one for shear modulus measurement it is not considered suitable for the sonar dome laminate.

6.9.3 Picture Frame Shear Test

Under this heading are considered a number of test methods which aim to overcome the free edge effects of the rail shear tests by loading all four edges of a square plate specimen. A large number of variations of this method are reported in the literature most of which rely on some sort of linked or pin jointed frame surrounding the test panel to apply the load. The basic arrangement is shown schematically in Figure 6.6.

Variations of this test have been in use for many years as a test for plywood and other wood based composites; in recent years it has been used for fibre composites by XINGHUA [77] and others. Although the test appears very simple and superior to the rail tests in concept, it is actually a very difficult test to carry out accurately. The uniform shear state depends on very precise fitting of the specimen in the frame and the frame itself must be free moving but free from any slack. Specimens are normally strain gauged. If the test is not set up very precisely then the results can be totally invalid. Experiments at RNEC using a picture frame test rig on sonar dome laminates have proved unsuccessful. There may be scope for future developments of this test but at present it must be considered too unreliable to be used here.

6.9.4 Other Shear Tests

None of the shear tests so far mentioned is totally satisfactory and it seems likely that no test which is truly satisfactory for all composite materials, will ever be developed. The number of test methods which have been

tried or proposed in testimony to this. Many shear tests have been proposed which rely on unusual specimen geometries - these have been excluded here because the specimens are difficult to manufacture and the methods are generally very material specific. Several methods are available for determining elastic constants which are not in the strictest sense mechanical tests. Ultrasonic pulse propagation, Free vibration and Forced vibration methods are some of these. These methods can with some materials yield full sets of elastic properties but their applicability to hand lay up fibre composites is doubtful. Ultrasonic and vibration methods by their very nature yield results for elastic properties at high strain rates. With non-metallic materials, properties at low or moderate strain rates may be very different.

6.10 Shear Tests used in the current work

6.10.1 Anticlastic Bending Test

This test utilises a state of shear induced in a square plate by the application of equal and opposite normal loads at adjacent corners, Figure 6.7. For the shear stress state, which is of a 'rotational transverse' nature, to be achieved, the loading must deform the plate into a state of anticlastic curvature, Figure 6.7(a). If the plate is arranged so that it is supported at 3 corners A, B and C, and loaded at the remaining corner D then this meets the loading requirement. If the load P necessary to produce a deflection x at the loaded corner is measured then it can be shown that the in plane shear modulus is given by:

$$G = \frac{3P\ l^2}{t^3\ x} \qquad (6.11)$$

where l is the length of one side of the plate and t is the plate thickness.

This test for shear modulus was first proposed by NADAI [78] and became quite extensively used as a quality control test for plywood in the aircraft industry. With the increasing use of composite laminates the method has undergone something of a revival. TSAI [79] has described a similar method for obtaining all the required elastic constants for an orthotropic plate, from one beam specimen and two twist specimens, when the principal material axes are known. BECKETT, DOHRMANN and IVES [80] have highlighted the dangers of large errors occuring if the plate does not bend into the particular 'anticlastic' surface that the equations require.

The limitation of this test for determination of in-plane shear modulus are:

(a) The principal axes of the material must be known.

(b) The specimen dimensions must be such that anticlastic bending occurs. If a synclastic bending mode develops gross errors will occur.

(c) Material thickness must be accurately determined. The calculated shear modulus is dependent on the cube of the thickness.

Provided that these limitations can be overcome the method offers a number of distinct advantages over other available methods:

(a) No strain gauging is required. No strain measurements are made.

(b) Specimen preparation is very simple. A square plate specimen is all that is required and provided this is flat and cut parallel to axes of material symmetry, it can be tested and repeatedly retested if necessary.

(c) The only measured parameters are load, deflection and specimen dimensions.

The requirement that the principal material axes should be known is met by the sonar dome laminate as specified. Anticlastic bending will be achieved if the specimen side/thickness ratio is selected carefully and deflections are kept small.

The transition from anticlastic bending to synclastic bending is rapid and easily detected. FOYE [81] has reported this as an instability problem influenced by specimen geometry, initial curvature and amount of deflection. Any anticlastic bending test should include some check that the proper bending mode is being achieved. If it is not then the test parameters should be changed accordingly.

For the sonar dome laminate the major defect of the method centres around accurate determination of specimen thickness, but this can be overcome by taking multiple thickness measurements of each test sample. After some initial experimental investigations the rail shear and picture frame shear arrangements were discarded and all of the in plane shear results for the sonar dome laminate, reported in this thesis, were obtained

from the anticlastic bending test.

6.10.2 Balanced Rail Shear Test

Although there are a multitude of shear tests available which may be used to obtain in plane shear modulus, admittedly none very satisfactory, through-plane shear has been largely neglected. This may be because there are fewer design situations where accurate values of through-plane shear modulus are required; thin shell analysis, for example, does not require it. It may also be because properties through the plane are very difficult to measure.

For the sonar dome laminate some assessment of the two through-plane shear moduli is desirable so that the validity of the thin shell analysis can be judged. No mechanical test has been reported which claims accurately to measure the through-plane moduli directly, but this is not really the requirement. What is required is some means of obtaining relative values to compare with the other elastic constants.

PURSLOW [82] suggested a modification of the balanced rail shear test which could be applied in all 3 material directions. This appears to have been simply a suggestion and it seems that no tests were carried out. PURSLOW's suggested arrangement is illustrated in Figure 6.8. The suggestion is that two small, (10 mm) cubes, of material should be strain gauged for shear deformation, and bonded to the symmetrical loading rig. The size of the specimens

is limited by the thickness of the laminate and the availability of short gauge length strain gauges.

All of the objections to the rail shear test apply to this test. There is no possibility of obtaining a state of pure shear in the material, the desirable aspect ratio of 10 to 12 is reduced to 1 and strain gauging is unavoidable.

Notwithstanding these serious objections, work has been undertaken at RNEC to develop this through-plane test and the results have been quite encouraging. This work has been reported by the author and associates - HARTSHORN, SMITH and SUMMERSCALES [83] and whilst the values for shear modulus obtained from this test are considered to be reasonably accurate, the main value of the test is as a comparative method, where one of the three shear moduli is known from other tests. Normally this known value would be the in-plane value.

This test has been used to obtain comparative through-plane shear moduli for the work reported here and the experimental method is detailed in Chapter 8.

6.11 Summary of Material Testing Techniques

In summary the number of test methods for the elastic characterisation of fibre reinforced composites such as GRP, reported in the literature, is vast. Most of the methods have disadvantages. For the shear properties none of the tests can claim to be truly satisfactory.

The test methods selected for the characterisation of the sonar dome laminate are:

(1) Uniaxial tension to determine E_1, E_2 and ν_{12}

(Some uniaxial compressive tests were undertaken to investigate possible bimodularity - none was found).

(2) Anticlastic bending to determine G_{12}

(3) Balanced rail shear to provide comparative values of G_{13} and G_{23}.

It is recognised that these tests do not give a complete characterisation of the laminate and are therefore less than ideal. They are however repeatable tests, and with the exception of the balanced rail shear test, they are all established techniques.

Test methods, specimen dimensions and loading regimes have been developed for each test, specifically for this project and for the sonar dome laminate. The tests selected are considered to be the best mix of tests available for this material and the detailed test methods, given in Chapter 8, should be considered specific to this material. Other laminates may be better evaluated with a different mix of tests and different test procedures.

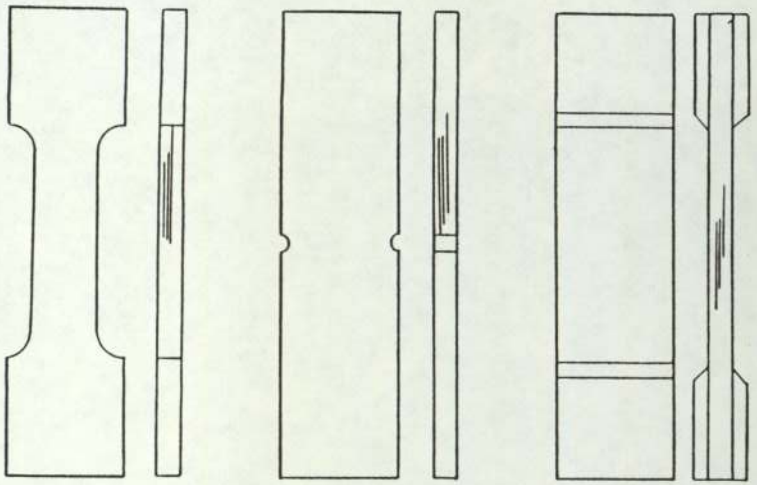

Note: Specimens not to scale.

Fig. 6.1 Uniaxial tensile test specimens

a) Dog bone
b) Straight sided with slight confluences
c) Straight sided with end tabs

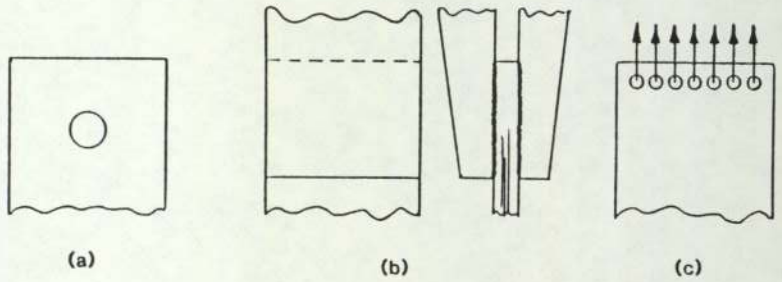

Fig. 6.2 Types of end connection

a) Single pin type
b) Serrated jaw type
c) Multi hole type

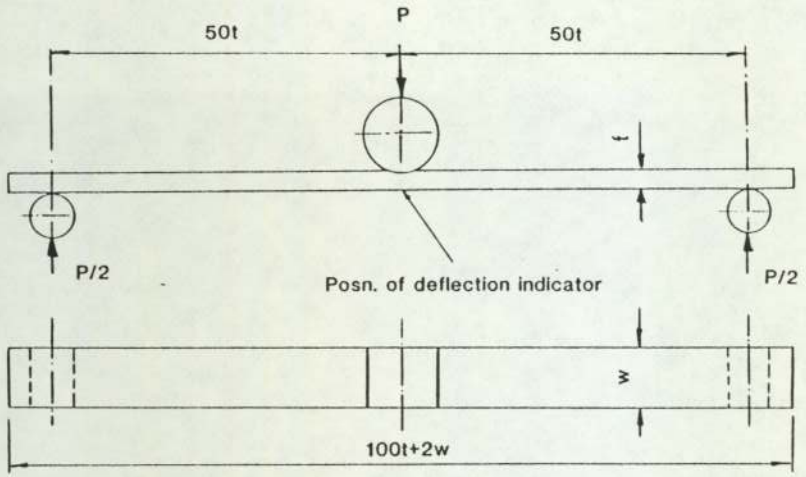

Fig. 6.3 Schematic arrangement for 3 point bend flexure test

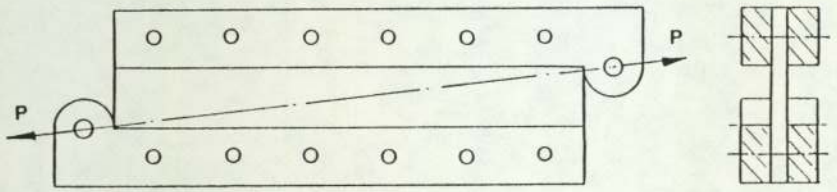

Fig. 6.4 Schematic arrangement for Single rail shear test

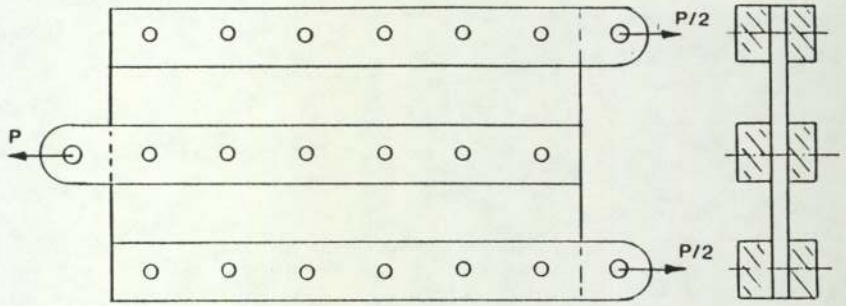

Fig. 6.5 Schematic arrangement for Double rail shear test

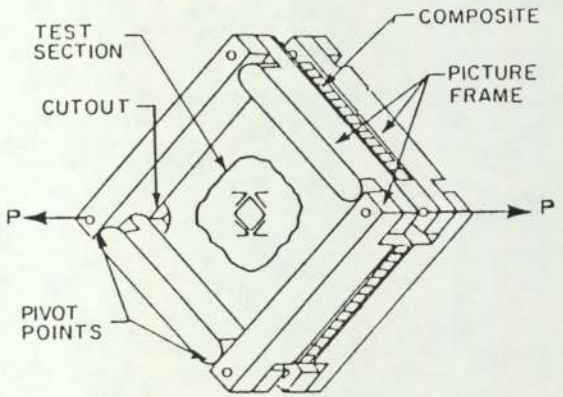

Fig. 6.6 Schematic arrangement for Picture frame shear test

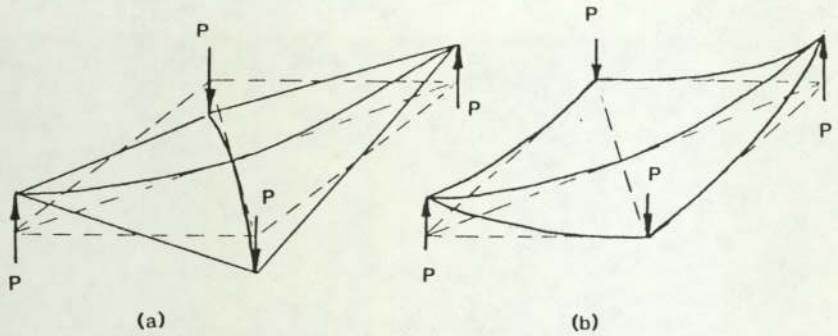

Fig. 6.7 a) Anticlastic bending of plate specimen
b) Synclastic bending of plate specimen

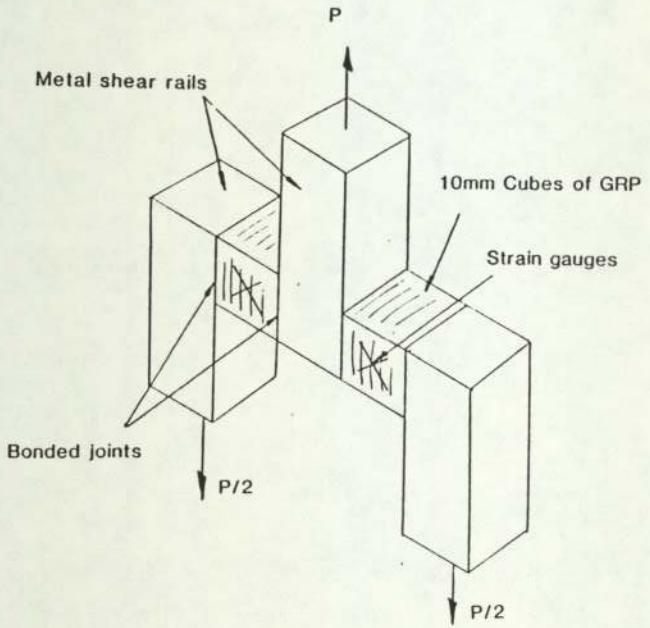

Fig. 6.8 Schematic arrangement for Balanced rail shear test

CHAPTER 7

INSTRUMENTATION, LOGGING AND EXPERIMENTAL PROCEDURES

7.1 Introduction

Experimental studies form a major part of this project both in evaluation of material properties and in large scale cylindrical panel testing. Accuracy and reliability of experimental data is thus very important. Procedures for obtaining the data, calibration of instrumentation, logging of data, and the processing of raw data are all possible sources of inaccuracy and error.

Because of the wide variety of experimental work carried out during the course of this project it has been necessary to employ a wide range of instrumentation and equipment and a number of different experimental procedures. Whilst some of these procedures may be regarded as fairly standard material tests, others have been developed specifically for this work. Additionally some of the procedures are common to several distinct parts of the work, for example the logging of strain readings from tensile tests on material samples is essentially similar to the logging of strains in the large scale sonar panel tests, also displacements of the anticlastic bending samples for the shear modulus measurement were logged in precisely the same way as were panel deflections in the large scale tests.

This chapter gives details of the test facility, equipment and instrumentation and describes the basic data logging procedures for all of the major tests described in later chapters. It therefore serves as an introduction to the experimental work of the project.

7.2 Structural Testing Facility

The experimental facility at RNEC consists essentially of a 9 x 4 metre strong floor with mounting frames, a multi-channel pneumatic loading system, a vacuum loading system, a servo-hydraulic multi-actuator system, a wide range of instrumentation and two control and data acquisition computers. The laboratory also has a Instron 8032 universal testing machine.

7.2.1 The Strong Floor

A 9 m x 4 m strong floor consisting of a series of linked I section RSJ's drilled at frequent intervals provides the main test area, further restraint of structures can be provided by a number of large vertical pillars. The floor area is serviced by two moveable gantries, each with 2 tonne winch, and a fork lift truck.

7.2.2 The Pneumatic Loading System

The laboratory has a 30 channel pneumatic control system designed to provide each channel with a separate predetermined pressure. Each channel may be controlled individually either manually or by using the load control amplifiers connected to the computer system. The system is able to control pressures to within 1 kPa over a range of 0-400 kPa.

For this project finer control over pressure was considered desirable and a Druck DPI 500 precision controller was used. This is a single channel instrument able to control both pressure and vacuum to within 0.1 kPa over a range +200 kPa to 0 kPa to -100 kPa.

7.2.3 Data Acquisition and Control Computers

The laboratory has two Intercole Systems Ltd. data acquisition computers. The original C2 machine is able to address 30 Digital to Analogue control channels and can log data from up to 400 voltage transducers and strain gauges. The logged data can be processed and the output presented in tabular and graphical form. All instrument calibration is carried out using laboratory standards and the logging system of the computer.

The more recent C3 computer has all the facilities of the C2 but is a very much more powerful machine and has a number of additional capabilities.

The central processor is a PDP 11/23 with 256 Kb of memory, the operating system is DEC RT11 version 5.0 and mass storage is by means of a multi-platter Winchester drive and floppy discs. The computer is coupled to a colour graphics terminal with a colour plotter and has access to all the original peripheral equipment.

The control system consists of D to A channels and 32 input/output status channels.

Both computer systems were used for these investigations, but most of the data logging was carried out using the C2 machine.

7.2.4 Universal Testing Machine

The laboratory has a material testing capability in the form of an Instron 8032 Test Machine. This machine has a microprocessor based control system coupled to a hydraulic actuator mounted in a two column loading frame and is suitable for both static and dynamic testing.

Output from the machine can be to a graph plotter, a small Instron based printer or to the Compulog C2 logging computer. In the latter case load, actuator position and up to six other transducers may be logged using a purpose written suite of programs.

For this project all testing was carried out using the machine in conjunction with the C2 logging system.

7.3 Instrumentation - Transducers

A range of laboratory transducers was used for this project and these are described below. With the exception of the ultrasonic thickness gauge these are all standard laboratory instruments. The ultrasonic thickness gauge is basically a field instrument which has been adapted for use in the laboratory.

7.3.1 Displacement Transducers

The displacement transducers used for this study were of the Linear Variable Differential Transformer (LVDT) type manufactured by RDP Electronics Ltd.

Two models were used because sufficient of one model were not available, however over the limited displacement range required very little difference is apparent between the two types.

The models are:

Type 500A

Displacement Range	+/- 12.5 mm
Output Voltage at max displacement	approx +/- 2.0 V

Type 1000A

Displacement Range	+/- 25.0 mm
Output Voltage at max displacement	approx +/- 2.0 V

These transducers have an integral conditioning unit and only require connection to a 6 V dc power supply and the logging system.

7.3.2 Pressure Transducer

A single pressure transducer was used to measure the pressure loadings applied to the panels (positive and negative pressures). This transducer was incorporated in the Druck precision controller and only required connection to the logging system.

All displacement and pressure transducers were individually calibrated prior to use. (See Section 7.4).

7.3.3 Strain Gauges

As previously stated strain gauges can be an unreliable measure of strain on composite materials, however they are often the only practical method of obtaining strain data. In view of this strain gauges were not used for any material testing, but were used on the aluminium and GRP panels. Precautions were taken to minimise the adverse effects including careful selection of gauge length and the use of pulsed excitation.

The strain gauges used were two element rosettes with each element connected to a separate logging channel. A 120 ohm resistor was connected to each channel as a dummy gauge forming a half bridge input to the logging system. This arrangement is more economical on strain gauges than a system using real gauges as dummies but does carry the penalty of sensitivity to changes in ambient temperature. This effect was reduced to a minimum by careful monitoring

and control of the ambient temperature. Changes in lead wire resistance due to temperature were compensated for by use of a 3 wire system.

Strain Gauge Specification:

2 element 0-90 degree rosette

Gauge Length	6 mm
Resistance	120 ohm
Gauge Factor	2.08

7.3.4 Thermocouples

Temperature monitoring during panel testing was carried out using K type Chromo-alimo thermocouples.

Two thermocouples were used, one on the panel under test and one on the steel surface of the test rig. Thermal contact was obtained using heat sink compound and adhesive tape.

7.3.5 Ultrasonic Thickness Gauge

The thickness measuring device selected for use in this project was a Teledictor 2002 Ultrasonic Thickness Gauge complete with analogue output unit.

This unit operates on a "pulse echo" principle. A piezo electric probe is placed in contact with one face of the material to be measured with acoustic contact ensured by the use of an incompressible coupling medium. A short 1 MHz ultrasonic pulse travels through the material and is reflected back from the opposite surface. The time taken for the pulse to travel through the sample and back is related to the thickness and the velocity of sound in the material.

7.4 Instrumentation - Calibration

Calibration of all working transducers used in the current work was carried out using Laboratory Standards whose calibration can be traced to NPL Standards. These Laboratory Standard transducers are maintained for calibration purposes only.

As far as possible calibration of working transducers was carried out with the transducers connected to the same logging channels, power supplies, etc, that were to be used during subsequent experimental work. Software algorithms used in calibration programs were also identical to those used for the experimental work.

7.4.1 Displacement Transducers

The LVDTs were calibrated using a drum-micrometer calibrator (Figure 7.1). The purpose of the calibration was to provide a slope of mV/mm for each instrument for subsequent use in the experimental processing.

Each transducer was fixed into the calibrator, connected to the common LVDT power supply (6 V DC) and the logging system. The instrument was then set to a number of positions either side of the nominal zero and the transducer output logged at each position.

A value fot the slope of mV/mm was then computed using a least squares regression routine to obtain the best fit straight line. From this line a value of displacement was calculated at each point and compared with the set values. The difference between the two displacement values represents the error at that point in the range. A specimen output is shown in Table 7.1.

The maximum error accepted, over the range of use, was +/- 0.02 mm. Transducers that were required to read very small displacements were recalibrated over a smaller range.

7.4.2 Pressure Transducer

The pressure transducer was calibrated using a similar method to that used for the displacement transducers. Two Budenberg dead weight pneumatic calibrators were used to set a range of positive and negative pressures. Values of slope (mV/kPa) were obtained for a positive range of 0 to 200 kPa and a negative range of 0 to -95 kPa. As with the displacement transducers these slopes were obtained by a least squares regression routine and a value for the maximum error of +/- 0.1 kPa was obtained. Table 7.2.

7.4.3 Thermocouples

The thermocouples were not calibrated but were checked against a precision thermometer over a range of 10 to 40 degrees C. Over this range the maximum error was +/- 0.5 degrees C.

7.4.4 Extensometers

Extensometers used with the Instron testing were calibrated using the Instron Extensometer Calibrator. This instrument is similar to the drum micrometer used to calibrate LVDTs but has various profiles upon which the extensometers can be mounted. The normal method of attaching the transducer to the calibrator profile is by means of rubber bands or springs hooked into notches at the ends of the knife edges. However the standard methods of attachment were not used for the GRP tensile specimens, instead the knife edges were bonded directly to the GRP using cyanoacrylate adhesive (see Chapter 8).

In order to ensure that this method of attachment

did not introduce parallex errors by reason of rotational restraint of the knife edges, a pair of GRP profiles were made to fit the calibrator (Figure 7.2). The extensometers were bonded to these profiles in a manner identical to that used for the specimens.

All extensometers were set to a gauge length of 10 mm and were calibrated over a range of +/- 0.2 mm using a method similar to that used for the displacement transducers. Using the same calibration routines as used for the displacement and pressure transducers no errors were detected at the resolution of the calibrator (Table 7.3).

7.4.5 Ultrasonic Thickness Gauge

This instrument was found to require frequent calibration during use.

GRP calibration blocks cut from the panel test material were manufactured in two thicknesses representative of the panel thickness range.

7.5 Instrumentation - Logging

This section describes the Instrumentation Logging for all the experimental work described in the following chapters. Each type of transducer was interrogated using a slightly different method as described below.

7.5.1 Voltage Transducers

(LVDTs, Pressure Transducer, Extensometers (Instron) and Ultrasonic Thickness Gauge).

The first function of the logging program is to log and retain any initial transducer offsets. In the case of voltage transducers this value is the voltage difference between the transducer set position and its electrical zero. This value is stored for each instrument and deducted from subsequent measured values.

The voltage is logged by connecting a 16 bit digital voltmeter to the transducer using reed relays exclusive to that logging channel, thus ensuring isolation from all other voltage sources connected to the system. The full scale range of the DVM is software switchable and is determined from information stored in the experiment data file. The rate of sampling is locked to the zero crossing point of the 50 Hz mains supply, this has the penalty of reducing the overall speed of logging but ensures minimum mains interference.

To further improve measurement accuracy the channel is interrogated twice, once with the scanner open circuit and the input amplifier short circuit (to settle the amplifier) and once with the amplifier connected via the scanner to the transducer. At this point an integer value relative to the transducer voltage is obtained and is processed by the computer to produce a value in the appropriate engineering units.

The interrogation and processing procedures and parameters selected for logging the voltage transducers and all other types of transducer were identical to those used during calibration. This ensured that the errors introduced by the logging system were reduced to a minimum.

7.5.2 Strain Gauges

Strain gauges are connected to the logging system in a half bridge configuration with an active gauge in one arm and a resistor in the other. The logging system electronically completes the bridge network and provides a constant energising current.

As with the voltage transducers the initial offset of each strain gauge must be obtained. This offset is the

difference in electrical resistance between the strain gauge and the 'dummy' resistor. In relation to the change in gauge resistance caused by mechanical strain this offset resistance can be very large and if simply measured as an out-of-balance voltage could greatly reduce the DVM range. In order to use the full DVM scale for strain measurement an 'autobalance' system using a series of precision resistors in a R/2R ladder network is employed. The gauge and dummy resistances are balanced by up to 16 precision resistors and the binary value of the resistors required is returned to the computer and stored.

On subsequent channel selection the appropriate resistor pattern is connected to the circuit and an out-of-balance reading made. As with the voltage transducers the amplifier gain range is obtained from the data file, the scanning rate is locked to the mains supply zero crossing point and the channel is addressed twice. The strain gauge network is first connected to the input amplifier with no energising in order to settle the amplifier, the energising current is then applied and a reading relating to the applied strain is made.

A number of problems can arise when using strain gauges on GRP, one of the most significant is due to the poor thermal conductivity of the material. Large values of apparent strain caused by localised heating can occur when a gauge is continually energised. The Compulog method of intermittent channel interrogation and energising ensures that gauge heating, and therefore apparent strain, is kept to a minimum.

7.5.3 Thermocouples

Temperature measurements were made by single junction thermocouples connected to the remote satellite cabinets, the cold junction emf being generated at the input terminals. In order to provide a compensation for this emf the temperature of the terminal strip was measured using an auxiliary resistance thermometer connected to a logging channel in the satellite cabinet.

Unlike the previous transducers the reference point for the thermocouples can vary throughout the experiment. Because of this the temperature of the reference junction was measured before each thermocouple interrogation.

Although thermocouple output is not linear over a wide range of temperature a simple straight line approximation produced an acceptable result over the limited range of temperature measured in this project.

7.6 Experimental Techniques

Three differing data collection procedures were used in this work. Methods used for the measurement of panel thickness, for material tensile testing and for panel testing are described below.

7.6.1 Thickness Measurement

Thickness of the GRP panels was measured using the Ultrasonic thickness gauge (described above) connected to a Compulog voltage measuring channel. The analogue output of the thickness gauge was directly related to the measured panel thickness by a previously determined factor.

A computer program specially written to log and process thickness data was used for this aspect of the study.

The logging function is initiated by measurement of a pseudo 'zero offset' voltage at an indicated 0.5 mm. Up to 100 thickness measurements can then be made and stored in the computer. Throughout the measurement stage frequent checks were made to ensure that the instrument remained calibrated. This was done by reference to two accurately machined calibration blocks and where necessary adjustment of the instrument was made using the 'zero' and 'velocity' controls. Recalibration of the computer was unnecessary since the instrument analogue voltage output is related to its digital display.

Processing:

Once the required number of measurements had been taken the program calculated values for mean, standard deviation and limits. Since areas of the panel appeared noticeably different in thickness, measurements were made using a 6 x 6 mesh, this enabled further processing to provide analysis of variance for the data grouped in rows, columns and square groups. From this data it was possible to determine whether one area was significantly different in thickness to the rest of the panel.

The values of the thickness measurements and of the processed data were then printed in a hardcopy form.

7.6.2 Material Tensile Testing

Tensile testing of GRP and aluminium samples to determine elastic properties was carried out using the Instron 8032 test machine linked to the Compulog C2 computer.

While loading control was effected from the Instron control console, the computer was used solely for logging.

Measurements of load, actuator position and four extensometer displacements were made by means of connections between the Instron analogue output device and the voltage measuring channels of a Compulog satellite cabinet.

Testing:

A typical tensile test carried out for this project monitored load, actuator position, axial strain and transverse strain. After logging the zero offsets, with the specimen unloaded, the load was applied as a slow ramp function. Once a preset minimum load had been detected (to allow settling of the load chain) logging of the four parameters continued at 1 second intervals.

Unlike loading during panel testing, a continuously increasing or decreasing load was applied to the specimen. Because the logging system operates sequentially it was not possible to measure the four parameters simultaneously, therefore at each logging interval the instrumentation was interrogated as follows:

Transverse Strain

Axial Strain

Actuator Position

Load

Actuator Position

Axial Strain

Transverse Strain

The means of the values obtained for strains and actuator position were then stored together with the value for load. The time taken to complete a logging cycle was less than 0.5 seconds, therefore any errors in this procedure would be due only to any small perturbations present in the ramp function.

Processing:

At the end of a test, or series of tests, the measured data was processed and displayed. The data was also used to produce a graphical display and by further processing to produce values of Tensile Modulus and Poisson's Ratio.

Values of Tensile Modulus and Poisson's Ratio were calculated over the range 10% - 60% of the maximum test load to ensure reasonable linearity. A least squares regression algorithm was used to produce a slope of load/strain for the Modulus calculation and Transverse Strain/Axial Strain for the calculation of Poisson's Ratio.

7.6.3 Panel Testing

A typical panel test was run under computer control using the Compulog C2 computer. The software suite allowed load control and data collection with a range of options. Positive pneumatic loading was provided by a dry air from a Hydrovane compressor and negative loading by a vacuum pump, pressure control was provided in both cases by the Druck pressure controller.

The logging system is shown schematically in Figure 7.3 and the pneumatic loading systems in Figures 7.4 - 7.6.

Test Preparation:

In order to carry out a test the system was connected as shown for positive or negative loading; various engineering programs were then used to ensure correct setting and operation of the instruments and a data file was constructed containing test and channel identification data together with instrument calibration values.

This information was used for description, logging and processing both in the experiment control program and the post processing programs.

Testing:

The experiment program had two main functions, logging and load control. The program also allowed the operator to select various features such as manual or automatic control, logging at preset time intervals, selection of pneumatic bypass circuit, etc.

Initially the program measured and recorded the offset voltages and strain gauge autobalance patterns as discussed above. The system was then ready to control the applied load and measure the test structure reaction. Using the computer, load control was achieved by generating a +/- 5 V analogue voltage using the Digital to Analogue Convertors (DACs). This voltage was proportional to a preset value of load, the relationship between voltage and load having been determined prior to testing.

In the case of the Druck pressure controller an input of +/- 2 V produced a full scale demand of +/- 200 kPa, in order to make full use of the DAC output a simple potentiometer was connected between the DAC and the pressure controller.

In manual mode the pressure was set by the computer or from the pressure controller. When the required pressure had been achieved logging was initiated manually. When used in automatic mode the computer set the load and waited to receive an 'in balance' signal from the controller, the computer then logged the instrumentation and set the next level. In the automatic mode preset time intervals were used to control logging.

Both manual and automatic modes allowed the use of the pneumatic bypass circuit to increase the flow rate to and from the test structure. Intended primarily for use with the vacuum tests because of the lower differential pressure, the system was also be used to increase the speed of positive pressure testing. The bypass system (Figure 7.6) is part of an outer control loop which is closed by the logging software. This allowed a simple on/off valve to connect the positive pressure or vacuum source directly to the test structure until the pressure was within 0.5 kPa of that demanded, the valve then closed and the Druck pressure controller achieved the fine control.

At each control level the logged data was filed to disc to increase security.

Processing:

Following the collection of experimental data a post processing program was employed. This program collated the logged data in a selected format, calculated the various displacements and stresses and presented the required information as a hardcopy output.

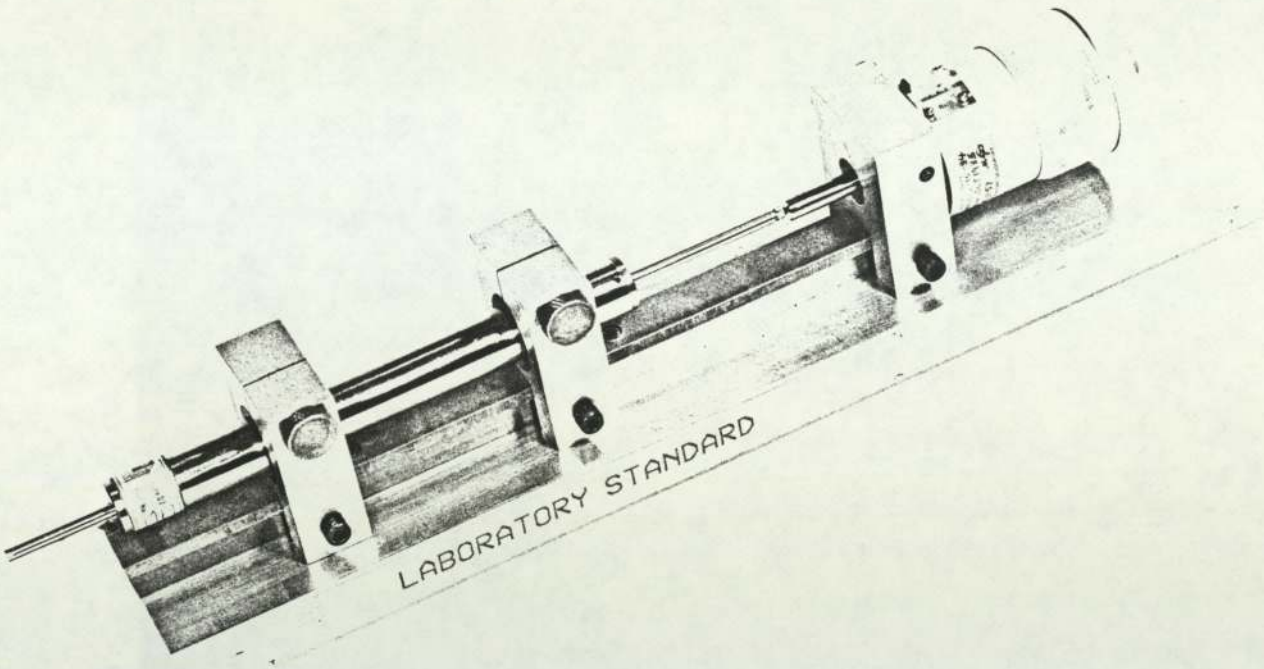

Fig. 7.1 Drum micrometer calibrator for calibration of LVDT's

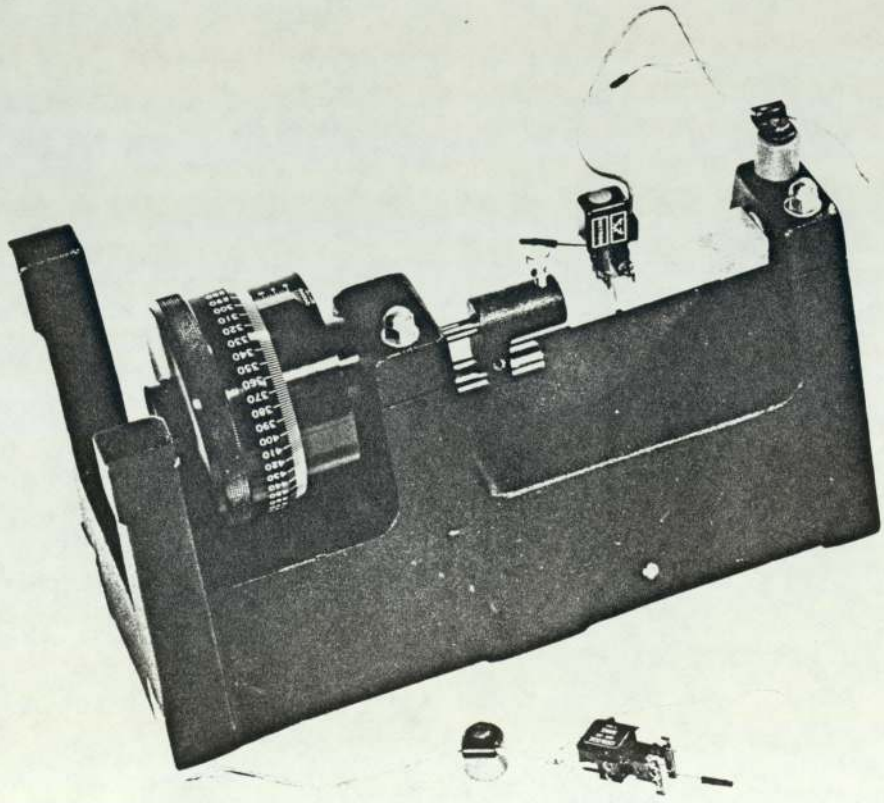

Fig. 7.2 Drum micrometer calibrator for calibration of extensometers (Note GRP profiles)

DISPLACEMENT TRANSDUCER CALIBRATION

Calibration date : 14-Feb-85
Type : 500A
Serial No. : 696
Power supply voltage : 6.000

Displacement (mm)	Readings (mV)	Error (mm)*
-10.00	1155.83	0.01
-9.00	1040.50	0.01
-8.00	924.50	0.01
-7.00	808.66	0.00
-6.00	693.00	0.00
-5.00	576.83	-0.00
-4.00	461.00	-0.01
-3.00	345.33	-0.01
-2.00	230.16	-0.01
-1.00	114.33	-0.01
0.00	1.50	-0.00
1.00	-111.50	-0.02
2.00	-225.83	-0.02
3.00	-340.50	-0.03
4.00	-455.50	-0.03
5.00	-570.83	-0.03
6.00	-686.50	-0.03
7.00	-802.66	-0.02
8.00	-920.00	-0.00
9.00	-1037.33	0.01
10.00	-1155.33	0.03

Slope = -115.226 mV/mm
Correlation coefficient = -0.9999
Amplifier gain range 8

* Error calculated using calibration readings and derived value of slope.

Stability Check
Mean = 0.00 : Values range from 0.00 to 0.00

Reading Check

Target (mm)	Reading (mm)
-5.00	-4.99
5.00	4.96

Table 7.1 Displacement Transducer Calibration

PRESSURE TRANSDUCER CALIBRATION

Calibration date : 11-Feb-85
Type : DPI 500
Serial No. : 5001

Pressure (kPa)	Readings (mV)	Error (kPa)*
0.00	0.00	0.00
9.99	99.80	-0.01
19.99	199.46	-0.04
29.99	299.53	-0.03
39.99	399.53	-0.03
49.98	499.86	0.00
59.98	599.73	-0.00
69.98	700.07	0.02
79.98	800.13	0.03
89.97	900.13	0.04
99.97	1000.14	0.04
109.97	1100.40	0.07
119.97	1200.47	0.08
129.96	1300.47	0.08
139.96	1400.47	0.09
149.96	1500.20	0.06
159.96	1599.87	0.03
169.95	1699.61	0.01
179.95	1799.14	-0.02
189.95	1898.54	-0.08
199.95	1997.94	-0.14

Slope = 9.9992 mV/kPa
Correlation coefficient = 0.9999
Amplifier gain range 8

* Error calculated using calibration readings and derived value of slope.

Stability Check
Mean = -0.00 : Values range from -0.02 to 0.00

Reading Check

Target (kPa)	Reading (kPa)
99.97	100.02

Table 7.2 Pressure Transducer Calibration

INSTRON EXTENSOMETER CALIBRATION

Calibration date : 17-Jun-85
Type : 2620-603
Serial No. : 118
Code Colour : Green

Extension(mm)	Readings (mV)	Error (mm)*
-0.10	-1027.15	0.00
-0.09	-928.65	0.00
-0.08	-828.19	0.00
-0.07	-727.25	0.00
-0.06	-629.12	0.00
-0.05	-528.49	0.00
-0.04	-428.56	0.00
-0.03	-326.99	0.00
-0.02	-266.96	0.00
-0.01	-126.33	0.00
0.00	-26.39	0.00
0.01	73.06	-0.00
0.02	171.76	-0.00
0.03	270.79	-0.00
0.04	372.76	-0.00
0.05	471.69	-0.00
0.06	572.46	-0.00
0.07	671.19	-0.00
0.08	771.89	-0.00
0.09	870.42	-0.00
0.10	968.95	-0.00

Slope = 9993.3400 mV/mm
Correlation coefficient = 0.9999
Amplifier gain range 6

* Error calculated using calibration readings and derived value of slope.

Stability Check
Mean = 0.00 : Values range from 0.00 to 0.00

Table 7.3 Instron Extensometer Calibration

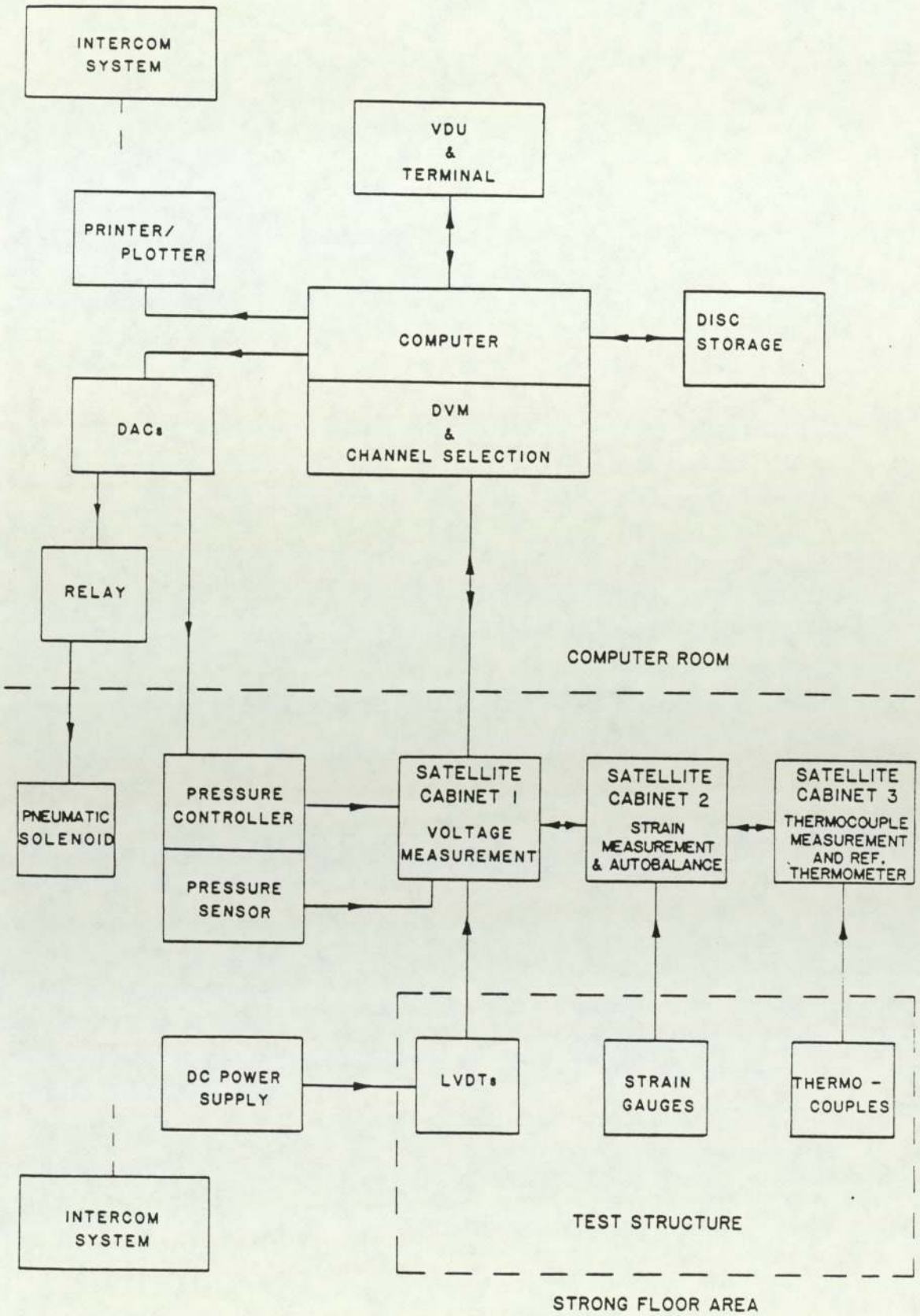

Fig. 7.3 Schematic diagram of computer controlled data acquisition and control system

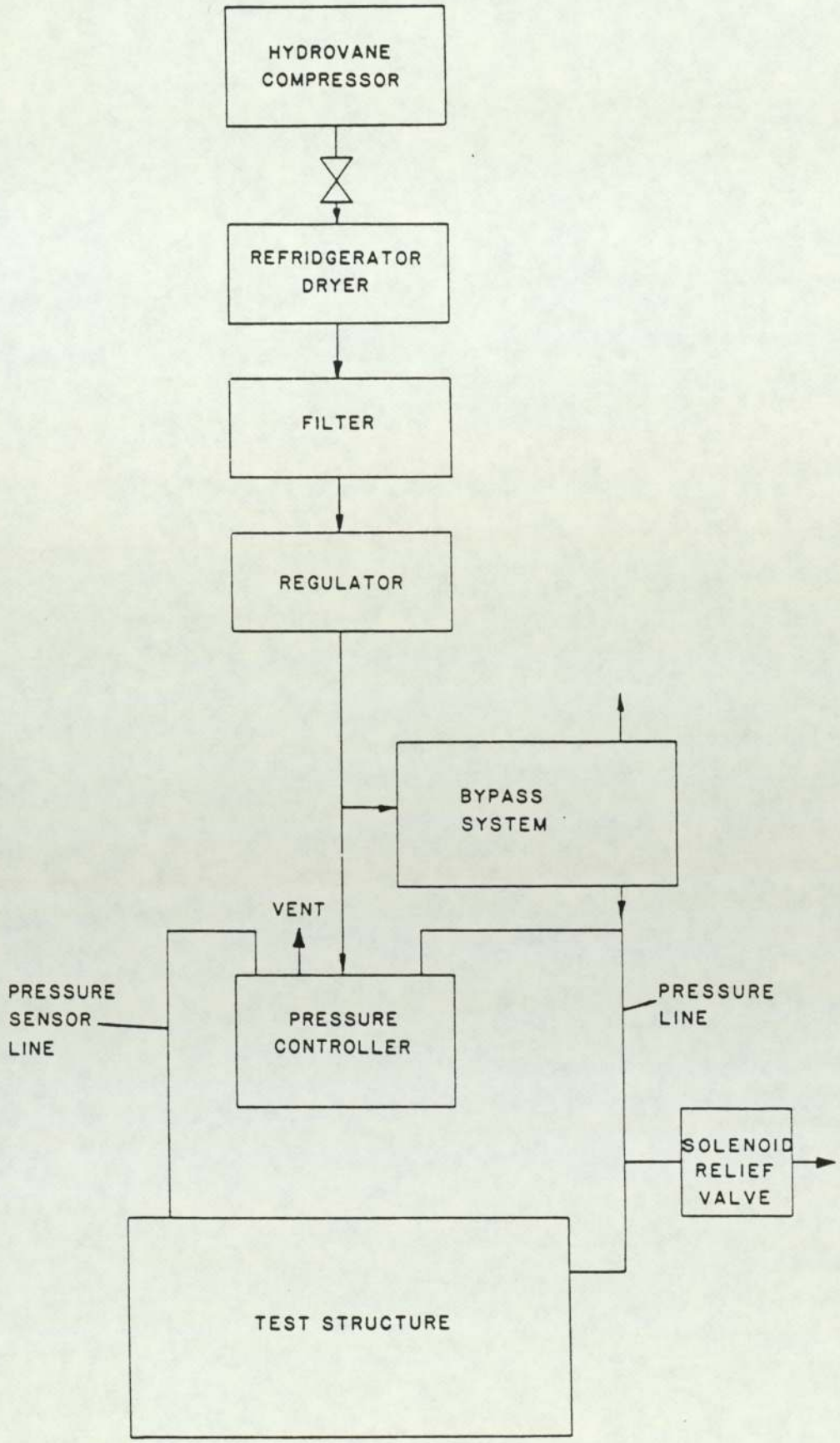

Fig. 7.4 Schematic diagram of pneumatic loading system (Positive pressure)

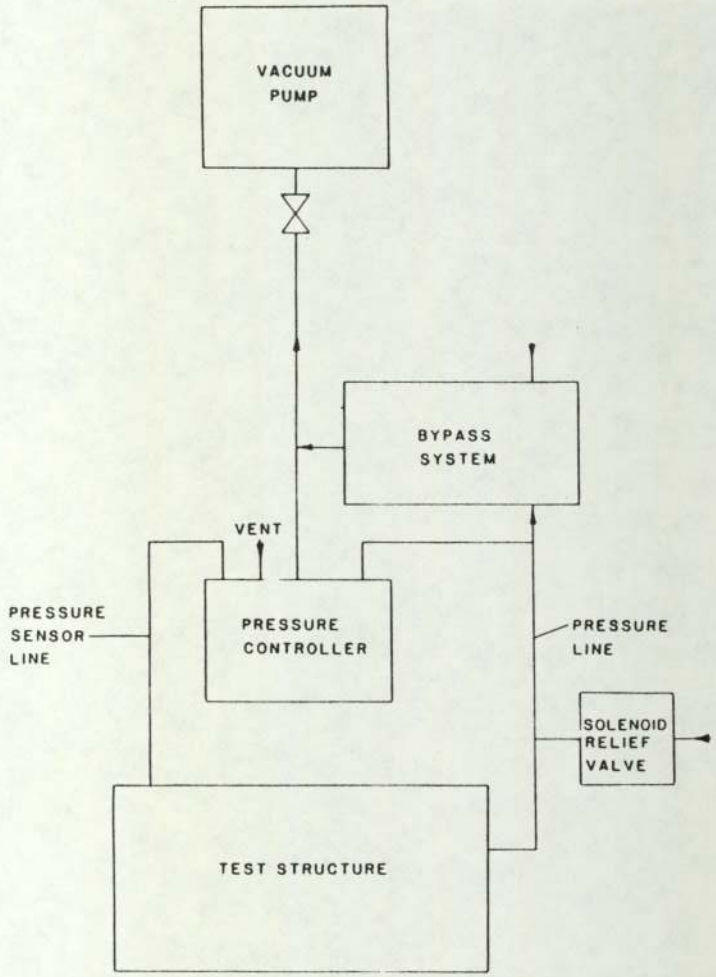

Fig. 7.5 Schematic diagram of pneumatic loading system (Negative pressure)

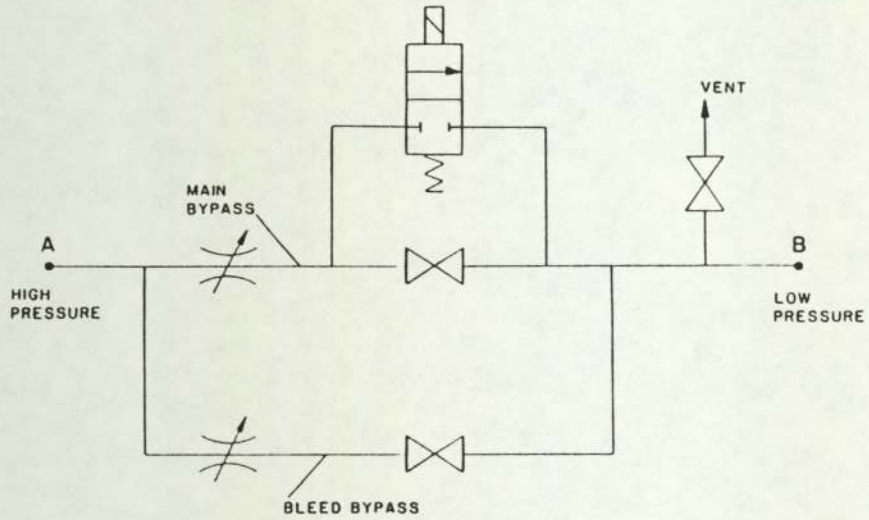

POSITIVE PRESSURE TESTS — A = PRESSURE LINE; B = TEST RIG

NEGATIVE PRESSURE TESTS — A = TEST RIG; B = VACUUM LINE

Fig. 7.6 Schematic diagram of pneumatic bypass system (Positive & negative pressure)

CHAPTER 8

EXPERIMENTAL DETERMINATION OF MATERIAL PROPERTIES

8.1 Introduction

In order to ensure that as far as was possible material samples for the various mechanical tests were truly representative of the lay up and properties of the main test panels, all of the specimens whose testing is described here were cut from the main panels. The panels were manufactured oversize to allow for this.

For the aluminium test specimens, strips of material were cut from the edges of the panel in its two principal directions prior to the panel being formed into its cylindrical shape. These strips were then annealed with the main panel and suitable tensile test specimens were then cut from the strips. This procedure was obviously not possible with the GRP panels since these were of course laid up in cylindrical form.

In order to obtain flat specimens of GRP from the cylindrical panels the mould used to lay up the panels was extended tangentially so that a flat extension piece of identical laminate could be laid up with each main panel. After curing the extension pieces were cut from the panels and then cut into individual material test specimens as shown in Figure 8.1(a). The whole panels including tangential extensions were laid up 50 mm oversize all round to eliminate immediate edge effects.

In order to ensure that the panels were laid up uniformly and that unrepresentative care was not taken in the region of the test specimens the panel manufacturers were not informed that the tangential extensions were required for material testing purposes.

8.2 Cutting of test specimens

The main mechanical tests performed on the material were tensile tests in the two principal material directions and the anticlastic bending of square plate specimens. The cutting regime shown in Figure 8.1(b) resulted in two square specimens from each panel, suitable for the anticlastic bending tests, together with a number of tensile specimens in each of the two principal material directions. The remaining material was available for minor tests and for spare specimens as required. Specimens were cut using a band saw and were not machined further. The cutting plan shown was designed to take specimens from different areas of the available material, tensile specimens for testing were selected from those specimens cut, so that adjacent specimens were not used.

Three GRP panels were produced for this study; these are described later in Chapter 10 For the purposes of material testing however, the three panels were identical except for thickness. Test specimens were cut from each panel as described above.

8.3 Tensile testing

Tests were carried out on 6 tensile specimens from each GRP panel, 3 specimens from each principal panel direction (x longitudinal and ϕ tangential). Three tensile tests were performed on each specimen making a total of 54 tests in all.

All tensile specimens were the same length (330 mm) but because they had been saw cut, the width of specimens was subject to some variation. Also the thickness of specimens varied both between and within panels. Specimen details are shown in Figure 8.2 and specimen dimensions and numbering system in Table 8.1. Specimen cross section dimensions were measured with a micrometer at several

points for each specimen and the values given in the table are mean figures. It should be noted at this stage that since the test panels were laid up against a mould, one face of panel was smooth and one rough. For the purposes of material testing the smooth surface is referred to here as the front face of a specimen and the rough surface as the back face. Note that the smooth surface was produced by contact with the smooth surface of the mould only. No gel-coat was used.

8.3.1 Loop Shaping

All tensile tests were carried out under load control using the Instron testing machine. Since the specimen under test forms an integral part of the load chain of the machine it is necessary before testing commences to set up appropriate shaping parameters for the control loop. The method of loop shaping is not of interest here but the loop shaping parameters are dependent on the stiffness of the specimen. To achieve best control performance loop shaping should therefore be done with a specimen identical to the one under test; using the test specimen itself for loop shaping is not desirable since the procedure is quite vigorous and the specimen might be damaged. To overcome this difficulty loop shaping was carried out on spare GRP specimens taken from the same panel and the same direction as subsequent test specimens. After each series of 9 tests (one panel in one direction) the control loop was reshaped.

8.3.2 Specimen preparation

Each test specimen was marked as shown in Figure 8.2(a) for extensometer positions and for test machine jaw positions. For each test 4 extensometers were fixed to the

specimen using cyanoacrylate adhesive.

The front surfaces of the specimens (smooth) were prepared by very light sanding with 400 grit abrasive paper to remove any residual mould release agent and to key the surface. Thin lines of adhesive were placed along the marked gauge lines and the knife edges of the extensometers were painted with adhesive catalyst. The extensometers were then placed in contact with the specimen and held in position until bonded. Great care was taken to ensure that the knife edges were fixed parallel to the gauge lines.

The rough back surfaces of the specimens did not form a suitable base for extensometer bonding. In order to provide a suitable base for the extensometers it was found necessary to make shallow grooves in the specimen using the blade of a hacksaw. These grooves were very shallow, just deep enough to provide a firm base for bonding of the extensometers. The arrangement is shown diagrammatically in Figure 8.2(b).

8.3.3 Test Parameters

All tests were done using the Instron 'Block' program. This allows the test parameters to be set in a series of blocks which are executed sequentially under either manual or automatic control. Each block has its own control parameters which are set prior to the test. 4 blocks were used for all of the tensile tests on the GRP specimens, these were:

Block 1 : Sine wave input

Mean level 0.0 kN

Amplitude 0.01 kN

Trigger manual

This is a holding block which has the effect of holding the specimen at zero load with the control system active. The small amplitude of load gives stability to the system. The manual trigger moves the program to the next block.

Block 2 : Ramp input

Start level 0.0 kN

Finish level 3.0 kN

Ramp rate 0.05 kN/s

Trigger automatic

This is the loading block. The specimen is loaded to 3.0 kN in a ramp fashion with the loading taking one minute to complete. At full load the control switches automatically to the next block.

Block 3 : Ramp input

Start level 3.0 kN

Finish level 0.0 kN

Ramp rate -0.05 kN/s

Trigger automatic

This block unloads the specimen at the same ramp rate as the loading.

Block 4 : Sine wave input

Mean level 0.0 kN

Amplitude 0.01 kN

Trigger manual

This is a second holding block identical to Block 1. This ensures nominal zero load when the jaws are opened and the test ended.

8.3.4 Testing

Each specimen, with extensometers attached, was placed in the hydraulic jaws of the testing machine. The hydraulic jaw pressure had been previously set to give a pressure on the specimen low enough to avoid matrix crushing yet sufficient to prevent slip. The specimen was carefully aligned to ensure that the axis of the specimen was parallel to the axis of the load chain.

When positioning was complete the extensometer safety pins were removed and the extensometers were zeroed. The load cell was zeroed and calibrated using the self-calibrate routine.

The load chain was then closed and the block program started. At this stage some pre-load was usually apparent due to the gripping action on an imperfectly smooth specimen. The sine wave input of block one stabilised this pre-load but would not remove it completely. If this pre-load exceeded 0.1 kN then the setting up procedure was repeated which because the specimen was released and regripped normally reduced the pre-load. Pre-loads of less than 0.1 kN (3% of maximum load) were considered acceptable and once a stable condition was achieved block 2 of the program was triggered and logging initiated. The logging procedure has been described fully in Chapter 7. Control of blocks 2 and 3 (loading and unloading) was then automatic and as soon as the program switched to block 4 logging was halted, the top set of jaws were opened and the test ended.

8.3.5 Processing of tensile test results

On completion of each tensile test the logged data was plotted as load against axial extension, load against transverse extension and as axial extension against transverse extension. The plotting was done automatically using all of the logged data and without any curve fitting so that in each case the plotted line passed through every point logged. A single example of the resulting graphs is shown in Figure 8.3(a, b and c). These plotted results were then examined for any irregularities or non-linearities which might have had influence on the calculation of either Young's modulus or Poisson's ratio. In general the plots showed good linearity, a minimum of hysteresis and few irregularities. See Figure 8.3.

The final processing of the test results to give values of Young's modulus and Poisson's ratio was done from the original data using a least squares regression routine between 10% and 60% of full load as described in Chapter 7 and based on cross sectional areas of the specimens as measured. Specimen results are shown for panel GRP 2 in Table 8.2. The results for the aluminium panel exhibited very little variation between specimens and no detectable anisotropy. Using the same test parameters and as used for the GRP the mean values for the aluminium samples were:

Young's Modulus $E = 74.7\ GN/m^2$

Poisson's Ratio $\nu = 0.31$

These values based on testing one sample from each principal panel direction three times are sufficiently close to

standard values for aluminium for their accuracy to be accepted.

The values calculated for the GRP specimens however cannot be accepted as representative of the GRP panels with the same confidence. Examination of the results for the GRP specimens shows a considerable spread of values for both Young's Modulus and Poisson's Ratio, but it can be clearly seen that the spread of values for tests on a single sample is considerably less than the spread of values between samples. This is the result that would be expected assuming the test method to be consistent but the material to be variable. Close examination reveals that the values obtained here for a single sample show a typical spread of 2% and a maximum spread of 4%. This indicates that the test procedure is consistent and that these values are thus likely to be accurate and representative of the particular specimens. It is of course essential to show that the specimens themselves were representative of the full panels from which they were cut.

Panels were laid up with a clearly defined number of layers of rovings and mat of specified weight. Under these conditions it is reasonable to assume that variations within a panel are mainly due to distribution of resin. Resin makes a relatively small (approx 10%) contribution to the in-plane stiffness of the panel but is the major cause of thickness variation. Small test coupons cut from a typical panel may therefore show marked thickness variation due to resin variation without marked change of stiffness. To allow for this effect all GRP moduli were

recalculated on the basis of new cross sectional areas on the assumption of all samples being the same thickness and this thickness being the mean thickness for the whole panel. This procedure results generally in only slight changes to mean values but the standard deviation of results is reduced. This would seem to be a reasonable compromise between acceptance of original values based on measured cross-sections and more sophisticated correction procedures based on relative contributions to stiffness from fibres and matrix. Adoption of the later approach would obscure the experimental nature of the test results to an unacceptable degree. The adopted procedure is illustrated for panel GRP 2 in Tables 8.3 and 8.4.

8.3.6 Poisson's Ratio

Since tensile tests were carried out in the two principal material directions and with both longitudinal and lateral strain being measured for each test, the result is for each panel two values of Young's Modulus and two values of Poisson's ratio. Inevitably the simple mean values result in 4 values which violate the reciprocity relationship:

$$E_x \nu_{\phi x} = E_\phi \nu_{x\phi}$$

In an attempt to obtain the most representative values for each panel values were obtained for complementary Poisson's ratio based on each of the mean experimental values for each panel. These values are given in Table 8.5. For the purposes of subsequent analysis the values selected were those based on the mean experimental value of $\nu_{\phi x}$.

8.4 Anticlastic Bending Tests

The anticlastic bending test for the determination of in-plane shear modulus for laminated materials was discussed briefly in Chapter 6. The essential feature of the test is that a square specimen of laminate is loaded at its 4 corners and so deflected into an anticlastic shape. In-plane shear modulus may then be calculated from measured corner deflections and knowledge of specimen dimensions.

8.4.1 Anticlastic bending test rig

To apply this test to the sonar dome laminate a special test rig illustrated in Figure 8.4 was developed. This rig was designed to give three point support to a square test specimen and to allow the fourth corner to be loaded either with dead weight or by universal testing machine. The three support points are steel balls 36 mm diameter. The whole arrangement is equipped with levelling screws and axis tilt facility and is adjustable to take panels up to side length 1.2 m and down to side length 150 mm. Measurement of deflections is by LVDTs as described in Chapter 7.

8.4.2 Validation of the anticlastic test method

Development of the test rig and validation of the test method has been reported elsewhere [84] and [85] and is not detailed here. Essentially the method used was applied to both isotropic (aluminium) and orthotropic (sonar laminate) specimens of various dimensions and the results compared for the isotropic samples with the known shear modulus from tensile testing. These comparisons demonstrated the method to be accurate within approximately ±5% provided that:

1. The plate thickness is accurately known.

2. The deflections are less than 0.5 x plate thickness.

3. The specimen side length/thickness ratio is in a range of approximately 20 to 60.

At high length to thickness ratio synclastic bending became a problem and at very low ratios errors due to inapplicability of the thin plate theory became apparent. The first of these effects, synclastic bending, represents a total cut off point for the method; if this type of behaviour occurs then no useful information can be obtained from the test. The second effect is a limit less easy to define since the results become simply less accurate as the test panel becomes smaller for any given thickness.

For this investigation all of the anticlastic samples were 330 mm square which with the variation of thickness between the panels gives a range of side/thickness ratios from 24 to 48. This is well within the acceptable range.

Although the highest value of this ratio (48) is well below the value at which synclastic bending has been observed for similar specimens it was considered prudent to monitor bending mode during the tests to confirm that anticlastic bending was taking place. All of the panels tested deformed anticlastically.

8.4.3 Testing Procedure

Panel preparation. Before testing, the thickness of each panel was determined from a mean of 36 thickness readings taken by ultrasonic thickness gauge.

The procedure used for this thickness measurement is described in Chapter 10 with reference to the large cylindrical test panels; the procedure used for the anticlastic samples was identical with this.

Testing. Each panel was inserted into the test rig supported at three corner points with the fourth corner point free for loading. LVDTs were arranged along the diagonals of the panels to monitor bending mode. Since the resolution of the LVDTs was no greater than 0.02 mm the deflection of the loaded corner was monitored using a dial gauge to improve accuracy. Loading at the free corner was applied by dead weight using a weight hangar and this too was manually logged.

Each panel was tested four times. After completion of the first test the panel was removed from the rig and reinserted with load and support diagonals interchanged. It was then re-tested. The third and fourth tests on each panel were conducted as for the first two but with the panel inserted in the test rig so that the load direction was effectively reversed.

In each test the load on the free corner was increased in increments and the load and corner deflection manually logged. At each increment the LVDTs were logged electronically. Load increments were selected for each panel such that maximum deflection of the loaded corner did not exceed 20% of the specimen thickness.

Processing of Results. For each test a load deflection curve was plotted and examined for anomalies. No detectable non-linearity was found for the small deflections used on any of the samples tested (example Figure 8.5). The diagonal deflections as measured by the LVDTs were also plotted as a check of anticlastic behaviour (example Figure 8.6). The slopes of the load deflection graphs were then found using a least squares regression routine as described in Chapter 7 and the shear moduli calculated using Equation 6.11. The results of the tests are given in Table 8.6 which gives the mean results for each main panel as well as for each sample and for each test. These results show only a minimum of scatter for each specimen quite within acceptable limits.

8.5 Summary of In Plane Elastic Properties

A summary of in-plane elastic properties as measured from the preceeding tests is given in Table 8.7.

This table gives orthotropic properties as measured together with mean values of the major constants as isotropic properties. These 'Isotropic' properties are given for comparison only.

8.6 Balanced rail shear test

This modification of the rail shear test was discussed briefly in Chapter 6. It is used here as a comparative test between through-plane and in-plane shear moduli.

8.6.1 Test rig and specimen preparation

The test rig for this test is shown in Figure 8.7. Two cubic samples of the test material are subjected to a state of simple shear between steel rails bonded to the specimens. Loading is provided by dead weight and strain is measured by strain gauges of very short gauge length.

Specimens were prepared from the intermediate thickness GRP panel (GRP 2). These specimens were cut from the spare test material and were then machined to accurate cubes of 10 mm side. 6 cubes were prepared in this way for testing in 3 pairs, one pair for each of the shear directions. Samples were carefully marked and kept in pairs to avoid any confusion.

The samples were then strain gauged using Techn-measure FCA-2-11 strain gauges of 2 mm gauge length. These are two gauge rosettes of 120 Ω gauges of gauge factor 2.08. The gauges were aligned with the diagonals of the cubes on the appropriate faces for each pair of samples.

Each pair of samples were then bonded to the shear arms of the test rig and the gauges connected to connector tabs on the central shear arm. Epoxy adhesive was used for this bonding in preference to cyanoacrylate. The gap filling properties of the resin adhesive ensured that good contact was obtained between specimens and shear arms. Since gauges were fitted to only one side of each specimen cube, correct alignment of the double cube/shear arm assembly was most important.

This alignment was achieved with the aid of a special jig and was aided by the use of a slow setting epoxy. The completed arrangement is shown in Figure 8.8. The gauges were connected in a half bridge network with each cube of the pair separately logged.

When the specimen assembly was completely set it was assembled into the test rig and carefully levelled so that the dead weight loading would provide an in-line pull. For each test weights were added to the weight hanger, and when all swinging had stopped the strain gauges were logged. The calibration and autobalance routines were as described in Chapter 7. Weights were added in steps of 1 kg up to 10 kg in each case. Each pair of specimen cubes were tested several times with strain logged during loading and unloading.

8.6.2 Processing of results

Graphs of shear strain against load were plotted for each test and for each block of each pair. Example graph Figure 8.9. Slopes of these graphs were then used to obtain shear modulus for each test. The results of these tests are given in Table 8.8.

8.7 Determination of fibre fraction

The mechanical properties of any composite are clearly influenced by the relative proportions of reinforcement and matrix. In principle the overall proportions of each constituent should be relatively easy to control even with an unsophisticated hand lay up procedure. Weight of reinforcement can be accurately determined before lay up either directly or from number of layers of known weight.

Wetting out of reinforcement can then be done with pre-weighed quantities of resin for each lamination. Unfortunately determination of fibre fraction for a cured laminate is more difficult and the only methods available are destructive ones. The two most common procedures are acid digestion, where the resin is removed by a concentrated nitric acid solution, and ashing where the resin is removed by burning. The method detailed here is ashing. This method is both quicker and safer than acid digestion methods for polyester resin. This method results in a mass fraction of glass fibres. This is then converted into the more commonly quoted volume fraction on the basis of the known densities of the two materials. Unfortunately it is not possible to take account of any voids present in the laminate but microscopic examination of the samples prior to ashing gave an estimated void content of less than 1%.

8.7.1 Ashing Method

9 specimens were tested, 3 from each of the three panels. Specimens were of roughly rectangular shape 40 mm x 20 mm x panel thickness. Each specimen was placed in a ceramic crucible and weighed. The crucibles were then heated at 50°C for several hours to drive off any residual moisture either in the specimens or in the crucibles. They were successively weighed until no change was apparent between weighings. In fact no change at all was detected indicating negligible initial moisture content. The crucibles were then heated with a naked flame until the resin ignited and as much as possible of the resin was burnt away. This was done under a fume hood. The crucibles were then placed in a muffle furnace at 625°C to complete the burning of the resin.

Had sufficient fume extraction been available in the furnace then the initial naked flame burning could have been avoided.

The crucibles were periodically removed from the furnace, cooled and reweighed until no further weight change took place. At this stage the final weights were noted and the mass fraction of each specimen was calculated. Volume fraction was also calculated based on:

SG. E Glass	2.54
SG. Cured resin	1.20

The results of this testing are summarised in Table 8.9.

It should be noted that this ashing technique leaves the glass reinforcement quite clean and intact so that it is possible to destack the laminations both to count them and to examine fibre orientation, see Figure 8.10.

8.8 Tensile Strength Testing

All of the mechanical tests described so far in this chapter have been tests for elastic properties rather than strength. This results from the need to reconcile predicted and measured deflection behaviour of sonar domes before ultimate strength can be confidently predicted. Failure criterion for composites both in terms of what exactly constitutes failure, and in terms of what degree of damage or degradation is acceptable is a complex area in itself and is outside the scope of this work. Nevertheless this work is concerned with the measurement and prediction of strains in composites, and in order to put these strains into perspective, some knowledge of the strength of the material is required.

A number of tensile tests to destruction were undertaken using the tensile specimens that had previously been used for the determination of the moduli.

One specimen was selected from each panel and in each principal panel direction giving six specimens in all.

8.8.1 Test Method

Each specimen was tested in the Instron test machine under position control using a single ramp input from start position to start position + 20 mm at a ramp rate of 0.01 mm/s. Actuator position and load were logged during the test at 4 second intervals using the C2 computer. This interval was chosen to meet the system limitation of 250 data loggings/ test. Load was monitored continuously and a note was made of load at first audible noise from the specimen. In addition acoustic emissions from the specimen were monitored using a AECL acoustic emission system with two sensors (175 kHz and 375 kHz) attached to the specimen.

Graphs of load/extension and acoustic emission/ extension were plotted for each specimen. An example is given in Figure 8.11. The acoustic emission plot should be regarded as a qualitative measure of cumulative damage only. A summary of the tensile strength testing is given in Table 8.10.

8.9 Accuracy of the material test results and concluding remarks

Clearly with a material as variable in quality as hand lay up GRP it is impossible to be completely certain of overall material properties from the results of tests on a relatively small number of samples.

The tests described in this chapter were made with fully calibrated instrumentation and using test procedures designed to eliminate known sources of error. All of the procedures have been proved consistent.

For repeated tests on individual samples the spread of results for the elastic constants E, G and ν is approximately ± 2%. The maximum spread of results for these constants between samples cut from any one panel is approximately ± 10%. This represents a measure of the variable quality of the material. It is likely that the total spread of these properties within any panel will be greater than this but this will be due in the main to small local variations. It is reasonable to assume that the mean properties given in Table 8.5 are representative of the whole panels to within ± 10% and probably to within ± 5%.

The balanced rail shear tests for through-plane shear moduli may be subject to absolute errors of ± 10% or more due to the nature of the method but the results are quite consistent. Such errors do not influence the conclusion drawn from these tests that the values of transverse shear moduli are approximately 50% of that of the in-plane shear modulus for this material.

The ashing test to determine fibre fraction is a very simple test and is subject only to errors in weighing of samples for mass fraction and to neglect of voids in calculation of volume fraction.

Assumed accuracy of this test is ± 1% for mass fraction and ± 5% for volume fraction.

Overall the test results obtained here are consistent and are considered to give a representation of the material properties of each of the GRP panels sufficiently accurate for structural analysis purposes.

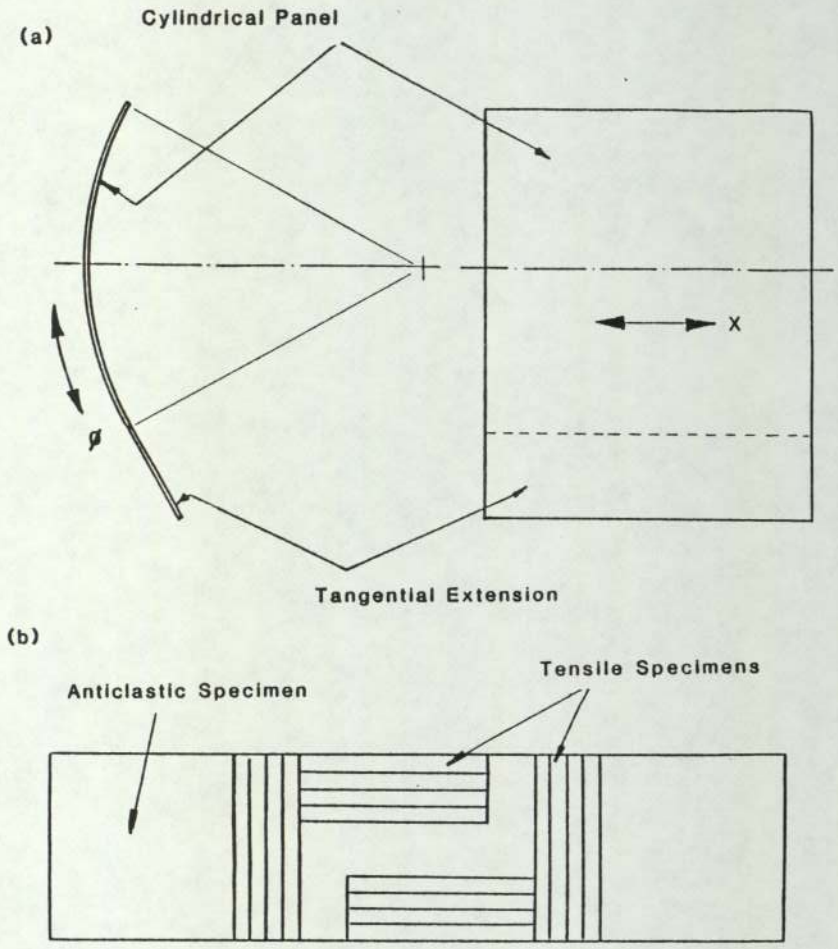

Fig. 8.1 a) Cylindrical panel showing tangential extension piece.
b) Material test specimen cutting regime.

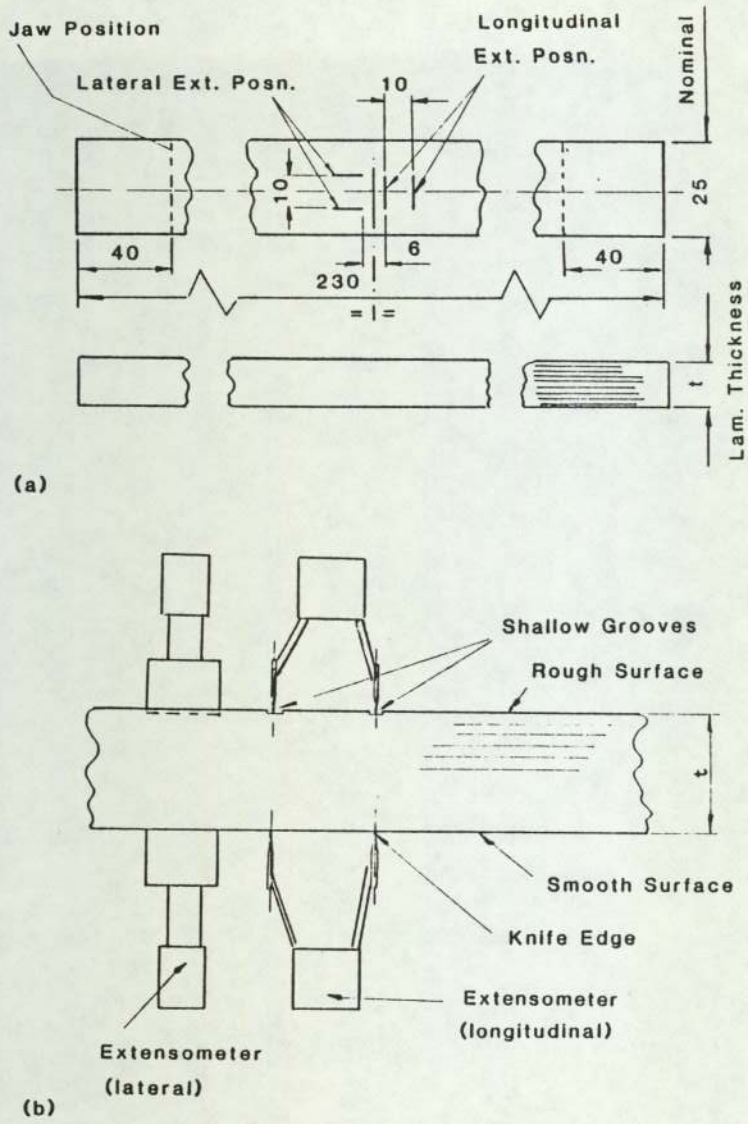

Fig. 8.2 a) Dimensions of tensile test specimen with gauge markings.
b) Details of extensometer fixings.

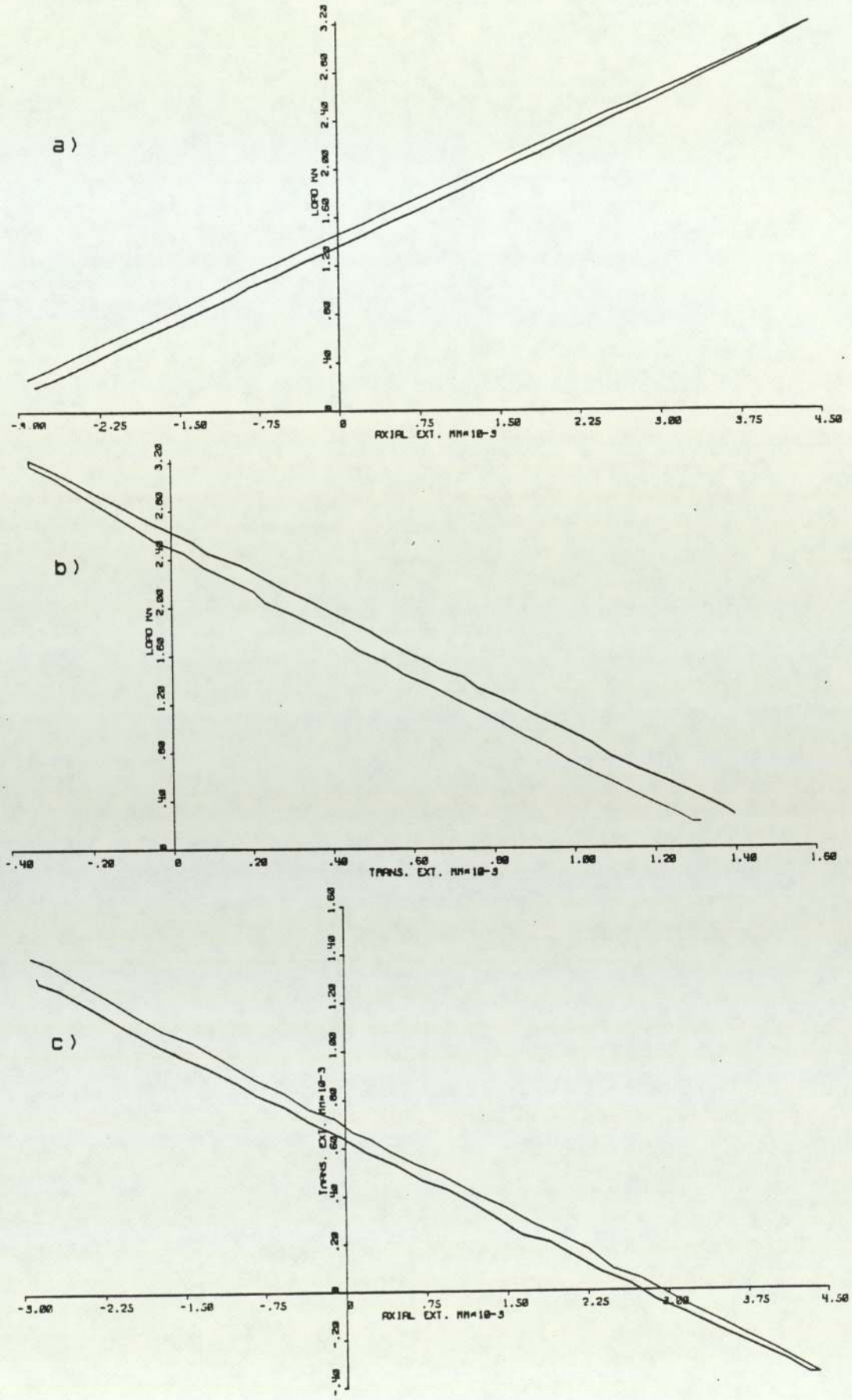

Fig. 8.3 Graphical example of tensile test results showing material linearity and hysteresis.
a) Load / axial extension
b) Load / transverse extension
c) Transverse extension / axial extension

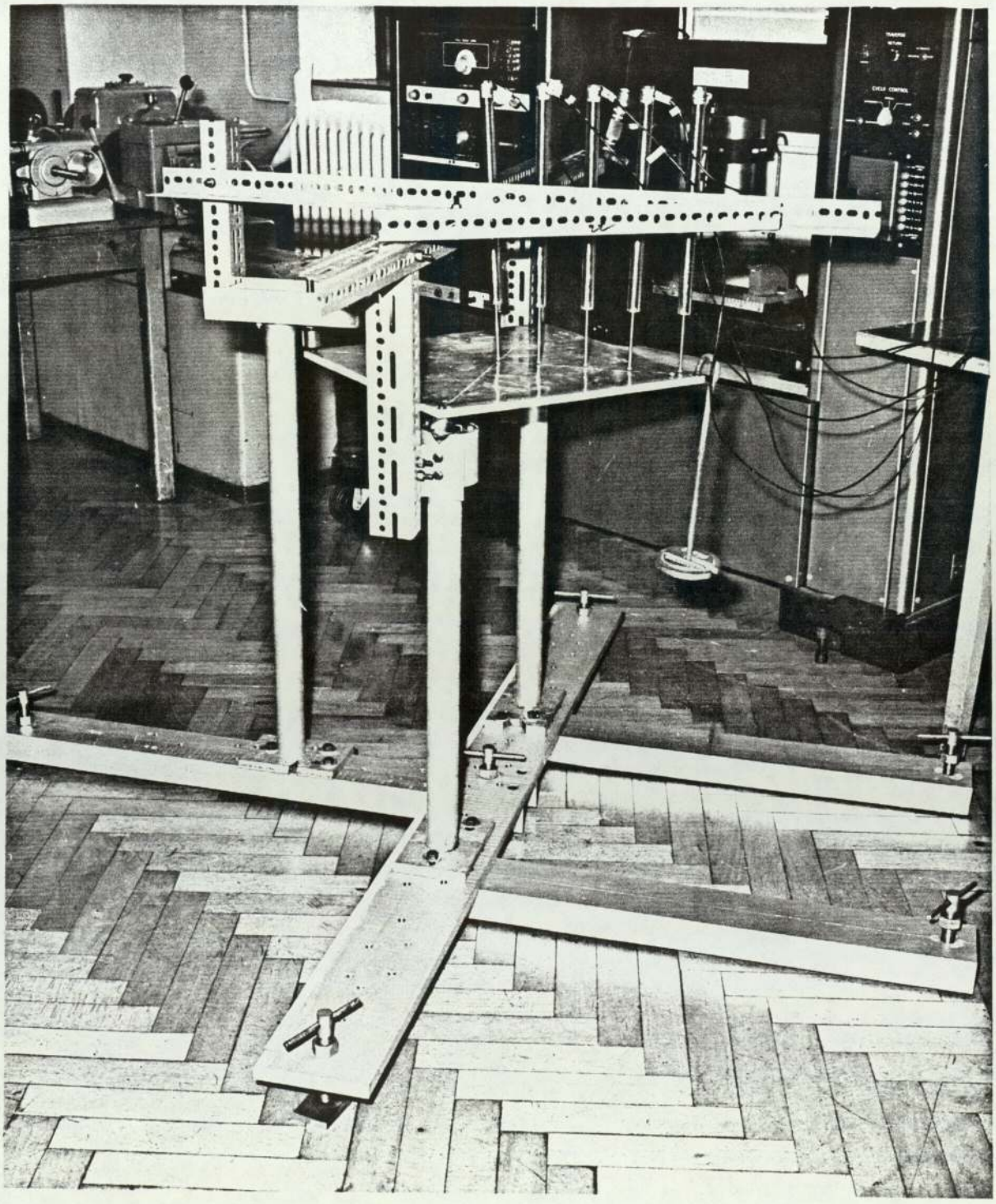

Fig. 8.4 Test rig for anticlastic bending tests.

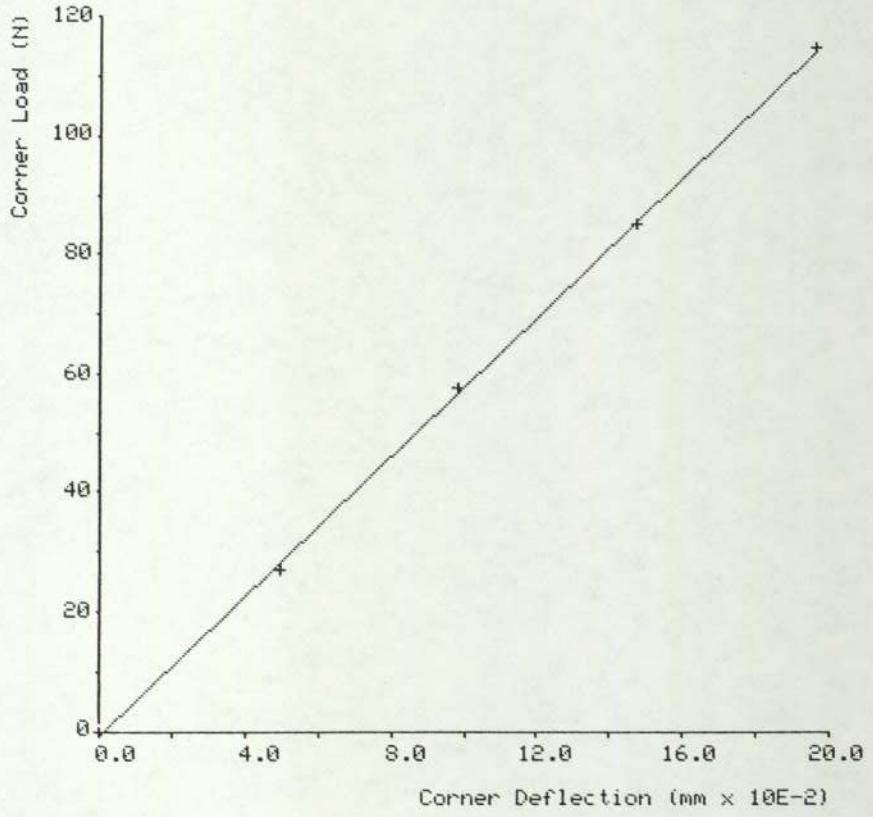

Fig. 8.5 Example of a corner load / deflection plot for an anticlastic bending test.

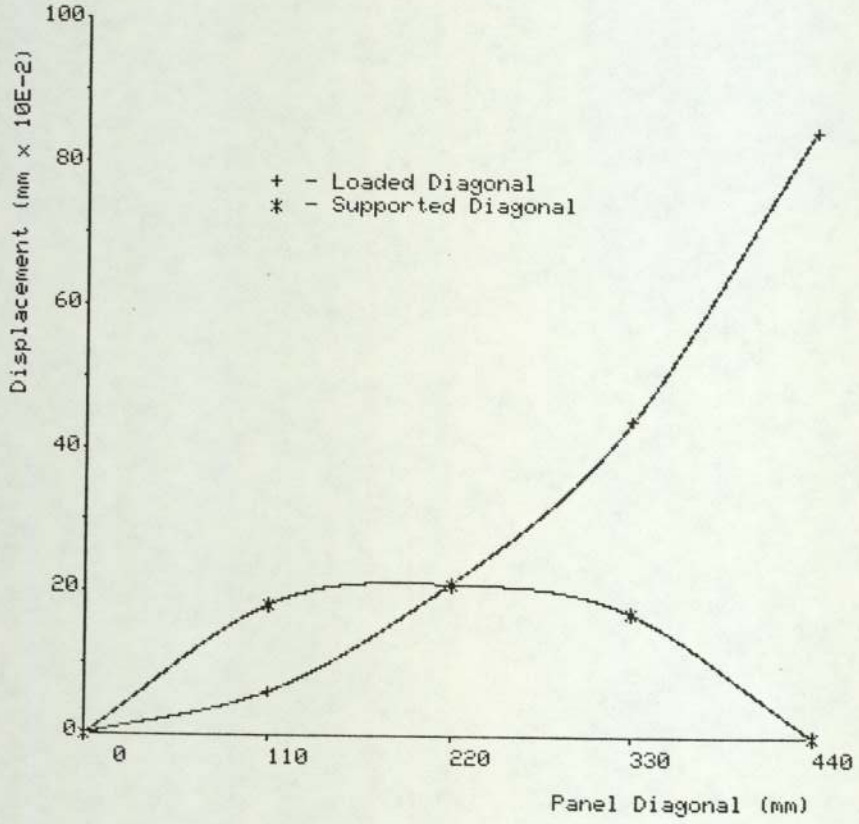

Fig. 8.6 Example plot of deflection along the loaded and supported diagonal of a test panel showing anticlastic curvature.

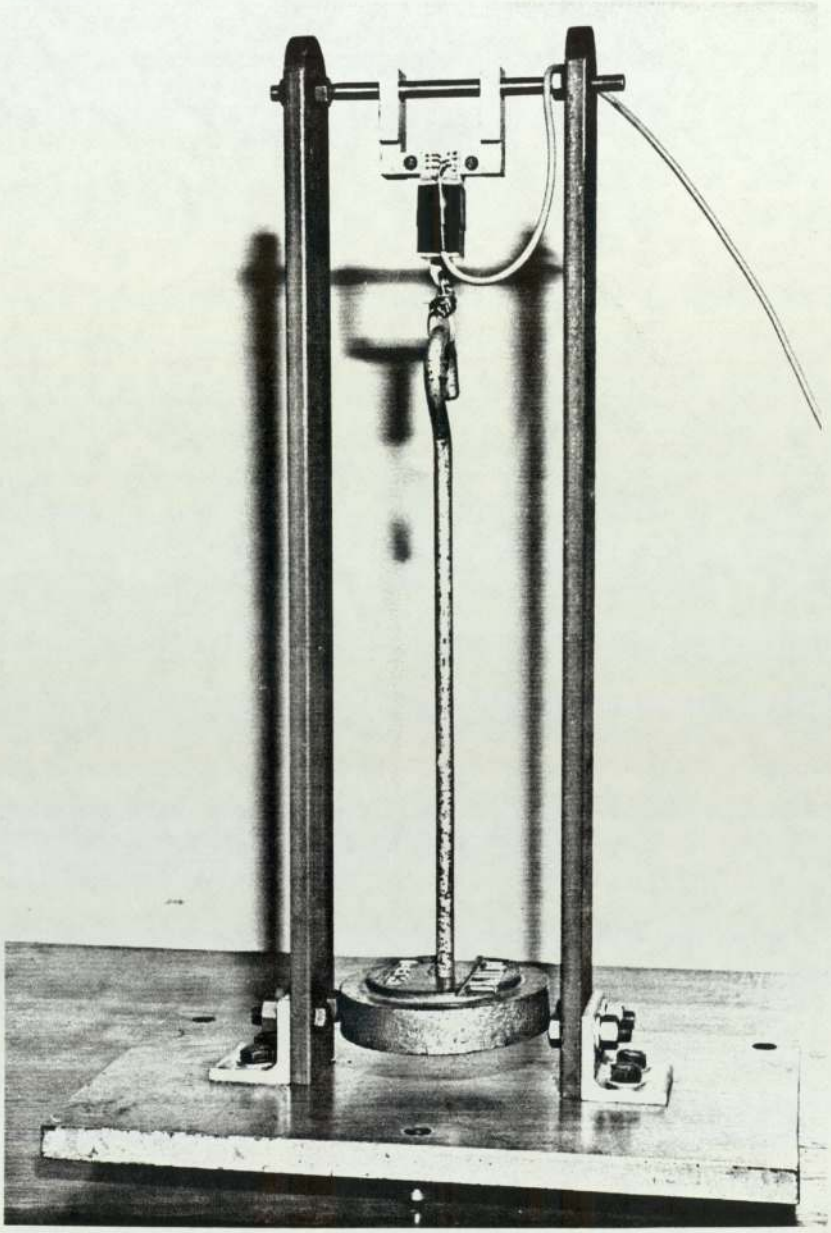

Fig. 8.7 Test rig for balanced rail shear test (through plane shear modulus measurement)

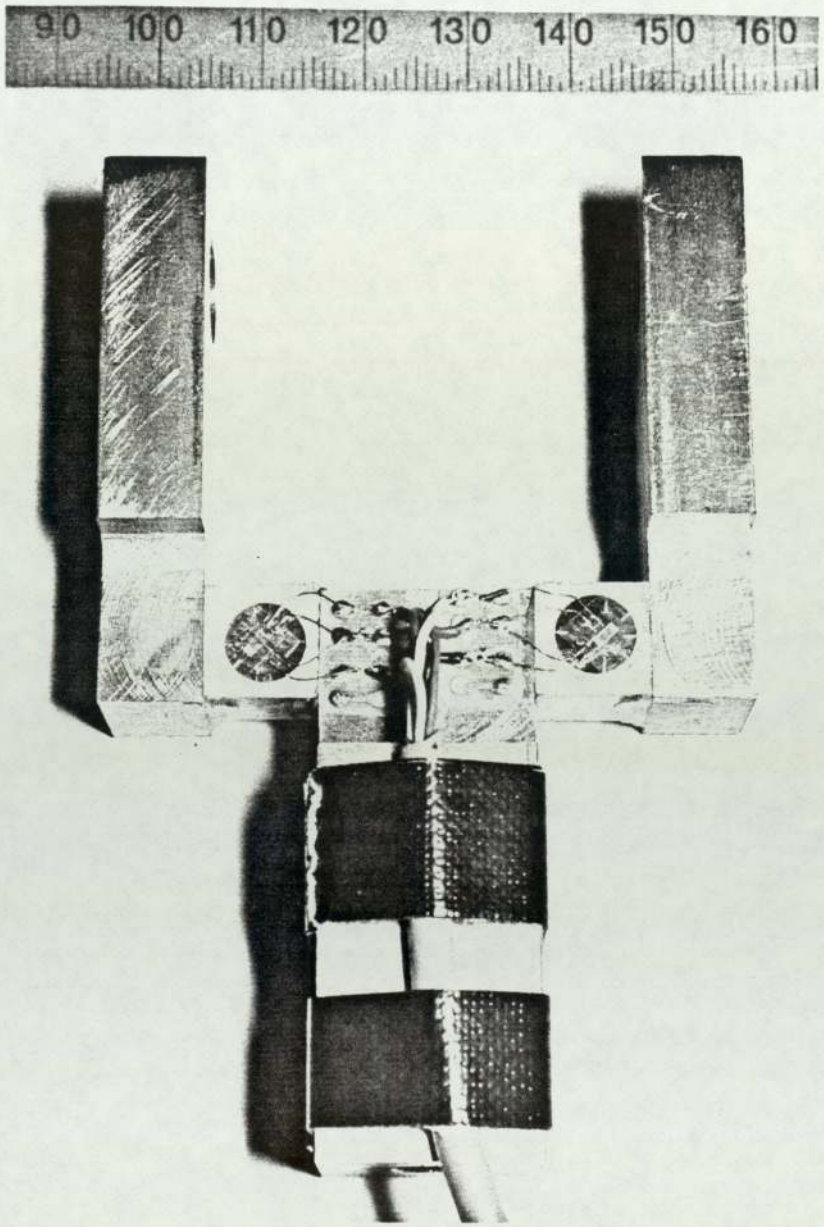

Fig. 8.8 Through plane shear samples strain gauged and bonded to shear arms prior to balanced rail shear test.

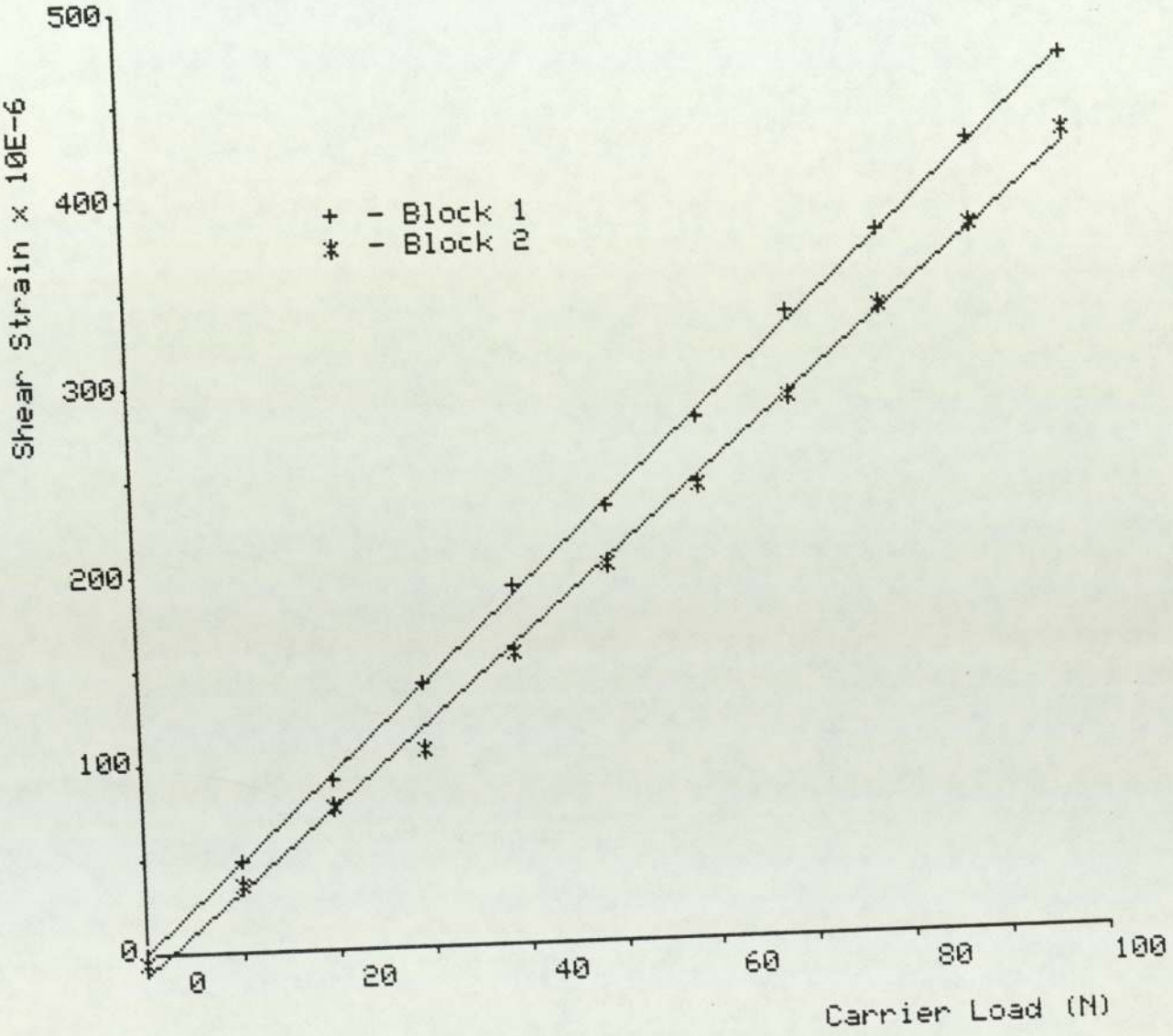

Fig. 8.9 Example plot of shear strain / carrier load for balanced rail shear test.

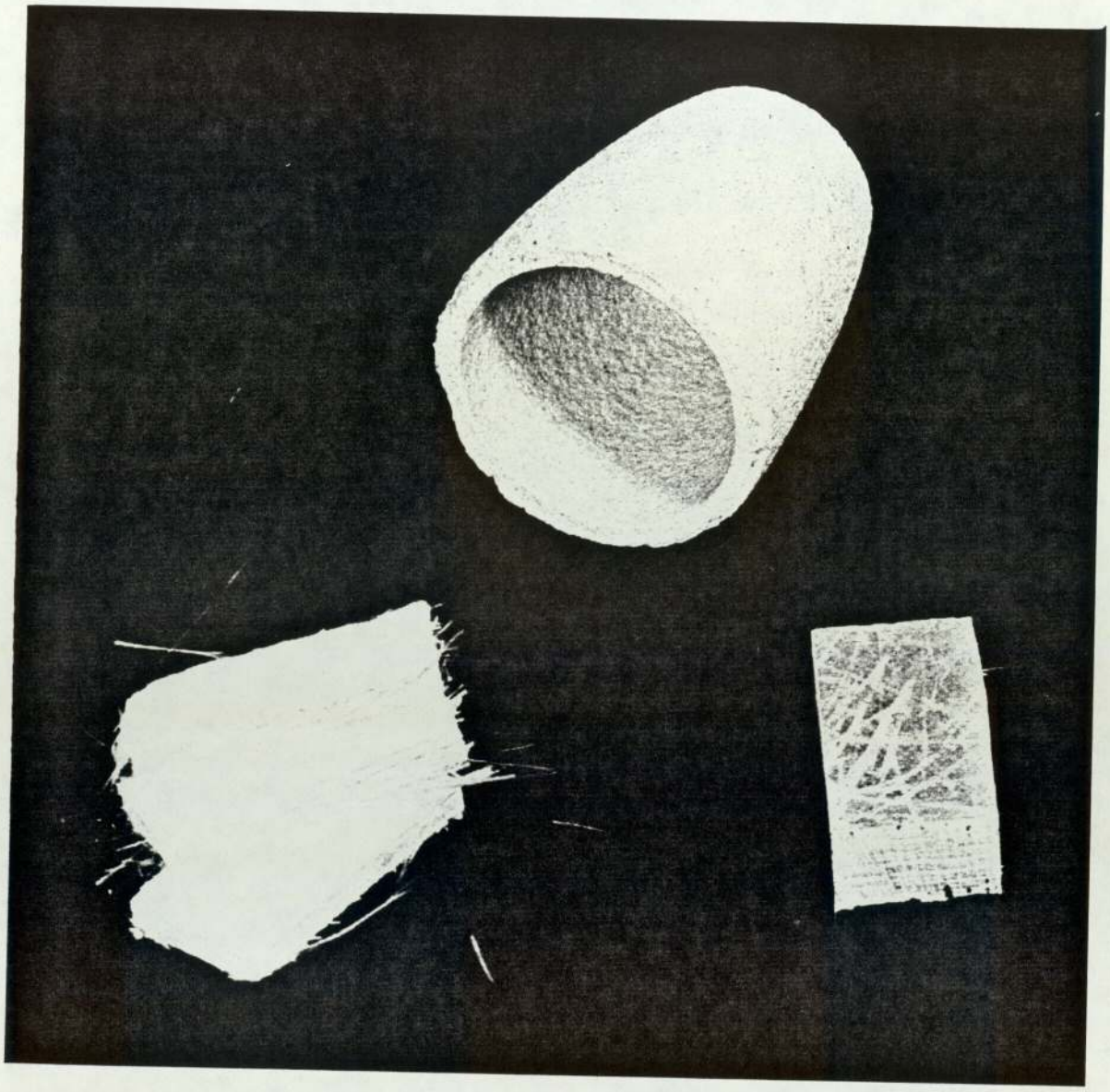

Fig. 8.10 Sample of GRP laminate after ashing. Similar sample shown prior to ashing.

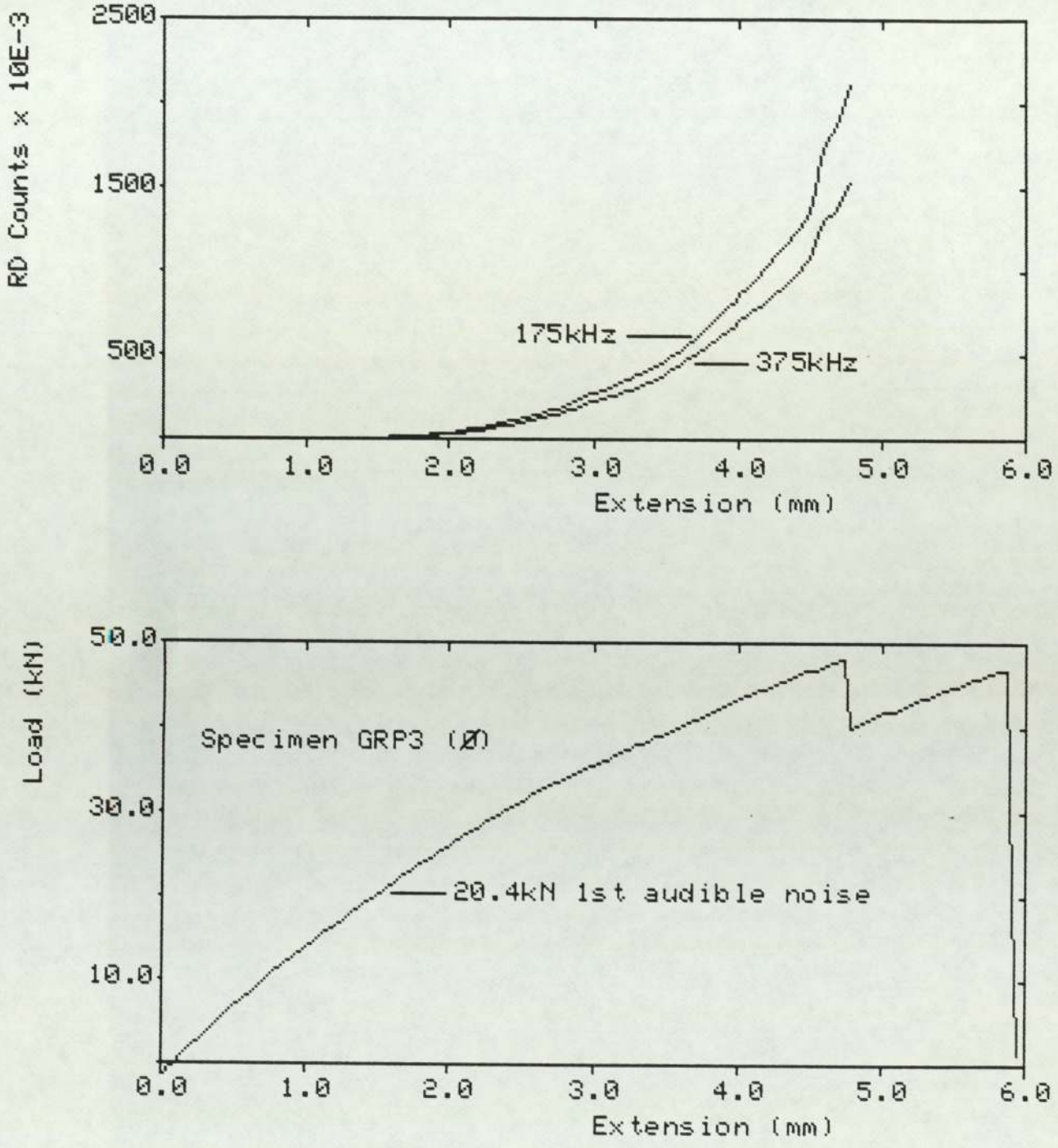

Fig. 8.11 Plots of acoustic emission / extension and load / extension for destructive tensile test on a GRP specimen.

	Panel No.1 Mean Thickness 8.18 mm		Panel No.2 Mean Thickness 11.33 mm		Panel No.3 Mean Thickness 15.62 mm	
Panel Direction	Spec. No.	C'Section (mm.)	Spec. No.	C'Section (mm.)	Spec. No.	C'Section (mm.)
ø	1.1	26.1 x 8.2	2.1	27.4 x 11.2	3.1	27.2 x 14.5
ø	1.2	25.9 x 7.6	2.2	27.1 x 11.5	3.2	27.2 x 14.7
ø	1.3	25.9 x 7.4	2.3	27.5 x 11.1	3.3	27.5 x 14.6
x	1.4	27.2 x 7.7	2.4	24.8 x 9.8	3.4	27.3 x 14.7
x	1.5	26.7 x 7.8	2.5	25.1 x 10.0	3.5	26.7 x 14.3
x	1.6	26.7 x 7.2	2.6	24.6 x 9.8	3.6	27.2 x 14.4

Table 8.1 Cross-section dimensions of GRP Tensile Specimens

		Test No.1		Test No.2		Test No.3	
Panel Direction	Spec. No.	E (GPa)	ν	E (GPa)	ν	E (GPa)	ν
ø	2.1	11.0475	0.2677	11.1760	0.2680	11.1836	0.2747
ø	2.2	10.0713	0.2565	10.1695	0.2592	10.4637	0.2496
ø	2.3	12.4081	0.2804	12.5601	0.2888	12.6030	0.2886
x	2.4	11.6465	0.1912	11.7381	0.1928	11.7893	0.1919
x	2.5	10.7525	0.2167	10.7226	0.2227	10.4864	0.2111
x	2.6	11.4322	0.1896	11.4874	0.1835	11.5443	0.1817

Table 8.2 Tensile Test Results GRP Panel No.2

(Moduli calculated on measured cross-sections)

		Test No.1		Test No.2		Test No.3	
Panel Direction	Spec. No.	E (GPa)	ν	E (GPa)	ν	E (GPa)	ν
ø	2.1	10.9207	0.2677	11.0478	0.2680	11.0552	0.2747
ø	2.2	10.2224	0.2565	10.3221	0.2592	10.5986	0.2496
ø	2.3	12.1558	0.2804	12.3049	0.2888	12.3468	0.2886
x	2.4	10.0738	0.1912	10.1530	0.1928	10.1972	0.1919
x	2.5	9.4903	0.2167	9.4639	0.2227	9.2554	0.2111
x	2.6	9.8380	0.1896	9.8855	0.1835	9.9344	0.1817

Table 8.3 Tensile Test Results GRP Panel No.2

(Moduli calculated on cross-section = measured width x mean panel thickness)

Panel Direction	Spec. No.	$\bar{E}$ (GPa) (Note 1)	Std. Dev.	$\bar{E}$ (GPa) (Note 2)	Std. Dev.	$\bar{\nu}$	Std. Dev.
ø	2.1	11.1357	0.0764	11.0079	0.0756	0.2701	0.0040
ø	2.2	10.2348	0.2042	10.3810	0.1949	0.2551	0.0050
ø	2.3	12.5237	0.1024	12.2692	0.1004	0.2859	0.0048
x	2.4	11.7246	0.0723	10.1413	0.0625	0.1920	0.0008
x	2.5	10.6538	0.1457	9.4032	0.1151	0.2168	0.0058
x	2.6	11.4879	0.0560	9.8860	0.0482	0.1849	0.0041

Table 8.4 **Mean & standard deviation of tensile test results for specimens from GRP Panel No.2**

Note 1 : Moduli calculated on measured cross-sections.

Note 2 : Moduli calculated on cross-section = measured width x mean panel thickness

Panel No.	Meas. $\bar{E}_{ø}$ (GPa)	Meas. $\bar{\nu}_{øx}$	Calc. ν_{ox}	Meas. $\bar{E}_{x}$ (GPa)	Meas. $\bar{\nu}_{xø}$	Calc. $\nu_{xø}$
1	9.6	0.25	0.225	11.1	0.26	0.289
2	11.2	0.27	0.229	9.8	0.20	0.236
3	10.6	0.24	0.245	9.1	0.21	0.206

Table 8.5 **Mean experimental values of Young's modulus & Poisson's ratio and calculated complementary values of Poisson's ratio.**

Calculated values based on $\nu_{ox} = \dfrac{\bar{E}_{ø} \times \bar{\nu}_{xø}}{\bar{E}_{x}}$ & $\nu_{xo} = \dfrac{\bar{E}_{x} \times \bar{\nu}_{øx}}{\bar{E}_{ø}}$

		In Plane Shear Modulus (GPa)					
Panel No.	Spec. No.	Test No. 1	Test No. 2	Test No. 3	Test No. 4	Mean Spec.	Mean Panel
1	1.1	3.73	3.67	3.73	3.61	3.68	3.62
	1.2	3.63	3.45	3.57	3.54	3.55	
2	2.1	3.76	3.76	3.66	3.82	3.75	3.82
	2.2	3.93	3.86	3.92	3.86	3.89	
3	3.1	4.08	3.93	4.08	4.08	4.04	4.03
	3.2	4.05	4.05	3.91	4.05	4.02	

Table 8.6 In-plane shear moduli of GRP panels from anticlastic bending tests

	Orthotropic Properties					Isotropic Properties		
Panel No.	E_ϕ (GPa)	E_x (GPa)	$\upsilon_{\phi x}$	υ_{xp}	$G_{\phi x}$ (GPa)	E (GPa)	υ	G (GPa)
1	9.6	11.1	0.25	0.289	3.62	10.35	0.255	4.12
2	11.2	9.8	0.27	0.236	3.82	10.50	0.235	4.25
3	10.6	9.1	0.24	0.206	4.03	9.85	0.225	4.02

Table 8.7 Summary of In-Plane Elastic properties of GRP panels

Note: Isotropic values of E & υ are means of measured orthotropic values.

Isotropic G calculated from $G = \frac{E}{2(1+\upsilon)}$

		Shear Modulus GPa			
Axis Direction	Test No.	Block 1	Block 2	Mean(Test)	Mean(Direction)
Xø	1.1	3.72	3.81	3.765	
(In plane)	1.2	3.43	3.62	3.525	3.66
	1.3	3.68	3.70	3.690	
XZ	2.1	1.86	1.87	1.865	
(Through plane)	2.2	1.77	2.07	1.920	1.91
	2.3	1.71	2.17	1.940	
øZ	3.1	1.78	1.92	1.850	
(Through plane)	3.2	1.75	1.87	1.810	1.80
	3.3	1.71	1.79	1.750	

Table 8.8 Comparative values of 'in plane' and 'through plane' shear moduli ($G_{x\phi}$, G_{xz} & $G_{\phi z}$) from balanced rail shear test.

Specimen No.	Mass of specimen (g)	Mass of fibres (g)	% fibre (mass)	% fibre (vol)	%fibre (mean vol)
1.1	8.5	3.8	44.7	27.6	
1.2	7.7	3.5	45.5	28.3	27.1
1.3	7.9	3.3	41.8	25.3	
2.1	11.8	5.6	47.5	29.9	
2.2	10.9	4.7	43.1	26.4	28.9
2.3	11.7	5.6	47.9	30.3	
3.1	15.3	7.6	49.7	31.8	
3.2	13.3	6.7	50.4	32.4	31.6
3.3	17.0	8.2	48.2	30.5	

Table 8.9 Fibre fraction of GRP specimens from ashing tests.

Note: Volume fraction (neglecting voids) based on :
S.G. (fibres) = 2.54
S.G. (matrix) = 1.20

Panel No.	Panel Direction	C'Section (mm)	Failure Load(KN)	Nominal Strain at failure(%)	Stress (MPa) Nominal Failure	Stress (MPa) 1st audible noise
1	ø	26.1x8.2	16.3	0.95	76.2(1)	46.8
1	x	27.2x7.7	26.7	1.76	127.5	43.5
2	ø	27.1x11.5	43.0	--(2)	138.0	42.7
2	x	24.6x9.75	28.0	1.33	116.7	52.9
3	ø	27.2x15.7	48.2	1.99	112.9	47.8
3	x	27.2x14.4	47.2	1.92	120.5	47.2

Table 8.10 Results of destructive tensile tests on GRP specimens

Note 1) Specimen failed at grip edge
2) Actuator position not logged

CHAPTER 9

TEST RIG DESIGN AND DEVELOPMENT

9.1 Introduction

The function of the test rig is to hold a cylindrical GRP panel of appropriate dimensions with all four of its edges encastre and to provide for the loading of the panel with uniform pressure on the convex side.

Most of the problems associated with the design of a test rig of this type are imposed by scaling effects. As has been stated earlier, structures of GRP, a laminated composite material, cannot easily be scaled either up or down and still retain their structural characteristics. For test purposes a scale of 1:5 has been found to be the smallest scale that can reasonably be employed for sonar panels. Although this figure is somewhat arbitrary, considerable practical experience suggests that it is about right. The size of typical Naval structures means that even a 1:5 scale model of a sonar dome is still a fairly large item. In this study a typical test panel is a little more than 1.4 m square in plan and up to 20 mm in thickness. Such a panel is very stiff and If its edges are to be held encastre in a test rig, then the rig itself and its support structure must be very rigid indeed.

Previous to the commencement of this project some testing of GRP panels had been attempted at RNEC using an earlier test rig [86] and [87]. These tests proved very unsatisfactory and no useful or reliable results were obtained. The main reason for this lack of success was that the test rig was deficient in several important respects including inadequate provision for immobilising the panel edges.

Although by extensive modifications to this rig it might have been possible to improve its performance it would still have had some important deficiencies. It was decided fairly early on in this work therefore that the best approach was to start afresh with a totally new test rig.

The test rig detailed here was designed specifically for the testing of cylindrical GRP sonar panels. It was designed to overcome most of the problems that had been previously encountered in [86] and [87] as well as others that could be foreseen at the time. Certain minor deficiencies of this new rig became apparent after manufacture but these were largely eliminated by subsequent modifications.

Appendix C contains principal reduced copy drawings of the test rig including some details of manufacture. The main design features are described here.

9.2 Overall design considerations

In view of the large size of the test panels it was clear that the test rig would be expensive to manufacture. Unfortunately since the rig was eventually manufactured in Devonport dockyard with some in-house modifications at RNEC, it is not possible to be precise about the actual final cost. However the approximate cost estimate made in 1982 of the basic rig excluding all instrumentation and test panels was £18000-£20000.

In view of this cost it was felt from the outset that the rig should be designed to be as versatile as possible so that on completion of this particular test program at least part of the rig might be salvaged for future use.

The particular panel dimensions for this investigation are fixed with respect to both radius of curvature and plan dimensions. Only the laminate thickness is variable. It would obviously be desirable if the rig could be designed so as to be useful for future testing, perhaps of panels with slightly different geometry. Furthermore, the loading case on the panels for this investigation is uniform pressure loading. Further investigations with other loading cases might be considered later if the rig could be designed from the outset with these possibilities in mind.

Unfortunately versatility of design can often only be achieved by compromising the primary function and the primary function in this case is the current investigation. Extra features were only added therefore, where they did not compromise the current work.

9.3 Description of test rig

9.3.1 Sectional design

The rig may be considered to be built up of four main sections, illustrated schematically in Figure 9.1.

(a) A base unit. This provides for the whole rig to be either fixed down to the strong floor of the structural testing facility or else to be free-standing and mobile. This part of the test rig should be usable for other future test programs with only a minimum of modification.

(b) An instrumentation frame. This carries the displacement transducers and is mounted on the base unit so as to be uninfluenced by the behaviour of the panel but to be an integral part of the rig for mobility and convenience.

(c) A guard frame. Guards serve a double purpose. Firstly the guards act as a safety feature in the event of a panel failure and secondly they provide protection from disturbance for the instrumentation frame.

(d) A special machined fixture to accommodate the test panel. This is the only part of the test rig that is totally specific to a particular panel geometry and which would be difficult to utilise in any other application. Unfortunately, due to the machining required it is also the most expensive part of the test rig to produce.

9.3.2 Base unit

This consists of a heavy frame support made up of steel box section and diagonally braced. The base stands on four pads which are designed to be bolted to the laboratory strong floor or alternatively to take heavy duty castors so that the rig can be mobile. The castors shown on the rig assembly drawing were, in fact, not used other than for convenience during the construction and finishing of the rig. All tests using the rig were carried out with the rig bolted to the strong floor. Three outrigged support pads are provided on each of the four sides of the base and each of these is drilled to take both the instrumentation frame and the guard frame.

The top of the base structure terminates in a flat 10 mm thick steel plate underbraced with box section and framed by a heavy steel flange 1440 mm square and of 100 mm x 25 mm section. The upper surface of this flange is machined and provided with 72 tapped holes for $\frac{3}{4}$" - 16 UNF bolts. The flange is seamwelded gastight to the plate and the plate has two $\frac{1}{2}$" BSP drain plugs. The drain plugs are provided so that the rig may be used with hydraulic as well as pneumatic loading.

9.3.3 Instrumentation frame

The main instrumentation frame is constructed of 25 mm square steel box section and is mounted outside of the main test rig. The two sides of the frame which run parallel to the straight sides of the test panel are used as rails for the mounting of a series of cross-members. Cross members can be clamped into position anywhere along the rails and take the form of curved angle bars arranged so that the arcs of the bars are concentric with the curvature of the test panels. LVDTs mounted on these bars are thus automatically a set distance from the test panel.

Each LVDT is individually mounted on its own non-magnetic fixture which can be positioned anywhere along the bars and automatically aligns the LVDT to measure panel displacements in the radial direction. Thus, it is possible using this arrangement to position an LVDT at any point on a cylindrical test panel without the need for checking that the LVDT is normal to the panel surface. This feature greatly simplifies the setting up procedure for a test.

The fixing of the instrumentation frame to the main test rig base was designed so that deflections or distortions of the test rig structure would not be transferred to the instrumentation. Such a transfer would, of course, result in false readings. Tests were done on the completed rig to confirm that no such interaction took place.

9.3.4 Guard frame

This frame is similar in construction to the instrumentation frame but is mounted outboard of it. Like the instrumentation frame it is a rigid structure of steel box section bolted to the base section of the rig and forming a cage around it to above head height.

The obvious difficulty with any guard system is that it restricts access to the equipment and makes setting up of tests more difficult. To minimise this the basic guard frame is of open construction so that access is only slightly hampered by the frame itself. The guards, made of 12 mm, 18 SWG weldmesh are permanently fixed to only two opposite sides of the cage so that access to the instrumentation can be gained through the remaining two sides. Screens (again of weldmesh) for these two sides are clipped to the frame just prior to each test. The top of the guard cage remains open.

9.3.5 Special panel fixture

This section of the test rig carries the test panel and may be considered as the test rig proper. Essentially it is a transition piece between the flanged top of the base unit and the flanged mounting of the test panel. It must be particularly rigid since it is to the top flange of this section that the test panels are bolted. The joint between the test panel and the rig effectively dictates the boundary conditions of the panel, which must be as near to fully encastre as possible.

To provide this rigidity, the panel fixture is heavily braced and webbed between the two main flanges. All welding is continuous. The structure is also designed to be exactly symmetrical in both of the test panel directions, so that the inevitable small deformations of the mounting flange will themselves be symmetrical, and will not induce asymmetric panel behaviour.

The outer faces of both flanges are machined surfaces (machined after fabrication), the lower plane flange is machined for a gasket joint to the base unit and the upper flange is cylindrically machined to conform accurately to the curvature of the test panels.

Because the test panels are all of the same outside radius (the same radius as the mould), all conform equally well to the machined flange and for the GRP test panels it is the smooth surface of the panel

which contacts the flange. In order to avoid the degradation of the clamped boundary condition that would have resulted from a gasket at this point, but still to maintain an airtight seal between the panel and the rig, the flange has a single groove for an 'O' ring type seal. The intention of this was to give a metal to metal or metal to GRP contact at the panel boundary. The detail of this joint is shown in Figure 9.2.

The panels are secured to this top flange by bolts, $\frac{3}{4}$" diameter and 72 in number passing through the flange, the test panel and securing rails. Four securing rails are required, two for the straight panel edges and two for the curved panel edges. The rails used on the straight panel edges are unaffected by test panel thickness since they have to conform only to a flat surface, but the curved rails must be bent to the inside radius of the panel which varies with panel thickness. To avoid the need to provide a set of curved rails for every variation of panel thickness a compromise was made. One set of rails was produced to accommodate panels up to 10 mm thick and another up to 20 mm thick. Aluminium packing pieces were then used to give final adjustments. This arrangement is illustrated schematically in Figure 9.3.

Two other features of this panel joint are worthy of note. Firstly, to achieve a more uniform clamping of a relatively wide flange joint the bolts are not arranged in a single row but in an alternate double

row pattern (see drawings). Secondly, the bolt pattern is designed to be symmetric so that a panel should be reversible on the rig without redrilling.

Since this section of the test rig forms four of the six sides of the pressure containment for pneumatic or hydraulic loading - the other two sides being provided by the test panel and the base - provision is made here for access to the convex side of the panel. Four access plates are provided, two on each side between the stiffening webs. In fact only two of these access plates were used for this work; one for air feed and pressure monitor lines and the other for strain gauge leads. Four bleed valves are also provided at the highest points of the containment. These are intended as air bleed points to be used with hydraulic loading. They were not used for this work since all loading was pneumatic.

Provision was also made in this section of the rig for a longitudinal dividing rail to be added to the rig to split the test panel in the ratio $\frac{1}{3} : \frac{2}{3}$. This was to allow testing of panels of different aspect ratio at a later date. The provision was not used for this work.

9.4 Development of the test rig

A number of minor changes were made to the test rig after its completion by the dockyard. Some of these changes were made in order to compensate for shortcomings of manufacture and others were made to improve the performance of the rig following initial experience of use.

Generally the deficiencies of manufacture were only minor ones and the rig performed adequately from the first test.

The most significant change made necessary as a result of deficiencies of manufacture was in the arrangement for sealing the test panels to the rig. The groove in the top flange, illustrated in Figure 9.2 proved difficult for the dockyard to machine accurately. On delivery of the rig the groove was found to have unacceptable variations in both its width and depth so that fitting of the rubber seal became difficult. Attempts to overcome this by using different sizes of seal proved only partially successful and finally the rubber seal was discarded altogether. For all of the subsequent tests a seal was formed by laying a bead of silicone rubber compound into the sealing groove before bolting down each test panel. This proved totally satisfactory as a seal but very much less convenient for panel changing.

The main developments made as a result of experience gained through testing were the addition of extra stiffening members to the rig for some of the tests. This extra stiffening was added in attempts to bring the boundaries of the panels closer to the ideal encastre condition.

The stiffening members were added across the open face of the rig in both panel directions in an attempt to close the rig and make it self reacting. Although even without the extra stiffening panel edge movements were very small, this modification had a considerable influence on panel behaviour in subsequent tests. The addition of these stiffeners and their effects are described in Chapter 11.

9.5 Test rig specification summary

Dimensions (overall)

Main test rig:	length	1465 mm
(excluding outriggers)	width	1515 mm
	height	810 mm
Instrumentation frame:	length	1595 mm
	width	1640 mm
	height	915 mm
Guard frame	length	1925
	width	1925 mm
	height	1820 mm
Total mass (estimated)		1200 kg

Panel flange dimensions:

Inside	length	1240 mm
	width	1240 mm
Outside	length	1440 mm
	width	1440 mm
Radius of curvature		1140 mm
Bolts	72 x $\frac{3}{4}$" UNF	

Pressure containment

Maximum working pressure		400 kPa
Access	4 x access panel	140 mm x 180 mm
	4 x vent	(see drawings)
	2 x drain	$\frac{1}{2}$" BSP.

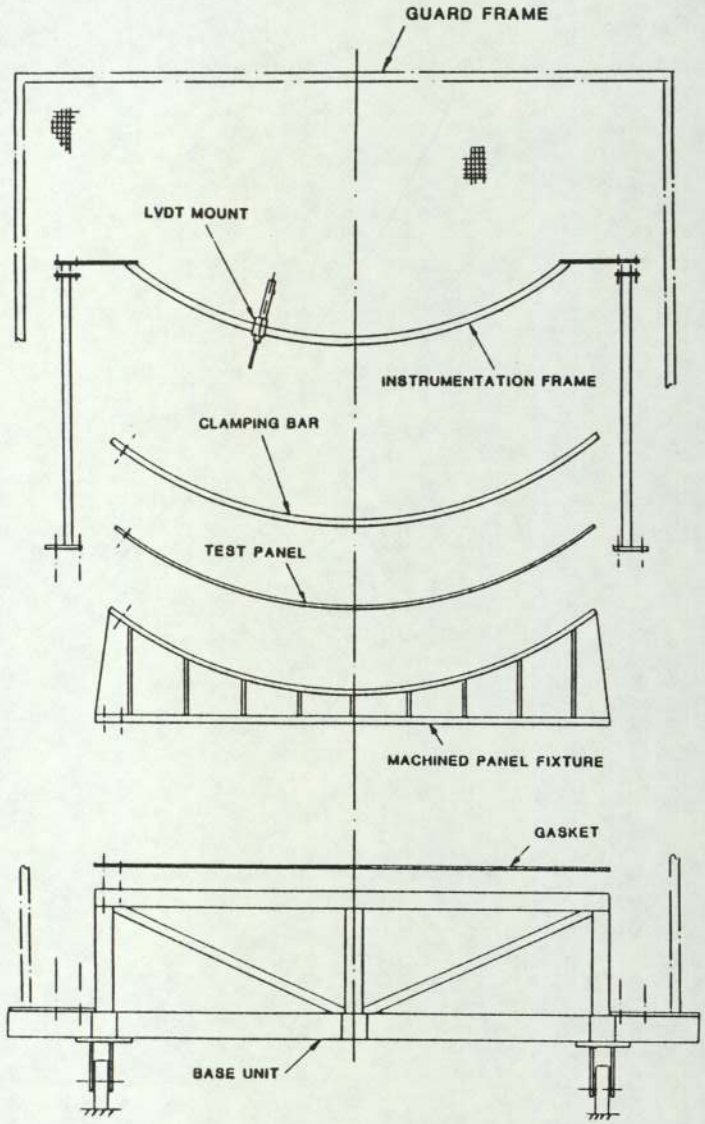

Fig. 9.1 Exploded schematic diagram of test rig (including guard and instrumentation frames)

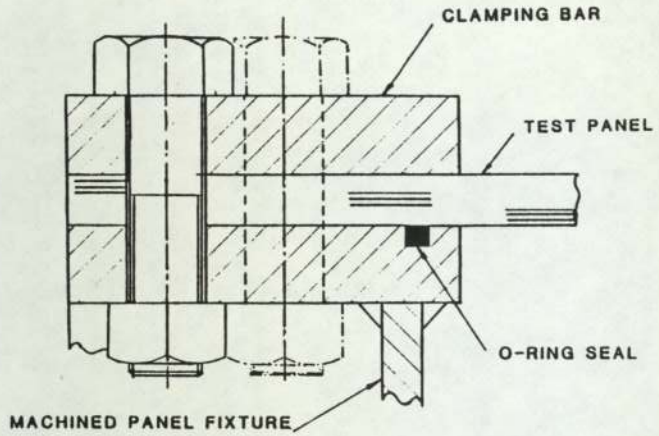

Fig. 9.2 Detail of panel edge seal and clamp arrangement.

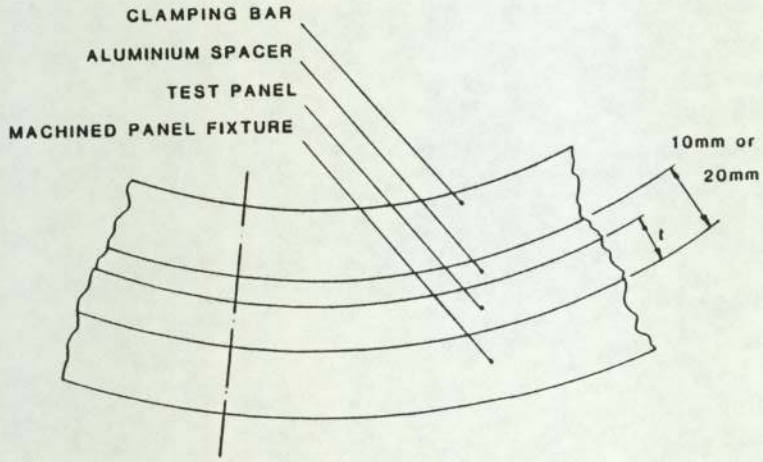

Fig. 9.3 Use of aluminium spacers to accomodate range of panel thickness.

CHAPTER 10

DESCRIPTION OF TEST PANELS AND HYDROSTATIC PANEL TESTING

10.1 Introduction

This chapter describes the large cylindrical test panels and details the full procedure adopted for their testing. It includes both the material thickness surveys of the panels using the ultrasonic thickness measurement and the hydrostatic load testing using the test rig described in Chapter 9.

Results of the thickness surveys are given here since they may be properly considered as part of the panel descriptions but results of the hydrostatic pressure testing are given separately in Chapter 11.

10.2 Panel manufacture

A total of 5 panels were tested in all. The dimensions of all 5 panels were identical except for panel thickness. Panel dimensions are given in Figure 10.1. The 5 Panels were:

AL1	Aluminium Panel (annealed)	6.4 mm thick
GRP1	GRP Panel (7 laminations)	
GRP2	GRP Panel (11 laminations)	
GRP3	GRP Panel (15 laminations)	
AL2	Aluminium Panel	1.2 mm thick

The panel AL1 was used as a panel of known isotropic properties and of uniform thickness to give basic information about, and to assist in the development of the test rig. No thickness survey was done on this panel but measurements around the edge indicated good dimensional accuracy. Samples of the panel material were subjected to mechanical testing as previously described in Chapter 8.

The 3 GRP panels were manufactured by W and J TOD PLC to

the standard ARE specification using a hand lay-up process. No special precautions were specified for these panels since it was intended that they be representative of normal sonar dome manufacturing practice. The plywood mould used in the manufacture of these panels was provided by RNEC. Lamination stacking was specified as alternate layers of woven rovings (WR) and chopped strand mat (CSM) with the roving warp and weft directions parallel to the panel edges. An odd number of laminations was specified for each panel with layers of CSM on each outside surface. Thus:

GRP1 3WR/4CSM

GRP2 5WR/6CSM

GRP3 7WR/8CSM

The final panel AL2 was a very thin aluminium one and was the only panel that was not formed to the cylindrical shape prior to being fitted into the test rig. This panel was selected for test because it had membrane stiffness comparable with the GRP panels, (approximately equivalent to a GRP panel of 8 mm thickness) combined with negligible bending stiffness. It was considered that testing this panel would give useful insight into panel bending behaviour.

10.3 Panel Preparation

10.3.1 Aluminium Panel AL1

This panel was manufactured in the dockyard at the same time as the test rig and was drilled with clearance holes to suit the top flange of the rig. No further machining of this panel was required.

10.3.2 GRP Panels 1, 2 and 3

The 3 GRP panels were initially prepared by cutting off the tangential extension pieces that were to form the material test samples (see Chapter 8) and were then drilled to suit the test rig top flange. In order to ensure

bolt hole alignment, an aluminium template was manufactured to assist in the drilling. All cut edges of the panels and the inside surfaces of the drilled holes were coated with polyester resin to seal the surfaces.

10.3.3 Aluminium panel AL2

This panel was prepared by drilling oversize holes only. On subsequent fitting into the test rig the panel was elastically deformed to conform to the cylindrical profile.

10.4 Thickness testing

Each GRP panel was marked out with a 6 x 6 grid of points for thickness testing with the panel standing upright on one of its curved edges. The upper edge was now designated North as a datum for identifying the panel disposition in the test rig.

Thickness readings were taken at each of the marked points using the ultrasonic thickness gauge.

The logged thickness readings were then processed to give mean and standard deviation as well as 95% and 99% confidence limits for the mean thickness. Each panel was surveyed 3 times and the mean panel thickness was taken as the mean of the 3 tests. Since it was not possible to measure the panels at exactly the same positions for repeated tests some variation between tests was found, however, the mean panel thicknesses lay within a band of $\pm$ 0.1 mm for repeated tests on each panel. A single sample survey for each panel is given in Table 10.1.

In addition to calculation of mean and standard deviation, the data from each thickness survey was grouped into rows, columns and blocks (see Figure 10.2), each of 6 readings. Sample means for these groups were calculated and an 'F' test for significance carried out. The detailed interpretation of the F ratios obtained from these

tests is not of concern here, however it can be seen that, for example, Panel GRP2 is significantly thicker in its South Westerly block and Panel GRP3 is significantly thinner in its Northern rows. This information is of use in explaining asymmetric panel behaviour under pressure load, (see later).

10.5 Strain Gauging

After the thickness survey all panels, including the aluminium ones, were marked out into a 12 x 12 grid system. This grid system was used to identify positions of strain gauge rosettes and LVDTs. Strain gauge positions were selected for panel AL1 and all three GRP panels, no strain gauges were used on panel AL2. 90° strain gauge rosettes with gauge axes aligned with panel edges were fixed to each panel in the selected positions. The strain gauged panel AL1 is shown in Figure 10.3, for gauge positions on each panel, see Chapter 11.

Strain gauges were connected with ribbon cables terminating in standard 7 pin connectors. For those gauges on the convex side of the panel (inside the pressurised section of the test rig). Plessey Type bulkhead connectors were used. All strain gauges were protected by an air drying protective coating.

10.6 Panel Testing

Each panel was subjected to a series of pressure tests. Slight variations of procedure were adopted for each panel but the typical procedure applied to a GRP panel is described below.

10.6.1 Panel fixing

Each panel was placed into the test rig with a seal effected by a double bead of silicone rubber compound as previously described. The 4 securing beams with appropriate packing pieces were then bolted down to give full contact at the sealing face. After a period of 24 hours to allow cure of the silicone sealant each of the 4

bars was removed in turn and coated with mould release agent. The area of exposed panel, rough surface uppermost under the sealing bar, was then coated with a polyester resin filler paste and the bar was then replaced and bolted down before the resin had cured. At this stage all clamping bolts were tightened to a torque of 150 Nm. After a further period of 24 hours to allow full cure of the resin, the 72 clamping bolts were retightened to this torque. The purpose of the resin was to level out the rough surface of the GRP to ensure an even clamping on the panel.

10.6.2 LVDT positioning and instrumentation checks

LVDTs were positioned on the instrumentation frame at selected grid points. Positions of LVDTs for each test are given in Chapter 11. Figure 10.4 shows a typical layout.

Where LVDT positions coincided with strain gauge rosette positions the strain gauges were protected by perspex discs 12 mm diameter x 1.5 mm thick, bedded onto the strain gauge protective coating. See Figure 10.5.

All LVDTs were then connected to the LVDT power supply and monitor unit and the LVDT compulog satellite cabinet. At this stage all LVDT channels were verified electrically.

Each LVDT was now moved in its carrier block to its electrical zero ± 10 mV. This zeroing was carried out to ensure that each LVDT was working close to the centre of its calibrated range.

10.6.3 Panel tests

With the pneumatic system connected as described in Chapter 7 and the guards in position, each panel was tested under computer control.

Each panel was tested a number of times with various changes of test parameters and in the case of AL1 and GRP3 with various degrees of test rig stiffening.

For each significant change of parameter or change of rig conditions 3 tests were done.

1. A set test to allow the panel to settle itself into the test rig for a particular loading.
2. A test from which test data was subsequently processed.
3. A confirmation test to check the data from 2 above.

A period of at least one hour was allowed between tests for panel relaxation. The majority of tests were carried out with increasing/decreasing pneumatic pressure or vacuum, with LVDTs strain gauges and pressure logged at preset pressure levels. For these tests pressure would be stabilised at each level prior to logging. A typical test, involving the logging at 20 pressure levels, having a duration of approximately 30 minutes. In addition a number of tests were conducted over longer periods to investigate the effects of creep and also of relaxation of the shell after removal of loading. A full list of tests together with representative test results is given in Chapter 11.

10.6.4 Side Jacks

On a limited number of tests, after the addition of cross stiffening members to the rig, further edge restraint was provided using hydraulic jacks at the mid-point of each longitudinal panel edge, see Figure 10.6. This edge jacking was done manually in an attempt to reduce panel edge translational displacements (measured with dial gauges) to zero. The method was partially

successful but was found difficult to control accurately. Results of this are given in Chapter 11.

Throughout a test the panel edge displacements, or more correctly the displacements of the top flange of the test rig, were monitored with dial gauges. Rotational as well as translational displacements were checked; rotations were measured using pairs of dial gauges across the width of the top flange.

The addition of stiffening members had a significant effect on edge displacements. With all stiffening members in place edge displacements were not measurable with dial gauges at rig pressures below 50 kPa (see Chapter 11).

10.7 Processing of Test Results

At the end of each panel test results were retrieved from the data file where they had been stored by the experiment program and printed out in hard copy form. The following information was available from each test.

1. Time of each logged pressure level from start of test to nearest minute.
2. Pressure at each level in kPa.
3. Displacement readings in mm at each LVDT channel at each pressure level.
4. Strain readings in microstrain from each strain gauge and at each pressure level.
5. Temperature readings at each pressure level.

(Note: for short duration tests no significant temperature variations were noted).

Where 3 tests (set(1), test(2), confirm(3)) were carried out these were compared at this stage. Generally values of displacement and strain were found to increase by around 10% between set test(1) and test(2) particularly where load direction had been reversed

from previous tests. Confirmation tests(3) gave results in agreement with tests(2) within the resolution of the instrumentation.

A total of 98 panel tests were carried out and logged in this way.

10.7.1 Membrane and bending stresses

A decision was made to express the stresses in the cylindrical panels in the form of bending and membrane components. This presents a slight disadvantage in that maximum values of stress are not given directly but it does give a better appreciation of the relative effects of bending and membrane action on the shell. Therefore at each panel location where strain gauge rosettes were fixed on both panel surfaces, strain gauge readings were processed first to give principal stresses and then to give bending and membrane stresses at that point. These stresses were calculated in the co-ordinate panel directions and were based on the elastic properties as measured for each panel material as described in Chapter 8.

10.8 Presentation of Results

The results from representative tests on each cylindrical panel are presented in Chapter 11. Displacement results are presented graphically in all cases. Due to the limited number of strain gauge rosette positions on each panel stress results are presented for gauged points in tabular form.

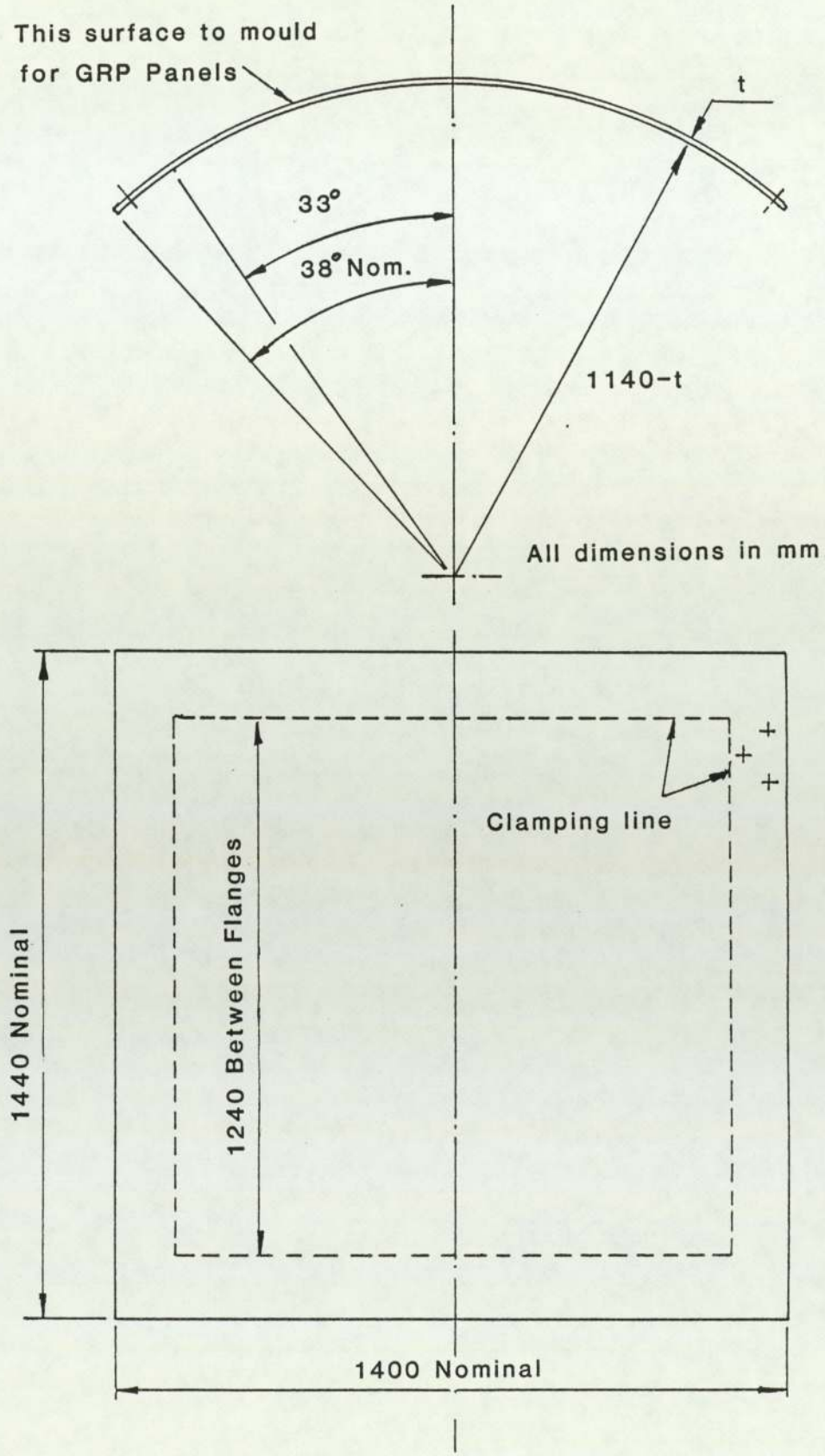

Fig. 10.1 Test Panel dimensions.

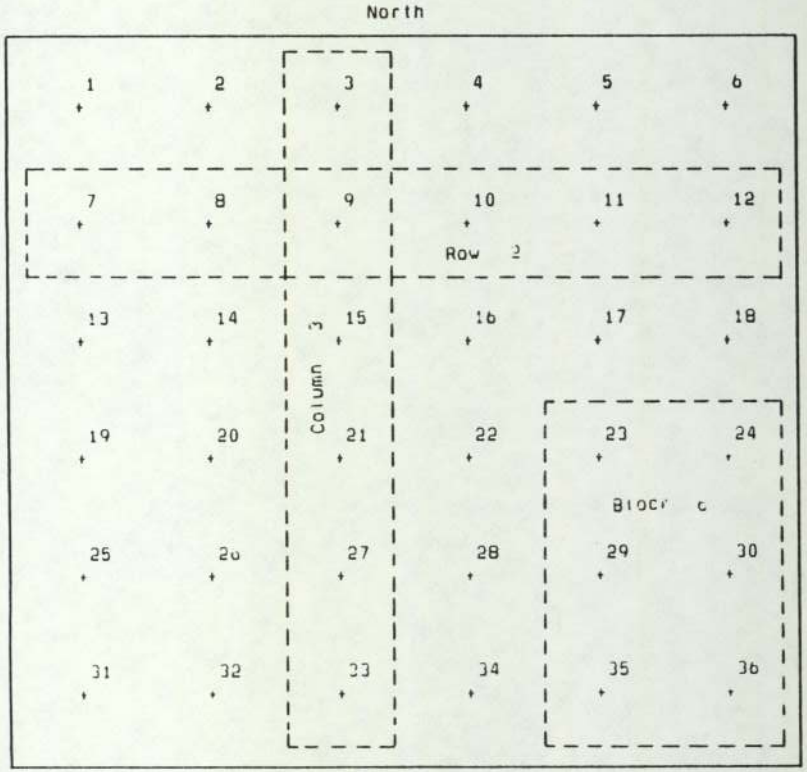

Fig. 10.2 Grouping of thickness data into rows, columns & blocks.

PANEL GRP1 (Test 1)

Mean Sample Thickness	:	8.22mm.
Standard Deviation	:	.59
Limits	:	+/- .19mm.
Probability that Mean will lie within Limits	:	95%
Number of Points	:	36

Thickness Readings (mm.)

1	7.86	8.35	8.79	8.04	9.14	8.40
7	7.63	8.17	8.05	8.87	8.80	8.50
13	7.87	8.75	8.74	7.72	9.07	8.68
19	7.86	7.67	8.11	7.56	8.44	8.60
25	9.30	8.34	7.44	8.59	8.17	9.12
31	6.59	8.02	7.58	7.45	8.07	7.45

The F ratio for the data grouped in Rows is 3.05

with a d.f. for the Numerator of 5
and for the Denominator or 30

The sample means are:

Group	1	2	3	4	5	6
	8.43	8.34	8.47	8.04	8.49	7.53

The F ratio for the data grouped in Columns is 1.38

with a d.f. for the Numerator of 5
and for the Denominator or 30

The sample means are:

Group	1	2	3	4	5	6
	7.85	8.22	8.12	8.04	8.61	8.46

The F ratio for the data grouped in Blocks is 2.35

with a d.f. for the Numerator of 5
and for the Denominator or 30

The sample means are:

Group	1	2	3	4	5	6
	8.10	8.37	8.76	7.96	7.79	8.31

Table 10.1a Thickness survey details (Panel GRP1)

PANEL GRP2 (Test 1)

Mean Sample Thickness	:	11.33mm.
Standard Deviation	:	.92
Limits	: +/-	.30mm.
Probability that Mean will lie within Limits	:	95%
Number of Points	:	36

Thickness Readings (mm.)

1	9.97	10.11	10.35	10.34	10.55	10.66
7	10.28	10.51	10.25	10.54	10.78	10.74
13	10.72	10.47	11.07	11.04	11.16	10.99
19	12.22	12.23	13.08	11.72	10.98	11.52
25	12.05	12.80	12.90	11.77	11.50	12.12
31	12.51	12.76	12.81	12.07	11.73	10.69

The F ratio for the data grouped in Rows is 15.41

with a d.f. for the Numerator of 5
and for the Denominator or 30

The sample means are:

Group	1	2	3	4	5	6
	10.33	10.52	10.91	11.96	12.19	12.09

The F ratio for the data grouped in Columns is .37

with a d.f. for the Numerator of 5
and for the Denominator or 30

The sample means are:

Group	1	2	3	4	5	6
	11.29	11.48	11.74	11.25	11.12	11.12

The F ratio for the data grouped in Blocks is 29.84

with a d.f. for the Numerator of 5
and for the Denominator or 30

The sample means are:

Group	1	2	3	4	5	6
	10.34	10.60	10.81	12.43	12.39	11.42

Table 10.1b Thickness survey details (Panel GRP2)

PANEL GRP3 (Test 1)

Mean Sample Thickness	:	15.65mm.
Standard Deviation	:	1.32
Limits	: +/-	.43mm.
Probability that Mean will lie within Limits	:	95%
Number of Points	:	36

Thickness Readings (mm.)

1	14.32	14.97	14.59	14.22	14.64	14.11
7	13.94	14.46	14.89	14.46	14.33	14.53
13	15.16	15.06	15.57	14.73	15.18	15.29
19	17.29	16.86	16.54	17.18	15.74	15.01
25	15.91	17.29	17.39	19.66	16.43	15.00
31	17.13	17.08	17.91	16.52	15.15	14.68

The F ratio for the data grouped in Rows is 11.11

with a d.f. for the Numerator of 5
and for the Denominator or 30

The sample means are:

Group	1	2	3	4	5	6
	14.55	14.46	15.20	16.36	16.52	16.53

The F ratio for the data grouped in Columns is 1.02

with a d.f. for the Numerator of 5
and for the Denominator or 30

The sample means are:

Group	1	2	3	4	5	6
	15.58	15.92	16.18	15.76	15.32	14.86

The F ratio for the data grouped in Blocks is 34.71

with a d.f. for the Numerator of 5
and for the Denominator or 30

The sample means are:

Group	1	2	3	4	5	6
	14.72	14.70	14.79	16.78	17.25	15.39

Table 10.1c Thickness survey details (Panel GRP3)

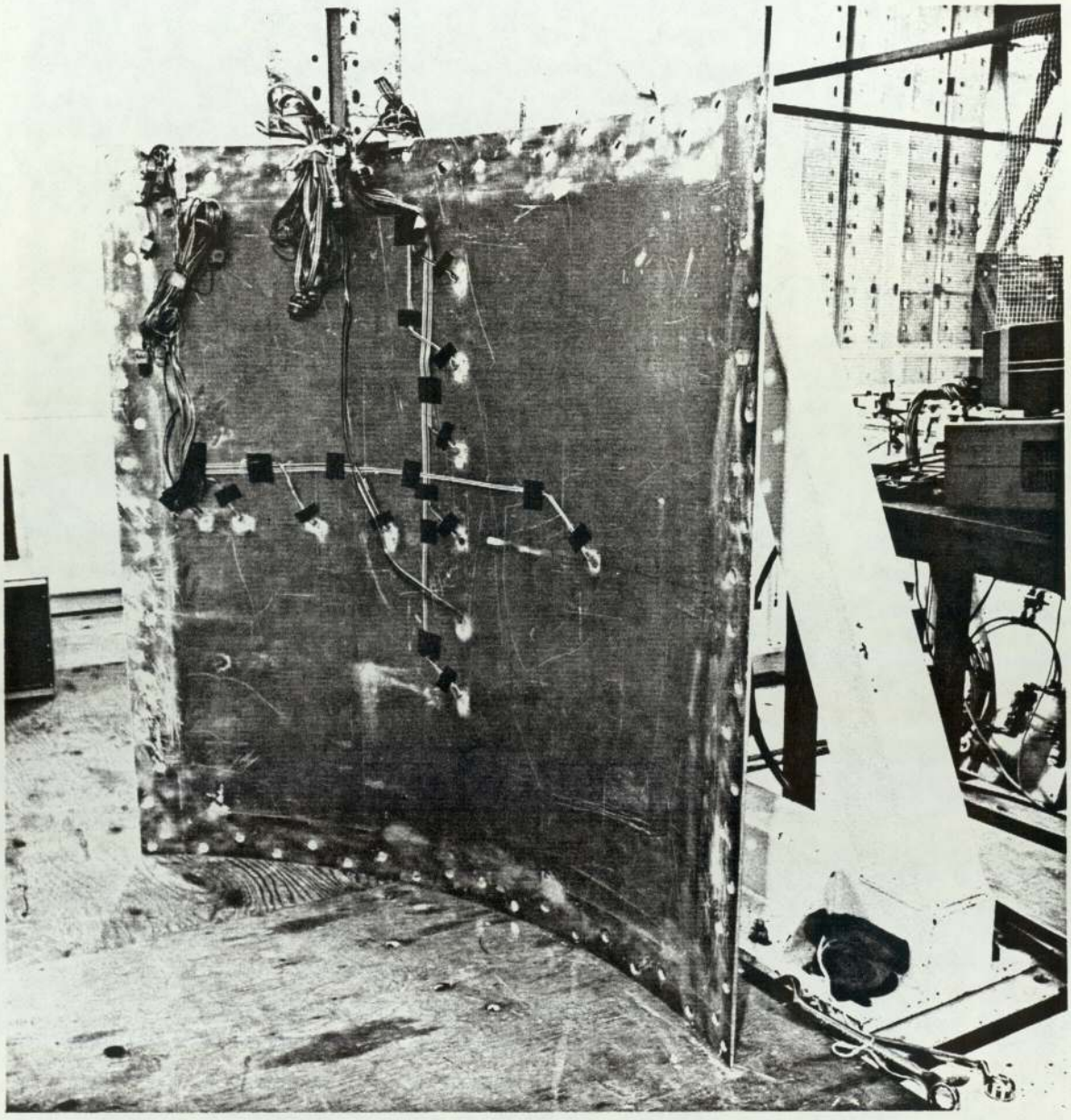

Fig. 10.3 View of test panel showing strain gauges.
(Panel AL1 shown)

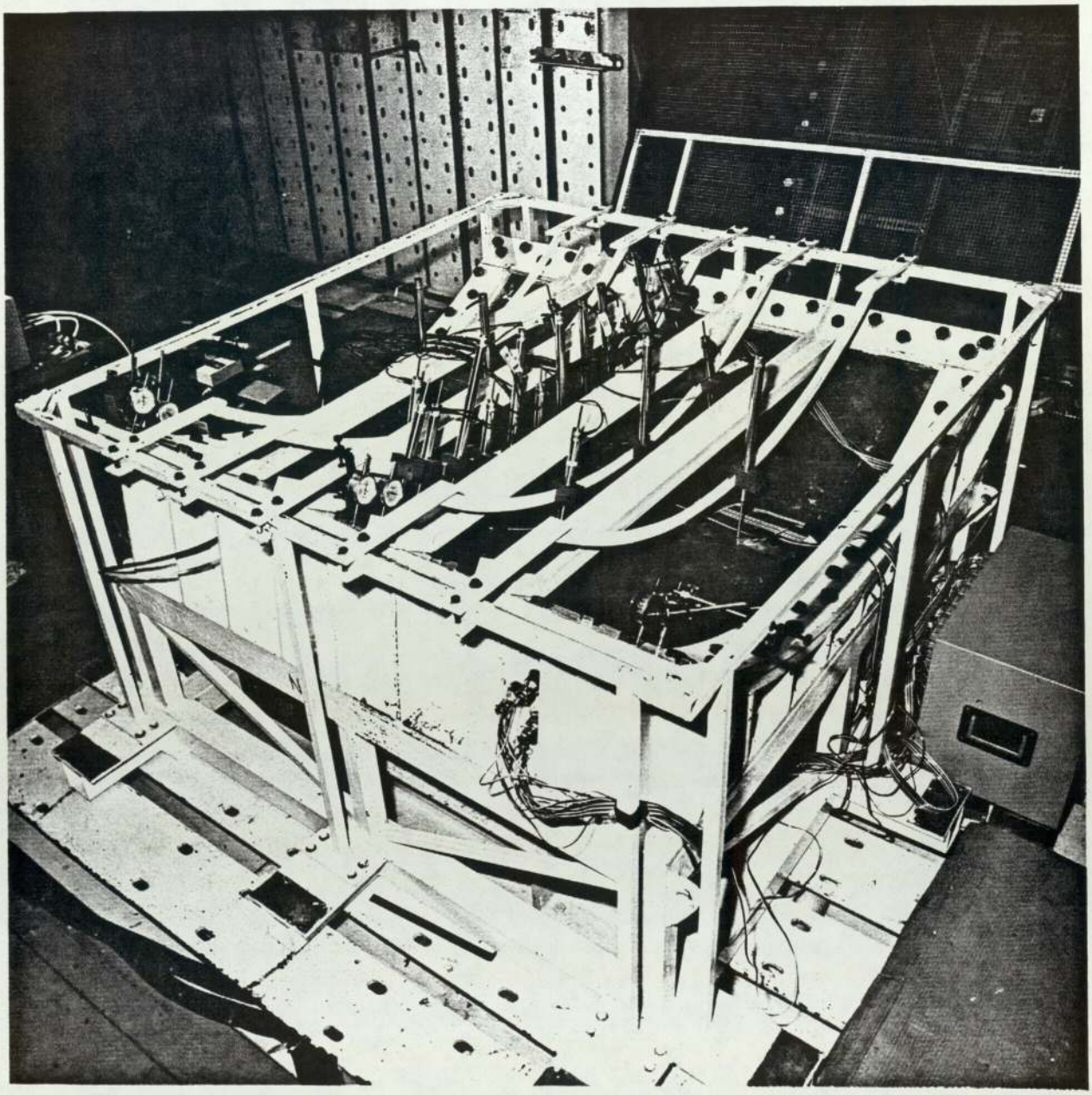

Fig. 10.4 View of test rig showing LVDT's positioned.

(Note: longitudinal rails and guard frame not fitted)

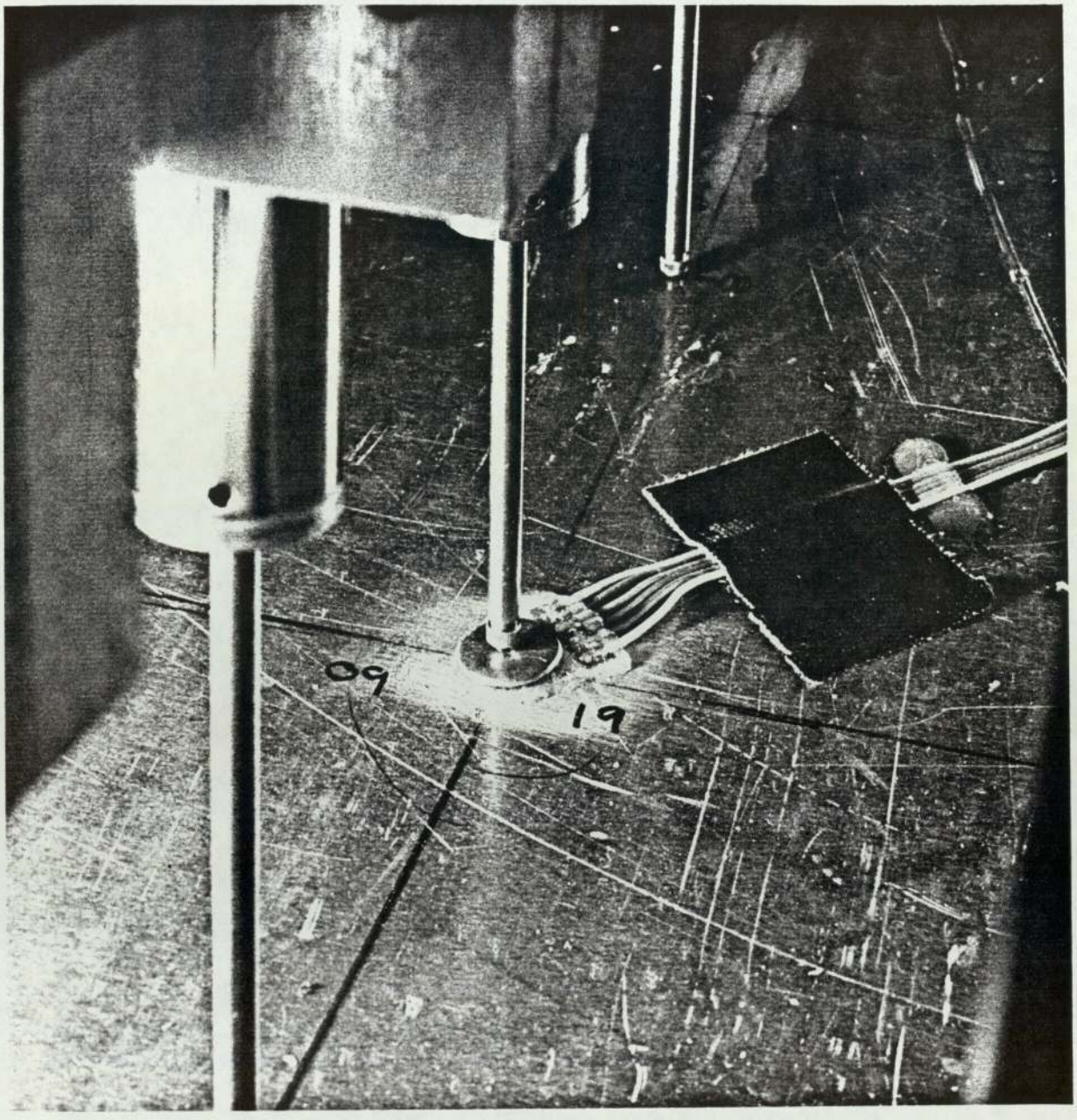

Fig. 10.5 Strain gauge rosette protected from LVDT shaft by a perspex disc.

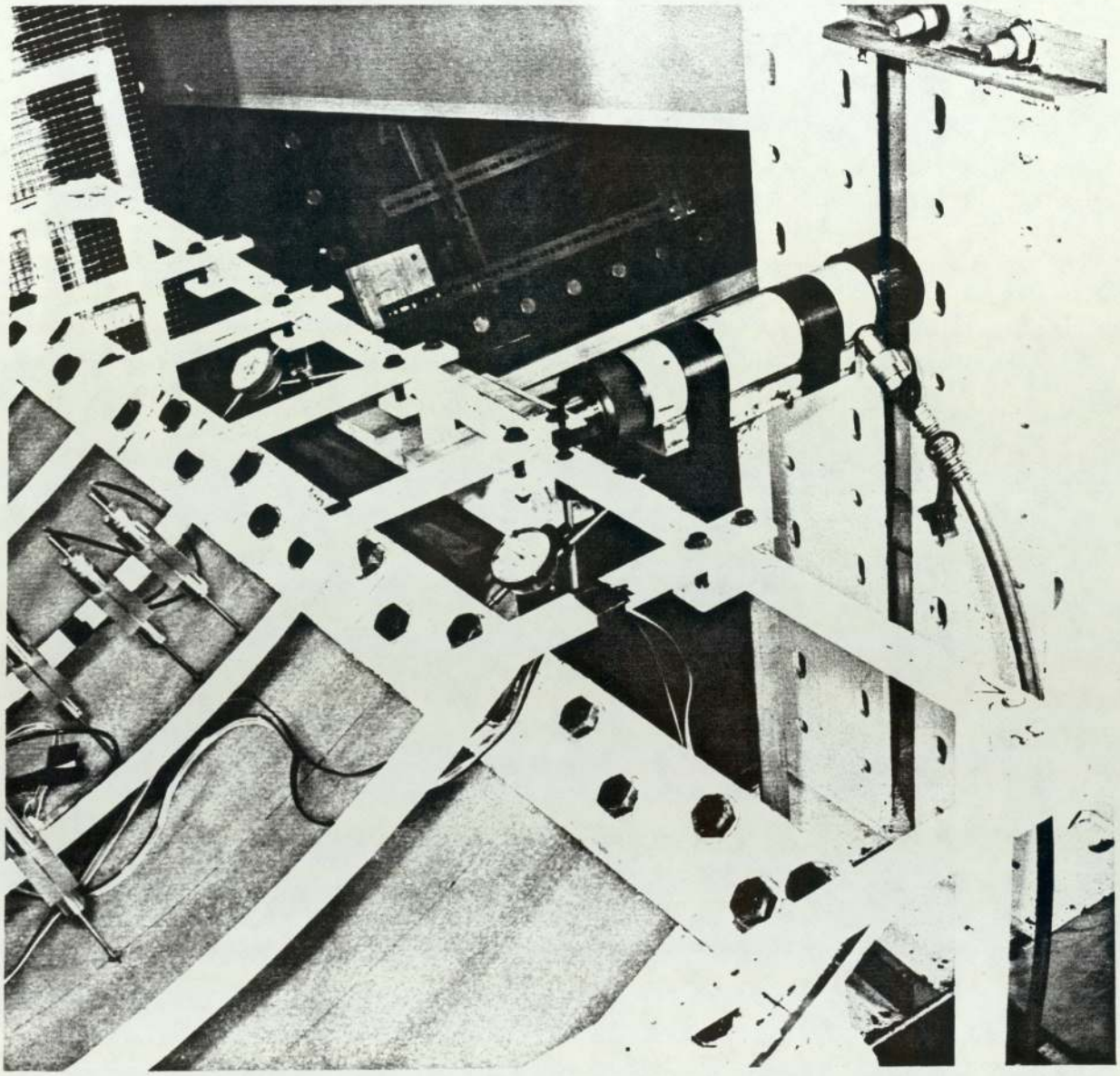

Fig. 10.6 Hydraulic jack at mid-point of longitudinal edge.
(Note: identical jack on opposite side of test rig.)

CHAPTER 11

RESULTS OF PANEL TESTING

11.1 Introduction

A total of 98 pressure and vacuum tests, as described in Chapter 10, with full instrumentation and logging of results, were carried out on the 5 test panels. A full catalogue of tests is given in Table 11.1.

In this chapter only representative results are presented for each panel under conditions of pressure and vacuum loading. In the cases of panels AL1 and GRP3 additional results are given to show the effect of the addition of stiffening members to the test rig.

All displacements of panels, measured with LVDTs normal to the panel surface are presented graphically. Stresses in the panel material, calculated at the positions of the strain gauge rosettes, are presented in tabular form because insufficient data points were available to allow realistic plotting of stress distributions. All the graphical and tabular information is cross referenced, where appropriate, to the catalogue of tests.

Observations and conclusions concerning the behaviour of the panels, based on the experimental results are made at the end of the chapter.

11.2 Interpretation of the displacement results

In order that the overall panel displacement profiles may be shown, displacements have been plotted along the axes of symmetry of the panels, X and ϕ (see Figure 11.1). These axes have been non-dimensionalised to run from -1 to +1 in each case so that the centre of the panel is zero for both axes.

All displacement graphs have been plotted for the full panel axis so as to give a displacement profile for the full length of the panel (X axis) or right across the panel (ϕ axis) so that asymmetry in behaviour can be clearly seen. Panel displacements are in mm in all cases and represent the actual radial displacements of the panels. All data points are shown and correspond to LVDT positions. The LVDT array for each test is shown in Figure 11.2. For the purposes of the displacement profiles, positive displacements are displacements in the direction radially inwards. This is in the direction of a positive pressure load applied to the test rig. This is contrary to the usual convention for shells but is consistent with previous work on sonar domes.

All curves are plotted using a modified cubic spline fit which has the characteristic of passing through all of the data points.

11.3 Interpretation of stress results

The values of stresses in Tables 11.2 to 11.9 were obtained by processing the strain readings from each strain gauge rosette using the material properties for each panel obtained from the testing described in Chapter 8. Strain gauge rosette positions shown in Figure 11.3.

For membrane and bending stresses the following convention was adopted.

Membrane stresses - tensile membrane stresses positive

Bending stresses - tensile stress on concave surface of panel indicates positive bending stress.

11.4 Effect of addition of stiffening members to the test rig

Figures 11.4 and 11.5 show the effect on displacement of the longitudinal panel edges, of increased rig stiffening. The results shown are those obtained with the aluminium panel AL1. Very similar results were obtained with the other panels. It should be noted that even before the addition of the cross members, edge displacements were small compared with panel thickness (approx 0.35 mm in the region of the centre of the longitudinal edge at a rig pressure of 50 kPa) but subsequent stiffening reduced these displacements by a factor of approximately 10. Figures 11.6 to 11.10 show the effect of this test rig stiffening on the deflection behaviour of the panel AL1 and it can be seen that panel displacements measured on the stiffened test rig are very significantly less than those measured before the addition of the extra members.

Since it is clearly impossible to achieve a zero edge displacement condition by means of stiffening alone, this condition was attempted by means of the hydraulic jacks. For a limited number of tests, jacks were used to return the longitudinal panel edges to their initial positions after application of the load. This could only be done for the case of positive pressure loading and was very difficult to control; the difficulties being to achieve equal effect on both sides of the test rig and to avoid overcorrection.

Because of these difficulties it was not possible to conclude that the edge condition achieved with the use of jacks was nearer to the ideal fully restrained condition than that achieved without jacks. Nevertheless, a significant effect on panel behaviour was observed when the jacks were used, (see Figure 11.11). This

demonstrates the sensitivity of panel behaviour to small transverse movements of the longitudinal panel edges.

It should be noted that the Figures 11.7, 8, 9 and 11 are based on average values of displacement from pairs of LVDTs symmetrically placed about the axis of symmetry of the panel. These figures therefore illustrate only the relative effects of the increasing edge restraint and are not true displacement profiles of the panel.

Using the test rig with all stiffening members added, but without the use of the hydraulic jacks, the displacement profiles of panel AL1 are shown in Figures 11.12 to 11.14. Some asymmetry is present in these profiles particularly along the ϕ axis of the panel. The reasons for this asymmetry will be explained later.

11.5 Displacement behaviour of GRP panels

The Figures 11.15 to 11.21 summarise the displacement behaviour of panel GRP1 and similarly Figures 11.22 to 11.30 and Figures 11.31 to 11.39, the behaviour of panels GRP2 and GRP3 respectively. The sequence for each set of figures is similar and will be discussed here with reference to panel GRP1 only.

Figures 11.15 and 11.16 show the displacements measured at a selection of LVDT positions and show clearly the onset of non-linearity in the panel behaviour for both positive pressure and vacuum loading. For this panel reasonable linearity is maintained up to about 20 kPa. Figures 11.17 to 11.19 show displacement profiles along the principal panel axes at a selection of loadings and Figure 11.20 shows displacement profiles along several rows of

LVDTs at 20 kPa (highest linear load). The final figure, Figure 11.21 shows the displacement profile along the ϕ axis of the panel at both positive pressure and vacuum loading but with symmetry imposed about the X axis of the panel.

This symmetry is achieved by plotting average values from pairs of LVDTs as before.

11.6 Additional tests on Panel GRP3

11.6.1 Relaxation of edge restraint

A number of additional tests were carried out on the thickest GRP panel, GRP3. After having completed the program of tests on this panel as for the other panels with the fully stiffnened test rig, a further series of tests was done but with progressive removal of the stiffening members. These tests were carried out to confirm that the stiffening of the test rig produced similar effects in the orthotropic and isotropic cases. The displacement results for these tests are given in Figures 11.40 and 11.41.

11.6.2 Creep and Panel relaxation tests

As has been stated earlier, the duration for a typical test was 30 minutes and panels were allowed to relax for a minimum of 1 hour between tests. It was considered desirable to investigate to what extent duration of applied loading would influence panel behaviour and for how long any residual displacement would persist after removal of the load. Panel GRP3 was therefore loaded to 50 kPa and logged at 10 minute intervals for 8 hours.

The load was then removed and logging continued still at 10 minute intervals for a further 8 hours. The displacement measured at LVDT position K7 (the position of maximum displacement) is shown in Figure 11.42.

11.7 Displacement Behaviour of Panel AL2

This panel was tested for displacement only to confirm that no instability problems would be encountered. Displacement profiles along the ϕ axis of this panel are shown in Figures 11.43 and 11.44.

Although no overall instability of this panel was observed, preliminary examination of the raw data from the positive pressure test revealed an apparent step change in the displacement at LVDT position B7 at a pressure between 1 and 1.5 kPa., this step change occurring during both loading and unloading. To investigate this effect the panel was re-tested using a higher speed logging system which allowed logging of 1 LVDT at a logging rate of 25 loggings/second. Using this system the panel was loaded from 0 to 2 kPa and back to zero in 40 seconds giving 1000 logged data points. The displacement pressure plot for LVDT position B7 is shown in Figure 11.45.

This is a clear snap buckle effect localised to a small area of the panel. Examination of the panel in the area of position B7 revealed a clearly defined area of double curvature approx 3 mm deep in the region of LVDT B7. This indicates that although overall instability of a cylindrical sonar panel is not likely to be a problem, it is possible for a localised instability to occur in the region of a panel defect. This might have important implications for sonar dome design.

11.8 Discussion of test results

A number of observations can be made directly from the experimental results.

11.8.1 Deflection behaviour

The first observation concerning the deflection behaviour of the test panels is that the radial deflections were found to be very sensitive to small translational movements of the panel edges, particularly to transverse displacements of the longitudinal edges. Sensitivity to longitudinal displacements of the transverse edges was observed to be very much less.

The second observation concerns the lobed pattern of the deflection profile along the transverse (ϕ) axis of each panel. This pattern of deflection was evident on all of the panels tested but was most pronounced on the thinner panels. It was particularly pronounced on the aluminium panels, both of which were thinner than any of the GRP panels, and in the case of the very thin aluminium panel, AL2, two additional lobes were produced across the width of the panel.

A third important observation is that all of the panels tested exhibited asymmetric deflection profiles. That the GRP panels should exhibit some degree of asymmetry in behaviour was to be expected in view of the thickness, lay up, and quality variations of the material, and in general the asymmetry shown by these 3 panels was far more severe than that shown by the aluminium panel AL1 (conclusions cannot be drawn from the behaviour of AL2 in this respect because as an unformed panel its initial curvature was not uniform).

However, the panel AL1 did still show a quite marked degree of asymmetry in its deflection behaviour.

Since this panel was fabricated from rolled plate material with good dimensional control it is unlikely that property variation alone can explain this behaviour. Two other possibilities may be considered. The first is that the test rig itself was responsible for inducing the asymmetry by virtue of some inbuilt asymmetry in the rig. Whilst the test rig was designed to be axisymmetric, some slight variation in manufacture cannot be ruled out. However, it should be noted that the asymmetry exhibited by one of the GRP panels, GRP1, was in the opposite sense to that shown by the panel AL1 so if the rig was exerting some influence it was not an overriding one. The second possibility is that the asymmetry might have been induced by uneven clamping of the panel in the rig. This seems more likely even though every effort was made to ensure that all bolts were tightened to the same torque. When the panel AL1 was removed from the rig and then refitted the same asymmetry was present.

The conclusion that must be drawn from this is that although some slight non-uniformity of either panel or constraint must be responsible for the asymmetry the geometry of the test panel is very sensitive to such influence. The sensitivity of panel behaviour to the restraint of the longitudinal edges has already been demonstrated. This is discussed further in Chapter 15.

As a final observation on the general deflection results it can be seen that all panels exhibited an initial phase of linear behaviour before the onset of quite complicated non-linear behaviour, involving the structure softening in some regions and appearing to harden in others, in no case was any tendency to instability encountered with panels AL1 or the GRP panels. The interesting snap buckle incident, encountered with panel AL2, was a very localised effect, being confined to an area of panel which was clearly non-uniform, and in fact had a double curvature. This incident does illustrate however, as mentioned before, that with an imperfect panel localised snap buckling is possible, and might have important implications for sonar dome design.

11.8.2 Panel stresses

Examination of the stress results for the test panels reveals that the major contribution to panel stress near the centre of each panel is membrane action. This is as would be expected for pressure loading of shells of this geometry.

For all tests a fairly uniform state of membrane stress (compressive for positive pressure load and tensile for vacuum load) was evident over most of the centre area of each panel; in all cases the stresses in the ϕ direction (hoop stresses) being significantly greater than those in the longitudinal direction.

Bending stresses, although significantly smaller in all cases than membrane stresses showed much greater variation over the area of the panels.

This variation of bending stress is certainly significant for the overall panel behaviour and ultimately for panel failure.

The main implication of these observations is that any analysis of the panel behaviour must take account of both bending and membrane actions even though membrane action would seem to be predominant. For finite element analysis for example, a combined membrane and bending element is appropriate whereas a simple membrane element is not.

11.9 Concluding Remarks

The above observations are based on the experimental results alone. More detailed observations concerning particularly the observed asymmetric behaviour, the sensitivity to edge condition and the implications for design of sonar domes are made later in the light of the numerical and finite element analysis presented in the following chapters.

Test No.	Panel	Load Profile (kPa)	Test Type (See Key to table)	Logging LVDTs	SGs	Comments
01	AL1	0 +50 0(Step 10)	S	D1	-	Leak Test - No leaks
02	AL1	0 +50 0(Step 10)	T	D1	-	1st Test
03	AL1	0 +100 0(Step 10)	S	D2	-	Set Test, extra LVDTs
04	AL1	0 +100 0(Step 10)	T	D2	-	Test
05	AL1	0 +100 0(Step 10)	C	D2	-	Confirmation Test
06	AL1	0 +50 (Step 10)	T	D3	-	Half Plate Scan (Col 6)
07	AL1	0 +50 (Step 10)	T	D3	-	Half Plate Scan (Col 5)
08	AL1	0 +50 (Step 10)	T	D3	-	Half Plate Scan (Col 4)
09	AL1	0 +50 (Step 10)	T	D3	-	Half Plate Scan (Col 3)
10	AL1	0 +50 (Step 10)	T	D3	-	Half Plate Scan (Col 2)
11	AL2	0 +2 (Step 0.5)	S	D2	-	Leak Test - No leaks
12	AL2	0 -5 0 (Step 0.5)	T	D2	-	
13	AL2	0 +3 0 (Step 0.5)	T	D2	-	
14	AL2	0 +3.5 0(Step 0.5)	T	D2	-	Local snap buckle
15	AL1	0 +60 (Step 5)	S	D2	S1	Strain Gauges fitted
16	AL1	0 +60 0 (Step 5)	T	D2	S1	
17	AL1	0 +60 0 (Step 5)	C	D2	S1	
18	AL1	0 -60 0 (Step 5)	S	D2	S1	
19	AL1	0 -60 0 (Step 5)	T	D2	S1	No confirmation test
20	AL1	0 +50 0 (Step 10)	T	D2	S1	Set prior to test. 2 Cross Stiffeners fitted
21	AL1	0 +50 0 (Step 10)	C	D2	S1	
22	AL1	0 +50 0 (Step 10)	T	D4	S1	2 LVDTs added
23	AL1	0 -50 0 (Step 10)	T	D4	S1	Set prior to test
24	AL1	0 -50 0 (Step 10)	C	D4	S1	
25	AL1	0 +50 0 (Step 10)	S	D4	S2	SGs repaired & added. Seal modified 2 extra Cross Stiffeners
26	AL1	0 +50 0 (Step 10)	T	D4	S2	
27	AL1	0 +50 0 (Step 10)	C	D4	S2	
28	AL1	0 -50 0 (Step 10)	S	D4	S2	
29	AL1	0 -50 0 (Step 10)	T	D4	S2	
30	AL1	0 -50 0 (Step 10)	C	D4	S2	
31	AL1	0 -50 0 (Step 10)	S	D5	S2	2 Longitudinal Stiffeners added. Revised LVDT chans.
32	AL1	0 -50 0 (Step 10)	T	D5	S2	
33	AL1	0 -50 0 (Step 10)	C	D5	S2	
34	AL1	0 +50 0 (Step 10)	S	D5	S2	
35	AL1	0 +50 0 (Step 10)	T	D5	S2	
36	AL1	0 +50 0 (Step 10)	C	D5	S2	
37	AL1	0 +50 (Manual)	T	D5	S2	Side Jacks operated at 20kPa & 50kPa
38	AL1	0 +50 (Manual)	T	D5	S2	Side Jacks operated at 50kPa
39	AL1	0 +100 0(Step 10)	S	D5	S2	
40	AL1	0 +100 0(Step 10)	T	D5	S2	
41	AL1	0 +50 0 (Step 10)	T	D5	S2	Rig evacuated to -90kPa with centre bolts loose. Bolts tightened before +ve pressure test
42	AL1	0 +50 (Manual)	S	D5	S2	Side Jacks operated at 10,20,30,40,50kPa
43	AL1	0 +50 (Manual)	T	D5	S2	As Test 42
44	AL1	0 +50 (Manual)	C	D5	S2	As Test 42
45	GRP2	0 -25 (Step 5)	S	D5	S3	
46	GRP2	0 -25 (Step 5)	T	D5	S3	
47	GRP2	0 -25 (Step 5)	C	D5	S3	
48	GRP2	0 -50 0 (Step 5)	S	D5	S3	
49	GRP2	0 -50 0 (Step 5)	T	D5	S3	
50	GRP2	0 -50 0 (Step 5)	C	D5	S3	
51	GRP2	0 +25 0 (Step 5)	S	D5	S3	
52	GRP2	0 +25 0 (Step 5)	T	D5	S3	
53	GRP2	0 +25 0 (Step 5)	C	D5	S3	
54	GRP2	0 +50 0 (Step 5)	S	D5	S3	
55	GRP2	0 +50 0 (Step 5)	T	D5	S3	
56	GRP2	0 +50 0 (Step 5)	C	D5	S3	
57	GRP2	0 +50 (Manual)	T	D5	S3	Side Jacks operated at 10,20,30,40,50kPa
58	GRP2	0 +50 (Manual)	C	D5	S3	As Test 57 Reversed jack heads

Table 11.1 List of Panel Tests cont.

Test No.	Panel	Load Profile (kPa)	Test Type (See Key to table)	Logging LVDTs	Logging SGs	Comments
59	GRP2	0 -50 (Creep)	T	D5	S3	Creep test at -50kPa for >1hr 30min. Set to -50kPa prior to test
60	GRP2	0 -94 0 (Step 10)	T	D5	S3	Max. vacuum
61	GRP1	0 -25 (Step 5)	S	D5	S3	
62	GRP1	0 -25 (Step 5)	T	D5	S3	
63	GRP1	0 -25 (Step 5)	C	D5	S3	
64	GRP1	0 -50 0 (Step 5)	S	D5	S3	
65	GRP1	0 -50 0 (Step 5)	T	D5	S3	
66	GRP1	0 -50 0 (Step 5)	C	D5	S3	
67	GRP1	0 +25 (Step 5)	S	D5	S3	
68	GRP1	0 +25 (Step 5)	T	D5	S3	
69	GRP1	0 +25 (Step 5)	C	D5	S3	
70	GRP1	0 +45 (Step 5)	S	D5	S3	Increasing non-linearity beyond 40kPa
71	GRP1	0 +40 0 (Step 5)	T	D5	S3	
72	GRP1	0 +40 0 (Step 5)	C	D5	S3	
73	GRP1	0 +25 0 (Manual)	T	D5	S3	Side jacks operated and released at 25kPa
74	GRP1	0 +40 (Manual)	T	D5	S3	Stability test at set loads
75	GRP1	0 -70 (Manual)	-	D5	S3	PR Test
76	GRP3	0 -25 (Step 5)	S	D5	S3	No unexpected behaviour
77	GRP3	0 -50 0 (Step 5)	S	D5	S3	
78	GRP3	0 -50 0 (Step 5)	T	D5	S3	
79	GRP3	0 -50 0 (Step 5)	C	D5	S3	
80	GRP3	0 -92 0 (Step 10)	S	D5	S3	Max. vacuum set
81	GRP3	0 -92 0 (Step 10)	T	D5	S3	
82	GRP3	0 -92 0 (Step 10)	C	D5	S3	
83	GRP3	0 +50 (Step 5)	S	D5	S3	
84	GRP3	0 +50 0 (Step 5)	T	D5	S3	
85	GRP3	0 +50 0 (Step 5)	C	D5	S3	
86	GRP3	0 +25 0 (Manual)	T	D5	S3	Side jacks operated at 25kPa
87	GRP3	0 +50 0 (Manual)	T	D5	S3	Side jacks operated at 50kPa
88	GRP3	0 -50 0 (Step 5)	S	D5	S3	Check instrumentation after period of non-use
89	GRP3	0 -50 0 (Step 5)	T	D5	S3	As Test 88
90	GRP3	0 -50 0 (Hold)	T	D5	S3	Creep test 8hr at -50kPa and 8hr recovery
91	GRP3	0 (Hold)	T	D5	S3	16hr instrumemt stability check.
92	GRP3	0 +50 0 (Step 5)	T	D5	S3	All stiffening bars in place. Set prior to test
93	GRP3	0 +50 0 (Step 5)	T	D5	S3	Longitudinal stiffeners removed
94	GRP3	0 +50 0 (Step 5)	C	D5	S3	As Test 93
95	GRP3	0 +50 0 (Step 5)	T	D5	S3	Outside cross stiffeners removed
96	GRP3	0 +50 0 (Step 5)	C	D5	S3	As Test 95
97	GRP3	0 +50 0 (Step 5)	T	D5	S3	Inside cross stiffeners removed
98	GRP3	0 +50 0 (Step 5)	C	D5	S3	As Test 97

Table 11.1(continued) List of Panel Tests

Key to Table:

Test type - *S = Set test, T = Test, C = Confirmation test*

Logging (LVDTs) - *D1 = 9LVDTs*
D2 = 19LVDTs
(See Fig 11.1) *D3 = 11LVDTs (Half plate scan)*
D4 = 21LVDTs
D5 = 21LVDTs (Some LVDTs exchanged for more suitable types. LVDTs recalibrated)

Logging (SGs) - *S1 = 18 x 2 gauge rosettes (2 gauges faulty)*
S2 = 21 x 2 gauge rosettes
(See Fig 11.2) *S3 = 6 x 2 gauge rosettes*

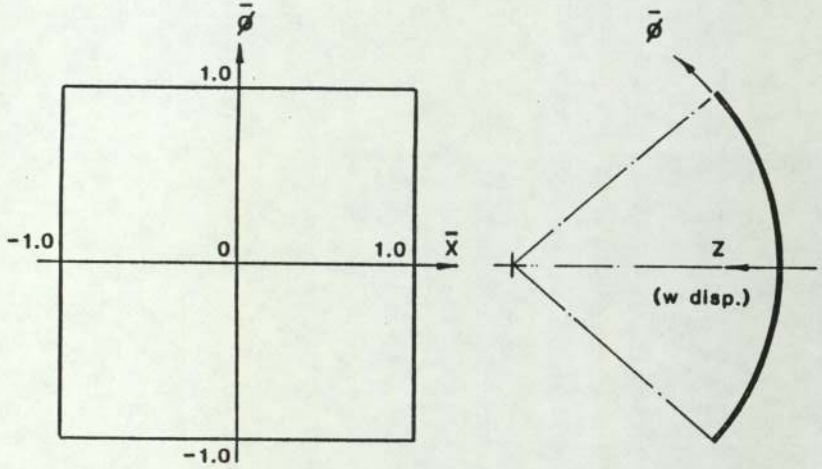

Fig. 11.1 Coordinate axes of cylindrical panels

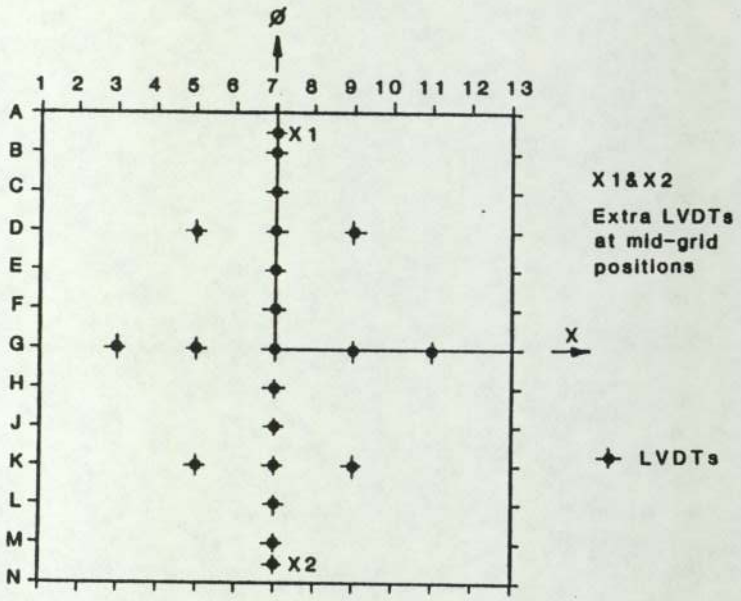

Fig. 11.2 Positions of LVDT's on experimental panels

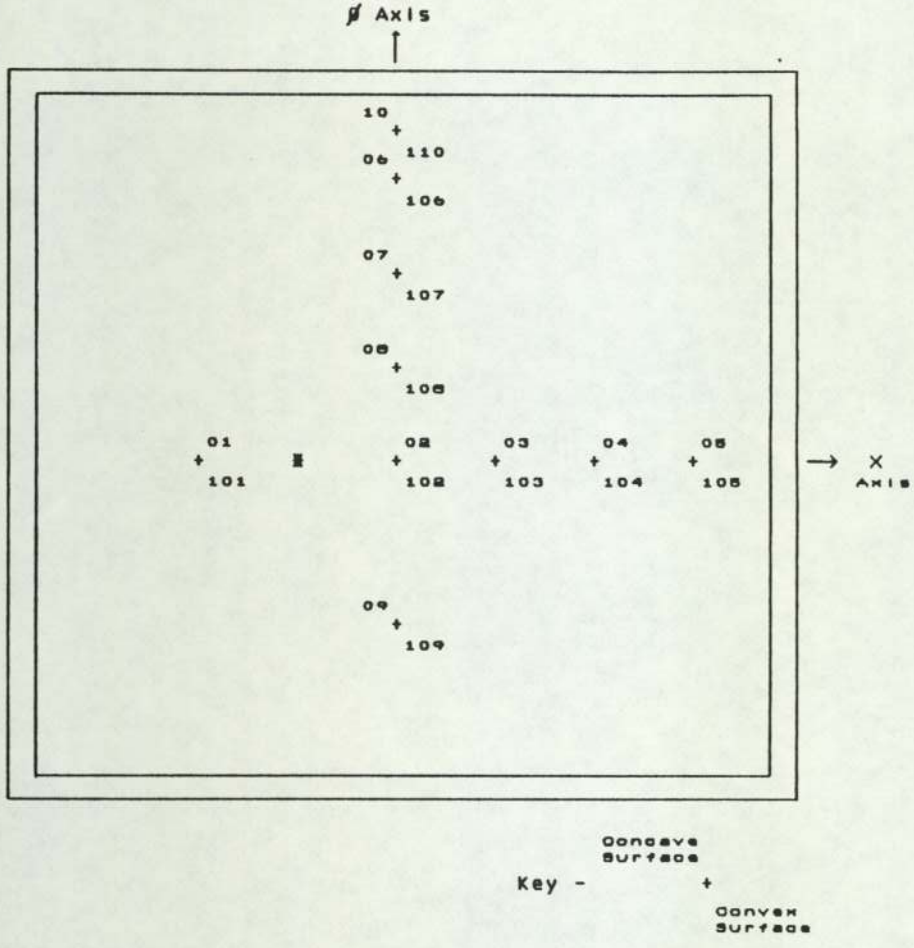

Notes: 1) AL1 Rosettes installed at all positions shown.
‡ denotes off-axis rosette, concave surface.
2) GRP1, 2 & 3 Rosettes installed at the following positions:
Concave Surface - 02, 04, 07
Convex Surface - 102, 104, 107

Fig. 11.3 Positions of Strain gauge rosettes on experimental panels

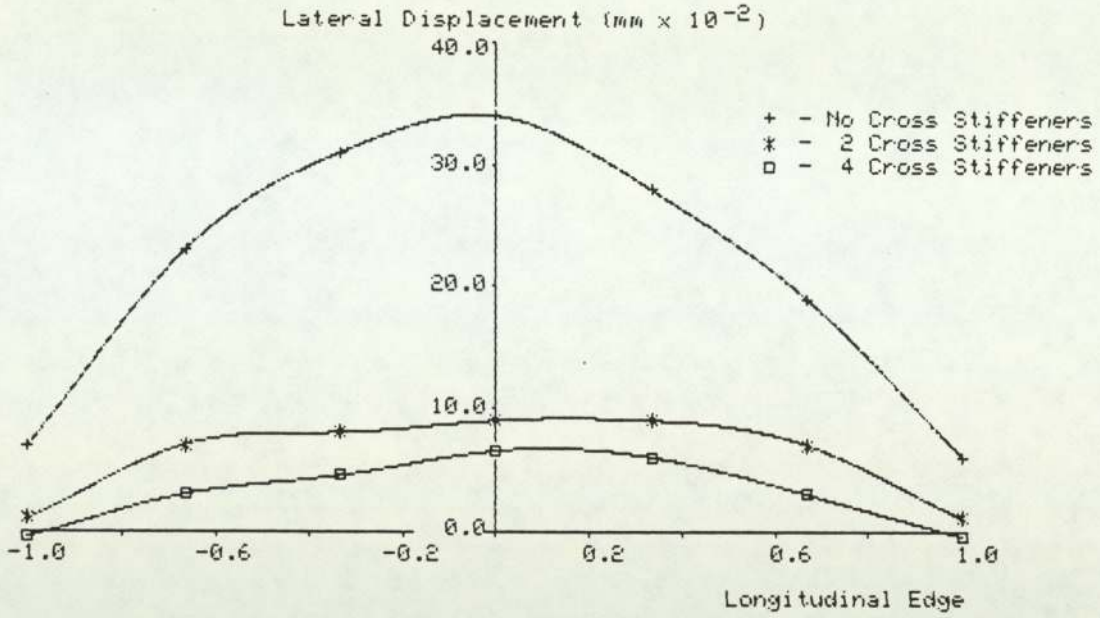

Fig. 11.4 Lateral edge displacements along longitudinal edge of test rig at a positive pressure of 50kPa

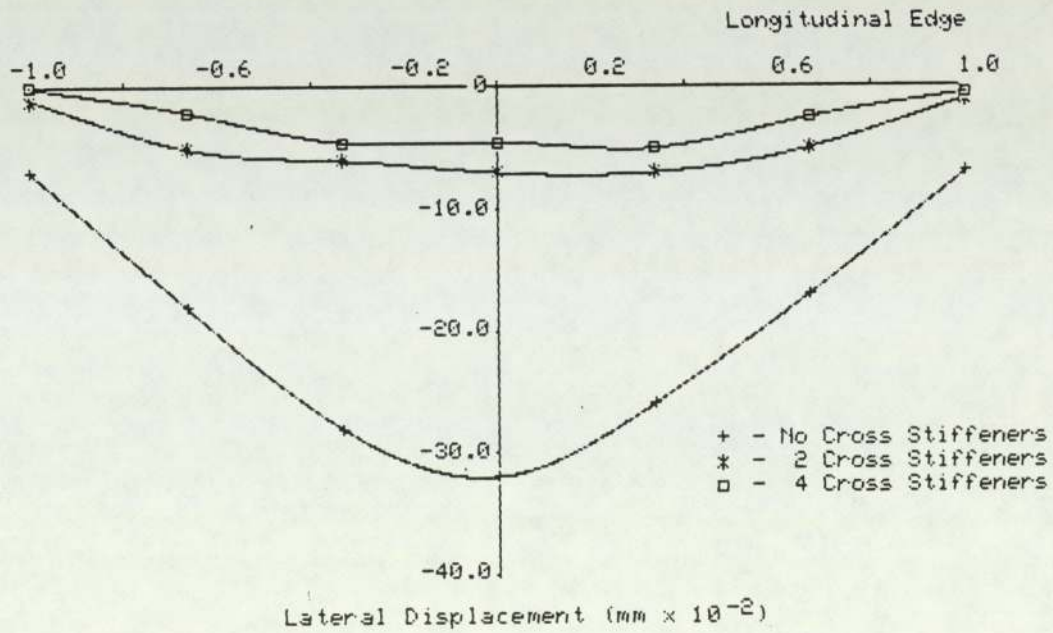

Fig. 11.5 Lateral edge displacements along longitudinal edge of test rig at a negative pressure of 50kPa

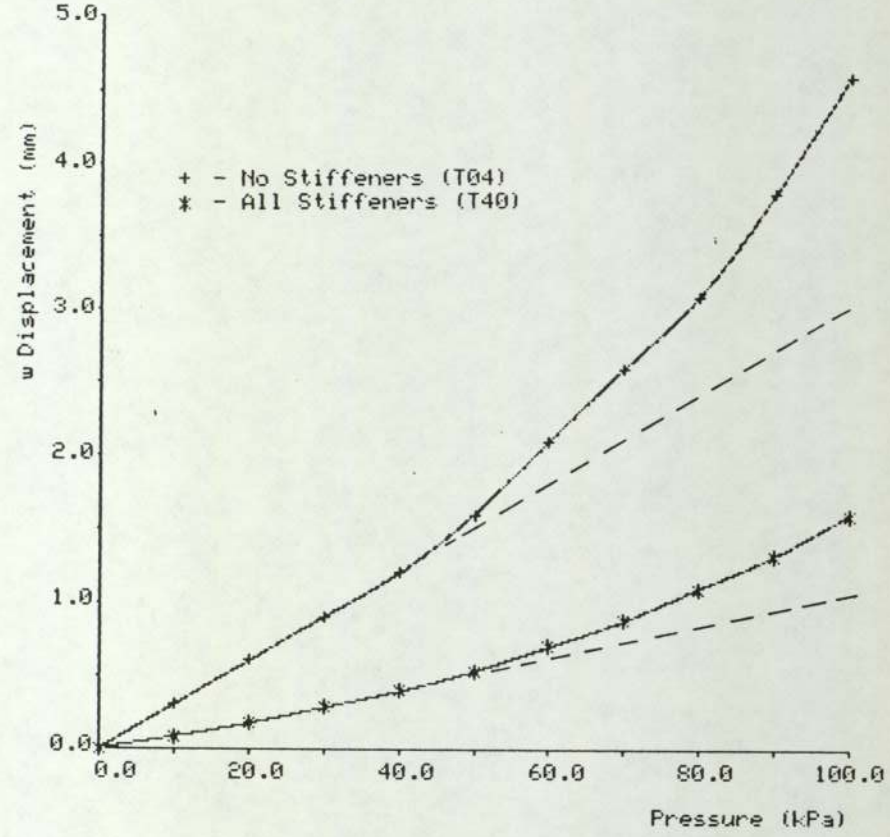

Fig. 11.6 Displacements at LVDT position D7 showing onset and form of non linear behaviour for panel AL1 (6.4mm Aluminium)

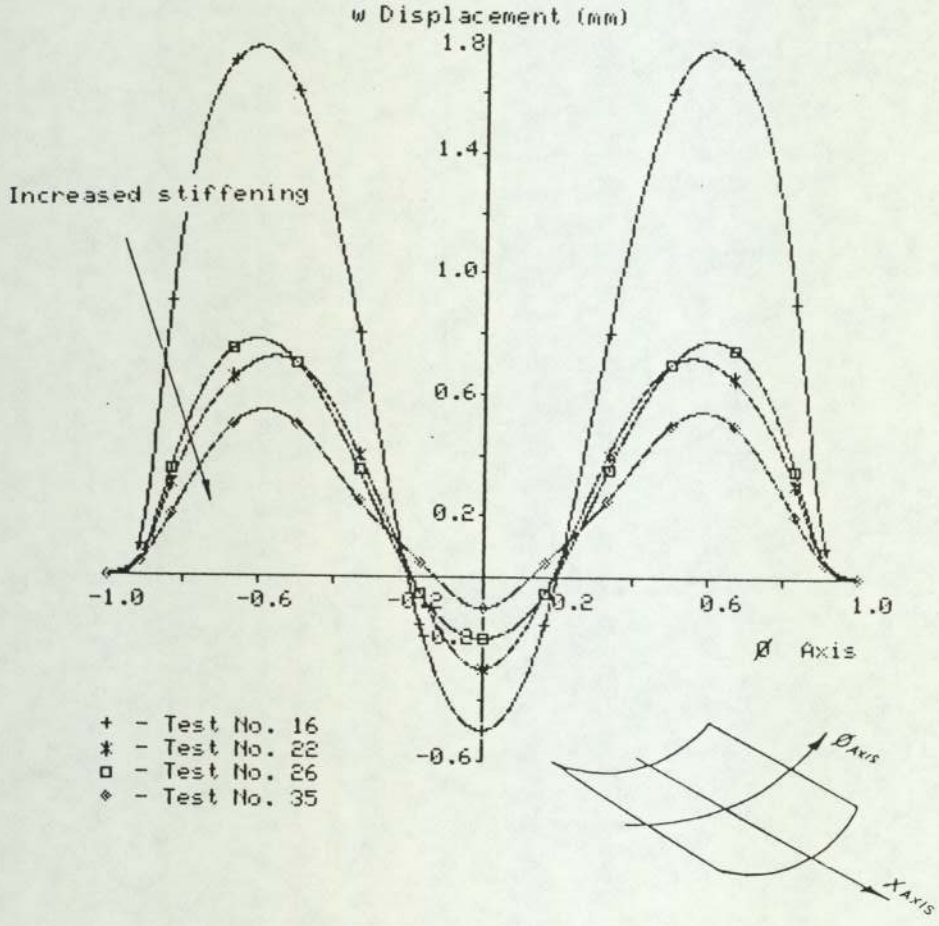

Fig. 11.7 Displacements along the Ø axis for panel AL1 showing the effect of increased rig stiffening (Positive pressure loading 50kPa)

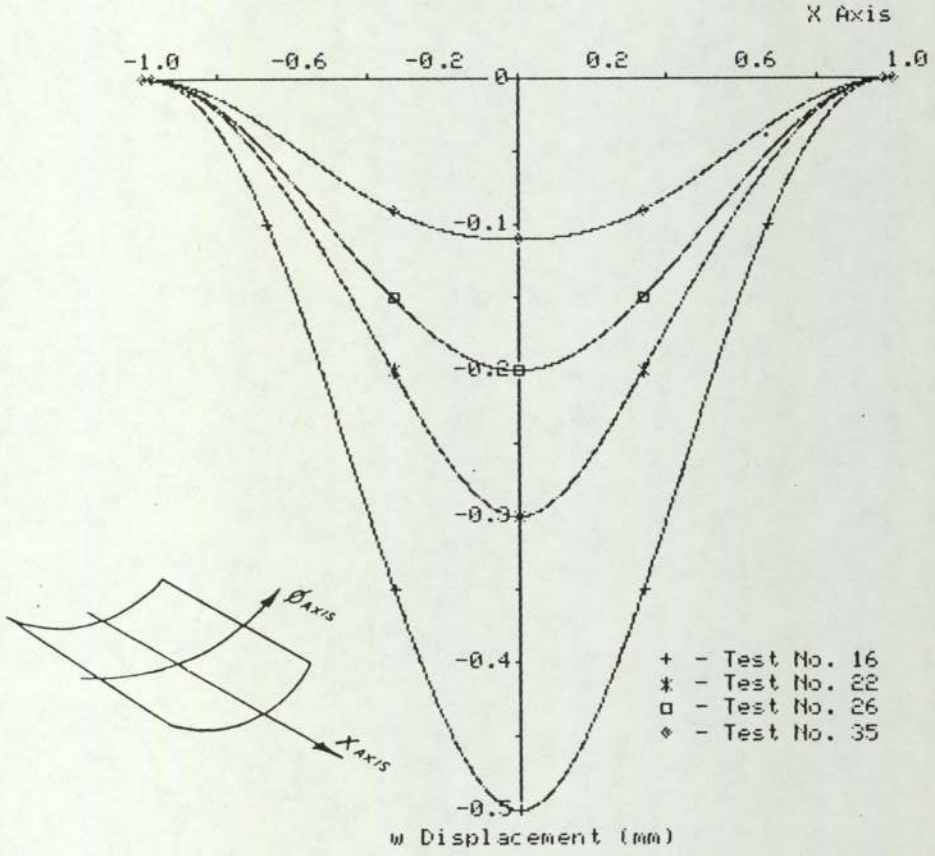

Fig. 11.8 Displacements along the X axis for panel AL1 showing the effect of increased rig stiffening (Positive pressure loading 50kPa)

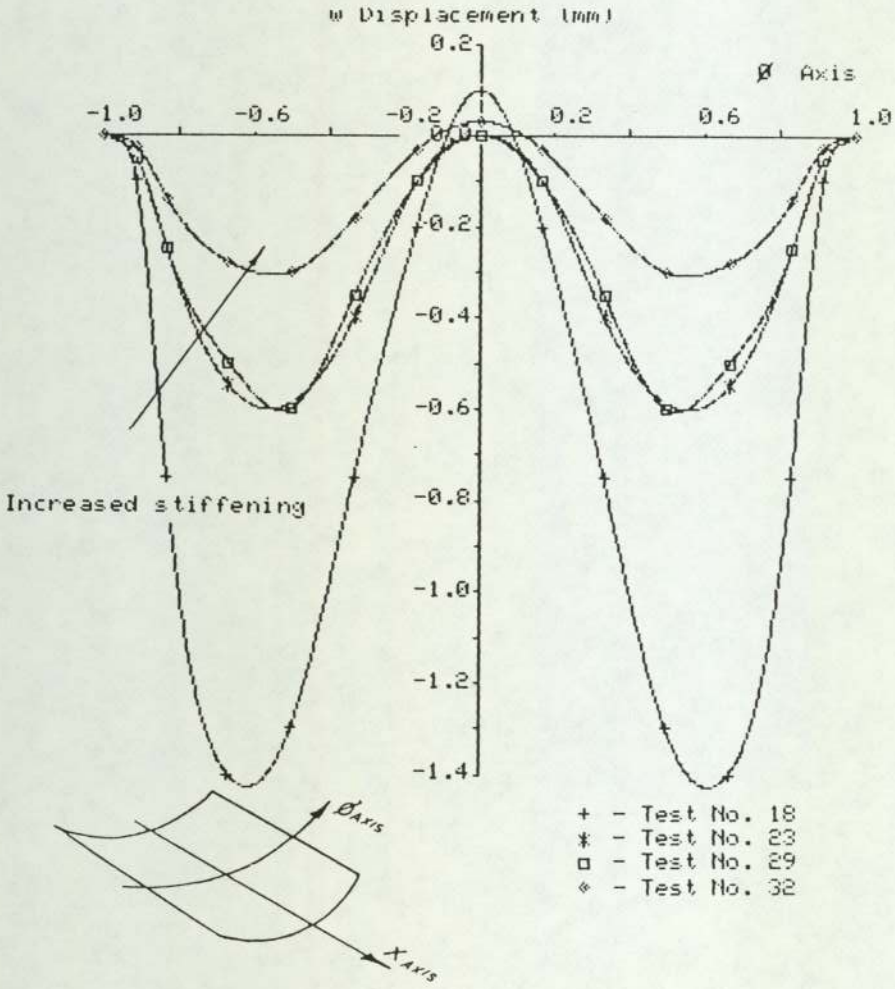

Fig. 11.9 Displacements along the Ø axis for panel AL1 showing the effect of increased rig stiffening (Negative pressure loading 50kPa)

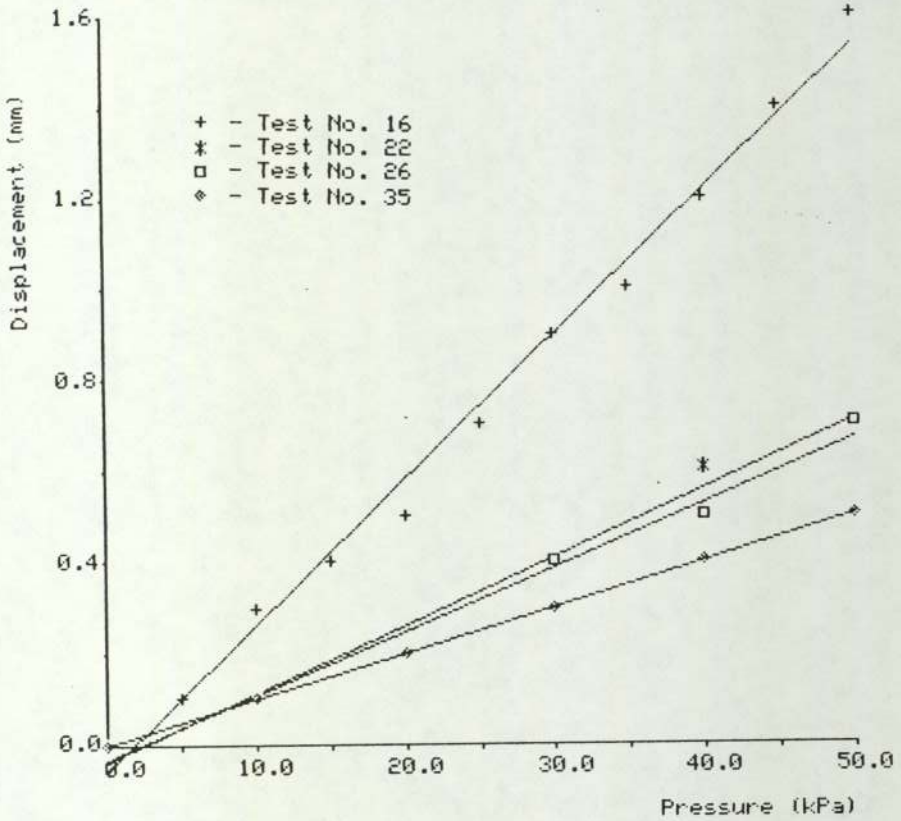

Fig. 11.10 Displacement at LVDT position D7 for panel AL1 showing the effect of increased rig stiffening with increasing positive pressure loading

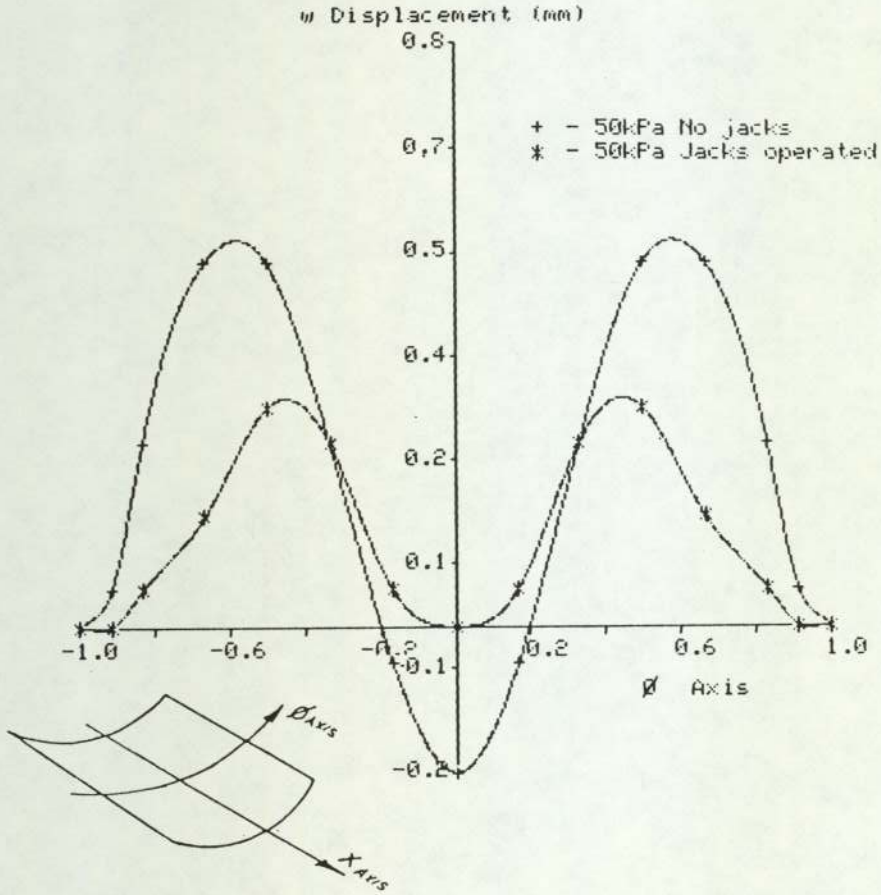

Fig. 11.11 Effect of operation of side jacks on displacements along the Ø axis of panel AL1 at a positive pressure of 50kPa (Test No.38)

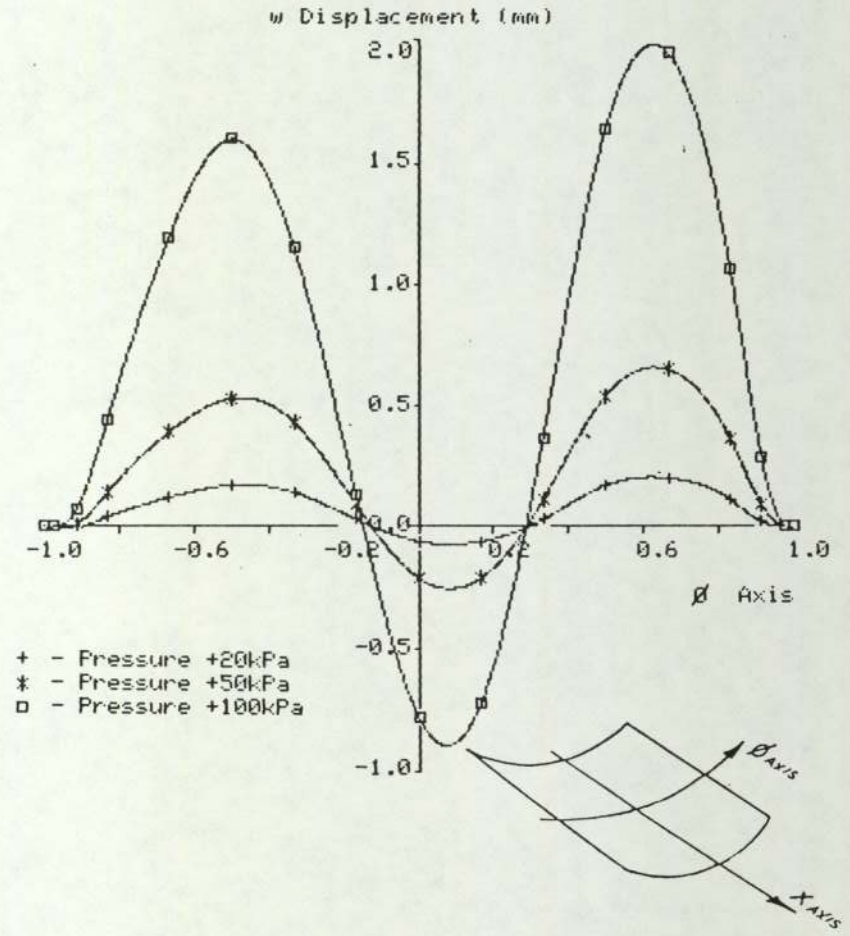

Fig. 11.12 Displacement along the Ø axis of panel AL1 showing development of asymmetric behaviour (Positive pressure loading)

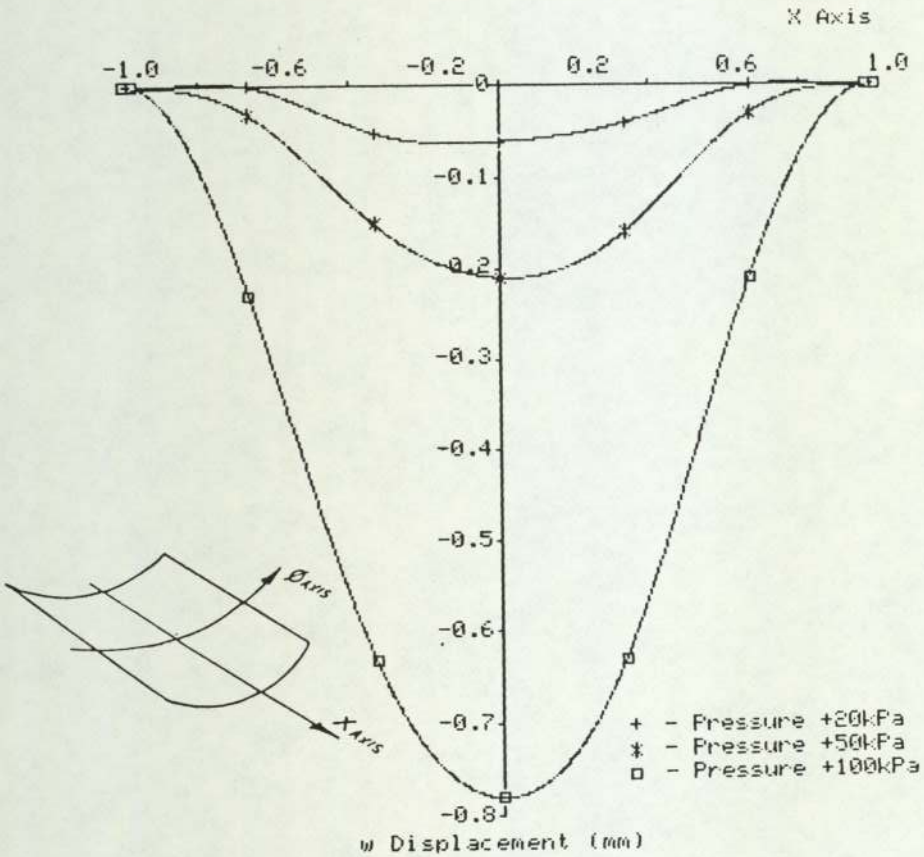

Fig. 11.13 Displacement along the X axis of panel AL1 showing development of asymmetric behaviour (Positive pressure loading)

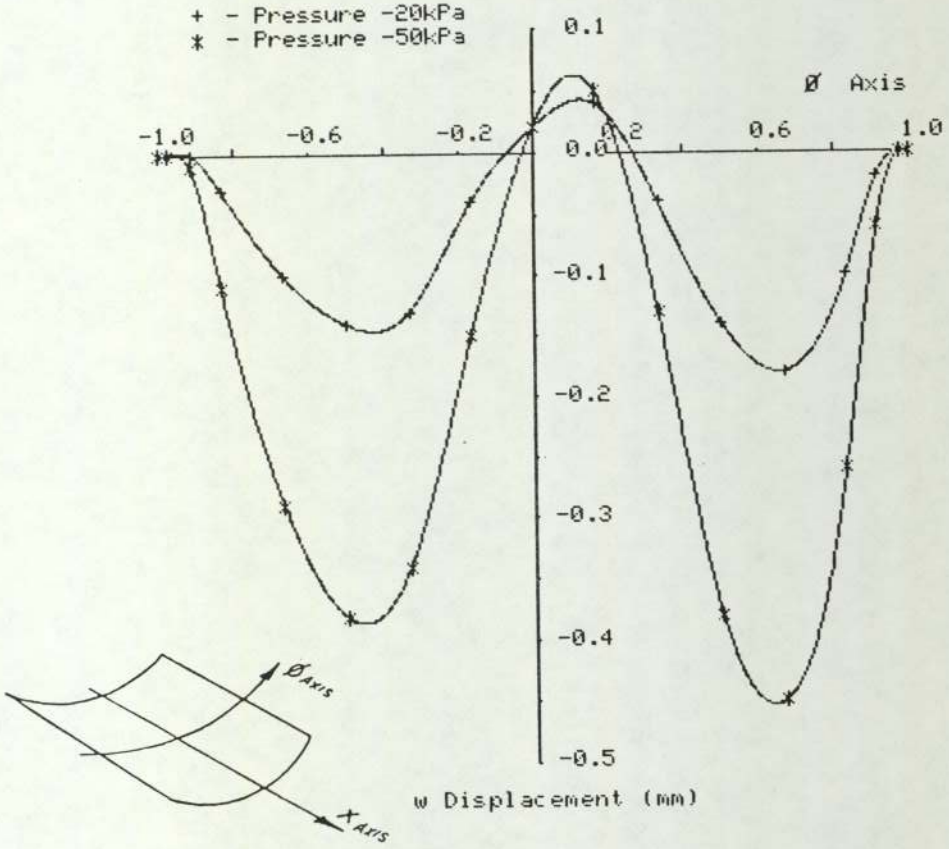

Fig. 11.14 Displacement along the Ø axis of panel AL1 showing development of asymmetric behaviour (Negative pressure loading)

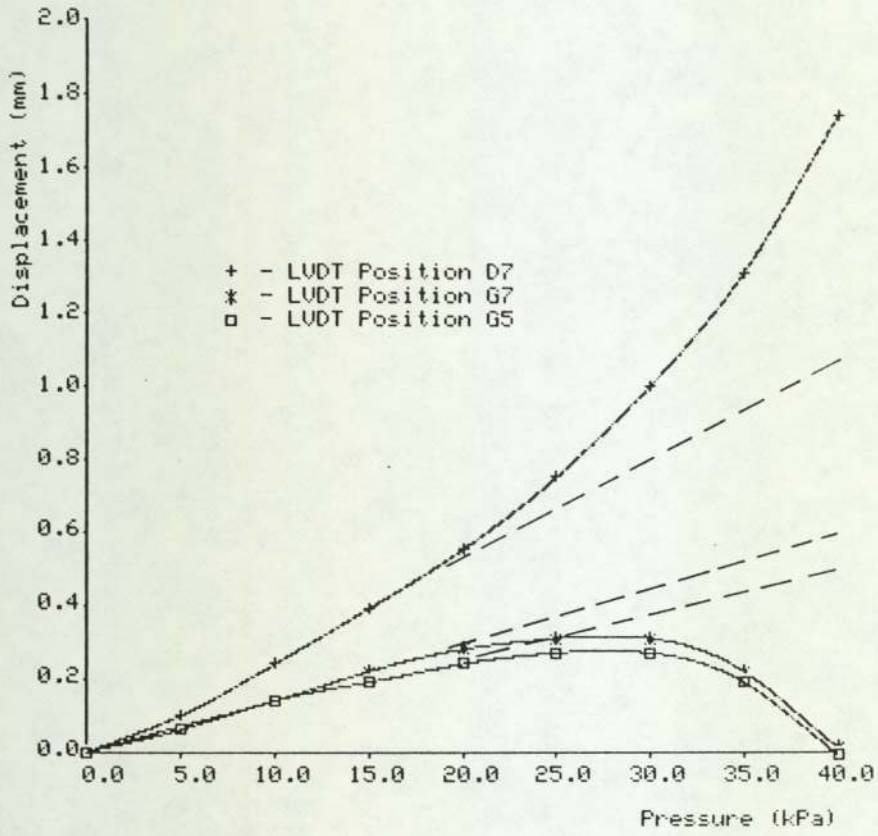

Fig. 11.15 Displacement at LVDT positions D7,G7 & G5 for panel GRP1 subject to positive pressure loading showing onset of nonlinear behaviour (Test No.71)

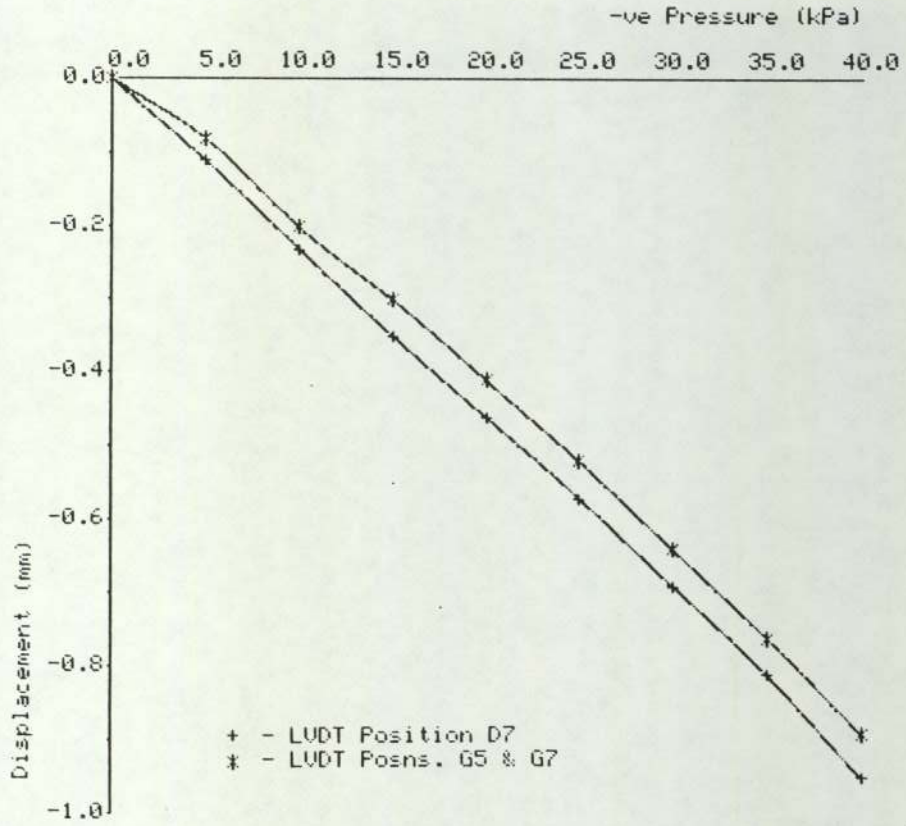

Fig. 11.16 Displacement at LVDT positions D7,G7 & G5 for panel GRP1 subject to negative pressure loading showing onset of nonlinear behaviour (Test No.65)

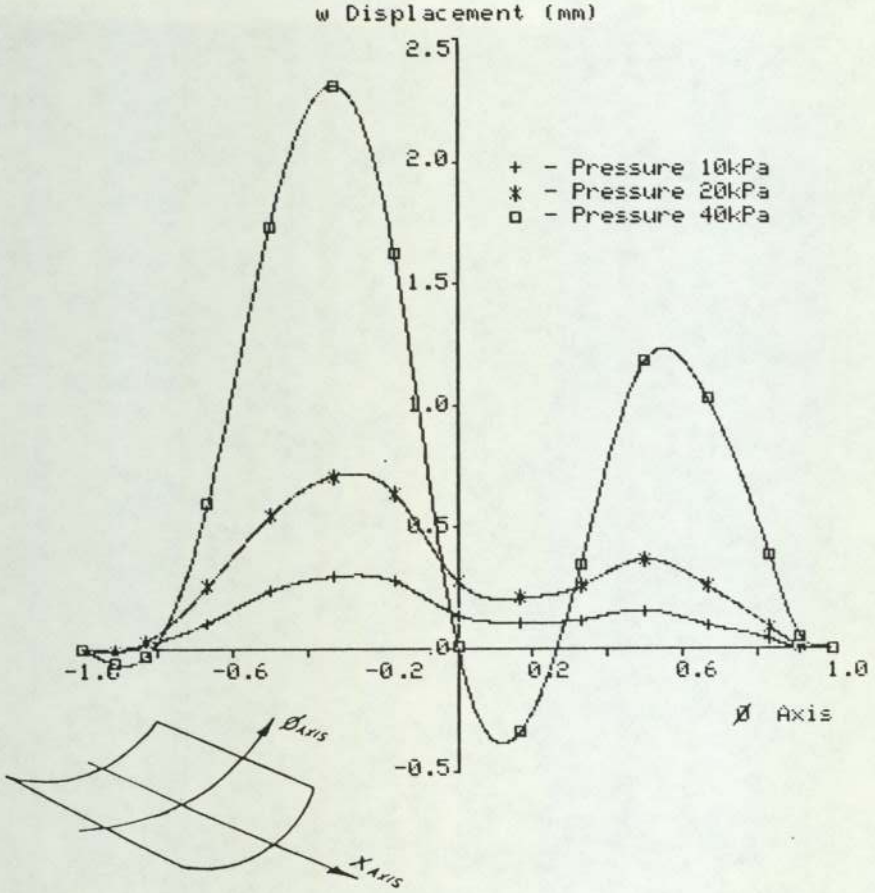

Fig. 11.17 Displacement along the Ø axis of panel GRP1 showing development of asymmetric behaviour (Positive pressure loading)

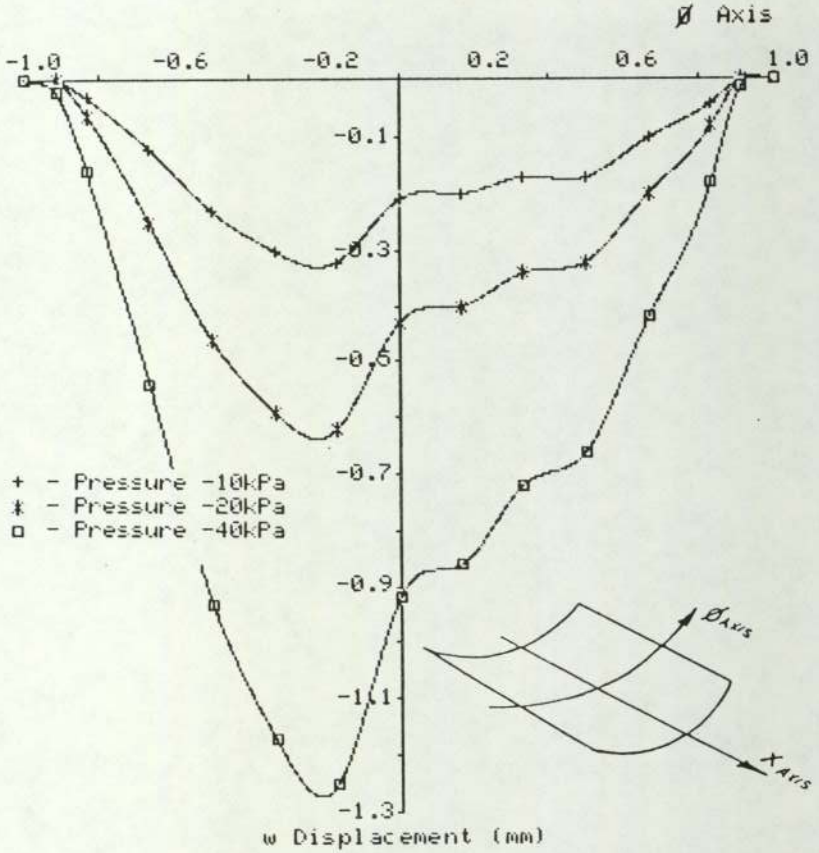

Fig. 11.18 Displacement along the Ø axis of panel GRP1 showing development of asymmetric behaviour (Negative pressure loading)

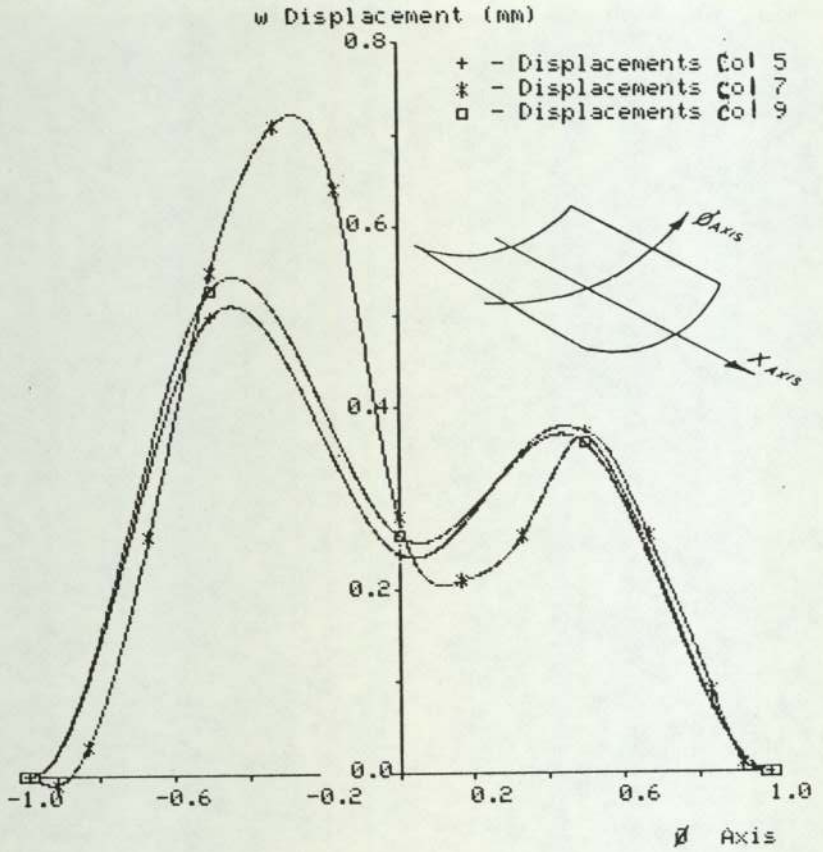

Fig. 11.19 Displacement of panel GRP1 along LVDT columns 5,7 & 9 at a positive pressure of 20kPa (Test No.71)

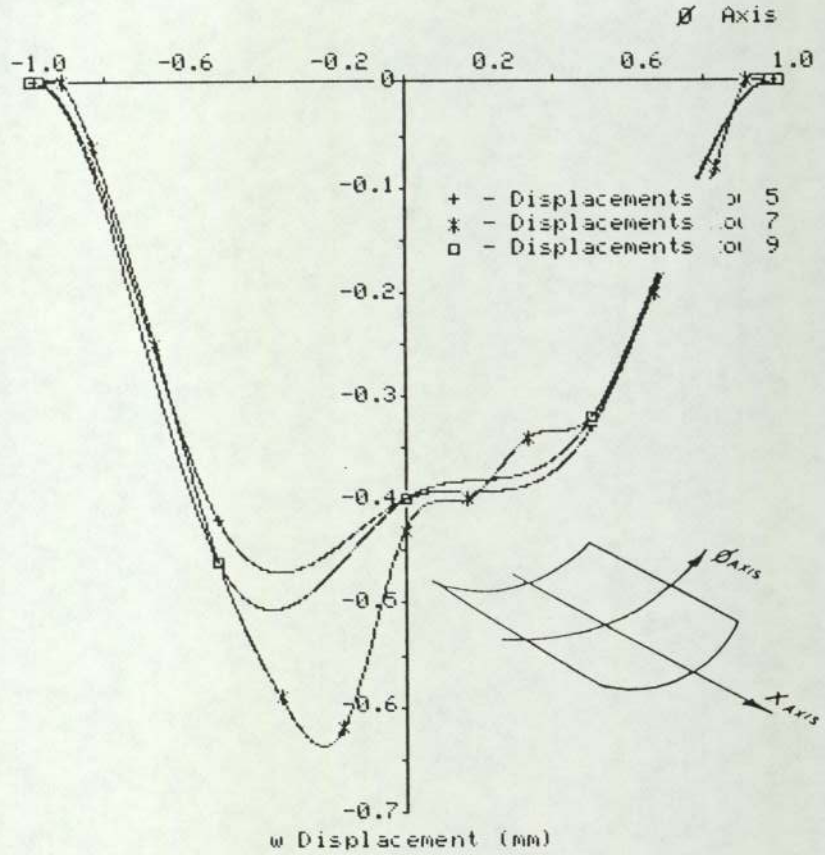

Fig. 11.20 Displacement of panel GRP1 along LVDT columns 5,7 & 9 at a negative pressure of 20kPa (Test No.65)

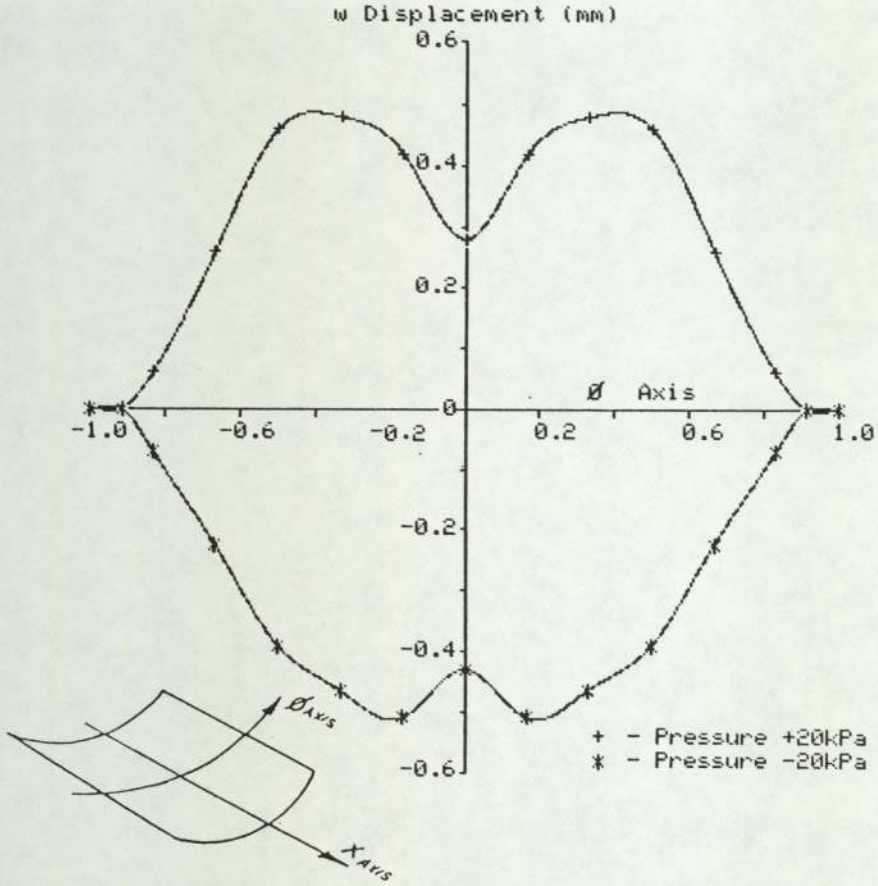

Fig. 11.21 Displacement of panel GRP1 along Ø axis at +20kPa and -20kPa. (Symmetry forced about X axis)

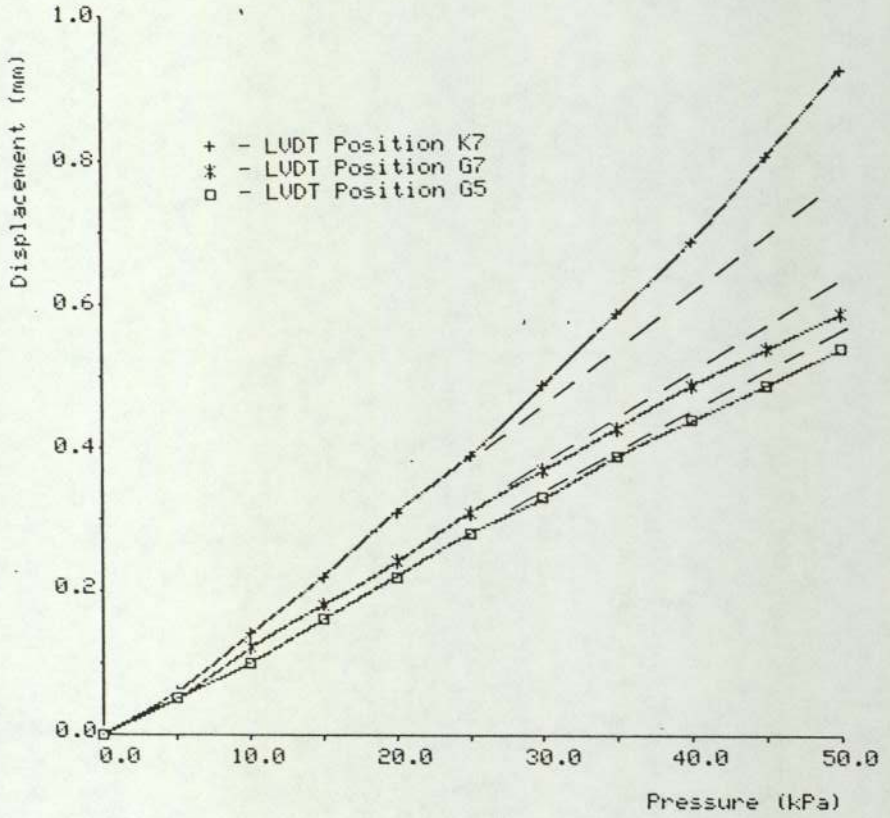

Fig. 11.22 Displacement at LVDT positions D7,G7 & G5 for panel GRP2 subject to positive pressure loading showing onset of nonlinear behaviour

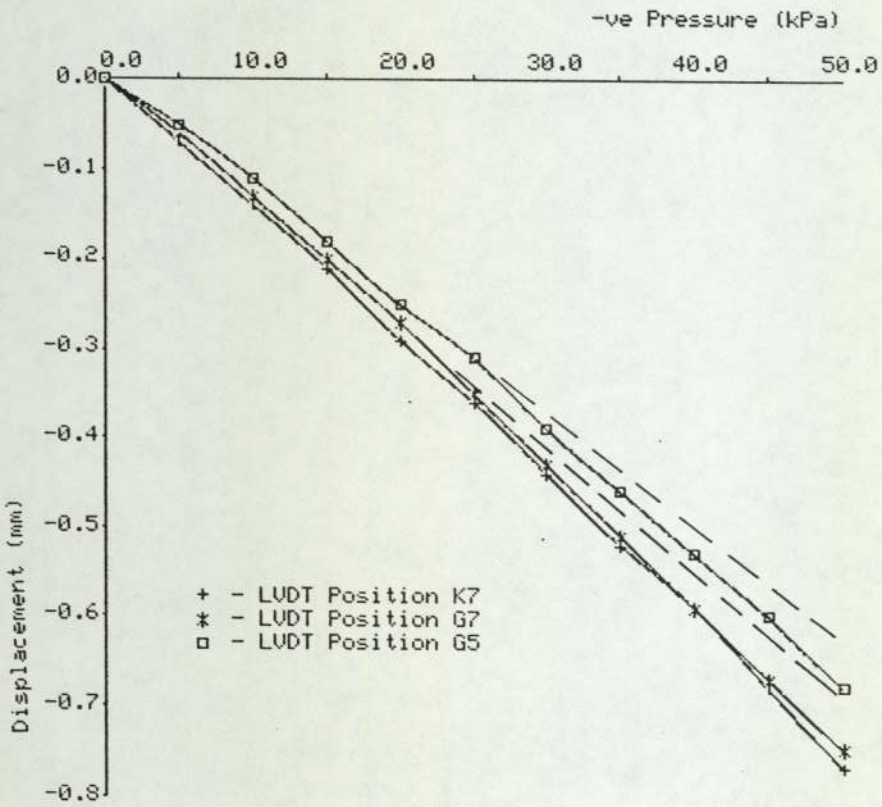

Fig. 11.23 Displacement at LVDT positions D7,G7 & G5 for panel GRP2 subject to negative pressure loading showing onset of nonlinear behaviour (Test No.49)

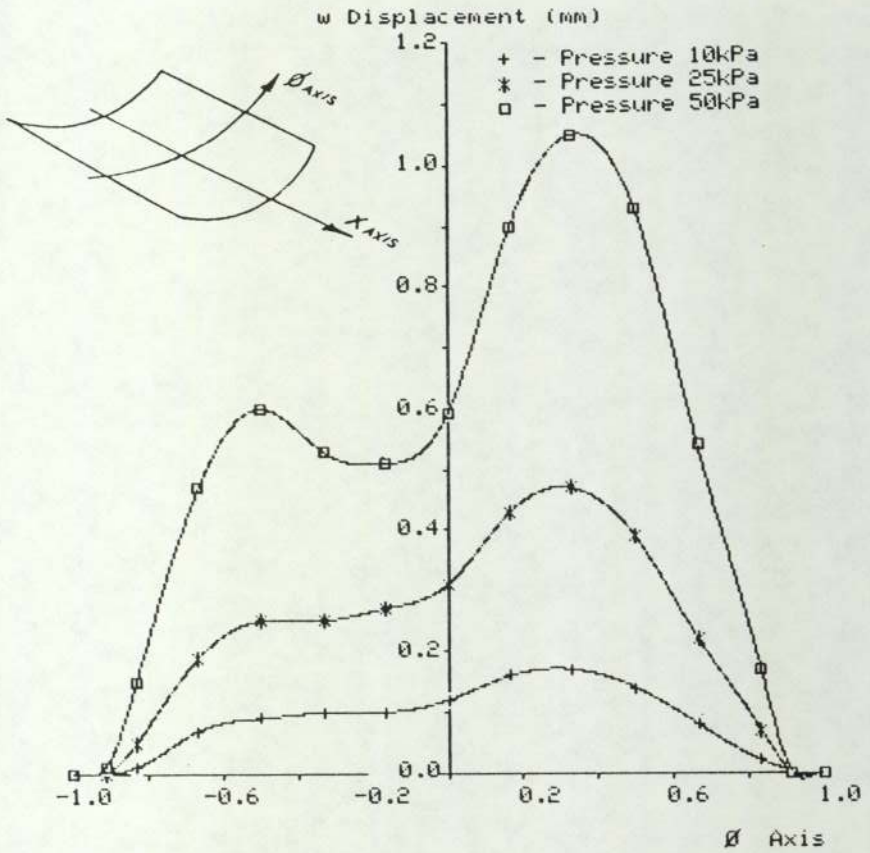

Fig. 11.24 Displacement along the Ø axis of panel GRP2 showing development of asymmetric behaviour (Positive pressure loading)

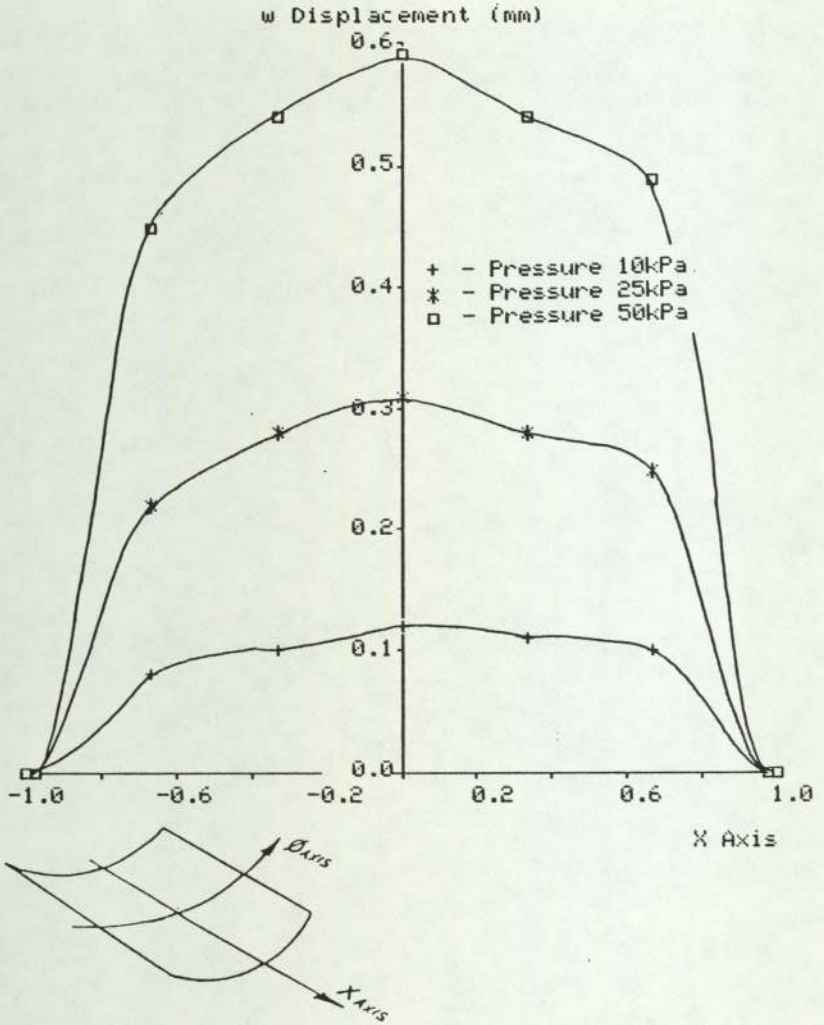

Fig. 11.25 Displacement along the X axis of panel GRP2 showing development of asymmetric behaviour (Positive pressure loading)

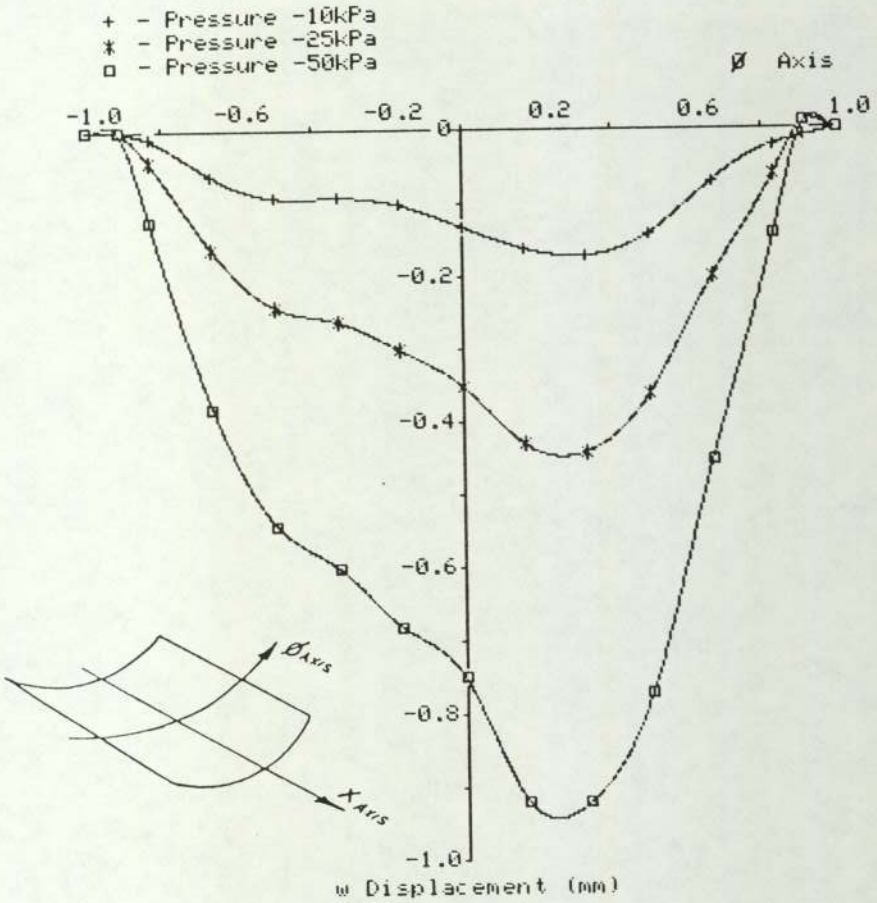

Fig. 11.26 Displacement along the Ø axis of panel GRP2 showing development of asymmetric behaviour (Negative pressure loading)

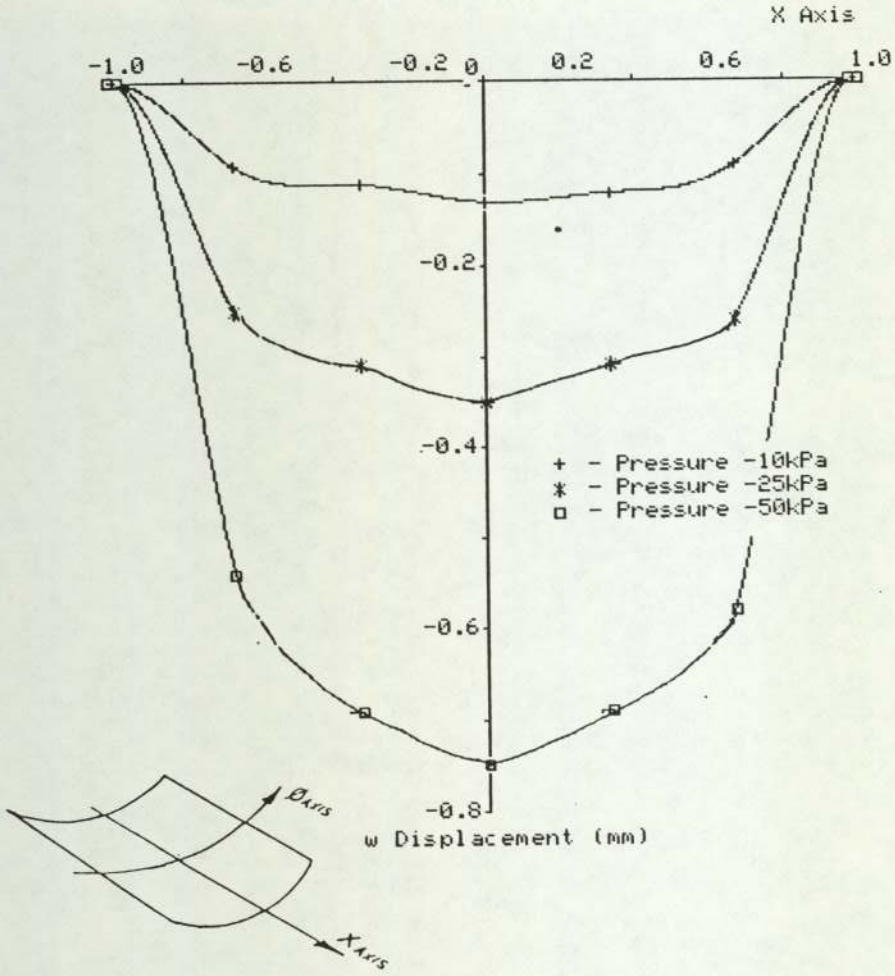

Fig. 11.27 Displacement along the X axis of panel GRP2 showing development of asymmetric behaviour (Negative pressure loading)

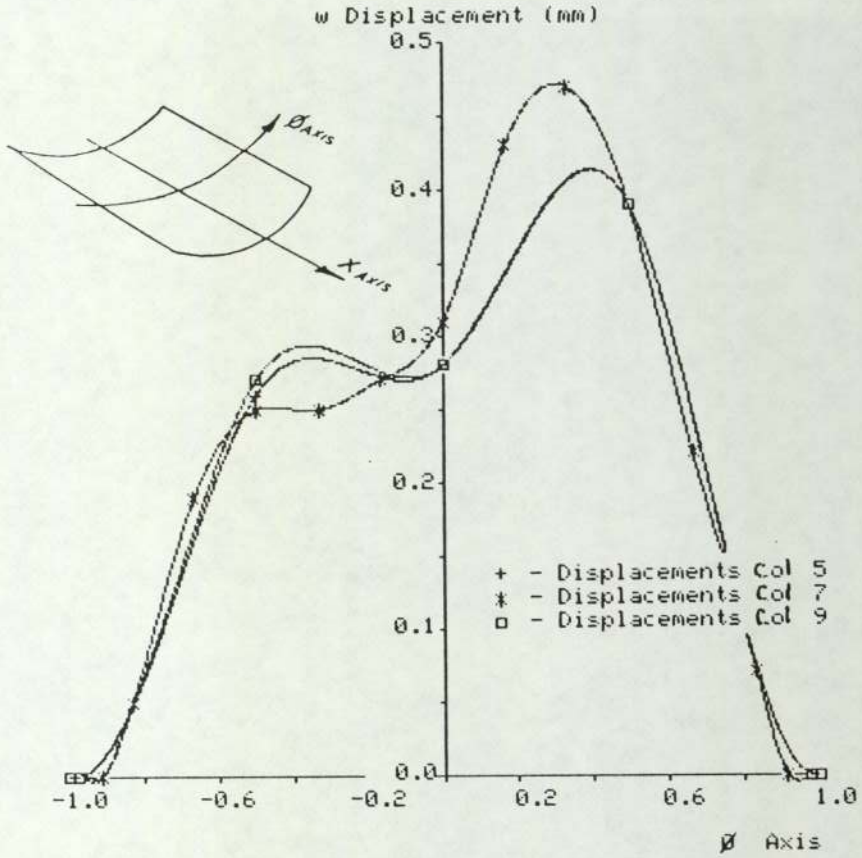

Fig. 11.28 Displacement of panel GRP2 along LVDT columns 5,7 & 9 at a positive pressure of 25kPa (Test No.55)

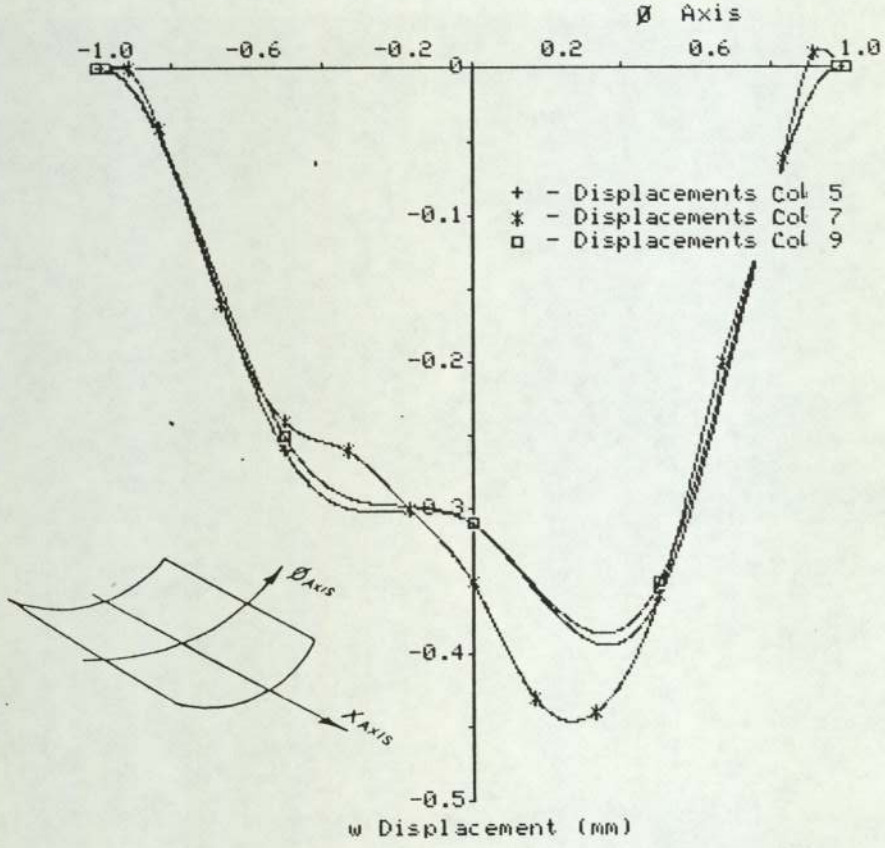

Fig. 11.29 Displacement of panel GRP2 along LVDT columns 5,7 & 9 at a negative pressure of 25kPa (Test No.49)

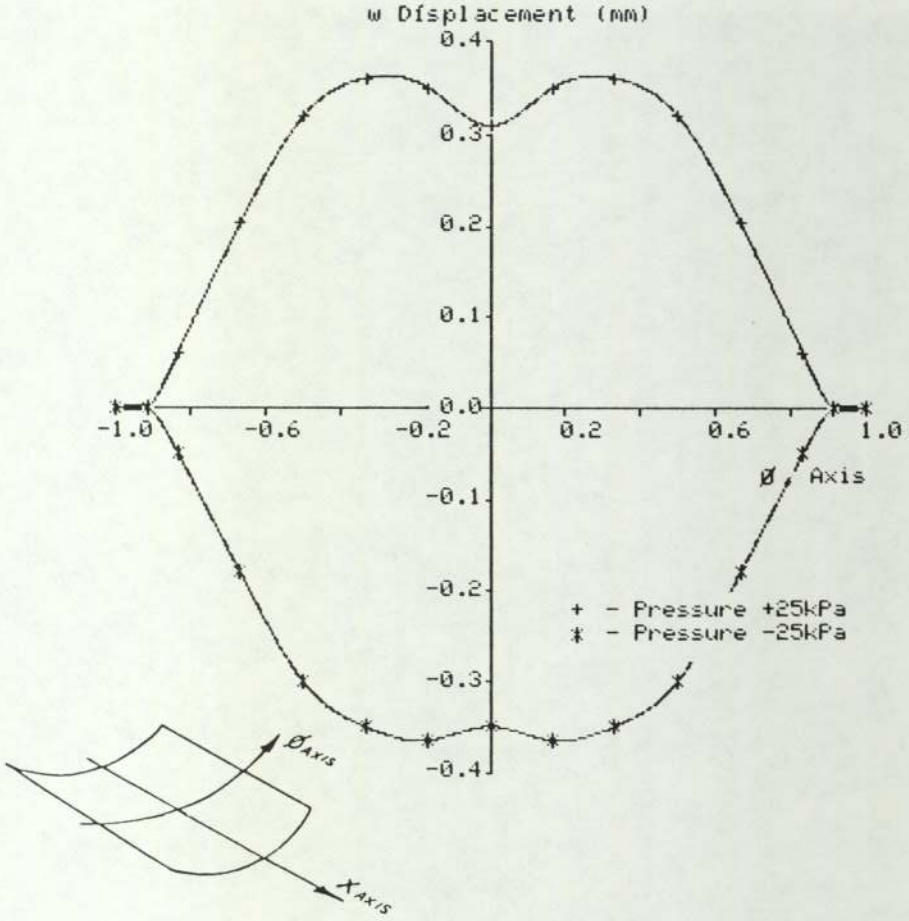

Fig. 11.30 Displacement of panel GRP2 along Ø axis at +25kPa and -25kPa.
(Symmetry forced about X axis)

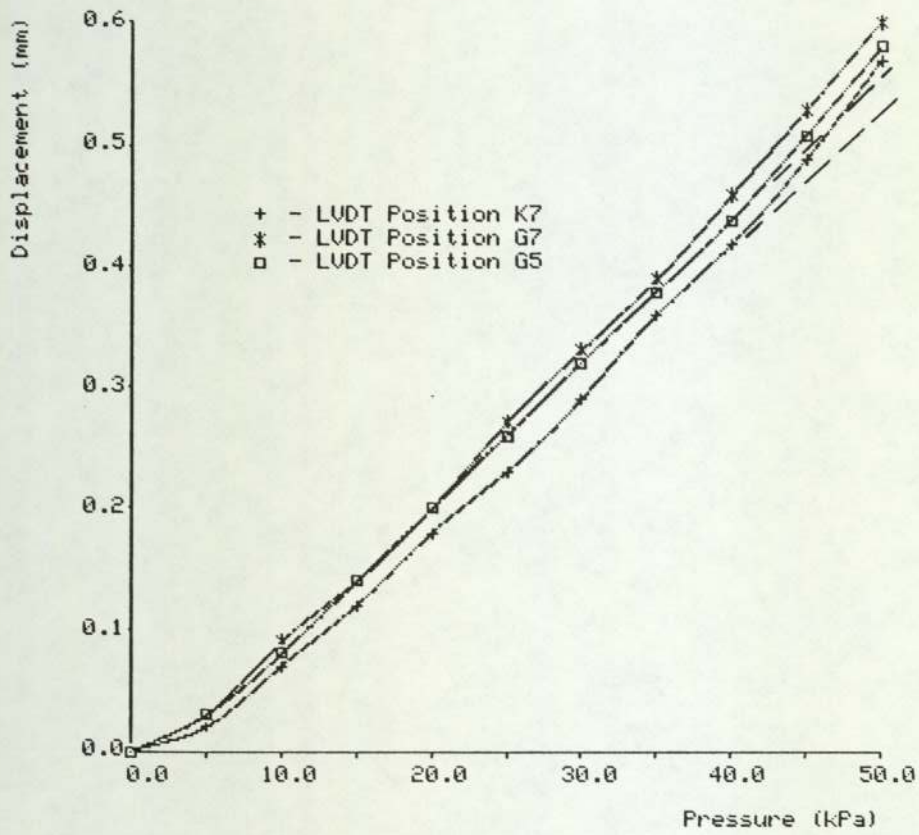

Fig. 11.31 Displacement at LVDT positions K7,G7 & G5 for panel GRP3 subject to positive pressure loading showing onset of nonlinear behaviour (Test No.84)

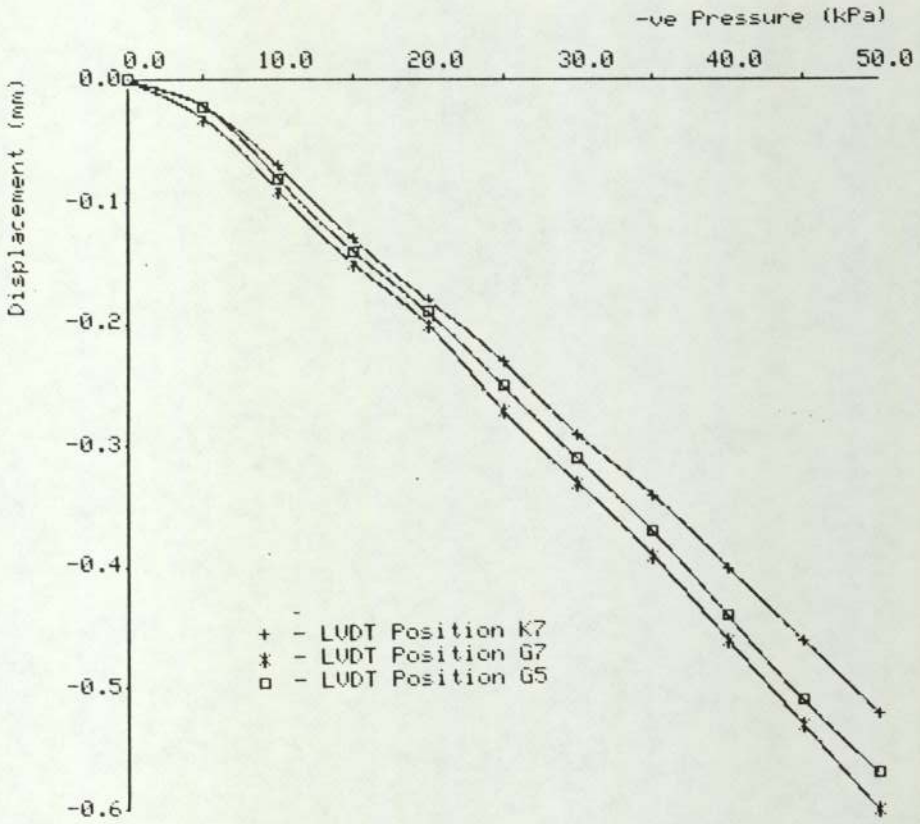

Fig. 11.32 Displacement at LVDT positions K7,G7 & G5 for panel GRP3 subject to negative pressure loading showing onset of nonlinear behaviour (Test No.78)

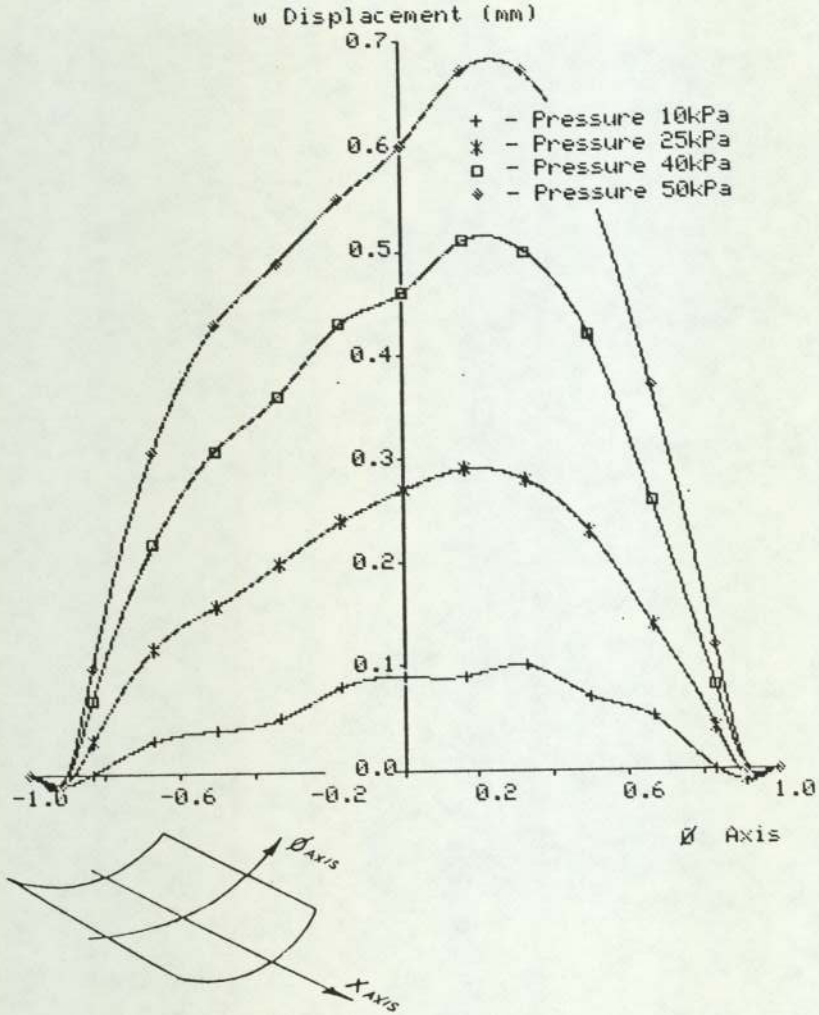

Fig. 11.33 Displacement along the Ø axis of panel GRP3 showing development of asymmetric behaviour (Positive pressure loading)

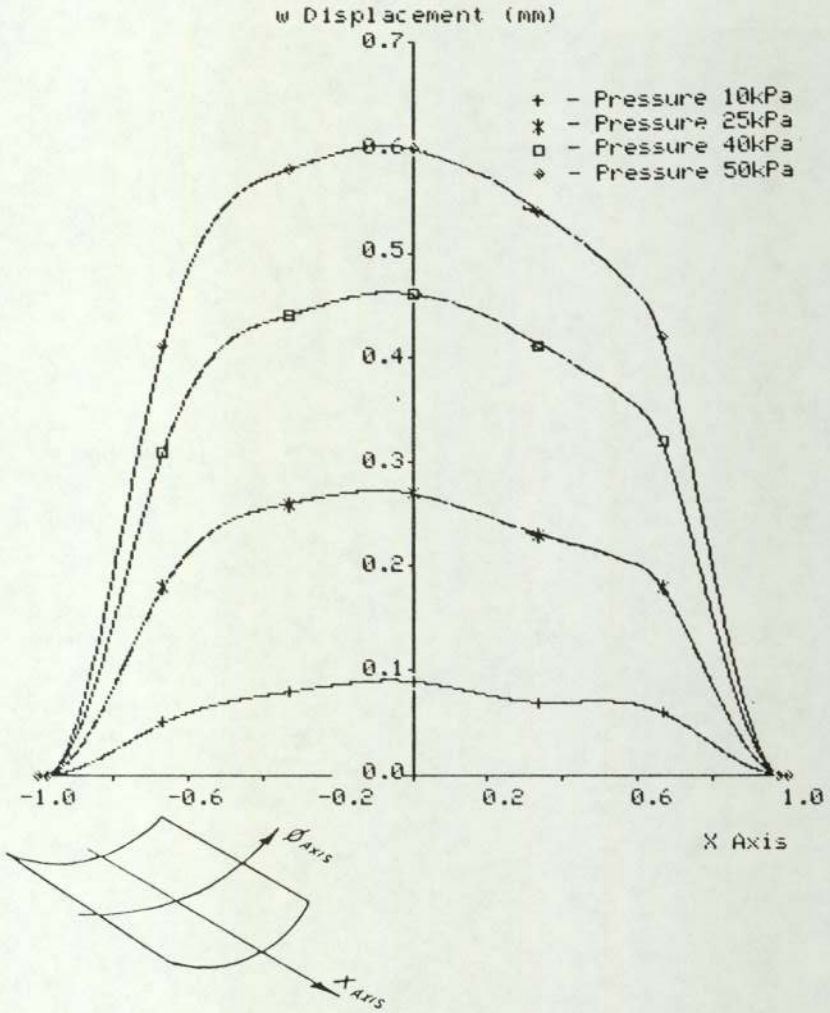

Fig. 11.34 Displacement along the X axis of panel GRP3 showing development of asymmetric behaviour (Positive pressure loading)

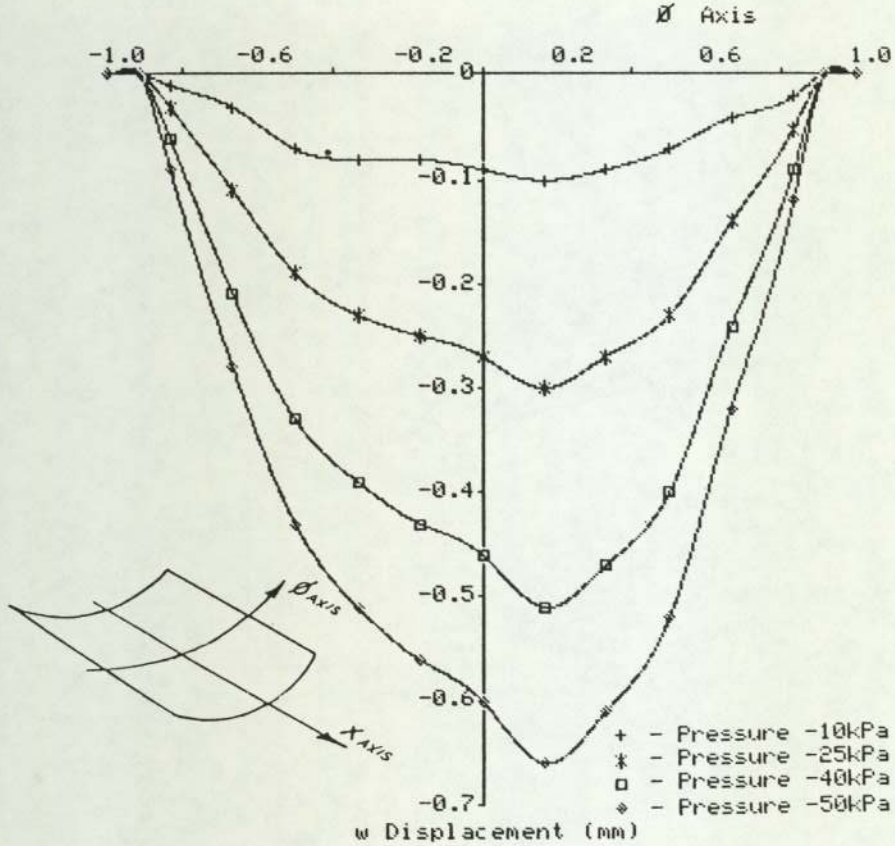

Fig. 11.35 Displacement along the Ø axis of panel GRP3 showing development of asymmetric behaviour (Negative pressure loading)

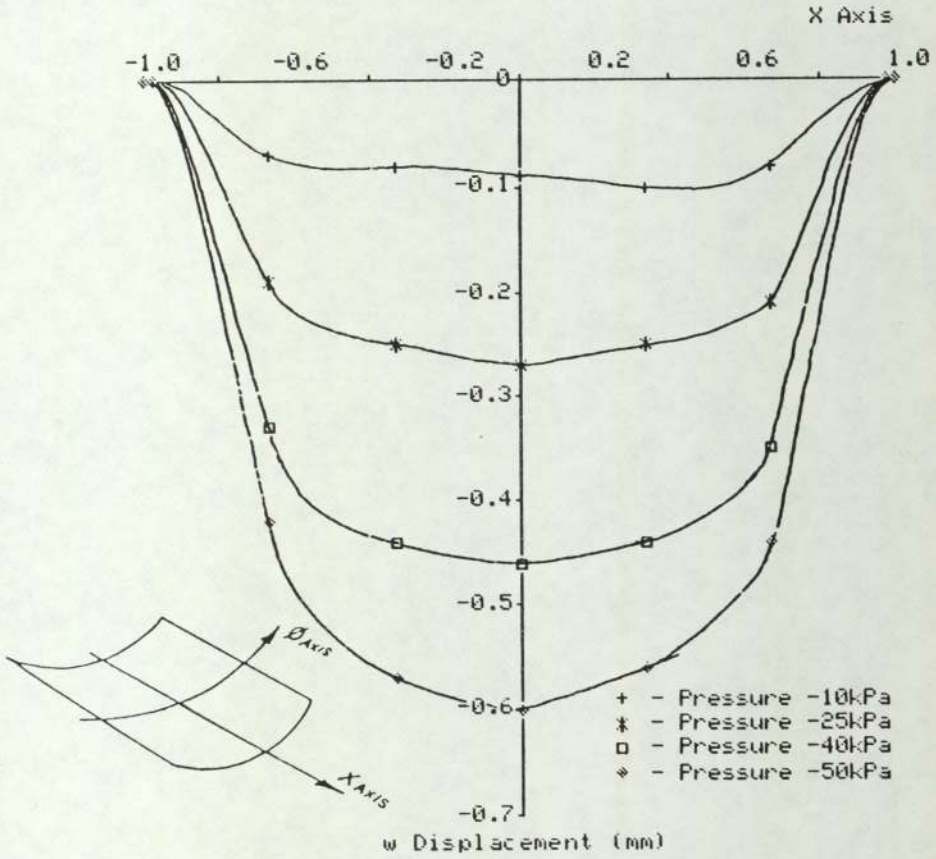

Fig. 11.36 Displacement along the X axis of panel GRP3 showing development of asymmetric behaviour (Negative pressure loading)

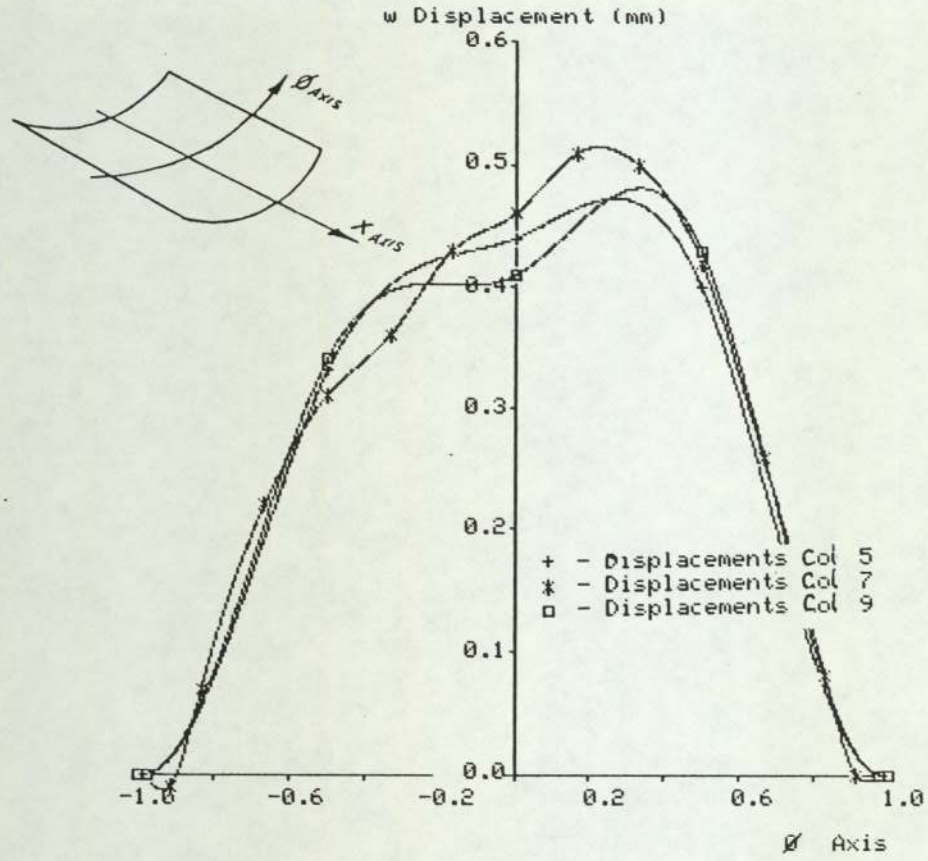

Fig. 11.37 Displacement of panel GRP3 along LVDT columns 5,7 & 9 at a positive pressure of 40kPa (Test No.84)

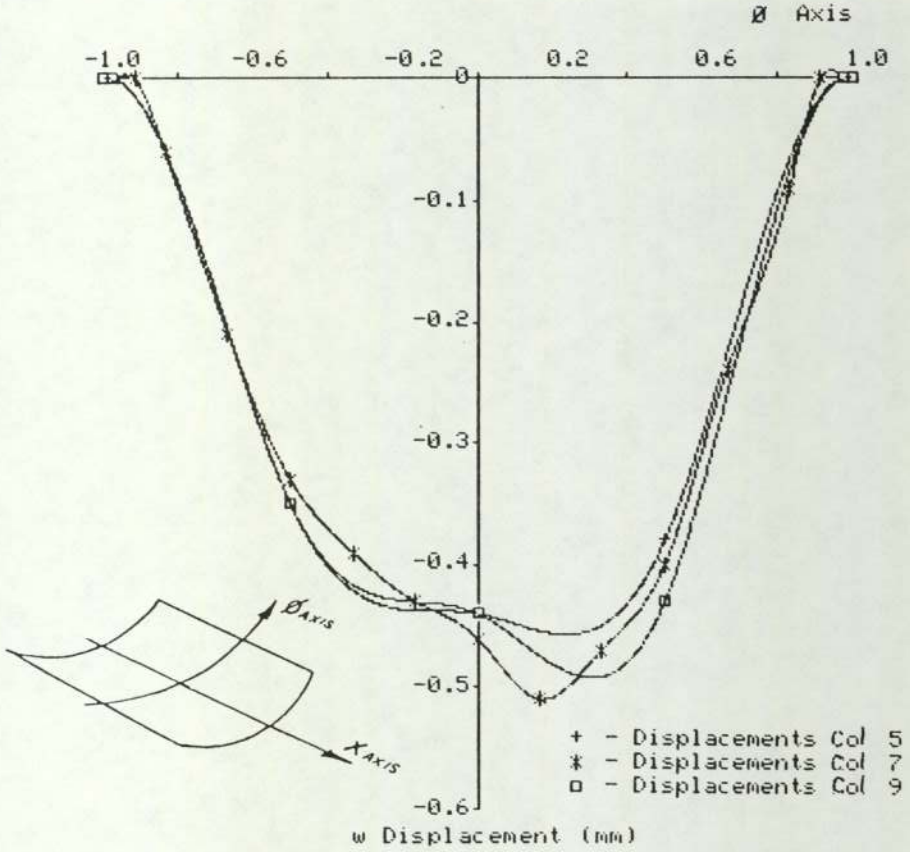

Fig. 11.38 Displacement of panel GRP3 along LVDT columns 5,7 & 9 at a negative pressure of 40kPa (Test No.78)

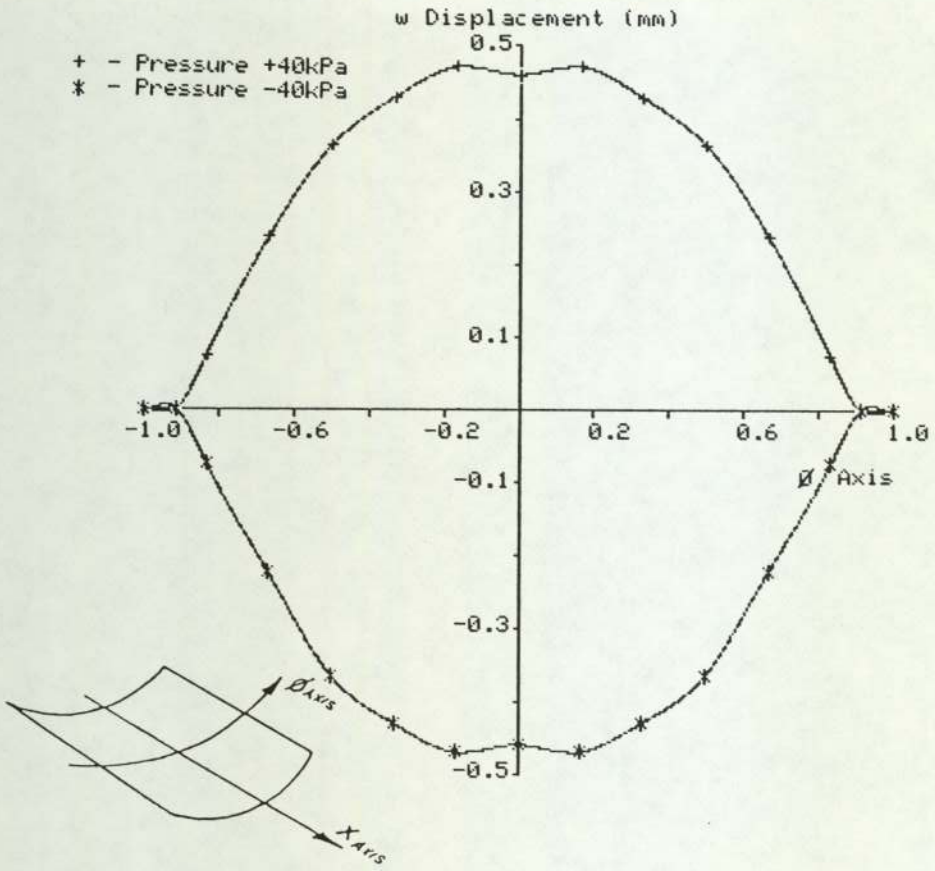

Fig. 11.39 Displacement of panel GRP3 along Ø axis at +40kPa and -40kPa. (Symmetry forced about X axis)

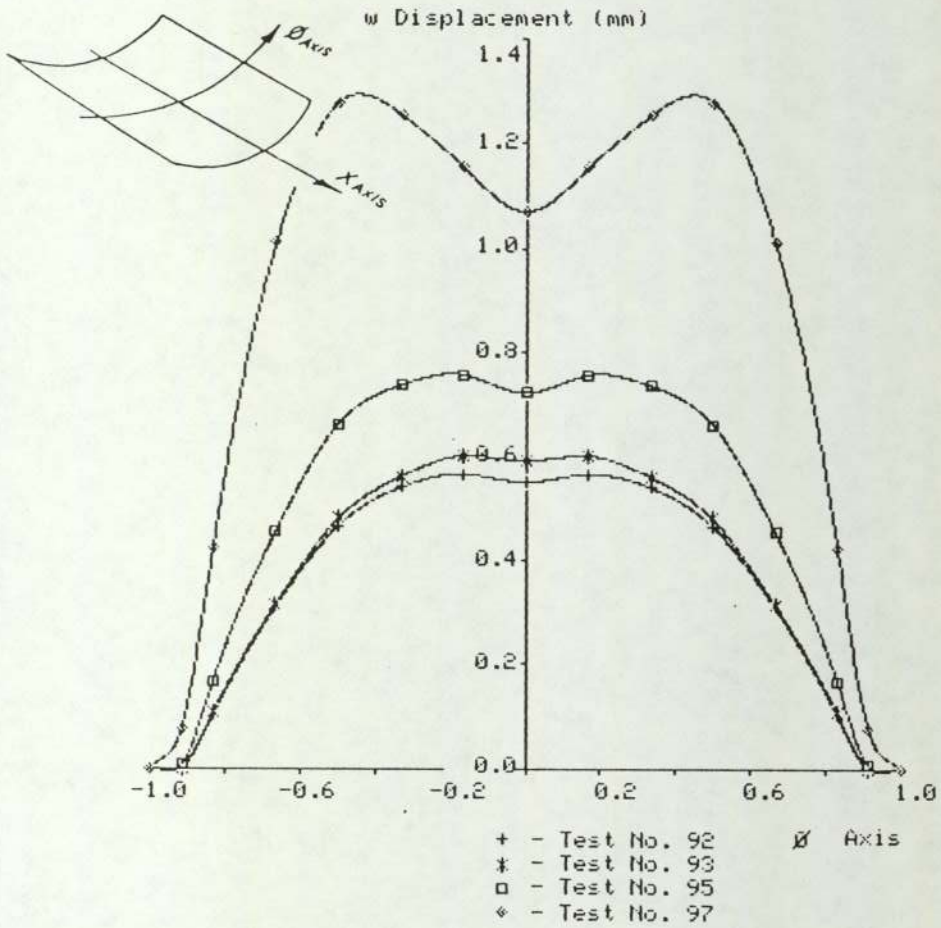

Fig. 11.40 Displacement along the Ø axis of panel GRP3 showing effect of relaxation of edge restraint (removal of cross stiffeners) at a positive pressure of 50kPa
(Symmetry forced about X axis)

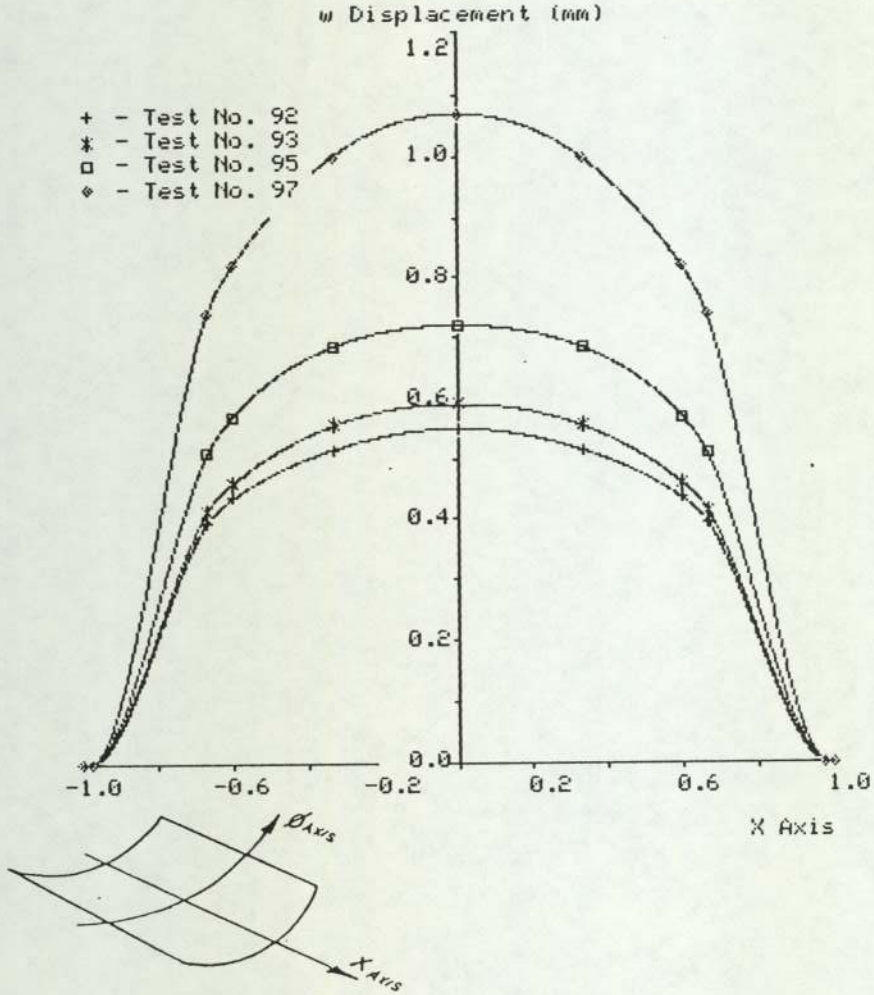

Fig. 11.41 Displacement along the X axis of panel GRP3 showing effect of relaxation of edge restraint (removal of cross stiffeners) at a positive pressure of 50kPa
(Symmetry forced about Ø axis)

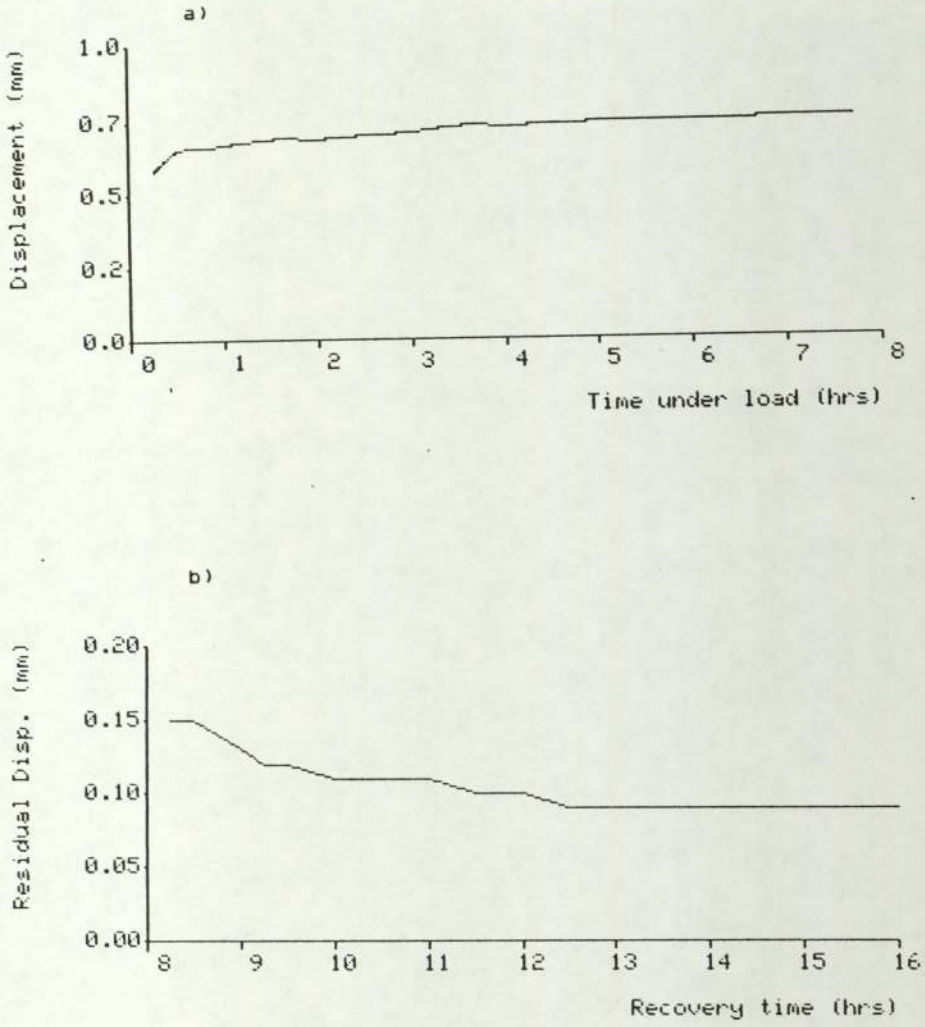

Fig. 11.42 Displacement at LVDT position K7 of panel GRP3 showing :
a) increase of displacement with time at 50kPa
b) reduction of residual displacement at 0kPa

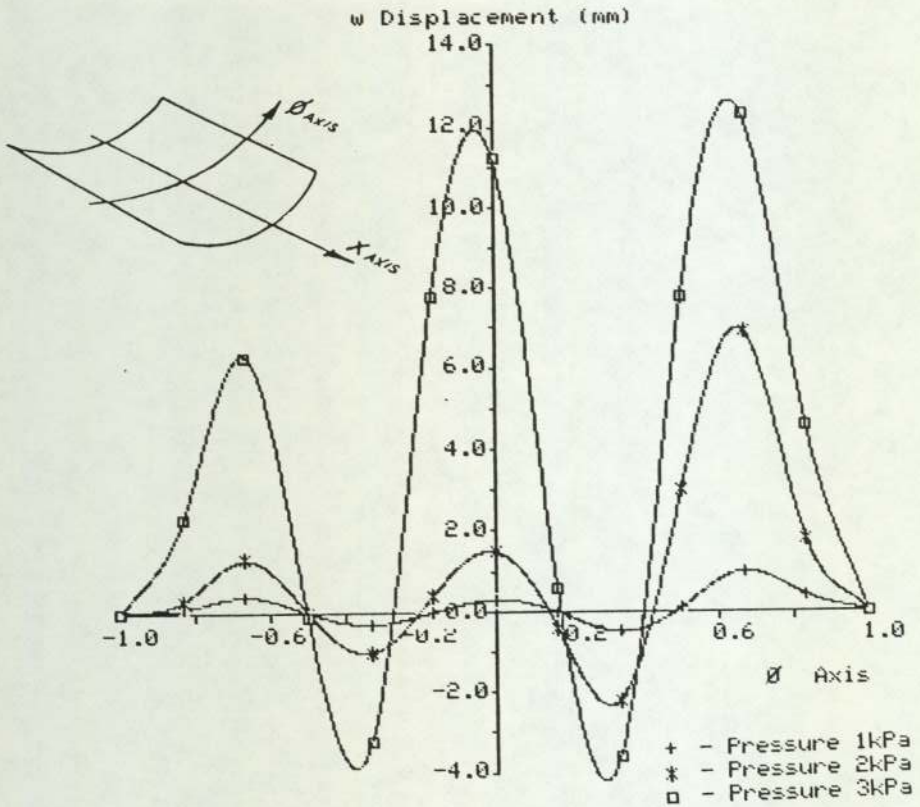

Fig. 11.43 Displacement along the Ø axis of panel AL2 (1.2mm Aluminium)
(Positive pressure loading)

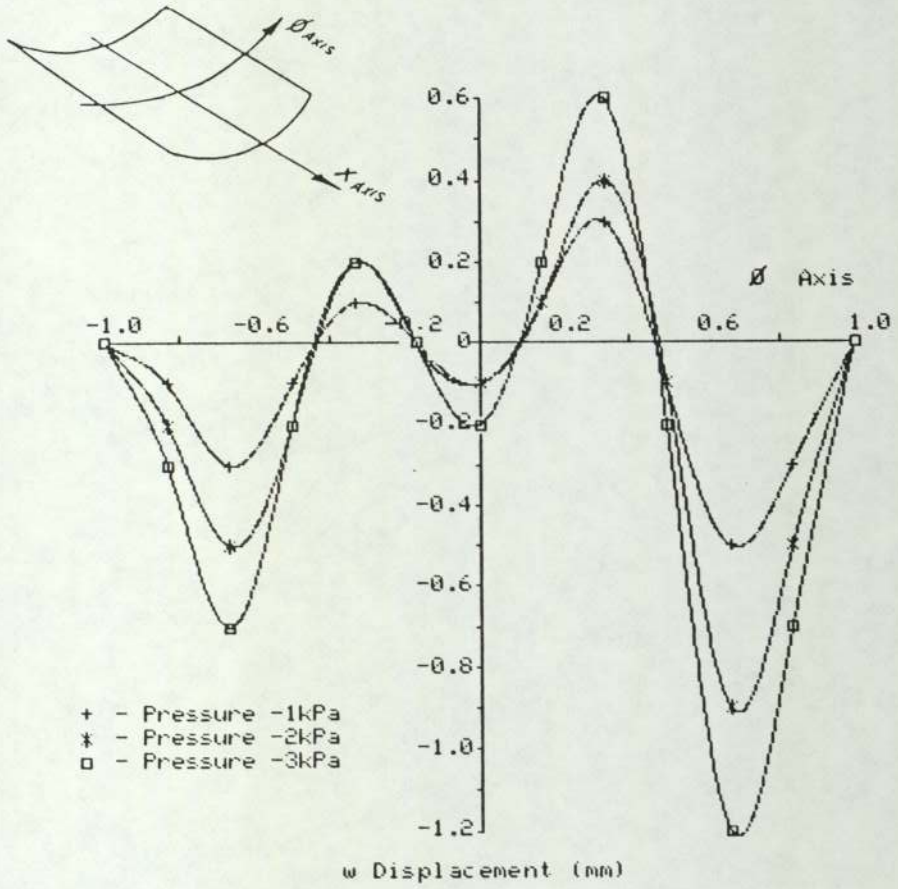

Fig. 11.44 Displacement along the ø axis of panel AL2 (1.2mm Aluminium)
(Negative pressure loading)

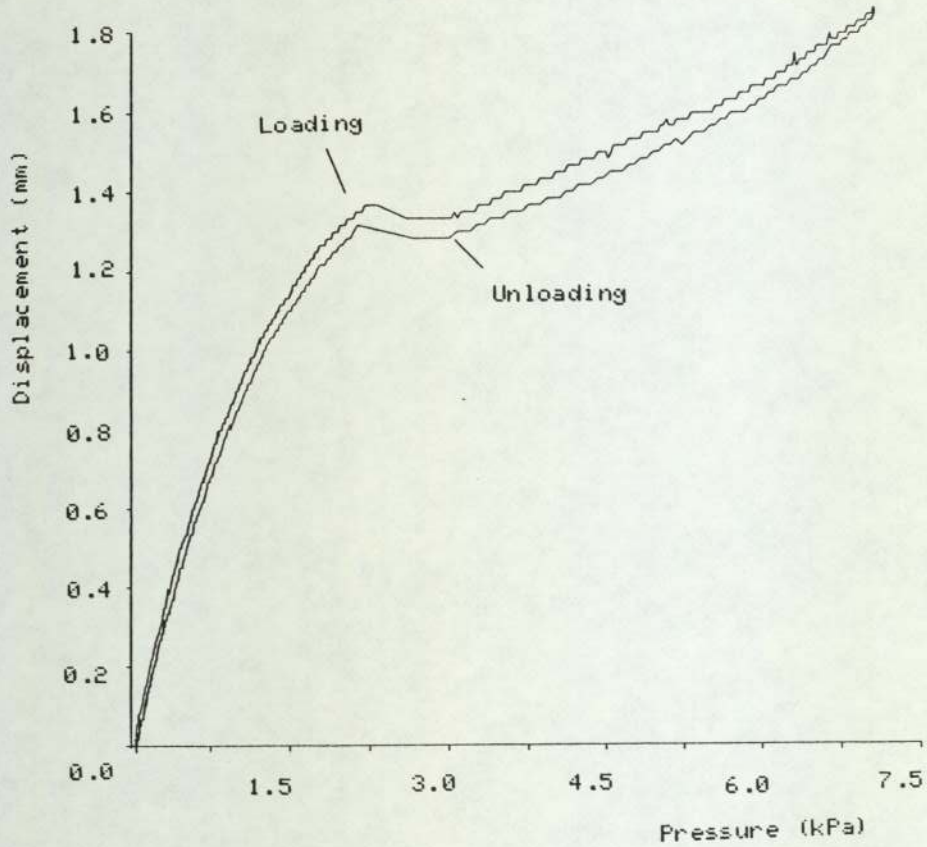

Fig. 14.45 Displacement at LVDT position B7 for panel AL2. (Test No. 14 - Loading and Unloading)

Note the snap buckle effect at approximately 1.3kPa and compare with Figure 4.2

Rosette No.	Panel Surface	Stress Values (MPa)					
				Membrane		Bending	
		σ_{ϕ}	σ_{θ}	σ_{ϕ}^{a}	σ_{θ}^{a}	σ_{ϕ}^{b}	σ_{θ}^{b}
01	Concave	-11.88	-3.52	-7.48	-1.92	-4.41	-1.60
101	Convex	-3.07	-0.32				
02	Concave	-14.50	-4.42	-7.81	-1.76	-6.69	-2.67
102	Convex	-1.12	0.91				
03	Concave	-13.38	-3.83	-7.76	-2.14	-5.62	-1.69
103	Convex	-2.14	-0.45				
04	Concave	-11.19	-3.31	-7.51	-1.90	-3.69	-1.42
104	Convex	-3.82	-0.48				
05	Concave	-9.64	-1.34	-8.22	-2.43	-1.43	1.09
105	Convex	-6.79	-3.51				
06	Concave	-6.62	-2.21	-7.69	-3.24	1.07	1.03
106	Convex	-8.75	-4.27				
07	Concave	-2.27	-1.80	-8.24	-4.28	5.97	2.48
107	Convex	-14.21	-6.75				
08	Concave	-5.31	-2.50	-8.43	-3.98	3.12	1.48
108	Convex	-11.54	-5.45				
09	Concave	-0.74	-1.63	-8.25	-4.55	7.51	2.92
109	Convex	-15.76	-7.46				
10	Concave	-8.96	-2.70	-6.80	-2.03	-2.16	-0.67
110	Convex	-4.64	-1.36				

Table 11.2 Experimental Stresses for 6.4mm Al Panel AL1 (Test No. 35) (subject to positive pressure of 50.0kPa)

Note: Positive bending stresses indicate tensile stress on concave surface.

Rosette No.	Panel Surface	Stress Values (MPa)					
				Membrane		Bending	
		σ_{ϕ}	σ_{x}	σ_{ϕ}^{a}	σ_{x}^{a}	σ_{ϕ}^{b}	σ_{x}^{b}
01	Concave	11.97	4.33	8.81	3.08	3.17	1.26
101	Convex	5.64	1.82				
02	Concave	13.19	4.95	9.24	3.69	3.95	1.27
102	Convex	5.29	2.42				
03	Concave	13.21	5.04	9.60	4.00	3.61	1.05
103	Convex	5.99	2.95				
04	Concave	11.77	4.43	9.34	3.64	2.44	0.80
104	Convex	6.90	2.84				
05	Concave	10.51	2.63	9.57	3.63	0.95	-1.00
105	Convex	8.62	4.62				
06	Concave	7.28	3.58	9.77	7.44	-2.49	-3.86
106	Convex	12.26	11.30				
07	Concave	5.64	4.09	8.87	5.06	-3.23	-0.97
107	Convex	12.10	6.02				
08	Concave	7.67	4.56	9.65	5.41	-1.98	-0.85
108	Convex	11.63	6.26				
09	Concave	4.84	3.76	8.94	5.00	-4.01	-1.24
109	Convex	13.03	6.23				
10	Concave	7.89	2.52	7.07	2.27	0.82	0.26
110	Convex	6.25	2.01				

Table 11.3 Experimental Stresses for 6.4mm Al Panel AL1 (Test No. 33) (subject to negative pressure of 50.0kPa)

Note: Positive bending stresses indicate tensile stress on concave surface.

Rosette No.	Panel Surface	Stress Values (MPa)					
				Membrane		Bending	
		σ_{ϕ}	σ_{κ}	σ_{ϕ}^{a}	σ_{κ}^{a}	σ_{ϕ}^{b}	σ_{κ}^{b}
02	Concave	-4.29	-0.96	-2.32	-0.68	-1.97	-0.28
102	Convex	-0.35	-0.40				
04	Concave	-3.53	-0.85	-2.32	-0.59	-1.21	-0.26
104	Convex	-1.11	-0.33				
07	Concave	-1.29	-0.39	-2.24	-0.67	0.95	0.28
107	Convex	-3.19	-0.95				

Table 11.4 Experimental Stresses for Panel GRP1 (Test No. 71)
(subject to positive pressure of 20.0kPa)

Rosette No.	Panel Surface	Stress Values (MPa)					
				Membrane		Bending	
		σ_{ϕ}	σ_{κ}	σ_{ϕ}^{a}	σ_{κ}^{a}	σ_{ϕ}^{b}	σ_{κ}^{b}
02	Concave	3.60	0.78	2.27	0.66	1.33	0.13
102	Convex	0.94	0.53				
04	Concave	3.15	0.70	2.27	0.54	0.89	0.16
104	Convex	1.38	0.38				
07	Concave	1.42	0.37	2.12	0.55	-0.70	-0.18
107	Convex	2.81	0.72				

Table 11.5 Experimental Stresses for Panel GRP1 (Test No. 65)
(subject to negative pressure of 20.0kPa)

Rosette No.	Panel Surface	Stress Values (MPa)					
				Membrane		Bending	
		σ_{ϕ}	σ_{κ}	σ_{ϕ}^{a}	σ_{κ}^{a}	σ_{ϕ}^{b}	σ_{κ}^{b}
02	Concave	-2.76	-0.72	-1.86	-0.57	-0.91	-0.15
102	Convex	-0.95	-0.42				
04	Concave	-2.56	-0.58	-1.97	-0.52	-0.60	-0.06
104	Convex	-1.37	-0.46				
07	Concave	-1.39	-0.41	-1.79	-0.46	0.40	0.05
107	Convex	-2.18	-0.50				

Table 11.6 Experimental Stresses for Panel GRP2 (Test No. 55)
(subject to positive pressure of 25.0kPa)

Rosette No.	Panel Surface	Stress Values (MPa)					
				Membrane		Bending	
		σ_ϕ	σ_x	σ_ϕ^a	σ_x^a	σ_ϕ^b	σ_x^b
02	Concave	2.59	0.62	1.83	0.52	0.77	0.11
102	Convex	1.06	0.41				
04	Concave	2.38	0.46	1.93	0.46	0.45	0.01
104	Convex	1.48	0.45				
07	Concave	1.49	0.39	1.78	0.42	-0.29	-0.03
107	Convex	2.07	0.44				

Table 11.7 Experimental Stresses for Panel GRP2 (Test No. 49) (subject to negative pressure of 25.0kPa)

Rosette No.	Panel Surface	Stress Values (MPa)					
				Membrane		Bending	
		σ_ϕ	σ_x	σ_ϕ^a	σ_x^a	σ_ϕ^b	σ_x^b
02	Concave	-2.29	-0.61	-2.00	-0.74	-0.29	0.13
102	Convex	-1.71	-0.86				
04	Concave	-3.08	-0.50	-2.34	-0.56	-0.75	0.06
104	Convex	-1.59	-0.61				
07	Concave	-1.43	-0.42	-1.91	-0.49	0.48	0.07
107	Convex	-2.38	-0.56				

Table 11.8 Experimental Stresses for Panel GRP3 (Test No. 84) (subject to positive pressure of 40.0kPa)

Rosette No.	Panel Surface	Stress Values (MPa)					
				Membrane		Bending	
		σ_ϕ	σ_x	σ_ϕ^a	σ_x^a	σ_ϕ^b	σ_x^b
02	Concave	2.25	0.53	1.96	0.65	0.29	-0.12
102	Convex	1.67	0.76				
04	Concave	2.91	0.39	2.27	0.49	0.65	-0.10
104	Convex	1.62	0.58				
07	Concave	1.45	0.37	1.87	0.45	-0.42	-0.08
107	Convex	2.29	0.52				

Table 11.9 Experimental Stresses for Panel GRP3 (Test No. 78) (subject to negative pressure of 40.0kPa)

CHAPTER 12

NUMERICAL SOLUTION

OF

CYLINDRICAL SHELL EQUATIONS

12.1 Introduction

This chapter details a numerical solution of Flügge's cylindrical shell equations using a Galerkin type procedure.

The Galerkin method has been described in many texts including KANTOROVICH and KRYLOV [88] and RICHARDS [89]. The principle of the method is described briefly in Appendix D of this thesis.

The case considered here, corresponding to the sonar panels of this study, is that of an orthotropic cylindrical shell panel subject to uniform radial pressure load and with the following three types of boundary condition.

(1) All edges simply supported.

(2) All edges hinged.

(3) All edges clamped.

The method of solution given here follows closely the procedure used in Reference [55], which considered the case of a clamped isotropic cylindrical shell panel subject to dead loading.

Beam eigen functions with undetermined constants are assumed for the panel displacements and were selected so as to satisfy the above boundary conditions. These functions which describe the normal modes of a vibrating beam have been tabulated by YOUNG and FELGAR [90].

It is a requirement of the Galerkin method that trial displacement functions must exactly satisfy all boundary conditions. These characteristic beam functions satisfy this

requirement. It may be noted that the requirements of the Galerkin method differ in this respect from those of the related Raleigh-Ritz technique. In using the latter technique it is only strictly necessary to satisfy the geometric boundary conditions.

These assumed displacement functions were then made to satisfy the governing differential equations in a weighted fashion according to Galerkin's procedure, resulting, for each set of boundary conditions, in a set of linear algebraic equations in terms of the unknown constants. By considering a finite number of terms these equations were solved to determine the unknown constants. Displacements were calculated and finally using the force displacement relationships the stress resultants and subsequently the stresses were determined.

Fortran programs of this solution for each of the three types of boundary condition are given in Appendix F.

Since only a finite number of terms were considered the convergence of the solution was investigated. Numerical results were then obtained for the particular geometries of cylindrical shell corresponding to the sonar panels of this study.

12.2 Non-dimensional form of the governing differential equations

The three approximate differential equations for an orthotropic cylindrical shell, subject to radial pressure loading are derived following Flügge [33] in Appendix E.

For the cylindrical panel shown in Figure 12.1 three non-dimensional displacement parameters may be introduced.

$$\bar{u} = \frac{u}{L} \quad ; \qquad \bar{v} = \frac{v}{R\alpha} \quad ; \qquad \bar{w} = \frac{w}{R}$$

In terms of these non-dimensional displacements the three governing differential equations may be written:

$$\left(\frac{R\alpha}{L}\right)^2 \bar{u}'' + \left(\frac{G}{E_1}\right)\bar{u}\cdot\cdot + \left(\frac{R\alpha}{L}\right)^2 \left(\frac{G + E_\nu}{E_1}\right)\bar{v}'\cdot + \left(\frac{E_\nu}{E_1}\right)\left(\frac{R\alpha}{L}\right)^2 \bar{w}' = 0 \qquad (12.1)$$

$$\left(\frac{G + E_\nu}{E_2}\right)\bar{u}'\cdot + \bar{v}\cdot\cdot + \left(\frac{G}{E_2}\right)\left(\frac{R\alpha}{L}\right)^2 \bar{v}'' + \bar{w}\cdot = 0 \qquad (12.2)$$

$$\left(\frac{E_\nu}{E_2}\right)\bar{u}' + \bar{v}\cdot + \bar{w} + \frac{h^2}{3R^2}\left[\left(\frac{R}{L}\right)^4 \left(\frac{E_1}{E_2}\right)\bar{w}'''' + \left(\frac{2E_\nu + 4G}{E_2}\right)\left(\frac{R}{\alpha L}\right)^2 \bar{w}''\cdot\cdot + \frac{1}{\alpha^4}\bar{w}\cdot\cdot\cdot\cdot\right] = -\frac{pR}{D_\phi} \qquad (12.3)$$

where $(\ )' = \frac{\partial}{\partial \bar{x}}$, $(\ )\cdot = \frac{\partial}{\partial \bar{\phi}}$, $\qquad \bar{x} = \frac{x}{L}$, $\bar{\phi} = \frac{\phi}{\alpha}$

These are the equations which will be solved here using the Galerkin method.

In terms of $\bar{u}$ $\bar{v}$ and $\bar{w}$ the force displacement relations can be obtained as:

$$N_x = D_x \bar{u}' + D_\nu(\bar{v}\cdot + \bar{w}) \qquad (12.4)$$

$$N_\phi = D_\phi(\bar{v}\cdot + \bar{w}) + D_\nu \bar{u}' \qquad (12.5)$$

$$N_{x\phi} = D_{x\phi}\left[\left(\frac{L}{R\alpha}\right)\bar{u}\cdot + \left(\frac{R\alpha}{L}\right)\bar{v}'\right] \qquad (12.6)$$

$$M_x = \left(\frac{K_x}{R}\right)\left(\frac{R}{L}\right)^2 \bar{w}'''' + \left(\frac{K_\nu}{R\alpha^2}\right)\bar{w}'' \qquad (12.7)$$

$$M_\phi = \left(\frac{K_\phi}{R\alpha^2}\right)\bar{w}'' + \left(\frac{K_\nu}{R}\right)\left(\frac{R}{L}\right)^2 \bar{w}'''' \qquad (12.8)$$

$$M_{x\phi} = \frac{2K_{x\phi}}{R}\left(\frac{R}{\alpha L}\bar{w}'\right) \qquad (12.9)$$

$$Q_x = \left(\frac{K_x R}{L^3}\right)\bar{w}''''' + \left(\frac{K_\nu + 2K_{x\phi}}{R\alpha^2 L}\right)\bar{w}''' \qquad (12.10)$$

$$Q_{x\phi} = \frac{K_\phi}{R^2\alpha^3}\bar{w}''' + \left(\frac{K_\nu + 2K_{x\phi}}{\alpha L^2}\right)\bar{w}'' \qquad (12.11)$$

where:

$$E_1 = \frac{E_x}{1 - \nu_{xy}\nu_{yx}}, \quad E_2 = \frac{E_y}{1 - \nu_{xy}\nu_{yx}}, \quad E_\nu = \frac{E_x\nu_{yx}}{1 - \nu_{xy}\nu_{yx}} = \frac{E_y\nu_{xy}}{1 - \nu_{xy}\nu_{yx}}$$

$$D_x = E_1(2h), \quad D_\phi = E_2(2h), \quad D_\nu = E_\nu(2h), \quad D_{x\phi} = G(2h)$$

$$K_x = \frac{2E_1h^3}{3}, \quad K_\phi = \frac{2E_2h^3}{3}, \quad K_\nu = \frac{2E_\nu h^3}{3}, \quad K_{x\phi} = \frac{2Gh^3}{3}$$

12.3 Solution

12.3.1 Assumed displacement functions

The following expressions can be assumed for the non-dimensional displacements $\bar{u}$, $\bar{v}$ and $\bar{w}$:

$$\bar{u} = \sum_{m=1}^{\infty}\sum_{n=1}^{\infty} A_{mn}\,\phi_{mn}(\bar{x}, \bar{\phi}) \qquad (12.12)$$

$$\bar{v} = \sum_{m=1}^{\infty}\sum_{n=1}^{\infty} B_{mn}\,\psi_{mn}(\bar{x}, \bar{\phi}) \qquad (12.13)$$

$$\bar{w} = \sum_{m=1}^{\infty}\sum_{n=1}^{\infty} C_{mn}\,\xi_{mn}(\bar{x}, \bar{\phi}) \qquad (12.14)$$

Where A_{mn}, B_{mn} and C_{mn} are undetermined constants, and the functions $\phi_{mn}(\bar{x}, \bar{\phi})$, $\psi_{mn}(\bar{x}, \bar{\phi})$ and $\xi_{mn}(\bar{x}, \bar{\phi})$ are selected so as to satisfy the boundary conditions.

Three types of boundary conditions are considered here:

(a) All edges simply supported (SS)

$$\bar{x} = \pm 1, \; N_x = \bar{v} = M_x = \bar{w} = 0$$

$$\phi = \pm 1, \; N_\phi = \bar{u} = M_\phi = \bar{w} = 0 \qquad (12.15)$$

(b) All edges hinged (CS)

$$\bar{x} = \pm 1, \; \bar{u} = \bar{v} = M_x = \bar{w} = 0$$

$$\bar{\phi} = \pm 1, \; \bar{u} = \bar{v} = M_\phi = \bar{w} = 0 \qquad (12.16)$$

(c) All edges clamped (CC)

$$\bar{x} = \pm 1, \; \bar{u} = \bar{v} = \bar{w} = \bar{w}' = 0$$

$$\phi = \pm 1, \; \bar{u} = \bar{v} = \bar{w} = \dot{\bar{w}} = 0 \qquad (12.17)$$

For simply supported boundary condition the functions can be taken as:

$$\left.\begin{aligned} \phi_{mn}(\bar{x}, \bar{\phi}) &= \sin\left(\frac{2m-1}{2}\pi\right)\bar{x} \;\; \cos\left(\frac{2n-1}{2}\pi\right)\bar{\phi} \\ \psi_{mn}(\bar{x}, \bar{\phi}) &= \cos\left(\frac{2m-1}{2}\pi\right)\bar{x} \;\; \sin\left(\frac{2n-1}{2}\pi\right)\bar{\phi} \\ \xi_{mn}(\bar{x}, \bar{\phi}) &= \cos\left(\frac{2m-1}{2}\pi\right)\bar{x} \;\; \cos\left(\frac{2n-1}{2}\pi\right)\bar{\phi} \end{aligned}\right\} \qquad (12.18)$$

For hinged boundary conditions, the functions can be taken as:

$$\left.\begin{aligned} \phi_{mn}(\bar{x}, \bar{\phi}) &= \sin m\pi\bar{x} \;\; \cos\left(\frac{2n-1}{2}\pi\right)\bar{\phi} \\ \psi_{mn}(\bar{x}, \bar{\phi}) &= \cos\left(\frac{2m-1}{2}\pi\right)\bar{x} \; \sin n\pi\phi \\ \xi_{mn}(\bar{x}, \bar{\phi}) &= \cos\left(\frac{2m-1}{2}\pi\right)\bar{x} \; \cos\left(\frac{2n-1}{2}\pi\right)\phi \end{aligned}\right\} \qquad (12.19)$$

For clamped boundary condition, the functions can be taken as:

$$\left.\begin{aligned}\phi_{mn}(\bar{x},\ \bar{\phi}) &= \sin m\pi\bar{x}\ \cos\left(\frac{2n-1}{2}\ \pi\right)\bar{\phi}\\ \psi_{mn}(\bar{x},\ \bar{\phi}) &= \cos\left(\frac{2m-1}{2}\ \pi\right)\bar{x}\ \sin n\pi\bar{\phi}\end{aligned}\right\} \qquad (12.20)$$

$$\xi_{mn}(x,\ \phi) = \left(\frac{\cos h\lambda_m\bar{x}}{\cosh\lambda_m} - \frac{\cos\lambda_m\bar{x}}{\cos\lambda_m}\right)\left(\frac{\cosh\lambda_n\phi}{\cosh\lambda_n} - \frac{\cos\lambda_n\phi}{\cos\lambda_n}\right) \qquad (12.20)$$

For the case of clamped boundary conditions λ_m and λ_n are determined from solution of the transcendental equations

$$\left.\begin{aligned}\tanh\lambda_m + \tan\lambda_m &= 0\\ \tanh\lambda_n + \tan\lambda_n &= 0\end{aligned}\right\} \qquad (12.21)$$

Substituting the assumed form of the displacements given in equations (12.12) to (12.14) into the differential equations (12.1) to (12.3) and using the Galerkin method results in:

$$\int_{-1}^{+1}\int_{-1}^{+1}\sum_{m=1}^{\infty}\sum_{n=1}^{\infty}\left[A_{mn}\left(\left(\frac{R\alpha}{L}\right)^2\phi''_{mn} + \frac{G}{E_1}\ \ddot{\phi}_m\right) + B_{mn}\left(\left(\frac{G+E_\nu}{E_1}\right)\left(\frac{R\alpha}{L}\right)^2\psi''_{mn}\right) + C_{mn}\left(\left(\frac{E_\nu}{E_1}\right)\left(\frac{R\alpha}{L}\right)^2\xi'_{mn}\right)\right]\phi_{mn}\,d\bar{x}\,d\bar{\phi} = 0 \qquad (12.22)$$

$$\int_{-1}^{+1}\int_{-1}^{+1}\sum_{m=1}^{\infty}\sum_{n=1}^{\infty}\left[A_{mn}\left(\left(\frac{G+E_\nu}{E_2}\right)\phi''_{mn}\right) + B_{mn}\left(\ddot{\psi}_{mn} + \left(\frac{G}{E_2}\right)\left(\frac{R\alpha}{L}\right)^2\psi''_{mn}\right) + C_{mn}\{\dot{\xi}_{mn}\}\right]\psi_{mn}\,d\bar{x}d\bar{\phi} = 0 \qquad (12.23)$$

$$\int_{-1}^{+1}\int_{-1}^{+1}\sum_{m=1}^{\infty}\sum_{n=1}^{\infty}\Bigg[A_{mn}\left(\left(\frac{E_\nu}{E_2}\right)\phi'_{mn}\right) + B_{mn}\{\psi^{\cdot}_{mn}\} + C_{mn}\Bigg\{1 + \frac{h^2}{3R^2}\left\langle\left(\frac{R}{L}\right)^4\cdot\left(\frac{E_1}{E_2}\right)\xi''''_{mn} + \left(\frac{2E_\nu + 4G}{E_2}\right)\left(\frac{R}{L\alpha}\right)^2\xi''''_{mn} + \frac{1}{\alpha^4}\,\xi^{\cdot\cdot\cdot\cdot}\right\rangle\Bigg\} + E_{mn}\left(\left(\frac{R}{D_\phi}\right)\xi_{mn}\right)\Bigg]\xi_{mn}\,d\bar{x}d\bar{\phi} = 0 \qquad (12.24)$$

where E_{mn} is determined from,

$$E_{mn} = \frac{\int_{-1}^{+1}\int_{-1}^{+1} p\xi_{mn}\,dx\,d\bar{\phi}}{\int_{-1}^{+1}\int_{-1}^{+1}\xi^2_{mn}\,d\bar{x}d\bar{\phi}} \qquad (12.25)$$

The derivatives of the functions can be expressed in terms of the other functions as follows:

$$\left.\begin{aligned}
\psi''_{mn} &= \sum_{i=1}^{\infty}\sum_{j=1}^{\infty} E^{mn}_{ij}\,\phi_{ij} && \text{(a)}\\
\xi'_{mn} &= \sum_{i=1}^{\infty}\sum_{j=1}^{\infty} F^{mn}_{ij}\,\phi_{ij} && \text{(b)}\\
\phi''_{mn} &= \sum_{i=1}^{\infty}\sum_{j=1}^{\infty} P^{mn}_{ij}\,\psi_{ij} && \text{(c)}\\
\xi^{\cdot}_{mn} &= \sum_{i=1}^{\infty}\sum_{j=1}^{\infty} Q^{mn}_{ij}\,\psi_{ij} && \text{(d)}\\
\phi'_{mn} &= \sum_{i=1}^{\infty}\sum_{j=1}^{\infty} K^{mm}_{ij}\,\xi_{ij} && \text{(e)}\\
\psi^{\cdot}_{mn} &= \sum_{i=1}^{\infty}\sum_{j=1}^{\infty} L^{mn}_{ij}\,\xi_{ij} && \text{(f)}\\
\xi''''_{mn} &= \sum_{i=1}^{\infty}\sum_{j=1}^{\infty} M^{mn}_{ij}\,\xi_{ij} && \text{(g)}
\end{aligned}\right\} \qquad (12.26)$$

Where E_{ij}^{mn}, F_{ij}^{mn}, ... etc can be determined using the orthogonality condition and the table of integrals YOUNG and FELGAR [91].

Substituting the function derivatives (equations 12.2.6(a) to (g)) into equations 12.22 to 12.24 results in a set of linear algebraic equations in terms of the unknown constants. A_{mn}, B_{mn} and C_{mn} for each set of boundary conditions.

12.3.2 Simply supported boundary condition

For the simply supported boundary condition the algebraic equations are:

$$a_1 A_{mn} + a_2 B_{mn} + a_3 C_{mn} = 0 \qquad (12.27)$$

$$b_1 A_{mn} + b_2 B_{mn} + b_3 C_{mn} = 0 \qquad (12.28)$$

$$c_1 A_{mn} + c_2 B_{mn} + c_3 C_{mn} = (R/D_\phi) E_{mn} \qquad (12.29)$$

where

$$a_1 = -\left[E_1 \left(\frac{R\alpha}{L}\right)^2 \left(\frac{2m-1}{2}\pi\right)^2 + G\left(\frac{2n-1}{2}\pi\right)^2\right]$$

$$a_2 = -\left[(E_\nu+G)\left(\frac{R\alpha}{L}\right)^2 \left(\frac{2m-1}{2}\pi\right)\left(\frac{2n-1}{2}\pi\right)\right]$$

$$a_3 = -\left[E_\nu \left(\frac{R\alpha}{L}\right)^2 \left(\frac{2m-1}{2}\pi\right)\right]$$

$$b_1 = -\left[(E_\nu+G) \left(\frac{R\alpha}{L}\right)^2 \left(\frac{2m-1}{2}\pi\right) \left(\frac{2n-1}{2}\pi\right)\right]$$

$$b_2 = -\left[E_2\left(\frac{R\alpha}{L}\right)^2 \left(\frac{2n-1}{2}\pi\right)^2 + G\left(\frac{R\alpha}{L}\right)^4 \left(\frac{2m-1}{2}\pi\right)^2\right]$$

$$b_3 = -\left[E_2 \left(\frac{R\alpha}{L}\right)^2 \left(\frac{2n-1}{2}\pi\right)\right]$$

$$c_1 = E_\nu\left(\frac{2m-1}{2}\pi\right), \quad c_2 = E_2\left(\frac{2n-1}{2}\pi\right)$$

$$c_3 = \frac{1}{3}\left[\left[\left(\frac{E_1}{E_2}\right)\left(\frac{R}{L}\right)^2\left(\frac{h}{L}\right)^2\left(\frac{2m-1}{2}\pi\right)^4 + \left(\frac{2E_\nu + 4G}{E_2}\right)\left(\frac{h}{L}\right)^2\left(\frac{1}{\alpha}\right)^2\right.\right.$$

$$\left.\left.\left(\frac{2m-1}{2}\pi\right)^2\left(\frac{2n-1}{2}\pi\right)^2 + \left(\frac{h}{R}\right)^2\left(\frac{1}{\alpha^4}\right)\left(\frac{2n-1}{2}\pi\right)^4\right]\right] + 1$$

and where:

$$E_{mn} = (-1)^{m+n}\frac{4p}{\left(\frac{2m-1}{2}\pi\right)\left(\frac{2n-1}{2}\pi\right)}$$

12.3.3 Hinged boundary condition

For this boundary condition the algebraic equations are:

$$a_1' A_{mn} + \sum_{i=1}^{\infty}\sum_{j=1}^{\infty} a_2' B_{ij} + \sum_{i=1}^{\infty} c_{in} a_3' = 0 \qquad (12.30)$$

$$\sum_{i=1}^{\infty}\sum_{j=1}^{\infty} b_1' A_{ij} + b_2' B_{mn} + \sum_{j=1}^{\infty} b_3' c_{mj} = 0 \qquad (12.31)$$

$$\sum_{i=1}^{\infty} c_1' A_{in} + \sum_{j=1}^{\infty} c_2' B_{mj} + c_3' c_{mn} = (R/D_\phi)E_{mn} \qquad (12.32)$$

Where

$$a_1' = -\left[\left(\frac{R\alpha}{L}\right)^2 (m\pi)^2 + \left(\frac{G}{E_1}\right)\left(\frac{2n-1}{2}\pi\right)^2\right]$$

$$a_2' = -\left(\frac{G}{E_1} + \nu_{yx}\right)\left(\frac{R\alpha}{L}\right)^2\left(\frac{2i-1}{2}\pi\right)(j\pi)\left(\frac{(-1)^{m+i}2m\pi}{(m\pi)^2 - \left(\frac{2i-1}{2}\pi\right)^2}\right)$$

$$\left(\frac{(-1)^{i+j}\left(\frac{2n-1}{2}\pi\right)}{(j\pi)^2\left(\frac{2n-1}{2}\pi\right)^2}\right)$$

$$a_3' = -\nu_{yx}\left(\frac{R\alpha}{L}\right)^2\left(\frac{2i-1}{2}\pi\right)\left[\frac{(-1)^{m+i}\,2m\pi}{(m\pi)^2-\left(\frac{2i-1}{2}\pi\right)^2}\right]$$

$$b_1' = -\left(\frac{G}{E_2}+\nu_{xy}\right)(i\pi)\left(\frac{2j-1}{2}\pi\right)\left[\frac{(-1)^{i+m}2\left(\frac{2m-1}{2}\pi\right)}{(i\pi)^2-\left(\frac{2m-1}{2}\pi\right)^2}\right]\left[\frac{(-1)^{n+j}2n\pi}{(n\pi)^2-\left(\frac{2j-1}{2}\pi\right)^2}\right]$$

$$b_2' = -(n\pi)^2-\left(\frac{G}{E_2}\right)\left(\frac{R\alpha}{L}\right)^2\left(\frac{2m-1}{2}\pi\right)^2$$

$$b_3' = -\left(\frac{2j-1}{2}\pi\right)\left[\frac{(-1)^{n+j}2n\pi}{(n\pi)^2-\left(\frac{2j-1}{2}\pi\right)^2}\right]$$

$$c_1' = \nu_{xy}(i\pi)\left(\frac{R\alpha}{L}\right)^2\left[\frac{(-1)^{m+i}\,2\left(\frac{2m-1}{2}\pi\right)}{(i\pi)^2-\left(\frac{2m-1}{2}\pi\right)^2}\right]$$

$$c_2' = (j\pi)\left[\frac{(-1)^{n+j}\,2\left(\frac{2n-1}{2}\pi\right)}{(j\pi)^2-\left(\frac{2n-1}{2}\pi\right)^2}\right]$$

$$c_3' = \frac{h^2}{3R^2}\left[\left(\frac{E_1}{E_2}\right)\left(\frac{R}{L}\right)^4\left(\frac{2m-1}{2}n\right)^4+2\left(\nu_{xy}+\frac{2G}{E_2}\right)\left(\frac{R}{\alpha L}\right)^2\left(\frac{2m-1}{2}\pi\right)^2\left(\frac{2n-1}{2}\pi\right)^2+\frac{1}{\alpha^4}\left(\frac{2n-1}{2}\pi\right)^4\right]+1$$

and where:

$$E_{mn} = (-1)^{m+1}\frac{4p}{\left(\frac{2m-1}{2}\pi\right)\left(\frac{2n-1}{2}\pi\right)}$$

12.3.4 Clamped boundary condition

For the clamped boundary condition the algebraic equations are:

$$a_1'' A_{mn} + \sum_{i=1}^{\infty}\sum_{j=1}^{\infty} a_2'' B_{ij} + \sum_{i=1}^{\infty}\sum_{j=1}^{\infty} a_3'' C_{ij} = 0 \qquad (12.33)$$

$$\sum_{i=1}^{\infty}\sum_{j=1}^{\infty} b_1'' A_{ij} + b_2'' B_{mn} + \sum_{i=1}^{\infty}\sum_{j=1}^{\infty} b_3'' C_{ij} = 0 \qquad (12.34)$$

$$\sum_{i=1}^{\infty}\sum_{j=1}^{\infty} c_1'' A_{ij} + \sum_{i=1}^{\infty}\sum_{j=1}^{\infty} c_2'' B_{ij} + \sum_{i=1}^{\infty}\sum_{j=1}^{\infty} c_3'' C_{ij} + c_4 C_{mn} = (R/D_\phi) E_{mn} \qquad (12.35)$$

where

$$a_1'' = -\left[\left(\frac{R\alpha}{L}\right)^2 (m\pi)^2 + \frac{G}{E_1}\left(\frac{2n-1}{2}\pi\right)^2\right]$$

$$a_2'' = -\left(\frac{G}{E_1} + \nu_{yx}\right)\left(\frac{R\alpha}{L}\right)\left(\frac{2j-1}{2}\pi\right)(j\pi)\left(\frac{(-1)^{i+m}\, 2m\pi}{(m\pi)^2 - \left(\frac{2i-1}{2}\pi\right)^2}\right)\left(\frac{(-1)^{j+n} 2\left(\frac{2n-1}{2}\pi\right)}{(j\pi)^2 - \left(\frac{2n-1}{2}\pi\right)^2}\right)$$

$$a_3'' = \nu_{yx}\left(\frac{R\alpha}{L}\right)^2 \lambda_i \left(\frac{(-1)^m\, 4\lambda_i^2\, (m\pi)\tanh\lambda_i}{(m\pi)^4 - (\lambda_i)^4}\right)\left(\frac{(-1)^n\, 4\lambda_j^2\left(\frac{2n-1}{2}\pi\right)}{\left(\frac{2n-1}{2}\pi\right)^4 - \lambda_j^4}\right)$$

$$b_1'' = -\left(\frac{G}{E_2} + \nu_{xy}\right)(i\pi)\left(\frac{2j-1}{2}\pi\right)\left(\frac{(-1)^{m+i} 2\left(\frac{2m-1}{2}\pi\right)}{(i\pi)^2 - \left(\frac{2m-1}{2}\pi\right)^2}\right)\left(\frac{(-1)^{n+j} 2(n\pi)}{(n\pi)^2 - \left(\frac{2j-1}{2}\pi\right)^2}\right)$$

$$b_2'' = \lambda_j \left(\frac{(-1)^m\, 4\lambda_i^2\left(\frac{2m-1}{2}\pi\right)}{\left(\frac{2m-1}{2}\pi\right)^4 - \lambda_i^4}\right)\left(\frac{(-1)^n\, 4\lambda_j^2\, (n\pi)\tanh\lambda_j}{(n\pi)^4 - \lambda_j^4}\right)$$

$$c_3'' = \left(2\nu_{xy} + \frac{4G}{E_2}\right)\left(\frac{R}{\alpha L}\right)^2\left(\frac{h^2}{3R^2}\right)\left[\frac{4\lambda_i^2\,\lambda_m^2}{\lambda_m^4 - \lambda_i^4}(\lambda_m \tanh\lambda_m - \lambda_i \tanh\lambda_i)\right.$$

$$\left.\left[\frac{4\lambda_j^2\,\lambda_n^2}{\lambda_n^4 - \lambda_j^4}(\lambda_n \tanh\lambda_n - \lambda_j \tanh\lambda_j)\right]\right] \quad \text{for } i \neq m,\ j \neq n$$

$$c_3'' = \left(2\nu_{xy} + \frac{4G}{E_2}\right)\left(\frac{R}{\alpha L}\right)^2\left(\frac{h^2}{3R^2}\right)\{\lambda_m \tanh\lambda_m(1 - \lambda_m \tanh\lambda_m)\}$$

$$\{\lambda_n \tanh\lambda_n(1 - \lambda_n \tanh\lambda_n)\} \qquad \text{for } i = m,\ j = n$$

$$c_4'' = \frac{h^2}{3R^2}\left[\left(\frac{R}{L}\right)^4\left(\frac{E_1}{E_2}\right)\lambda_m^4 + \frac{\lambda_n^4}{\alpha^4}\right] + 1$$

and where

$$E_{mn} = -\frac{4p \tanh\lambda_m \tan\lambda_n}{\lambda_m\,\lambda_n}$$

12.3.5 Solution of simultaneous equations

The unknown constants A_{mn} B_{mn} and C_{mn} are determined from solution of the three sets of simultaneous equations, (ie equations 12.27-12.29 or equations 12.30-12.32 or equations 12.33-12.35 depending on the boundary conditions).

It should be noted that the solution for the hinged boundary condition and that for the clamped boundary condition both require the solution of $3 \times m \times n$ simultaneous equations, where m and n are the number of terms considered in the two series.

In the Fortran programs in Appendix F these simultaneous equations are solved using a standard library routine (Crout's factorisation method).

In contrast, in the simply supported case the full benefits of the orthogonality of the assumed displacement functions are realised and solution is required for only three simultaneous equations for each harmonic (ie for each value of m and n).

12.3.6 Stress resultants and membrane and bending stresses

Once the constants A_{mn}, B_{mn} and C_{mn} have been determined the stress resultants can be found from the following equations:

$$N_x = \sum_{m=1}^{\infty} \sum_{n=1}^{\infty} \left[D_x A_{mn} \phi'_{mn} + D_\nu \{ B_{mn} \psi^{\cdot}_{mn} + C_{mn} \xi_{mn} \} \right] \tag{12.36}$$

$$N_\phi = \sum_{m=1}^{\infty} \sum_{n=1}^{\infty} \left[D_\nu A_{mn} \phi'_{mn} + D_\phi \{ B_{mn} \psi^{\cdot}_{mn} + C_{mn} \xi_{mn} \} \right] \tag{12.37}$$

$$N_{x\phi} = \sum_{m=1}^{\infty} \sum_{n=1}^{\infty} \left[D_{x\phi} \left(\left(\frac{L}{R\alpha} \right) A_{mn} \phi^{\cdot}_{mn} + \left(\frac{R\alpha}{L} \right) B_{mn} \psi'_{mn} \right] \right. \tag{12.38}$$

$$M_x = \sum_{m=1}^{\infty} \sum_{n=1}^{\infty} \left[\left(\frac{K_x}{R} \right) \left(\frac{R}{L} \right)^2 \xi''_{mn} + \left(\frac{K_\nu}{R} \right) \left(\frac{1}{\alpha^2} \right) \xi^{\cdot\cdot}_{mn} \right] \tag{12.39}$$

$$M_\phi = \sum_{m=1}^{\infty} \sum_{n=1}^{\infty} \left[\left(\frac{K_\phi}{R} \right) \left(\frac{1}{\alpha^2} \right) \xi^{\cdot\cdot}_{mn} + \left(\frac{K_\nu}{R} \right) \left(\frac{R}{L} \right)^2 \xi''_{mn} \right] \tag{12.40}$$

$$M_{x\phi} = \sum_{m=1}^{\infty} \sum_{n=1}^{\infty} \left(\frac{2K_{x\phi}}{R} \right) \left(\frac{R}{\alpha L} \right) C_{mn} \xi'^{\cdot}_{mn} \tag{12.41}$$

$$Q_x = \sum_{m=1}^{\infty} \sum_{n=1}^{\infty} \left[K_x \left(\frac{R}{L^3} \right) C_{mn} \xi'''_{mn} + (K_\nu + 2K_{x\phi}) \left(\frac{1}{R\alpha^2 L} \right) C_{mn} \xi'^{\cdot\cdot}_{mn} \right] \tag{12.42}$$

$$Q_\phi = \sum_{m=1}^{\infty} \sum_{n=1}^{\infty} \left[K_\phi \left(\frac{1}{R^2 \alpha^3} \right) C_{mn} \xi^{\cdot\cdot\cdot}_{mn} + (K_\nu + 2K_{x\phi}) \left(\frac{1}{\alpha L^2} \right) C_{mn} \xi'^{\cdot\cdot}_{mn} \right] \tag{12.43}$$

In the above expressions for the stress resultants appropriate functions, depending on the boundary conditions as defined in equations (12.18 to 12.20), are of course used in each case.

For the purposes of sonar dome design, results in the form of stress resultants are probably less useful than results in the form of stresses. It is however convenient to retain the distinction between membrane and bending action. The membrane and bending stresses are thus found from:

$$\sigma_x^{\,d} = \frac{N_x}{2h} \qquad (12.44)$$

$$\sigma_x^{\,b} = \pm \frac{3M_x}{2h^2} \qquad (12.45)$$

$$\sigma_\phi^{\,d} = \frac{N_\phi}{2h} \qquad (12.46)$$

$$\sigma_\phi^{\,b} = \pm \frac{3M_\phi}{2h^2} \qquad (12.47)$$

The panel displacements, which are of course of major interest, are found by substitution of the constants A_{mn}, B_{mn} and C_{mn} in the displacement functions 12.12 to 12.14 with the appropriate functions 12.18 to 12.20 depending on the boundary conditions.

12.4 The isotropic case

The solution detailed in Section 12.3 is a completely general one for an orthotropic cylindrical shell where the axes of material symmetry correspond with the axes of symmetry of the shell. This is the case for the cylindrical GRP sonar panels considered here.

This general solution can, of course, be applied to the more specific case of an isotropic cylindrical shell panel by making the following substitutions.

$$E_x = E_y = E \tag{12.48}$$

$$\nu_{xy} = \nu_{yx} = \nu \tag{12.49}$$

$$G = \frac{E}{2(1+\nu)} \tag{12.50}$$

12.5 Convergence Study

Rigorous proof of the convergence of this numerical solution is difficult; and complicated by the fact that the rate of convergence is dependent on the physical parameters of the shell. The study of convergence of the Galerkin method hinges on careful investigation of the behaviour of infinitely many linear algebraic equations and has been the subject of a number of monographs mainly in Russian, for example MIKHLIN [92]. For a particular shell however, convergence can be adequately demonstrated as below.

The particular shell geometry and properties of the middle thickness GRP sonar panel of this investigation, expressed in terms of the non-dimensional parameters of this solution are:

$R/L = 1.84$

$R/h = 200$

$\alpha = 33^{o}$

$E_x/E_y = 1$ (Isotropic case)

$\nu_{xy} = 0.235$ (")

$G_{xy}/E_x = 0.405$ (")

Using these parameters, numerical results were obtained for the fully clamped shell, using differing numbers of terms in the solution. These numerical results, in the form of non-dimensionalised displacements and stress resultants are given in Tables 12.1 to 12.7.

It can be seen from these results that whilst the convergence is not monotonic it is fairly rapid, particularly for displacement and for membrane stress. Convergence of bending stress is less rapid but nevertheless changes only at the 2nd significant digit after 5 terms and the 3rd significant digit after 8 terms.

All of the panels of this investigation are of broadly similar geometry (with the exception of panel AL2 which has an R/h ratio an order of magnitude higher than the other panels) so similar convergence can be reasonably expected in each case.

For most design purposes with panels of this general geometry, and to minimise computational effort, a solution to 7 terms would seem to be adequate. For the purposes of this particular investigation, including for the parametric study given in the next chapter, all cases were worked to 9 terms.

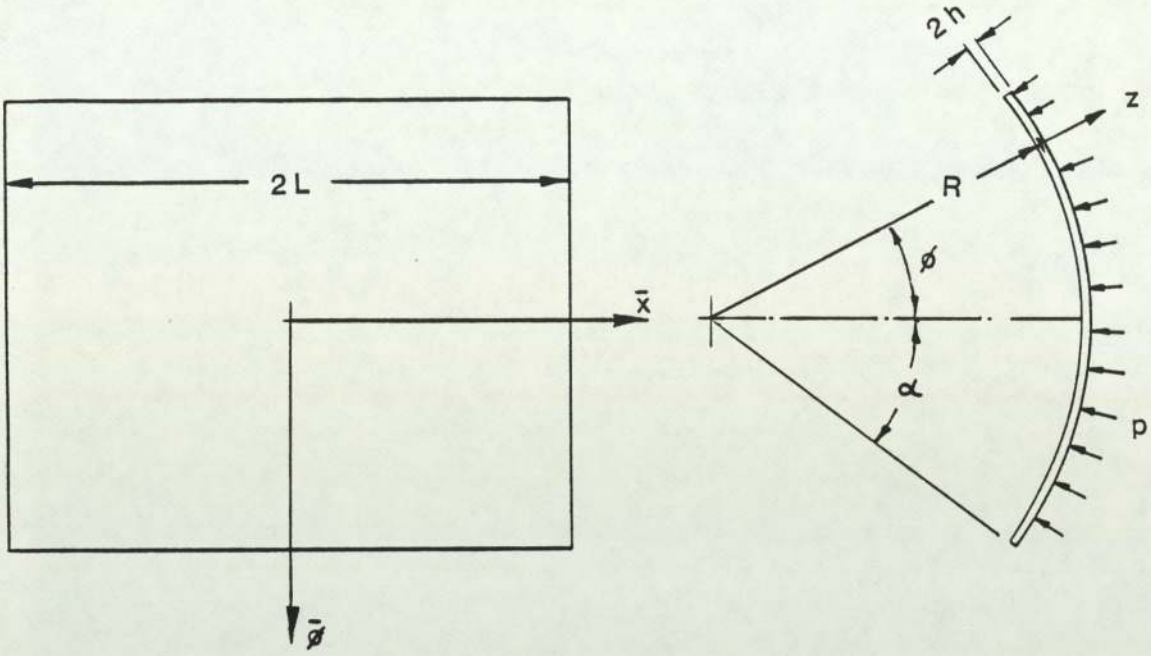

Fig. 12.1 Cylindrical shell panel

	Number of Terms								
ø/α	1	2	3	4	5	6	7	8	9
0.0	-225.2	-110.9	-131.8	-122.9	-126.2	-124.8	-125.5	-125.1	-125.3
0.2	-206.4	-115.5	-134.8	-127.0	-130.0	-128.8	-129.4	-129.0	-129.3
0.4	-155.4	-115.0	-135.3	-127.0	-130.2	-128.8	-129.4	-129.0	-129.3
0.6	-87.8	-86.3	-108.4	-99.9	-102.6	-101.4	-101.9	-101.7	-101.8
0.8	-26.8	-32.8	-44.7	-41.0	-43.3	-42.3	-42.8	-42.5	-42.6
1.0	0.0	0.0	0.0	0.0	0.0	0.0	0.0	0.0	0.0

Table 12.1 Variation of $\frac{wE}{PR}$ at $\frac{x}{L} = 0$

with number of terms taken in Galerkin solution.

	Number of Terms								
ϕ/α	1	2	3	4	5	6	7	8	9
0.0	-474	-891	-1687	-2103	-2440	-2599	-2732	-2801	-2862
0.2	-434	-999	-1651	-2187	-2446	-2650	-2762	-2839	-2899
0.4	-327	-1125	-1705	-2176	-2510	-2680	-2788	-2875	-2930
0.6	-185	-918	-1617	-2023	-2260	-2431	-2556	-2634	-2682
0.8	-56	-366	-781	-1116	-1334	-1466	-1545	-1595	-1629
1.0	0	0	0	0	0	0	0	0	0

Table 12.2 Variation of $\frac{M_x}{PR^2} \times 10^6$ at $\frac{x}{L} = 1$

with number of terms taken in Galerkin solution.

	Number of Terms								
x/l	1	2	3	4	5	6	7	8	9
0.0	-422	-599	-865	-798	-872	-852	-877	-870	-880
0.2	-387	-725	-785	-901	-866	-904	-903	-906	-914
0.4	-291	-903	-894	-944	-1025	-1023	-1021	-1037	-1042
0.6	-164	-781	-1122	-1170	-1176	-1210	-1247	-1265	-1269
0.8	-50	-321	-644	-872	-1001	-1068	-1102	-1119	-1131
1.0	0	0	0	0	0	0	0	0	0

Table 12.3 Variation of $\frac{M_\phi}{PR^2} \times 10^6$ at $\frac{\phi}{\alpha} = 1$

with number of terms taken in Galerkin solution.

	Number of Terms								
x/l	1	2	3	4	5	6	7	8	9
0.0	-1.430	-0.890	-1.061	-0.991	-1.017	-1.006	-1.011	-1.009	-1.010
0.2	-1.282	-1.035	-0.970	-1.037	-1.003	-1.016	-1.012	-1.012	-1.013
0.4	-0.889	-1.229	-1.005	-1.017	-1.041	-1.036	-1.032	-1.035	-1.035
0.6	-0.397	-1.041	-1.114	-1.071	-1.040	-1.042	-1.048	-1.050	-1.049
0.8	-0.023	-0.432	-0.593	-0.702	-0.714	-0.727	-0.720	-0.720	-0.718
1.0	-0.031	-0.021	-0.034	-0.028	-0.033	-0.029	-0.032	-0.030	-0.031

Table 12.4 Variation of $\frac{N_\phi}{PR}$ at $\frac{\phi}{\alpha} = 0$

with number of terms taken in Galerkin solution.

	Number of Terms								
β/α	1	2	3	4	5	6	7	8	9
0.0	-1.430	-0.890	-1.061	-0.991	-1.017	-1.006	-1.011	-1.009	-1.010
0.2	-1.409	-0.842	-1.048	-0.979	-1.014	-0.999	-1.005	-1.002	-1.004
0.4	-1.335	-0.794	-1.050	-0.969	-0.996	-0.984	-0.991	-0.988	-0.989
0.6	-1.197	-0.853	-1.026	-0.948	-0.985	-0.971	-0.977	-0.974	-0.975
0.8	-1.021	-0.918	-1.001	-0.958	-0.968	-0.962	-0.963	-0.963	-0.963
1.0	-0.923	-0.894	-0.928	-0.942	-0.944	-0.946	-0.948	-0.947	-0.949

Table 12.5 Variation of $\frac{N_\beta}{PR}$ at $\frac{x}{L} = 0$

with number of terms taken in Galerkin solution.

	Number of Terms								
x/l	1	2	3	4	5	6	7	8	9
0.0	-0.213	-0.256	-0.239	-0.249	-0.245	-0.248	-0.247	-0.247	-0.247
0.2	-0.202	-0.248	-0.238	-0.240	-0.242	-0.242	-0.241	-0.241	-0.241
0.4	-0.171	-0.229	-0.212	-0.227	-0.222	-0.224	-0.224	-0.224	-0.224
0.6	-0.131	-0.197	-0.183	-0.200	-0.195	-0.200	-0.198	-0.199	-0.198
0.8	-0.105	-0.138	-0.168	-0.169	-0.165	-0.169	-0.164	-0.167	-0.165
1.0	-0.130	-0.091	-0.145	-0.117	-0.138	-0.125	-0.136	-0.128	-0.134

Table 12.6 Variation of $\frac{N_M}{PR}$ at $\frac{\beta}{\alpha} = 0$

with number of terms taken in Galerkin solution.

	Number of Terms								
β/α	1	2	3	4	5	6	7	8	9
0.0	-0.213	-0.256	-0.239	-0.249	-0.245	-0.248	-0.247	-0.247	-0.247
0.2	-0.214	-0.234	-0.237	-0.242	-0.241	-0.242	-0.242	-0.242	-0.242
0.4	-0.215	-0.197	-0.216	-0.223	-0.219	-0.222	-0.222	-0.222	-0.221
0.6	-0.209	-0.190	-0.186	-0.195	-0.193	-0.195	-0.194	-0.195	-0.194
0.8	-0.202	-0.203	-0.187	-0.195	-0.187	-0.192	-0.189	-0.190	-0.190
1.0	-0.217	-0.210	-0.218	-0.222	-0.222	-0.222	-0.223	-0.223	-0.223

Table 12.7 Variation of $\frac{N_M}{PR}$ at $\frac{x}{L} = 0$

with number of terms taken in Galerkin solution.

CHAPTER 13

PARAMETRIC STUDY

13.1 Introduction

This chapter presents numerical results for a pressure loaded cylindrical shell panel, in the form of a parametric study, intended to be of use for preliminary design purposes.

The behaviour of a cylindrical panel, subject to pressure loading, is influenced by the panel boundary conditions, the elastic properties of the panel material, and by the geometry and physical dimensions of the panel. In the case of a GRP sonar panel, variations in any of these may occur either as a result of deliberate design changes or as a result of variations in manufacture or assembly. In either case, the effect of these variations on the mechanical behaviour of the panel can be investigated using the numerical solution detailed in Chapter 12.

Similar results to those presented here could, of course, have been obtained using finite element analysis. The numerical 'Galerkin' solution of Chapter 12 was used in preference, since to have used finite elements for this part of the study would have necessitated remeshing of the structure at each change of geometry, and whilst this would have been perfectly satisfactory, it would have been very time consuming. The Galerkin method, in contrast, is very straightforward in this respect, and the effect of parameter changes can be investigated very quickly.

Because of the number of parameters required, completely to describe a cylindrical panel, a comprehensive parametric study, adequate to predict, for design purposes, the behaviour of every possible case, is clearly impractical and also outside of the scope of this work. The graphs presented here therefore, are intended only to illustrate the effects of changes to the major panel parameters over limited ranges.

Within the ranges considered however, these graphs should find application in the preliminary design of future cylindrical panels. They may also be used to examine the effects of material and geometry changes. A more extensive range of design data can be generated, if required, simply by more computational work.

It is necessary in a study of this kind to begin by selecting a set of base parameters to which all independent parametric changes can be referred. In this study these common base parameters are the geometry parameters and approximate material properties of the middle thickness GRP panel GRP2. The approximate material properties are the mean values measured for this panel. These base parameters were selected because they are close to those of most interest for this work and they are also the parameters for which the convergence of the numerical solution has been investigated.

Using the numerical results obtained with these parameters as a comparator each of the following were examined in turn.

(1) Changes to panel boundary conditions.

(2) Changes to material elastic properties including orthotropy.

(3) Changes to panel geometry.

For a range of each panel parameter, results were obtained for radial displacement, membrane stress and bending stress.

All results are presented graphically, in non-dimensional form, along the axes of symmetry of the panel. Membrane and bending stresses are given in the directions parallel to the panel edges (the principal panel directions) and although the total principal stresses are not given directly, they can of course be obtained if required, by addition of the membrane and bending components.

13.2 Boundary conditions

Three types of boundary conditions were considered for this study:

(1) All edges simply supported. (SS)

(2) All edges hinged (membrane clamped). (CS)

(3) All edges clamped. (CC)

13.3 Material properties

For investigation of the effects of variation of material elastic properties, three non-dimensional parameters were considered:

(1) E_x/E_ϕ.

(2) $G_{x\phi}/E_\phi$.

(3) $\nu_{x\phi}$.

For each of these parameters a range of values was selected to cover all likely possibilities for the sonar dome laminate, and also to provide sufficient spread of values to indicate clearly any trends in behaviour. For example the ratio of Young's moduli E_x/E_ϕ is the fundamental measure of the material orthotropy and is considered here in the range 0.5 to 2. This is a greater range than would normally be expected for the standard sonar dome laminate but is nevertheless a relatively small range for composite laminates in general.

13.4 Panel geometry

Since the numerical solution is based on Flügge's cylindrical shell equations, which make no limiting assumptions about shell geometry except that the shell be thin, it is applicable to a wide range of geometries including long shells, short shells, shallow shells and deep shells. To examine geometry changes three non-dimensional parameters were considered.

(1) α (semi central angle).

(2) R/L (Radius/semi length).

(3) R/h (Radius/semi thickness).

Only limited ranges of these parameters were selected for this study. To cover all likely requirements for future sonar panel design wider ranges may need to be considered.

13.5 Parameters and key to figures

Base Parameters.

Material

$E_x/E_\phi = 1$ (isotropic case)

$G_{x\phi}/E_\phi = 0.405$ (")

$\nu_{x\phi} = 0.235$ (")

Geometry (see Figure 13.1)

$\alpha = 33^o$

$R/L = 1.84$

$R/h = 200$

Boundary conditions:	Figure Nos.
SS)	
)	
CS)	13.2 to 13.7
)	
CC)	

Material properties		
E_x/F_ϕ	= 0.5, 1.0, 2.0	13.8 to 13.12
$G_{x\phi}/E_\phi$	= 0.2, 0.405, 0.6	13.13 to 13.17
$\nu_{x\phi}$	= 0, 0.235, 0.5	13.18 to 13.22

Geometry		
α	= 20^o, 33^o 60^o	13.23 to 13.28
R/L	= 0.92, 1.84, 3.68	13.28 to 13.32
R/h	= 100, 200, 400	13.32 to 13.37

13.6 Notes on Interpretation of the graphical results

(1) Results are presented along axes of symmetry only and are plotted in each case, from the centre of the panel to the edge.

(2) Numerical values have been obtained at 6 points for each curve. Data points are shown and keyed.

(3) Cubic spline curve fitting has been used for all graphs. Zero slope has been enforced at clamped edges for displacement graphs and at axes of symmetry for all graphs.

(4) Displacements shown positive are radially inwards (in the direction of a positive pressure load to the convex surface of the panel).

(5) Bending stresses are shown as positive (tensile) on the concave surface of the panel.

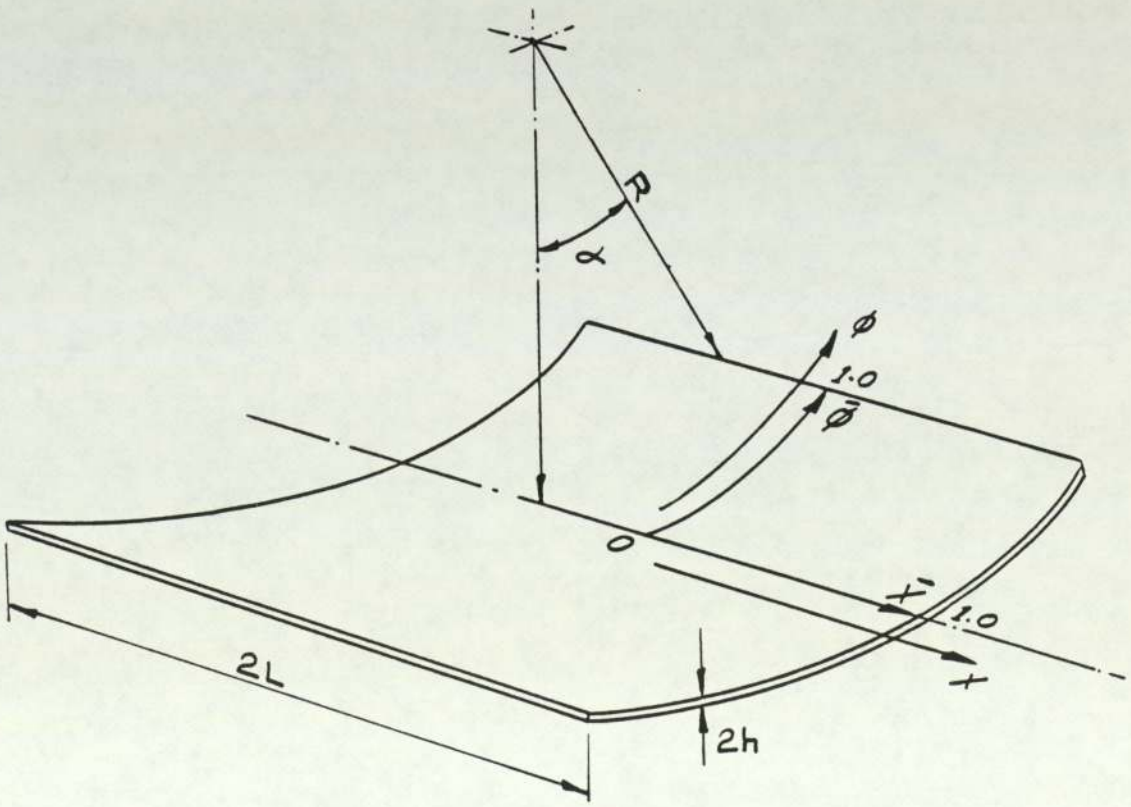

Fig. 13.1 Cylindrical shell panel

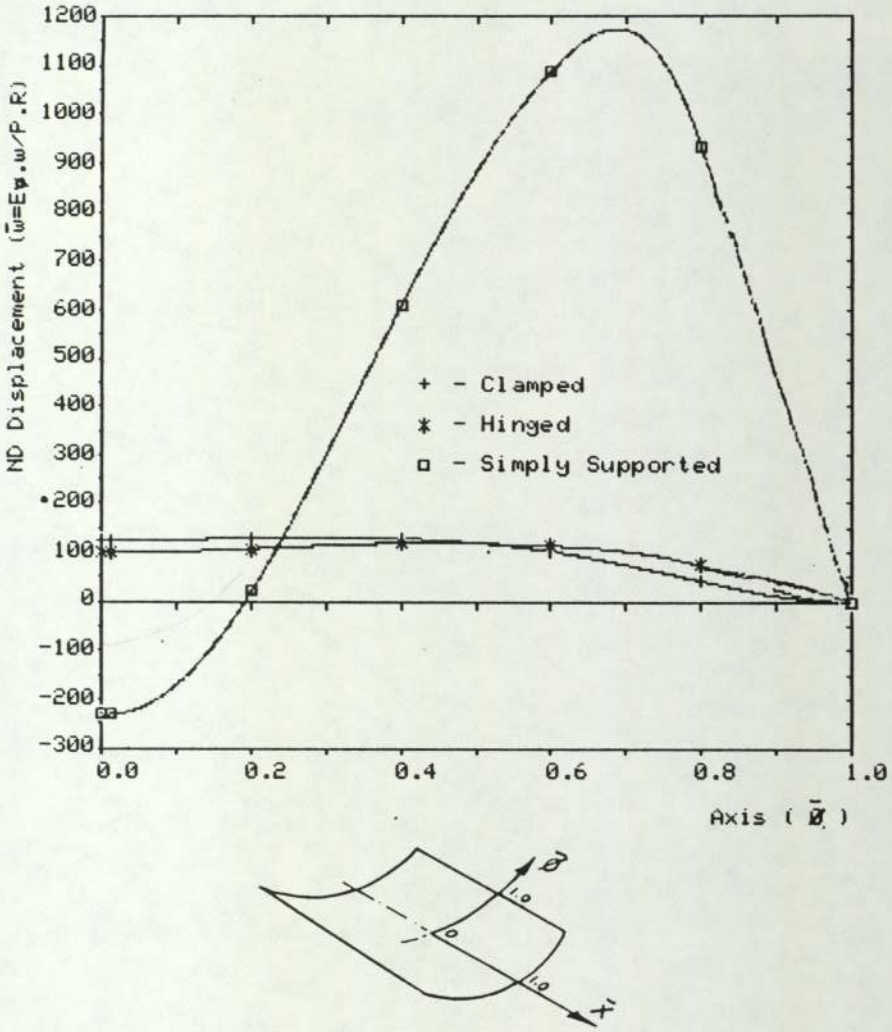

Fig. 13.2 Variation of nondimensional radial displacement ($\bar{w}$) along $\bar{x}$=0 for clamped, hinged & simply supported edges (Isotropic case)

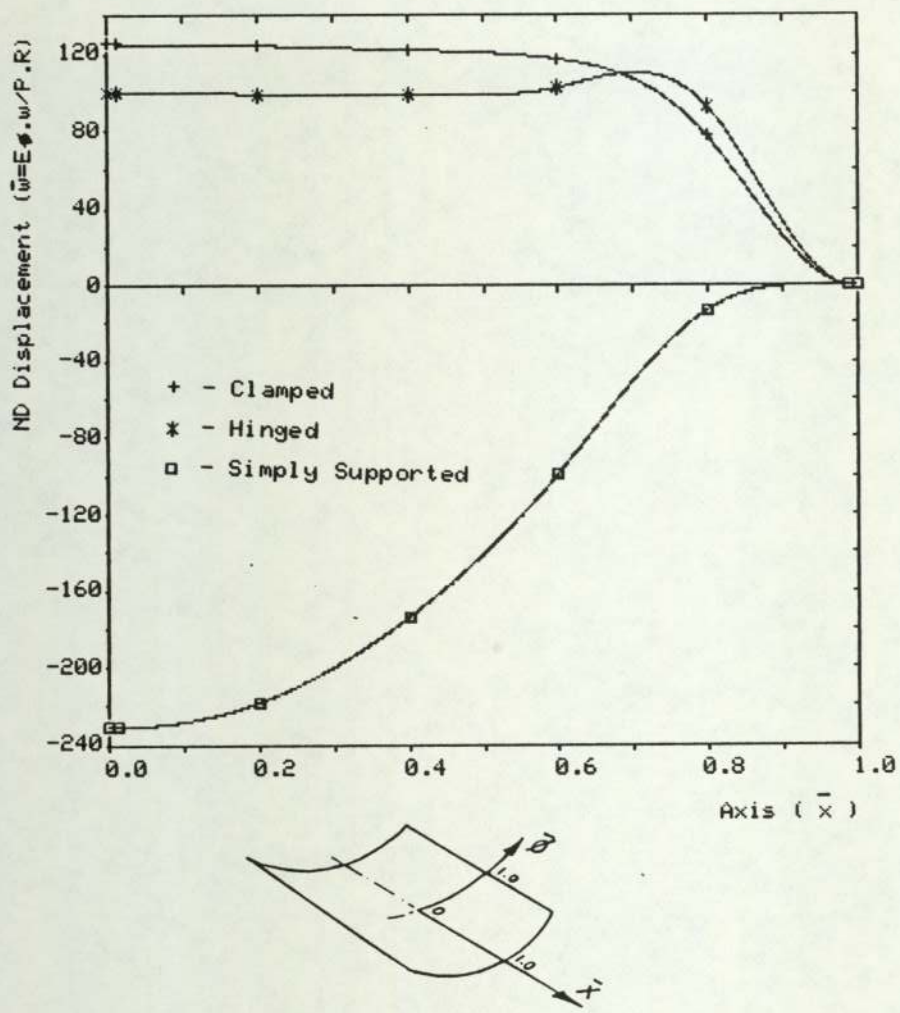

Fig. 13.3 Variation of nondimensional radial displacement ($\bar{w}$) along $\bar{\theta}$=0 for clamped, hinged & simply supported edges (Isotropic case)

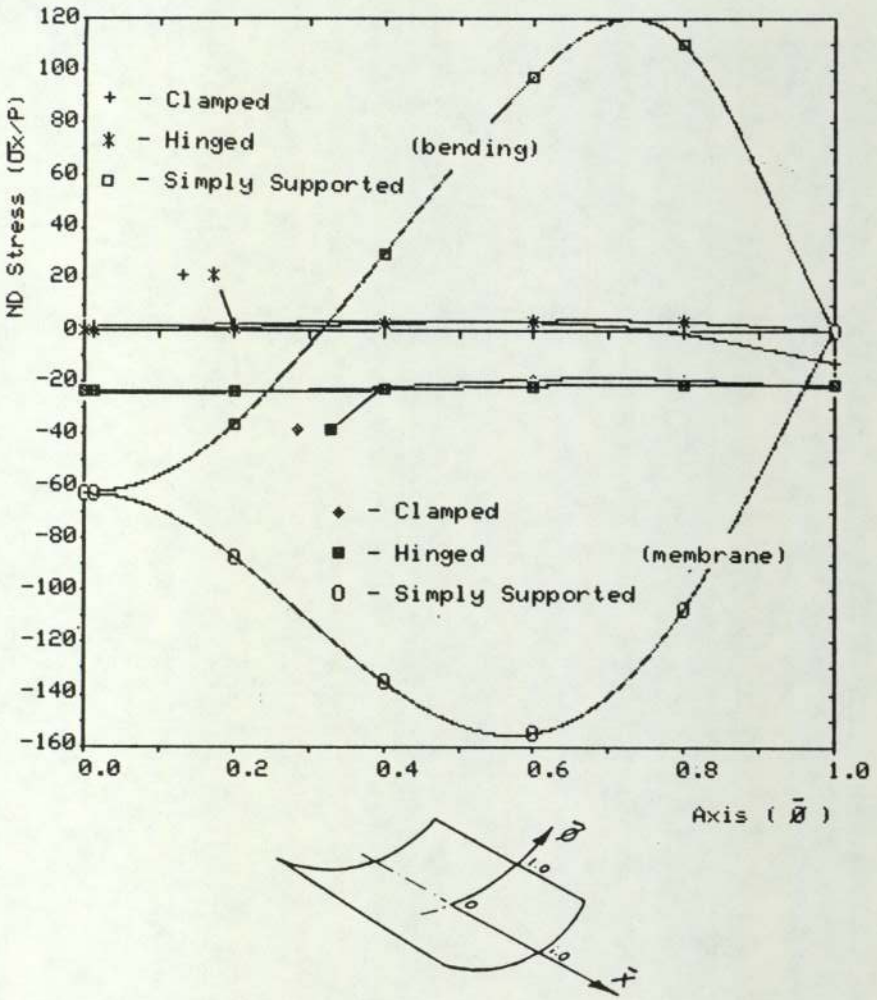

Fig. 13.4 Variation of Nondimensional stresses ($\bar{\sigma}_x$), bending and membrane along $\bar{x}$=0 for clamped, hinged & simply supported edges (Isotropic case)
Bending stress on concave surface.

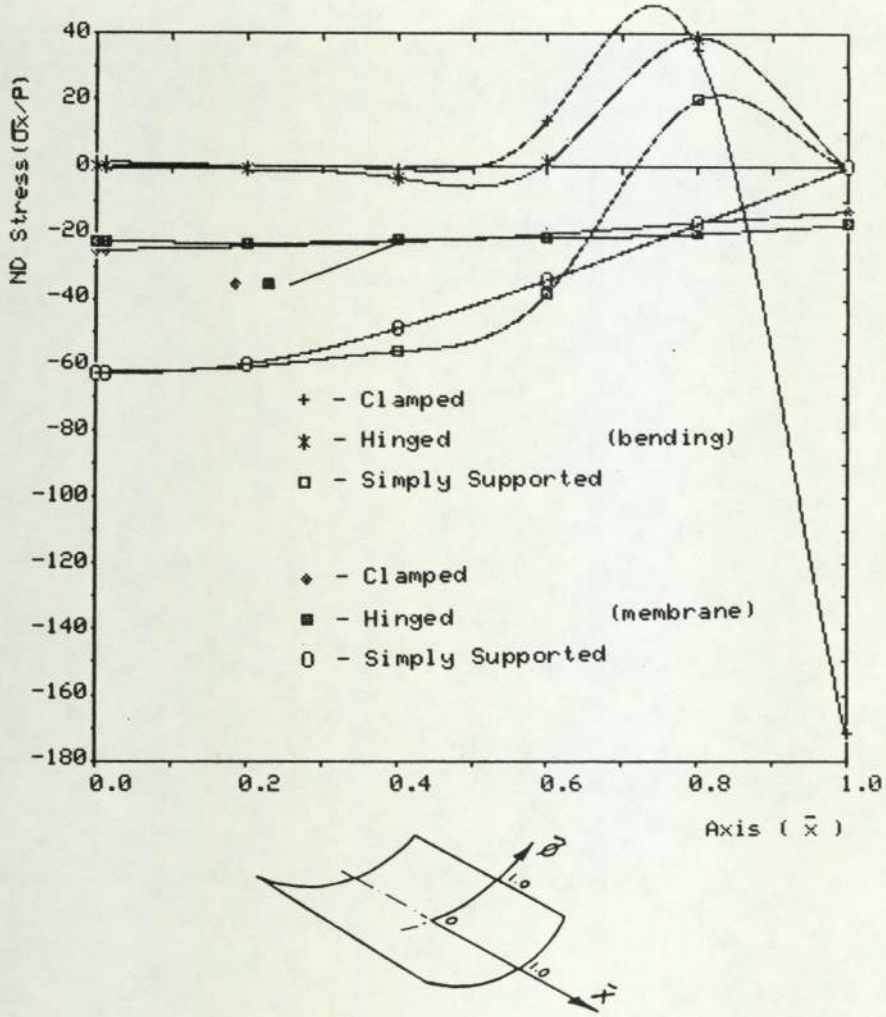

Fig. 13.5 Variation of Nondimensional stress ($\bar{\sigma}_x$), bending and membrane along $\bar{\beta}$=0 for clamped, hinged & simply supported edges (Isotropic case)
Bending stress on concave surface.

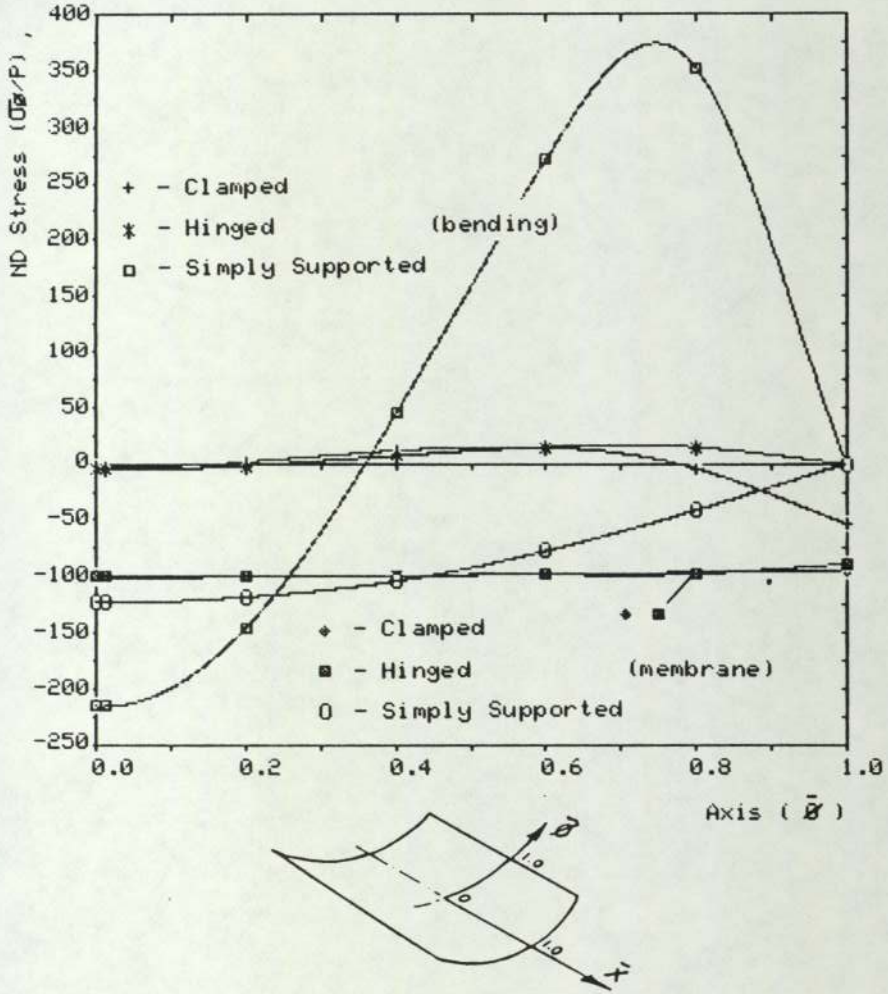

Fig. 13.6 Variation of Nondimensional stress (σ_{ϕ}), bending and membrane along $\bar{x}$=0 for clamped, hinged & simply supported edges (Isotropic case)
Bending stress on concave surface.

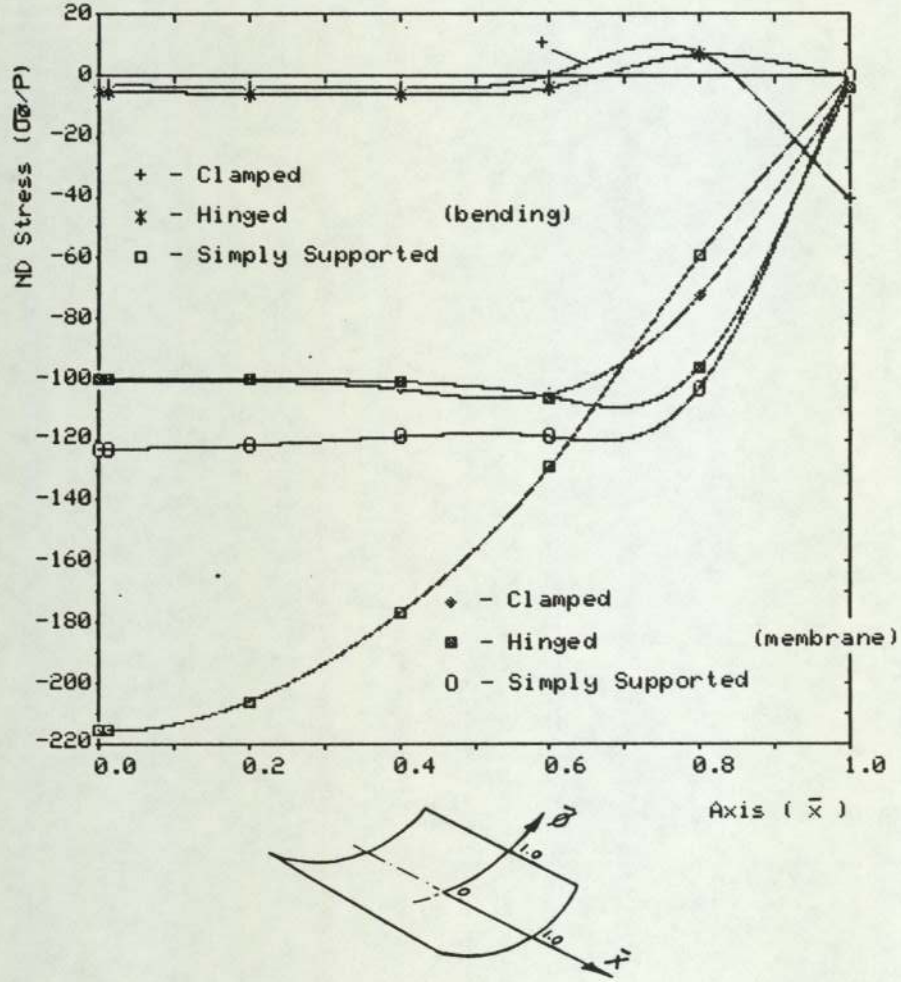

Fig. 13.7 Variation of Nondimensional stress (σ_{ϕ}), bending and membrane along $\bar{\phi}$=0 for clamped, hinged & simply supported edges (Isotropic case)
Bending stress on concave surface.

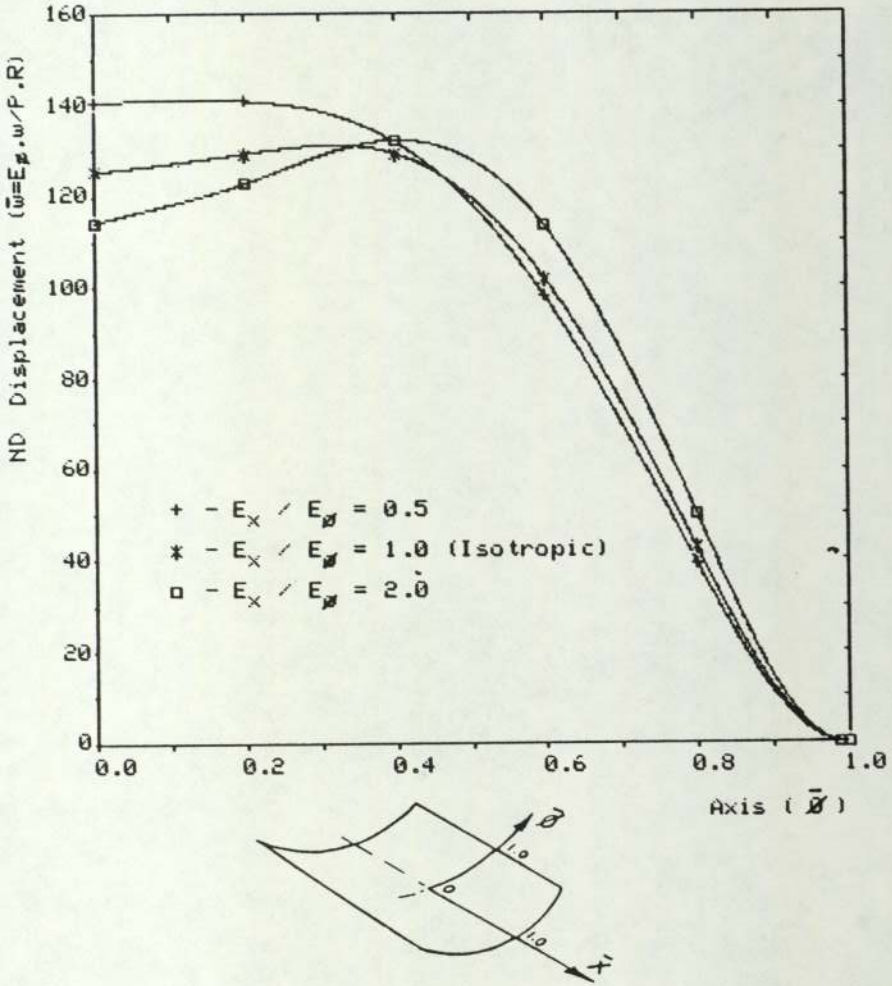

Fig. 13.8 Variation of nondimensional radial displacement ($\bar{w}$) along $\bar{x}$=0 for 3 cases of E_x/E_ϕ (Orthotropic case)

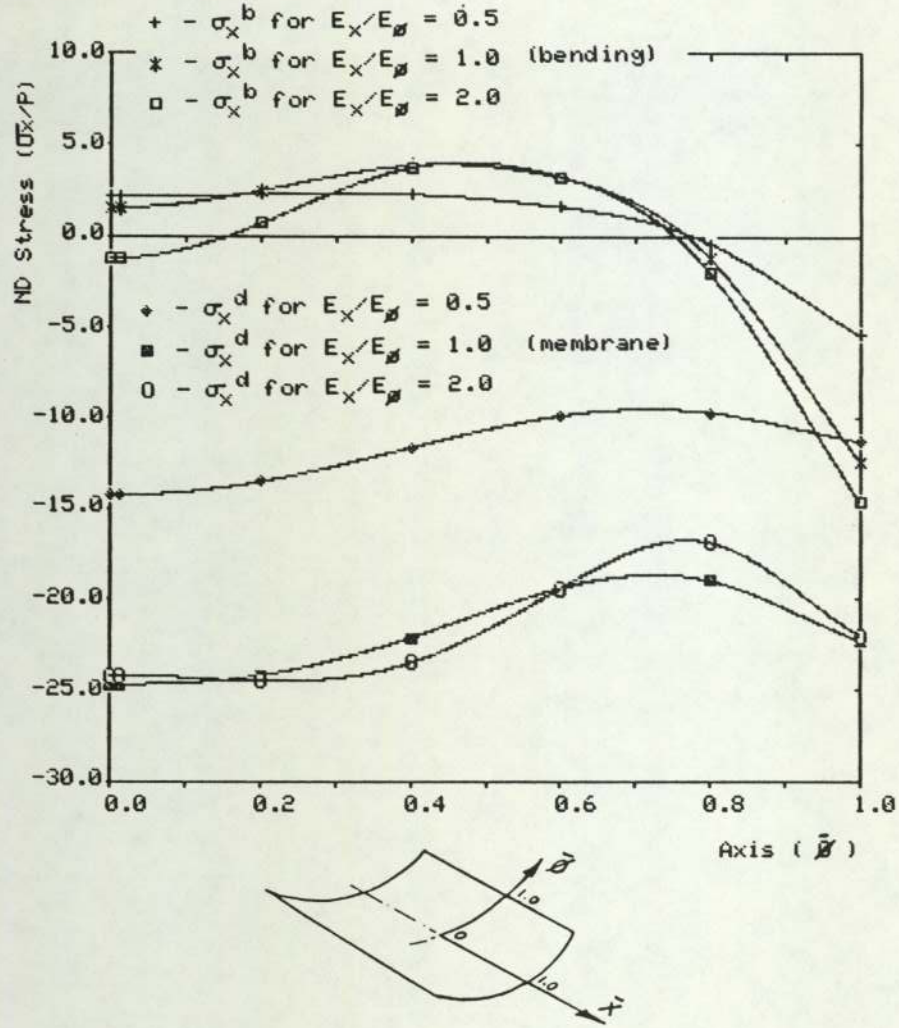

Fig. 13.9 Variation of Nondimensional stresses (σ_x), bending and membrane along $\bar{x}$=0 for 3 cases of E_x/E_ϕ (Orthotropic case)
Bending stress on concave surface.

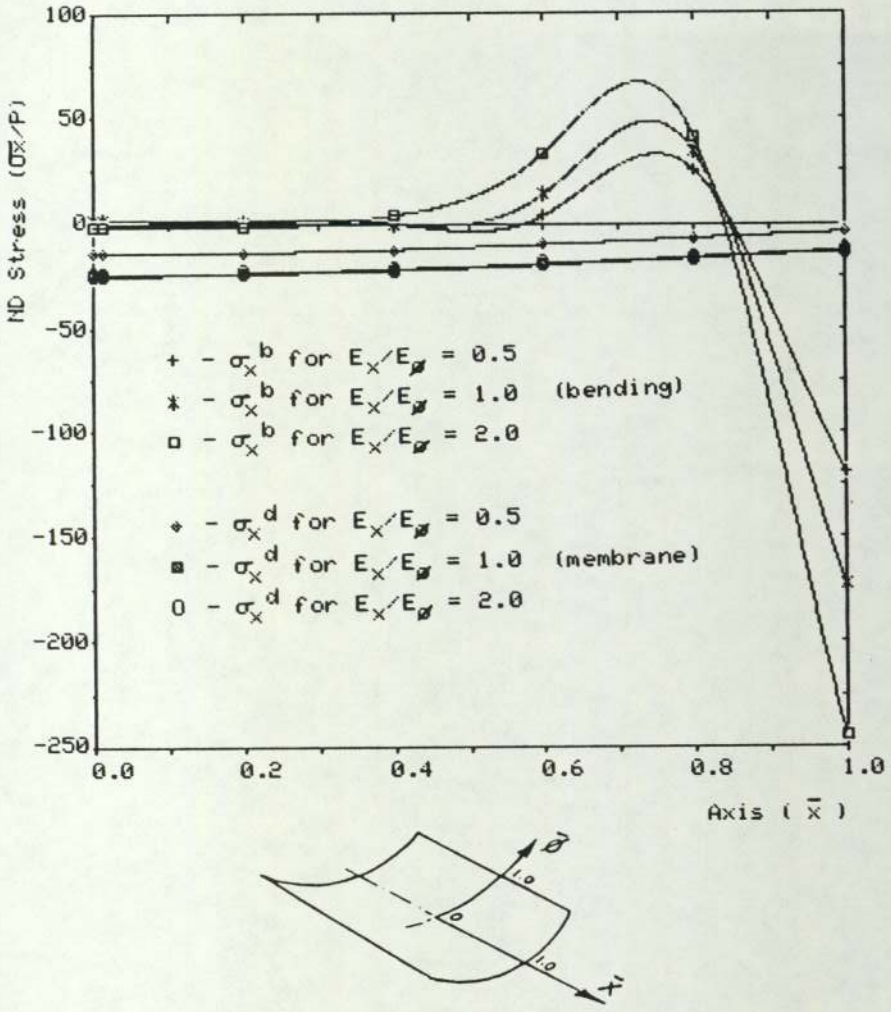

Fig. 13.10 Variation of Nondimensional stress ($\bar{\sigma}_x$), bending and membrane along $\bar{\phi}$=0 for 3 cases of E_x/E_ϕ (Orthotropic case)
Bending stress on concave surface.

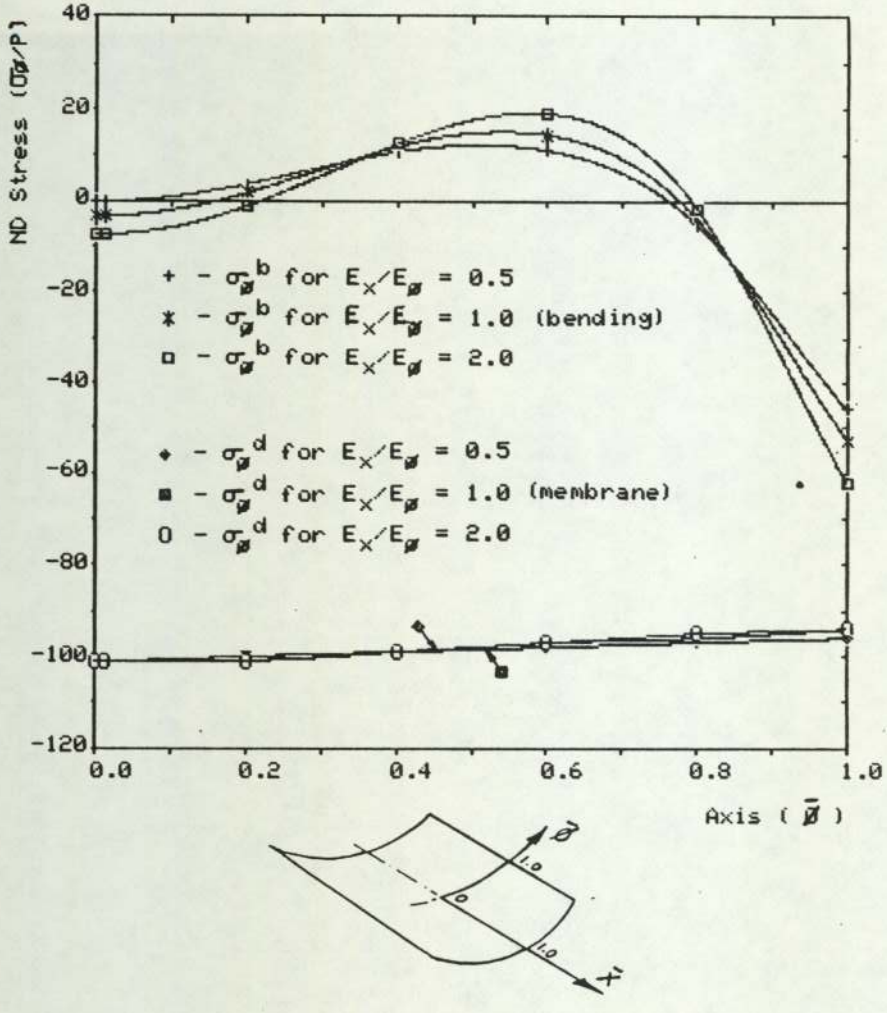

Fig. 13.11 Variation of Nondimensional stress ($\bar{\sigma}_\phi$), bending and membrane along $\bar{x}$=0 for 3 cases of E_x/E_ϕ (Orthotropic case)
Bending stress on concave surface.

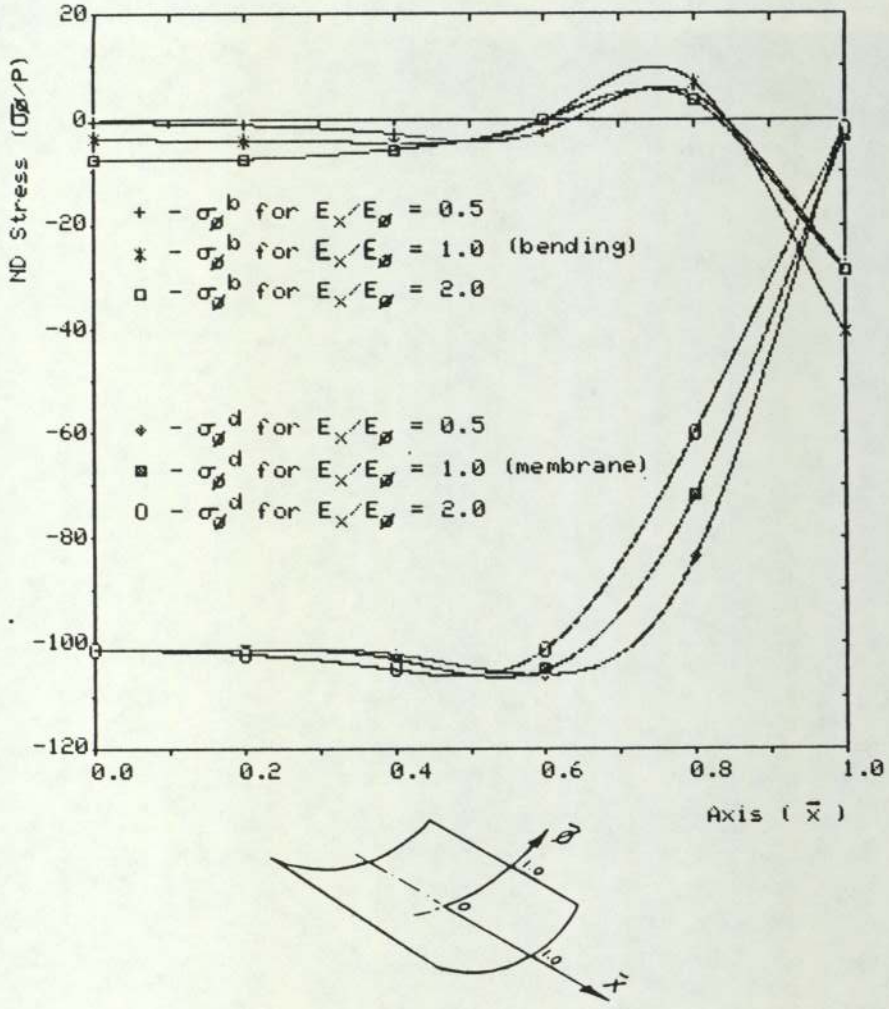

Fig. 13.12 Variation of Nondimensional stress (σ_{ϕ}), bending and membrane along $\bar{\phi}$=0 for 3 cases of E_x/E_{ϕ} (Orthotropic case)
Bending stress on concave surface.

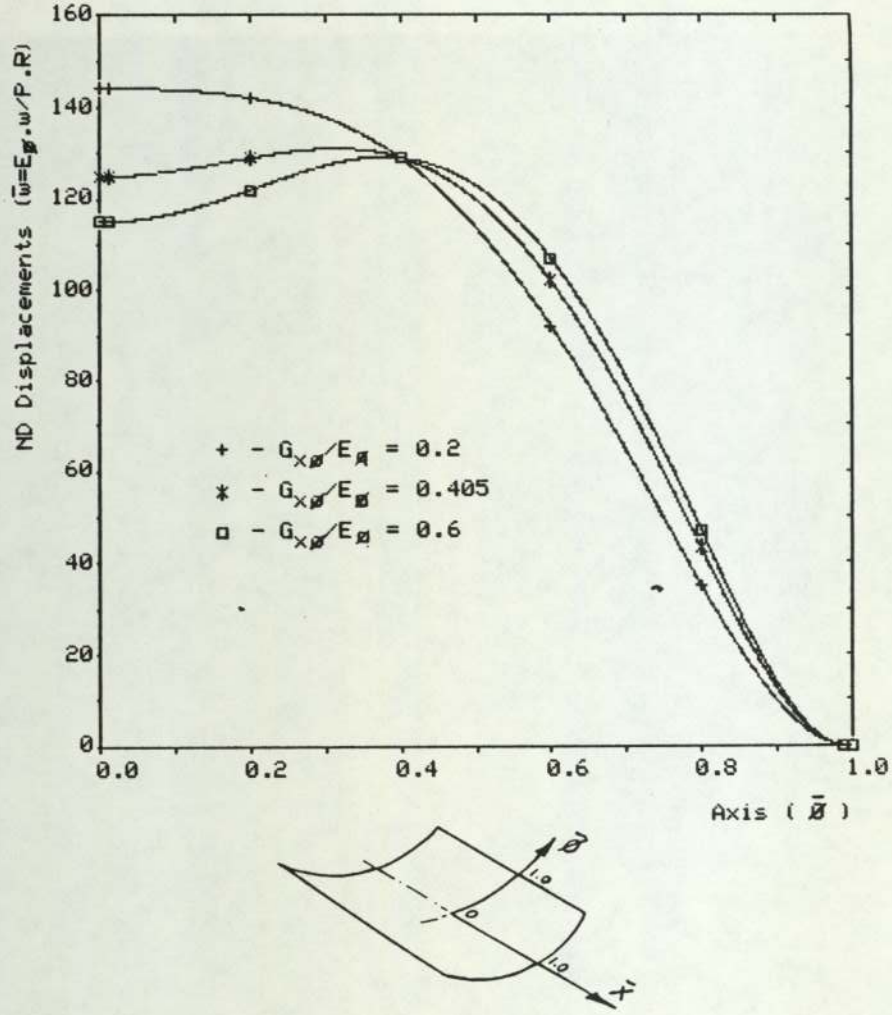

Fig. 13.13 Variation of nondimensional radial displacement ($\bar{w}$) along $\bar{x}$=0 for 3 cases of $G_{x\phi}/E_x$ (Orthotropic case)

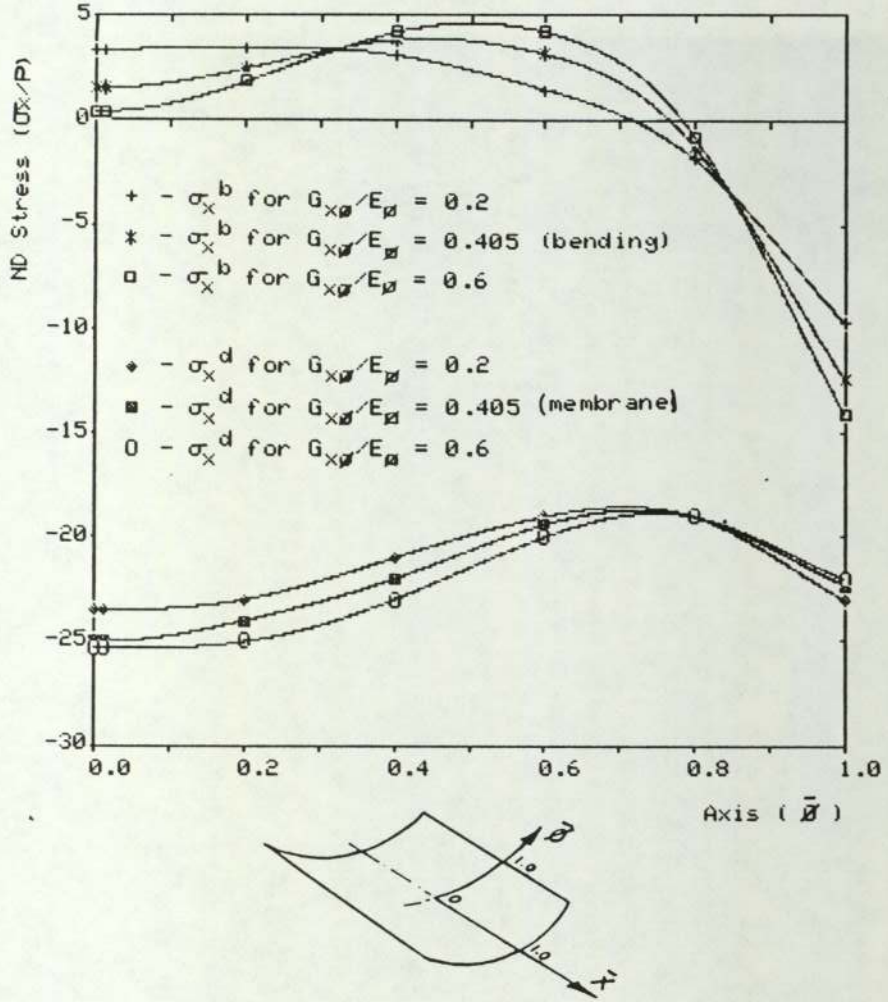

Fig. 13.14 Variation of Nondimensional stresses ($\sigma_{\bar{x}}$), bending and membrane along $\bar{x}$=0 for 3 cases of $G_{x\phi}/E_x$ (Orthotropic case)
Bending stress on concave surface.

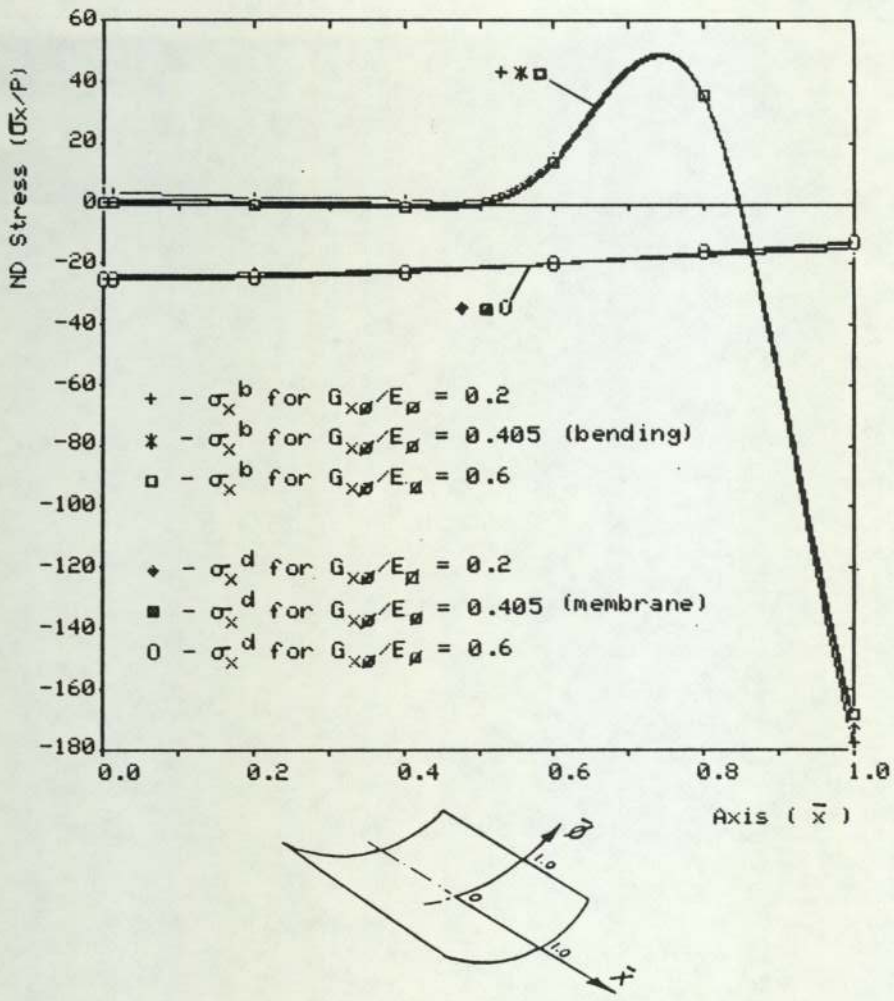

Fig. 13.15 Variation of Nondimensional stress (σ_x), bending and membrane along $\bar{\phi}$=0 for 3 cases of $G_{x\phi}/E_x$ (Orthotropic case)
Bending stress on concave surface.

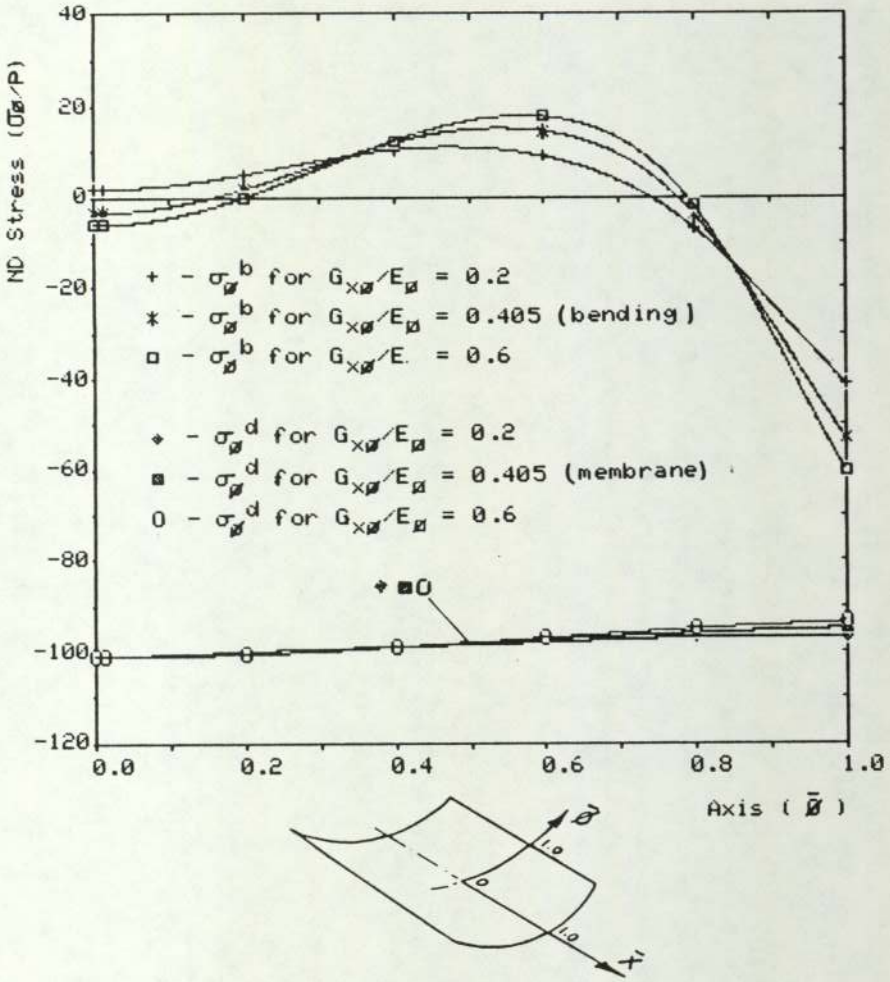

Fig. 13.16 Variation of Nondimensional stress ($\bar{\sigma}_{\phi}$), bending and membrane along $\bar{x}$=0 for 3 cases of $G_{x\phi}/E_x$ (Orthotropic case)
Bending stress on concave surface.

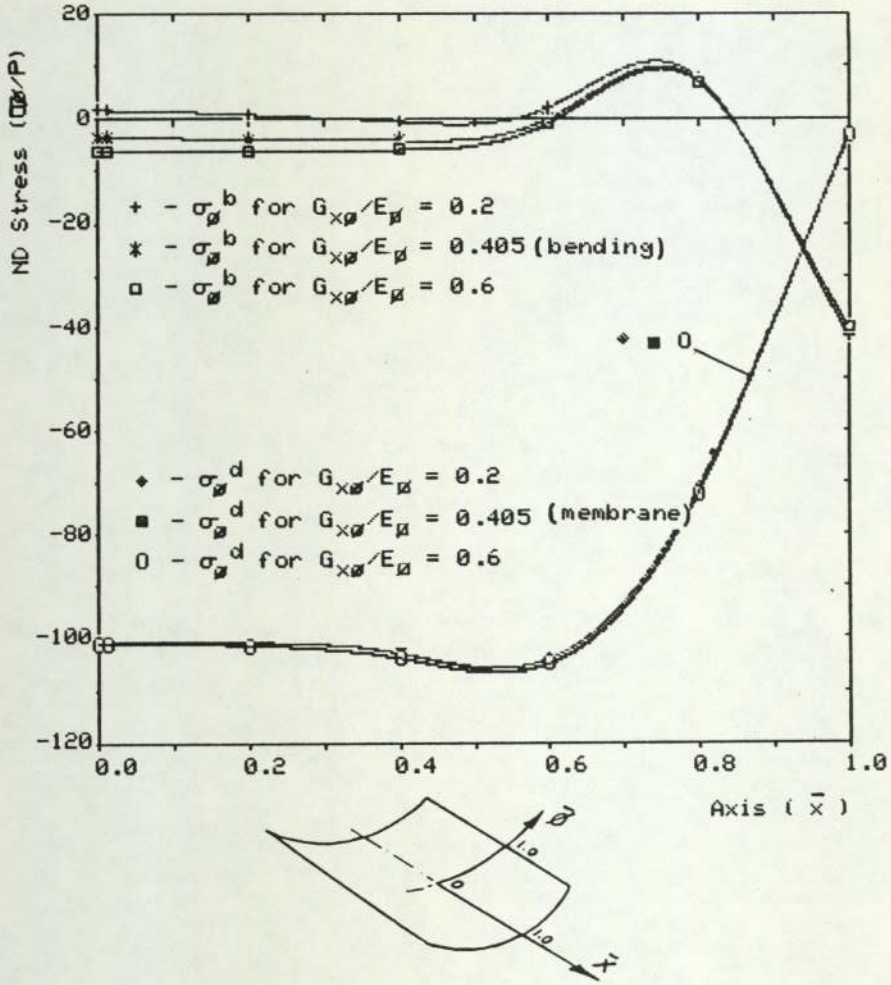

Fig. 13.17 Variation of Nondimensional stress ($\bar{\sigma}_{\phi}$), bending and membrane along $\bar{\phi}$=0 for 3 cases of $G_{x\phi}/E_x$ (Orthotropic case)
Bending stress on concave surface.

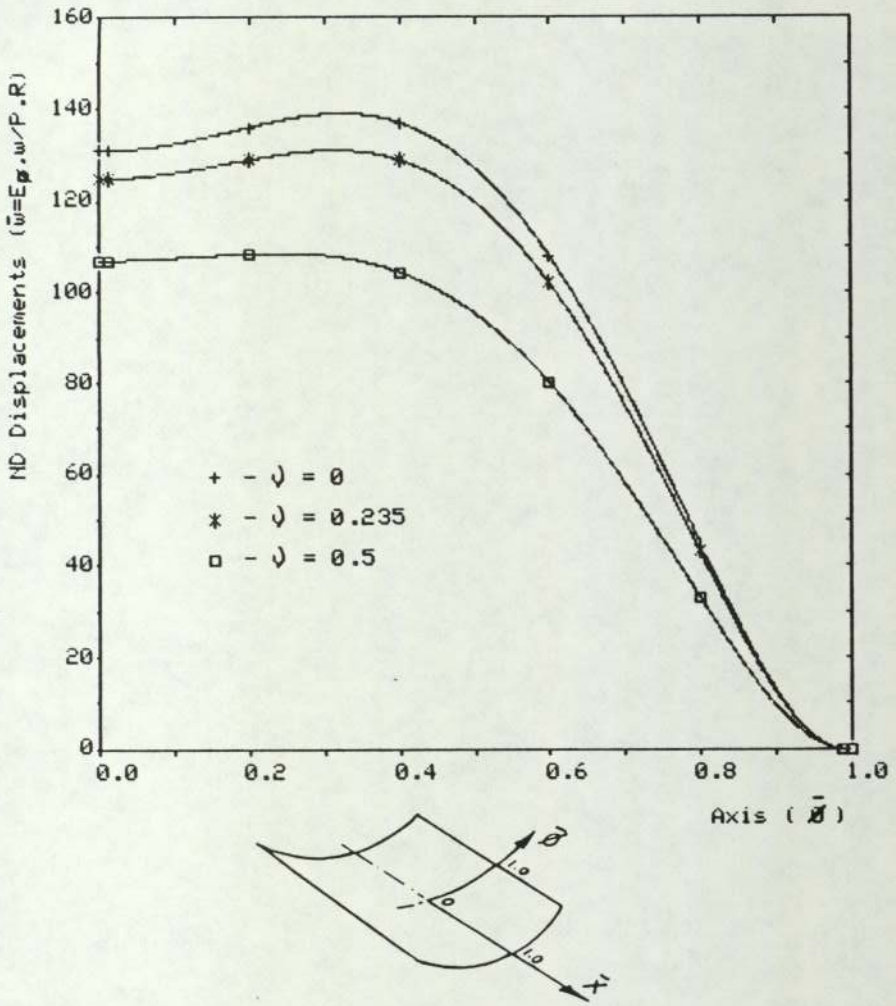

Fig. 13.18 Variation of nondimensional radial displacement ($\bar{w}$) along $\bar{x}$=0 for 3 values of Poisson's ratio (Isotropic case)

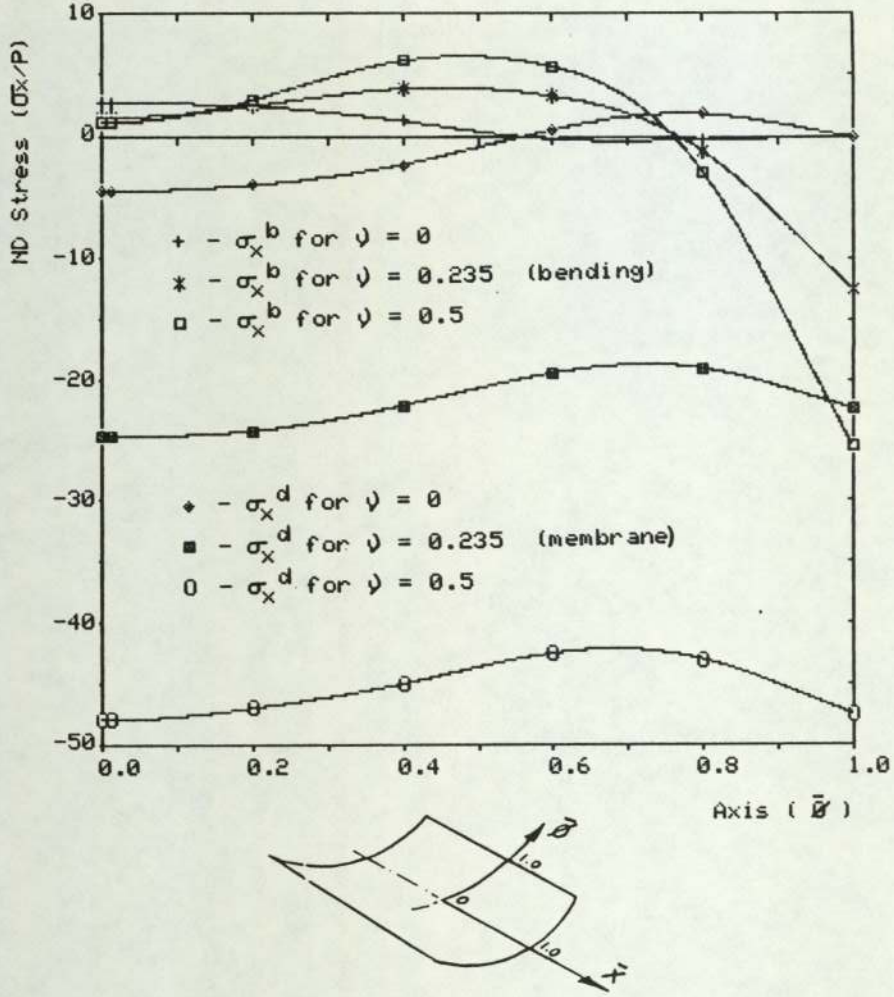

Fig. 13.19 Variation of Nondimensional stresses (σ_x), bending and membrane along $\bar{x}$=0 for 3 values of Poisson's ratio (Isotropic case)
Bending stress on concave surface.

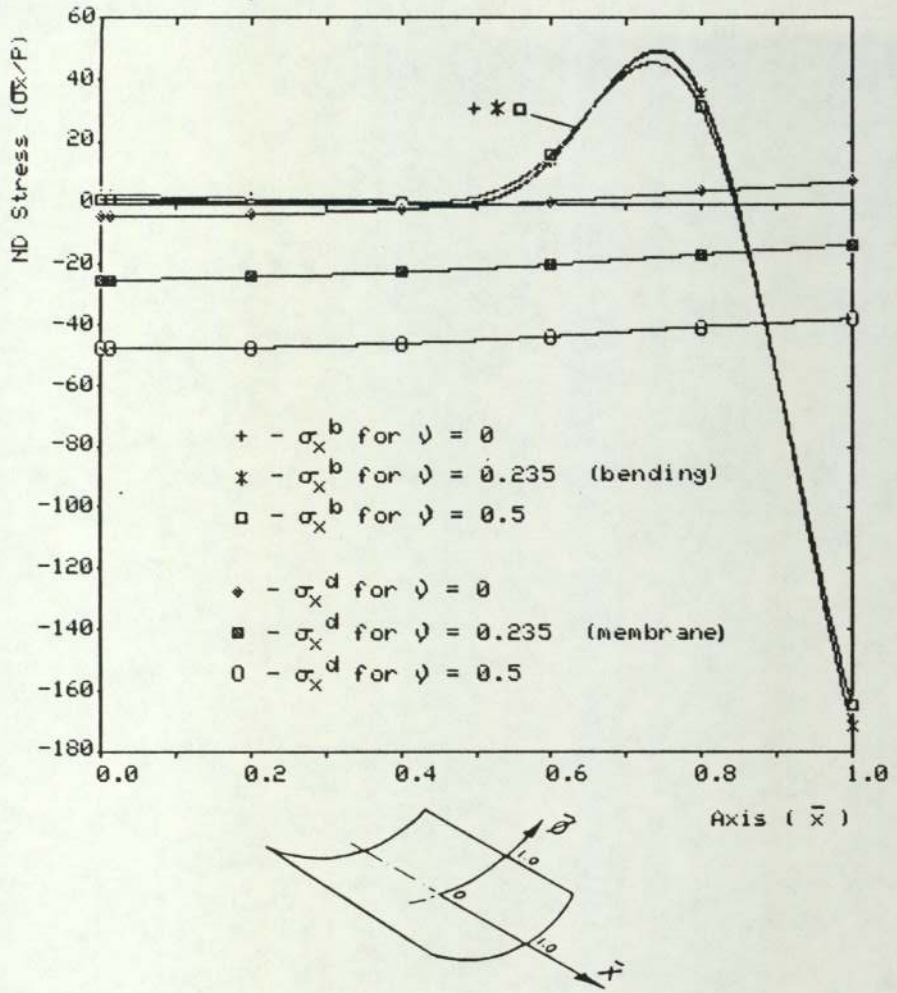

Fig. 13.20 Variation of Nondimensional stress ($\sigma_{\bar{x}}$), bending and membrane along $\bar{\theta}$=0 for 3 values of Poisson's ratio (Isotropic case)
Bending stress on concave surface.

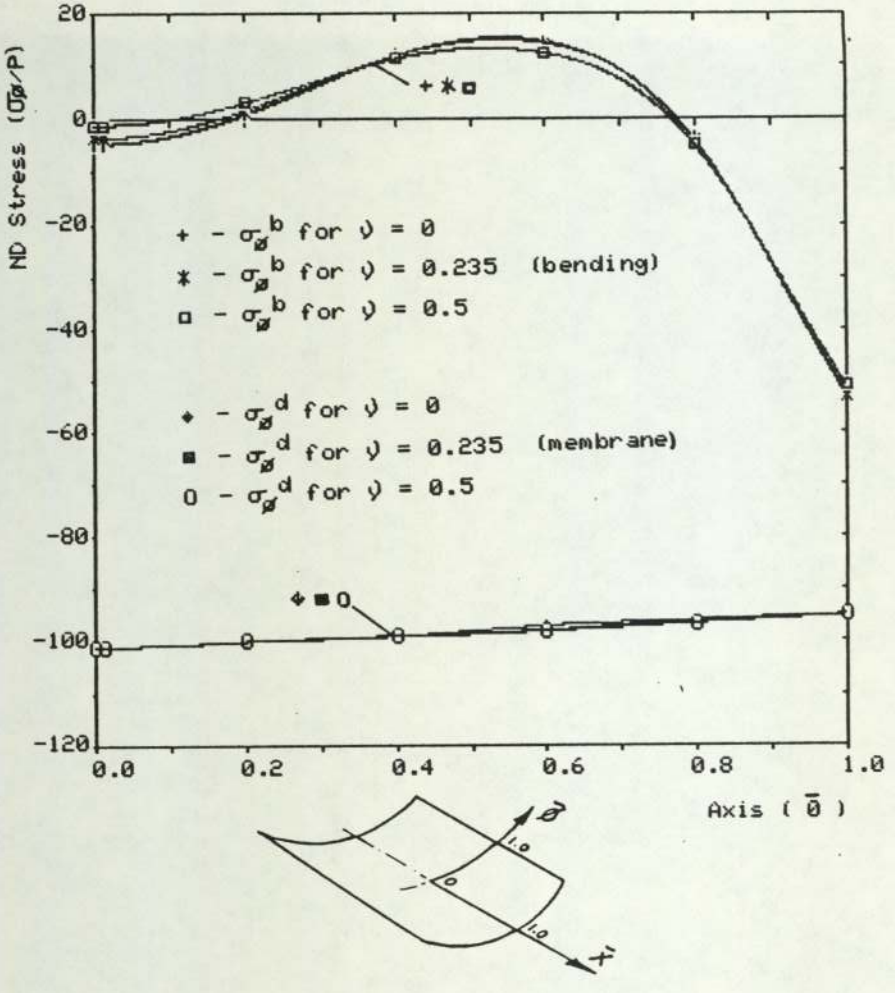

Fig. 13.21 Variation of Nondimensional stress ($\sigma_{\bar{\theta}}$), bending and membrane along $\bar{x}$=0 for 3 values of Poisson's ratio (Isotropic case)
Bending stress on concave surface.

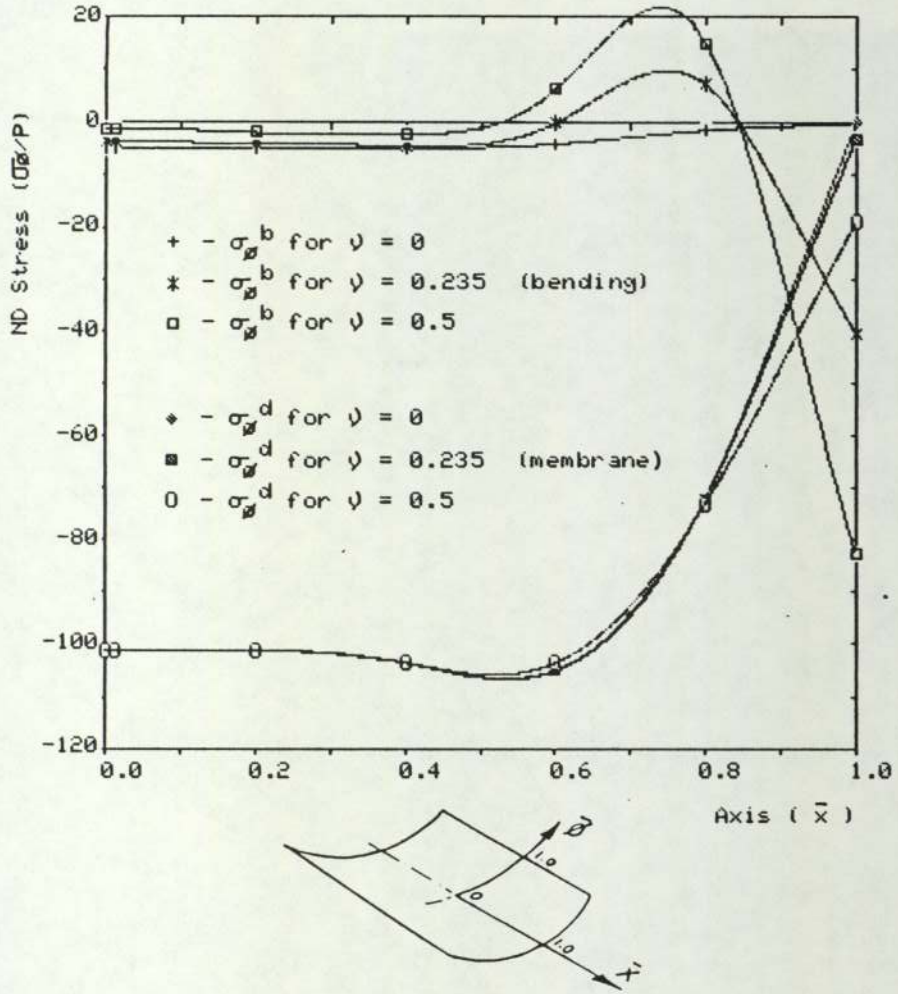

Fig. 13.22 Variation of Nondimensional stress ($\sigma_{\bar{\phi}}$), bending and membrane along $\bar{\phi}$=0 for 3 values of Poisson's ratio (Isotropic case)
Bending stress on concave surface.

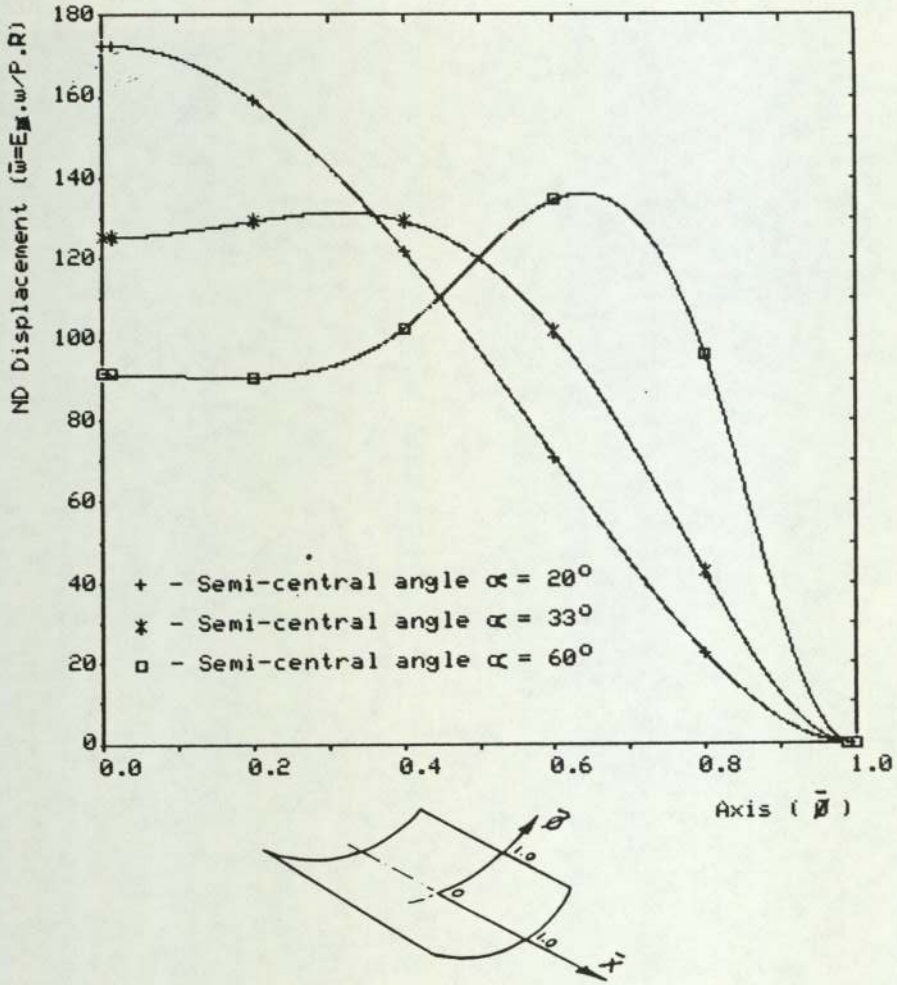

Fig. 13.23 Variation of nondimensional radial displacement (w) along $\bar{x}$=0 for 3 values of semi-central angle (Isotropic case)

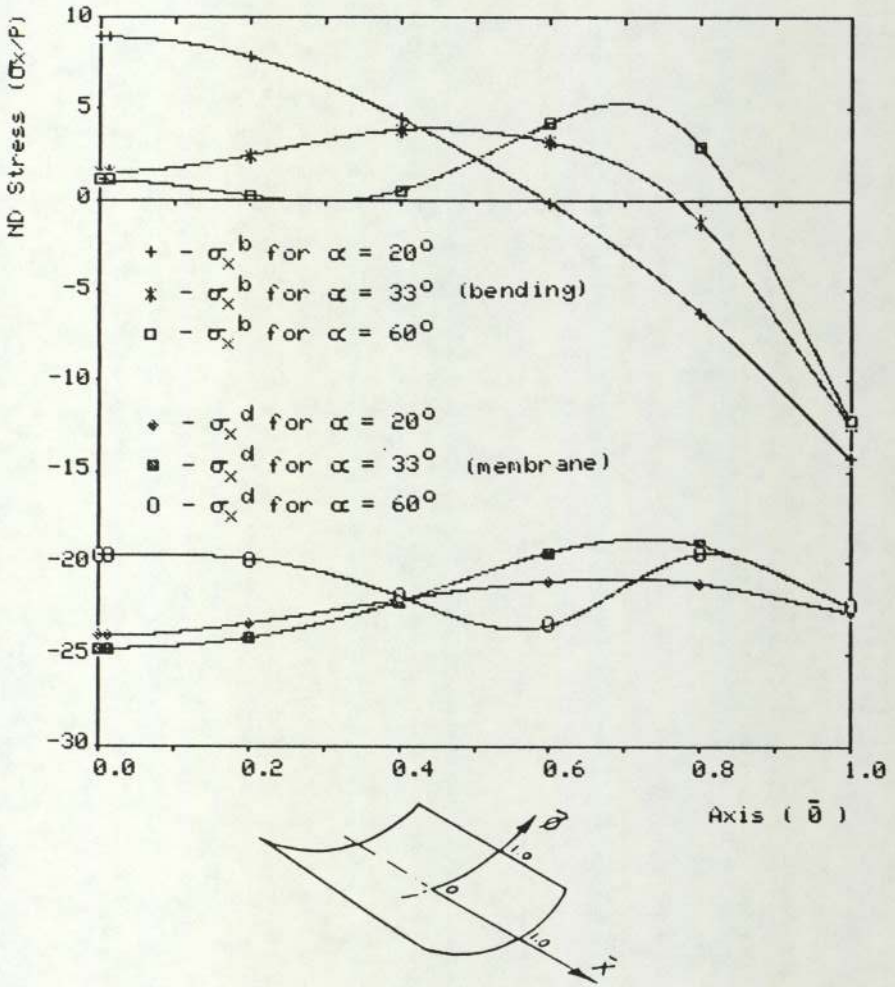

Fig. 13.24 Variation of Nondimensional stresses (σ_x), bending and membrane along $\bar{x}$=0 for 3 values of semi-central angle (Isotropic case)
Bending stress on concave surface.

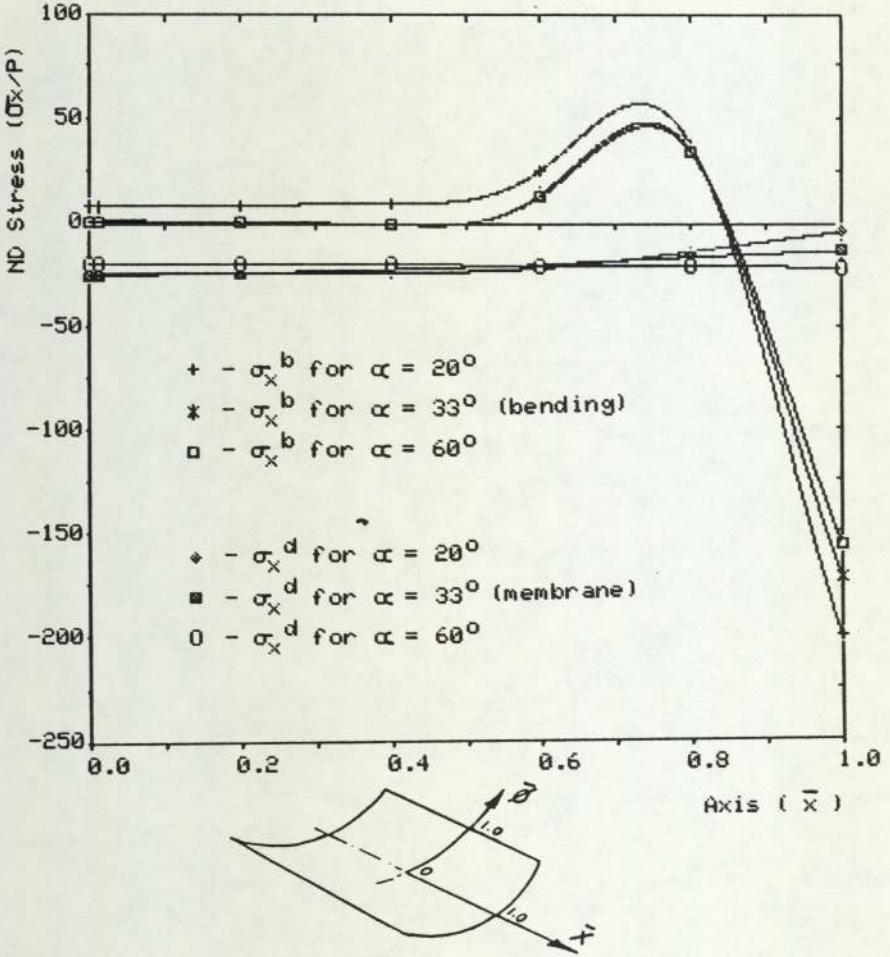

Fig. 13.25 Variation of Nondimensional stress (σ_x), bending and membrane along $\bar{\theta}$=0 for 3 values of semi-central angle (Isotropic case)
Bending stress on concave surface.

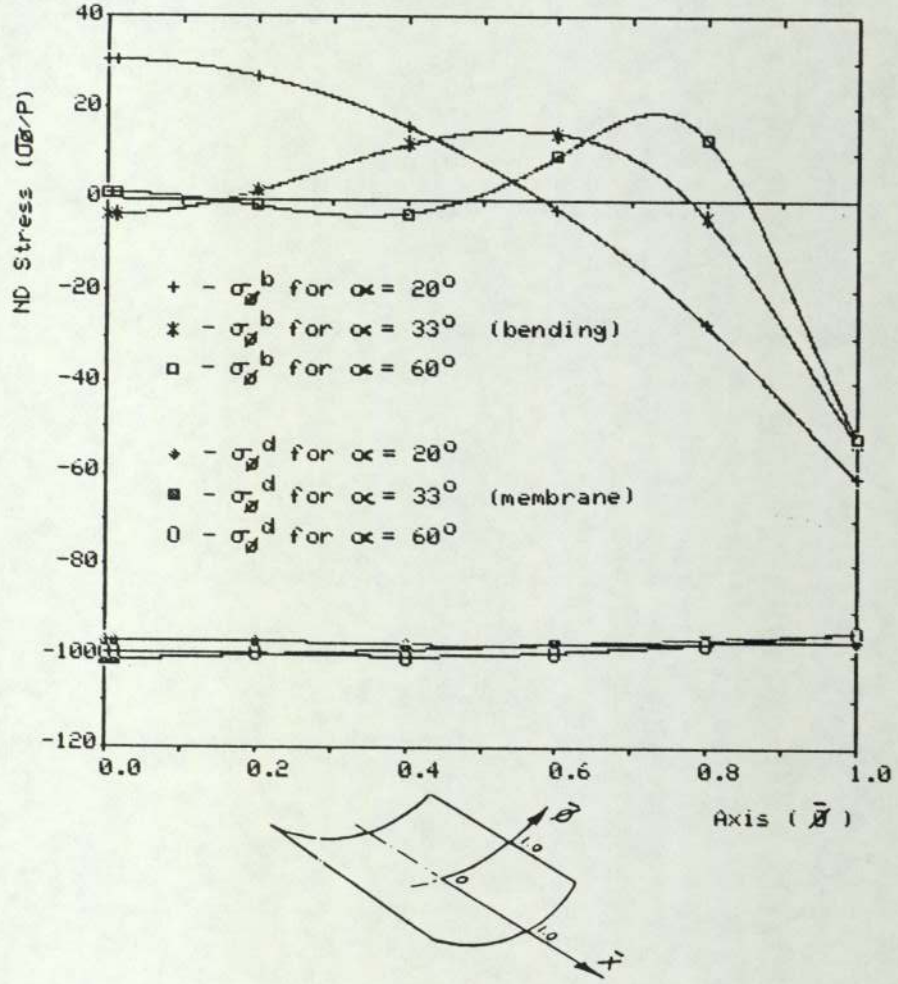

Fig. 13.26 Variation of Nondimensional stress ($\bar{\sigma}_{\phi}$), bending and membrane along $\bar{x}$=0 for 3 values of semi-central angle (Isotropic case)
Bending stress on concave surface.

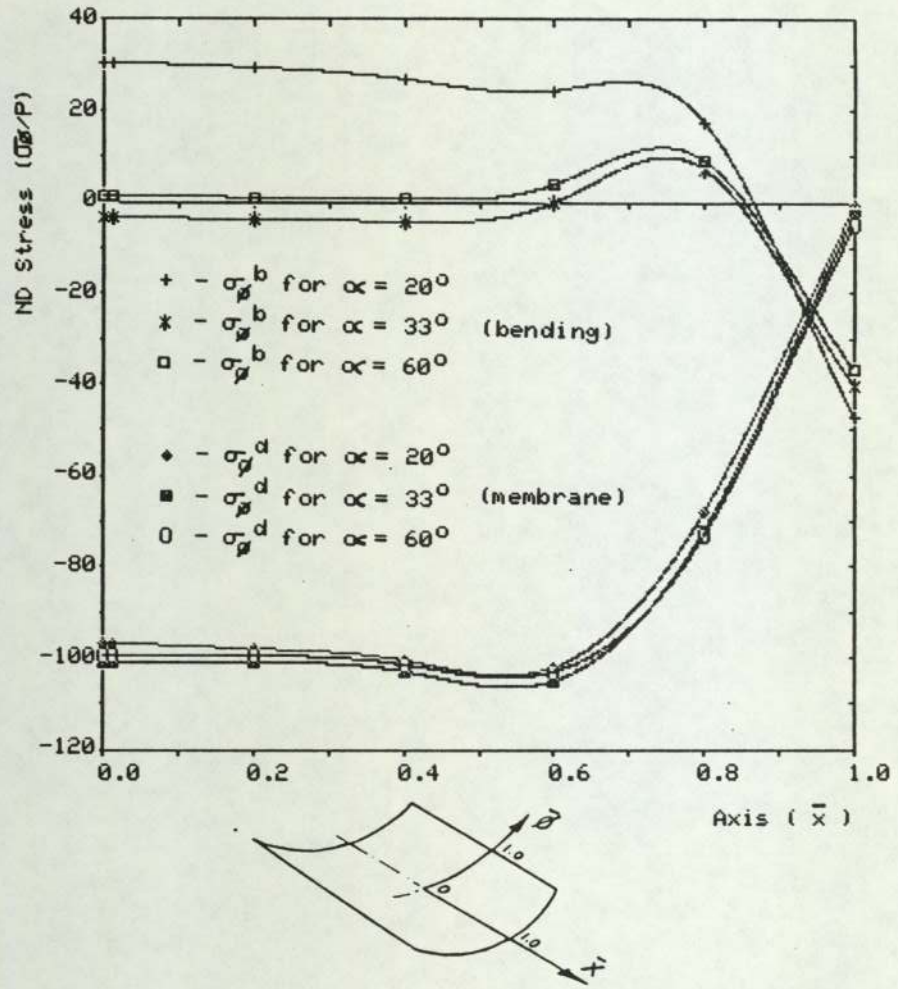

Fig. 13.27 Variation of Nondimensional stress ($\bar{\sigma}_{\phi}$), bending and membrane along $\bar{\phi}$=0 for 3 values of semi-central angle (Isotropic case)
Bending stress on concave surface.

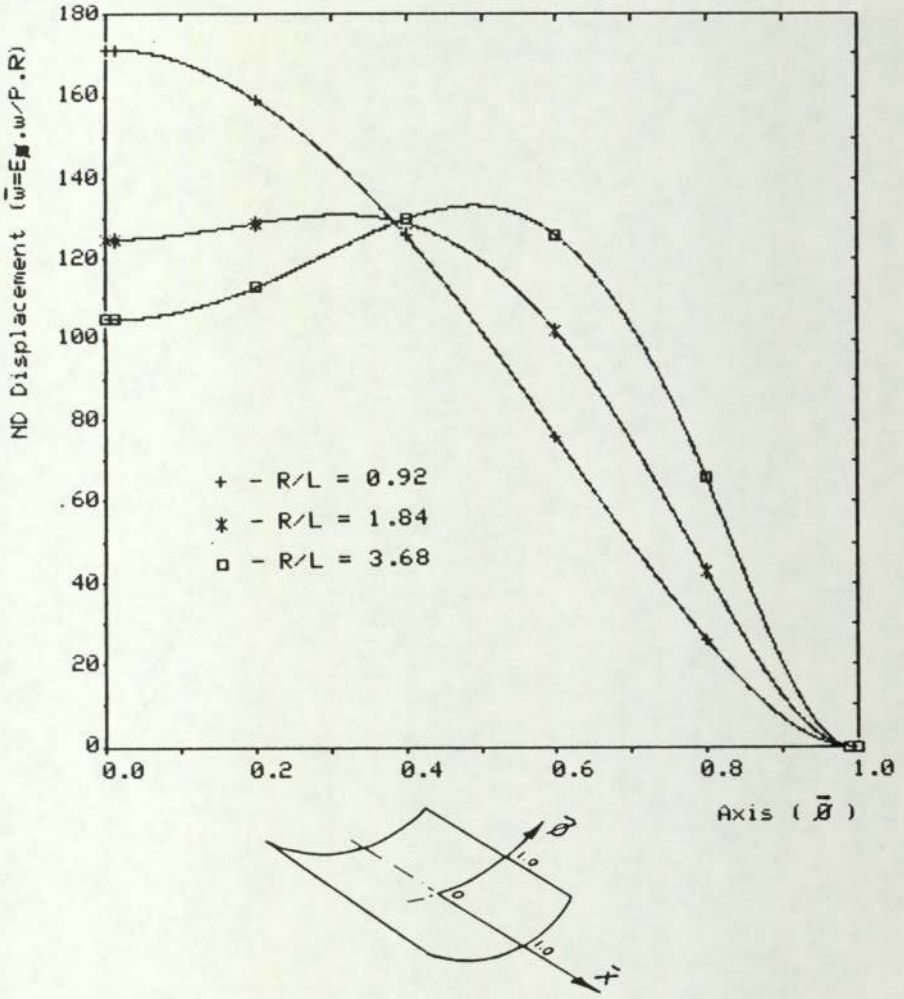

Fig. 13.28 Variation of nondimensional radial displacement ($\bar{w}$) along $\bar{x}$=0 for 3 cases of R/L (Isotropic case)

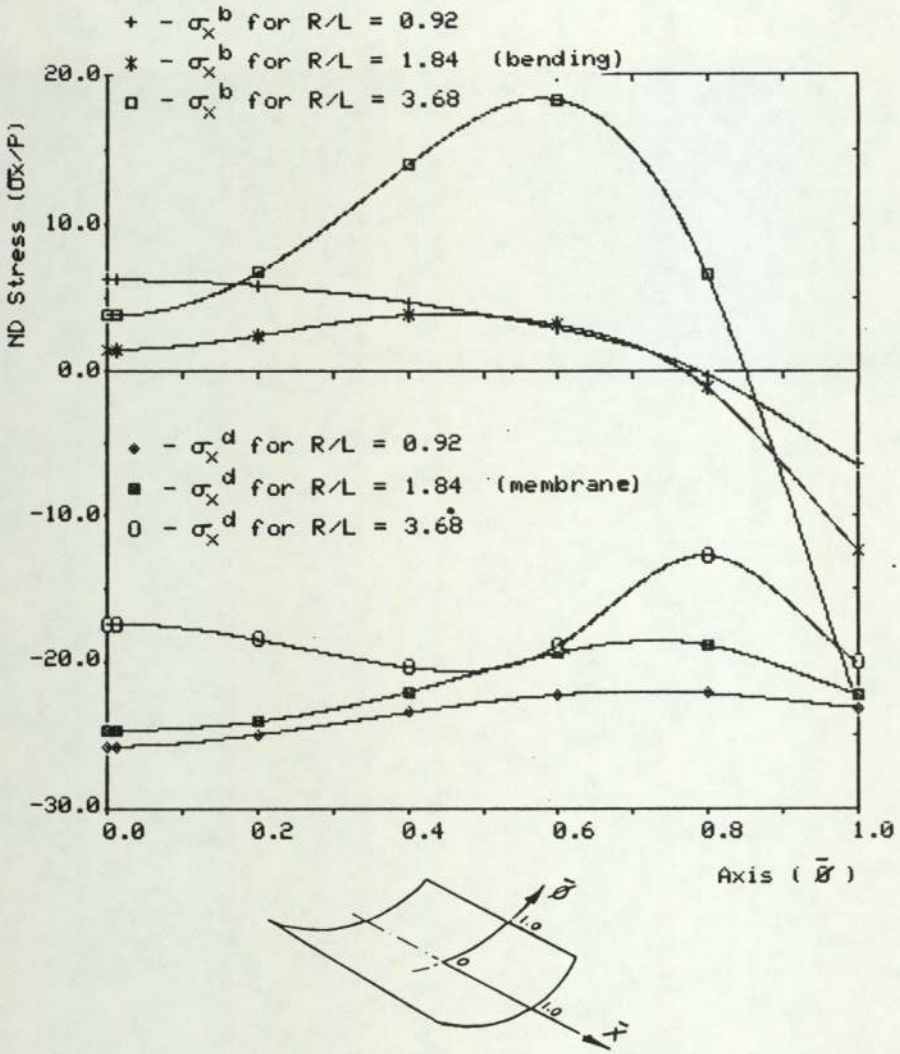

Fig. 13.29 Variation of Nondimensional stresses (σ_x), bending and membrane along $\bar{x}$=0 for 3 cases of R/L (Isotropic case)
Bending stress on concave surface.

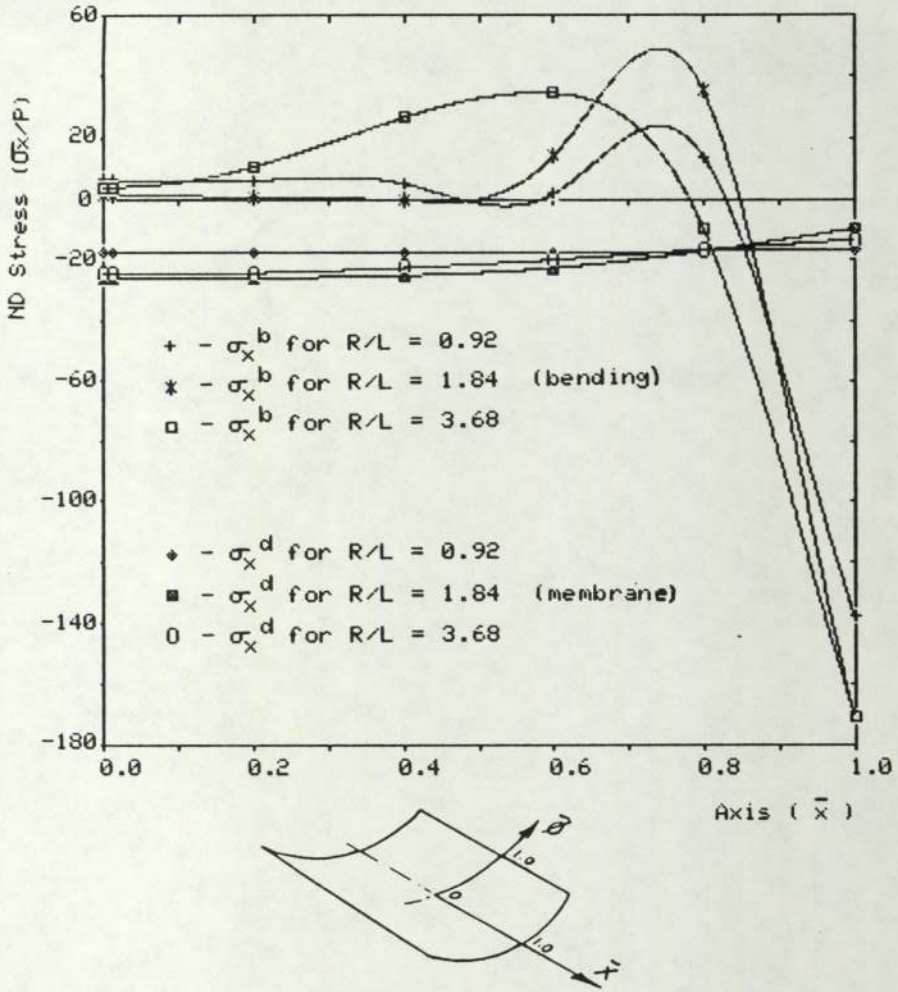

Fig. 13.30 Variation of Nondimensional stress (σ_x), bending and membrane along $\bar{\theta}$=0 for 3 cases of R/L (Isotropic case)
Bending stress on concave surface.

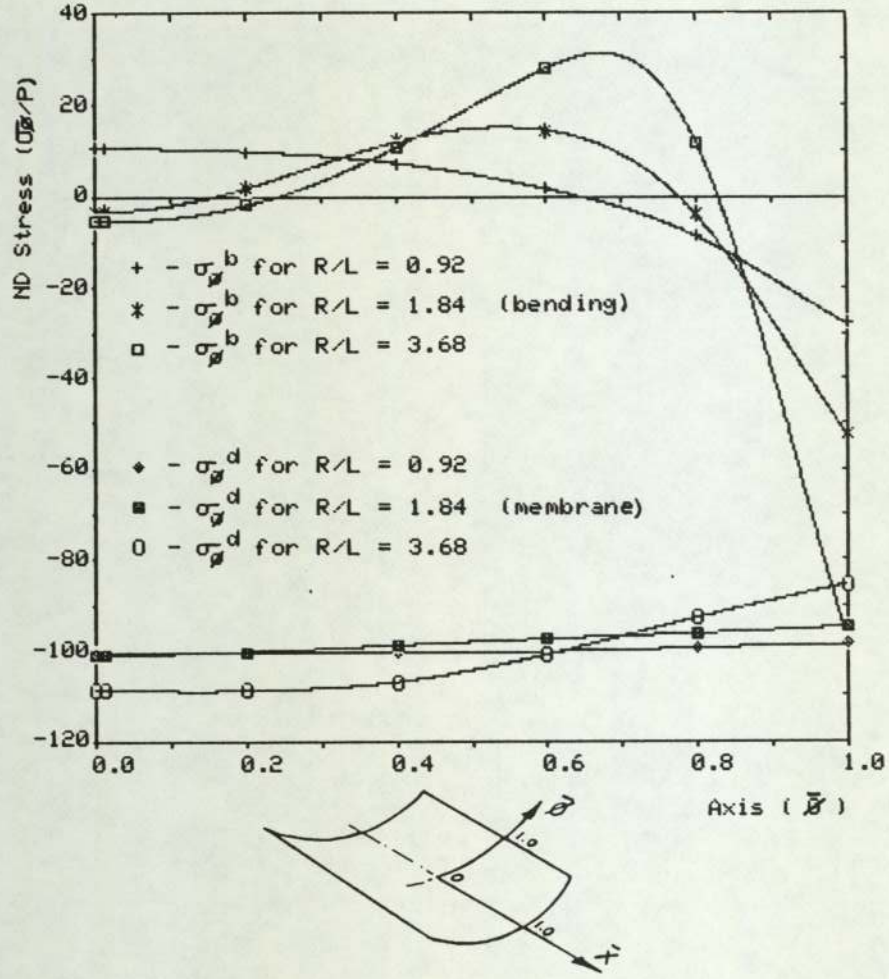

Fig. 13.31 Variation of Nondimensional stress (σ_θ), bending and membrane along $\bar{x}$=0 for 3 cases of R/L (Isotropic case)
Bending stress on concave surface.

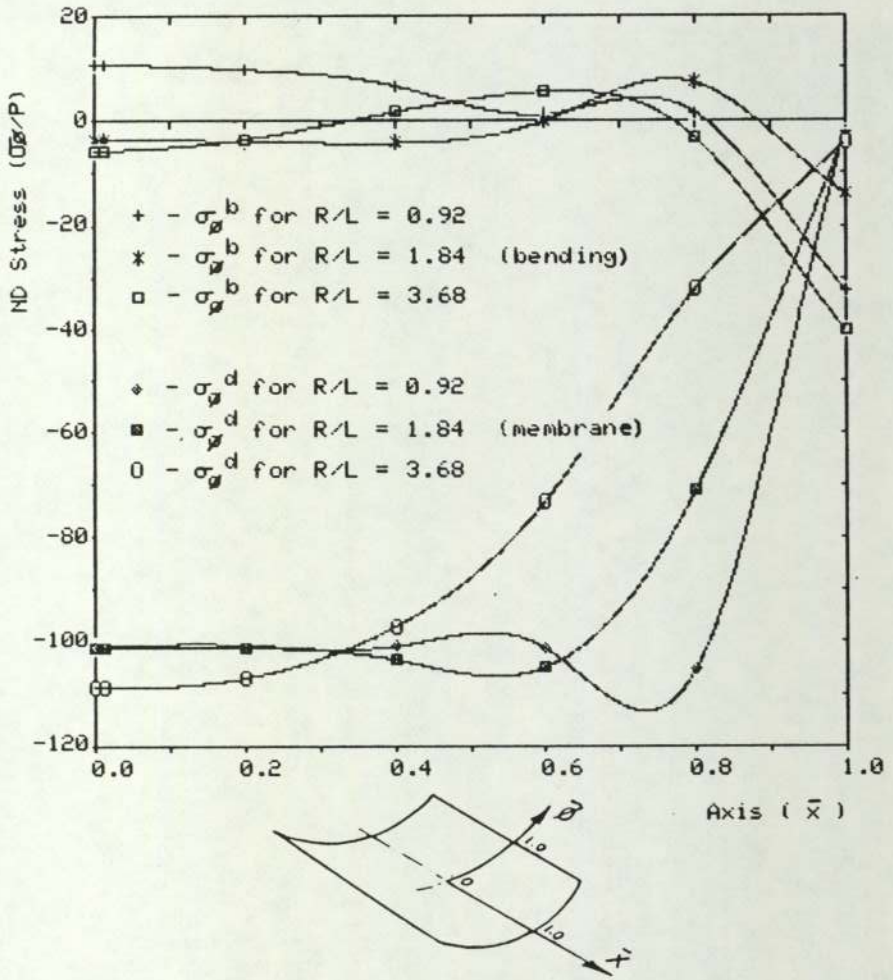

Fig. 13.32 Variation of Nondimensional stress (σ_{ϕ}), bending and membrane along $\bar{\phi}$=0 for 3 cases of R/L (Isotropic case)
Bending stress on concave surface.

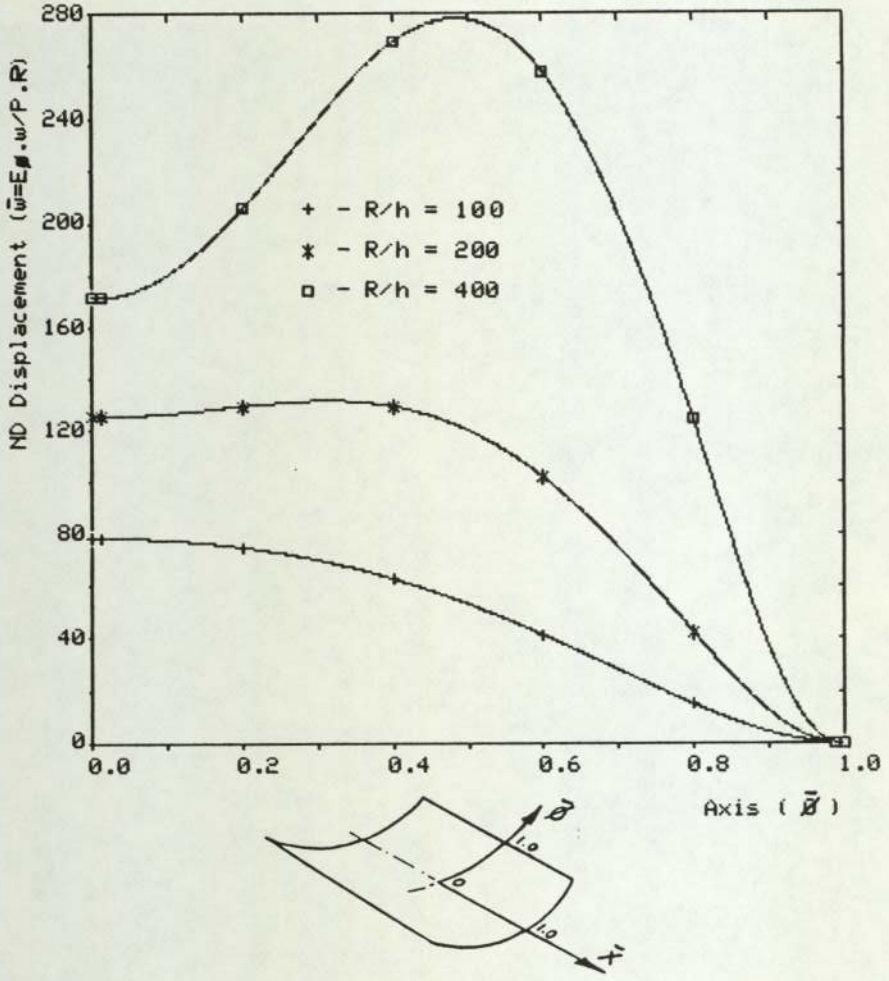

Fig. 13.33 Variation of nondimensional radial displacement ($\bar{w}$) along $\bar{x}$=0 for 3 cases of R/h (Isotropic case)

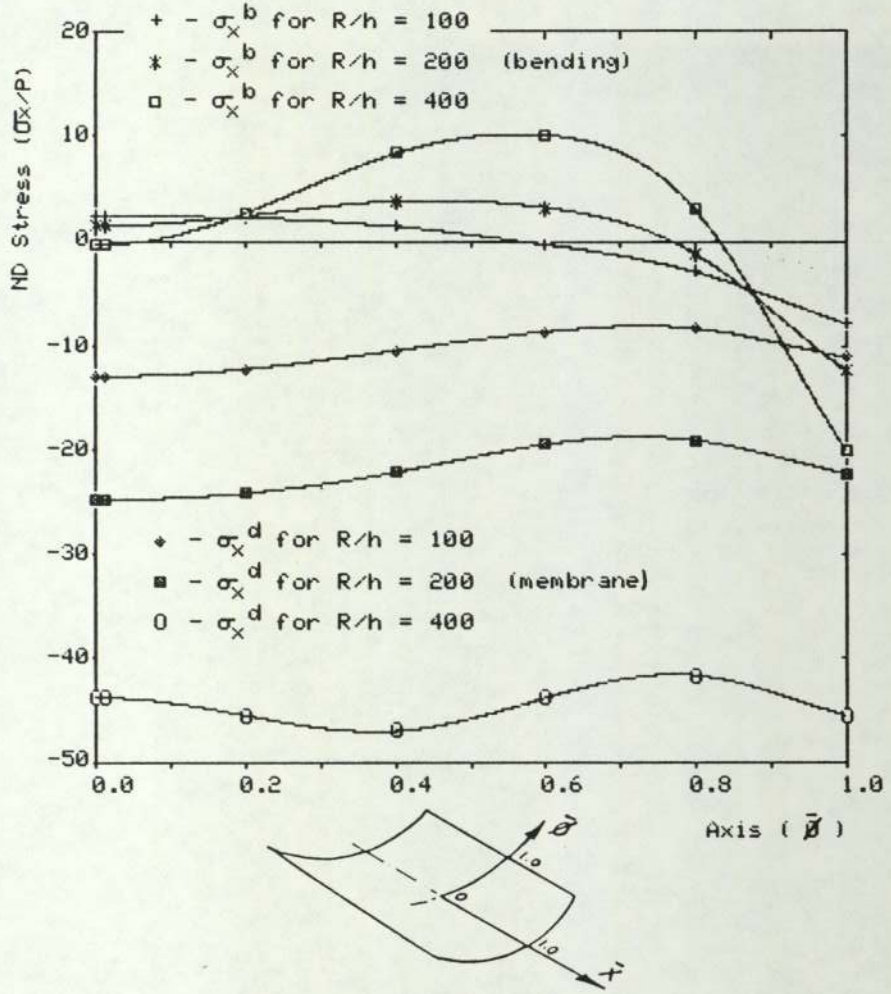

Fig. 13.34 Variation of Nondimensional stresses (σ_x), bending and membrane along $\bar{x}$=0 for 3 cases of R/h (Isotropic case)
Bending stress on concave surface.

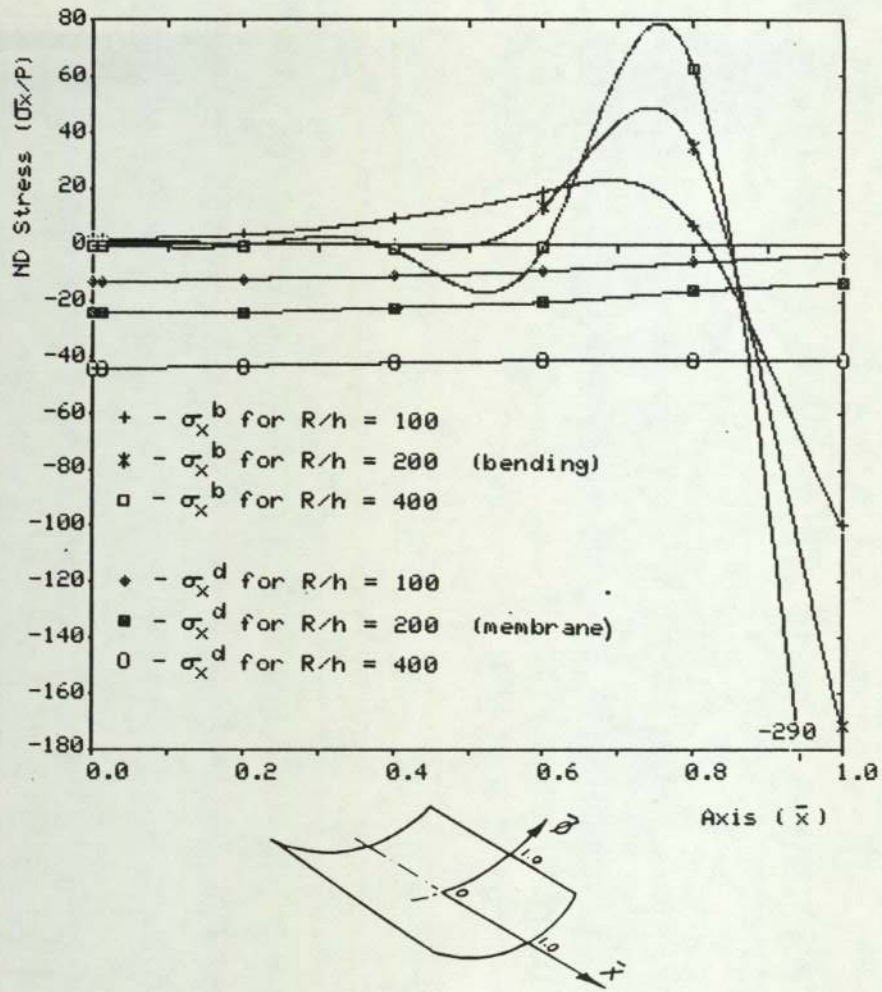

Fig. 13.35 Variation of Nondimensional stress (σ_x), bending and membrane along $\bar{\beta}$=0 for 3 cases of R/h (Isotropic case)
Bending stress on concave surface.

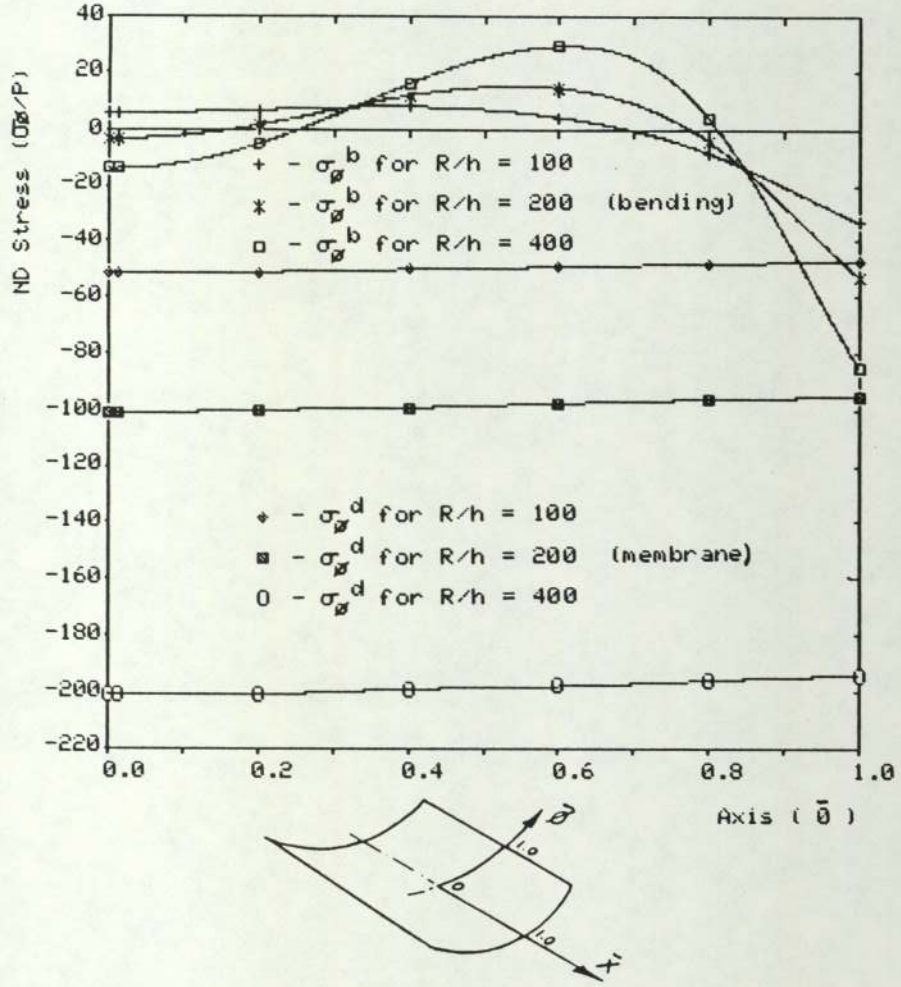

Fig. 13.36 Variation of Nondimensional stress ($\bar{\sigma}_{\phi}$), bending and membrane along $\bar{x}$=0 for 3 cases of R/h (Isotropic case)
Bending stress on concave surface.

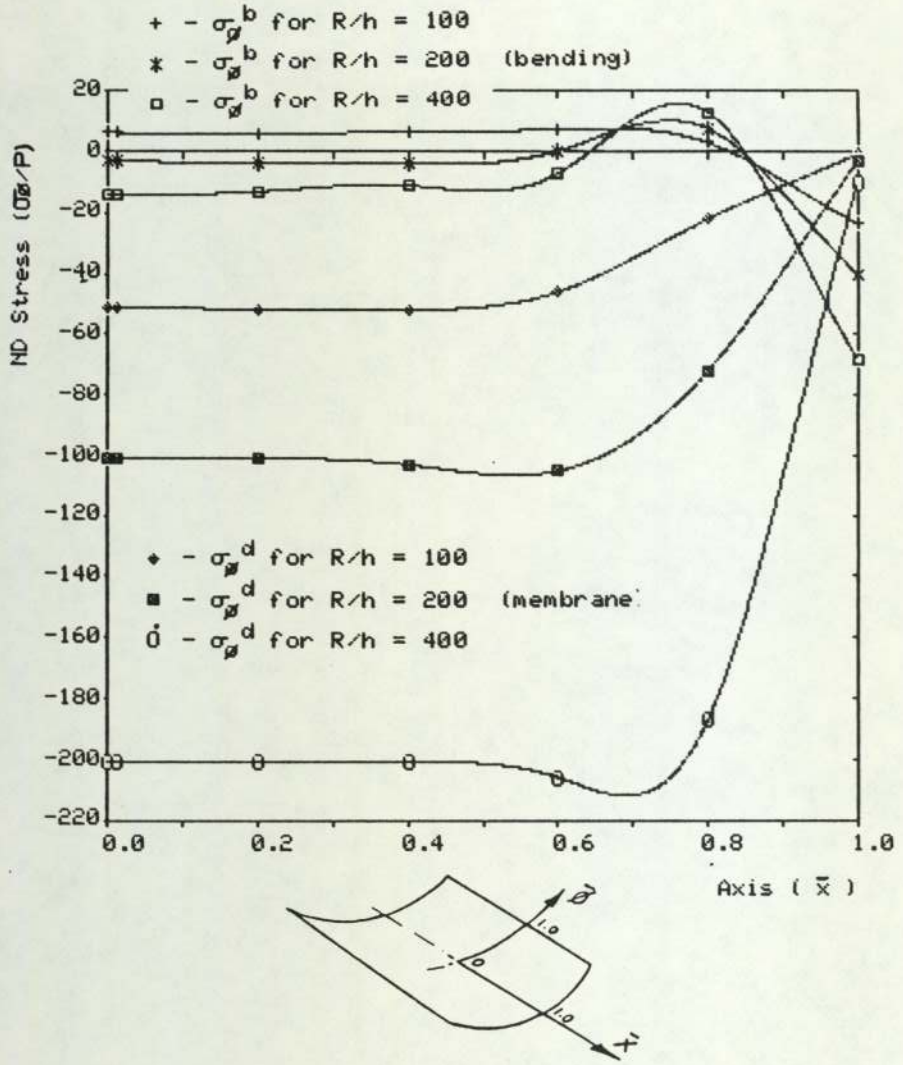

Fig. 13.37 Variation of Nondimensional stress ($\bar{\sigma}_{\phi}$), bending and membrane along $\bar{\theta}$=0 for 3 cases of R/h (Isotropic case)
Bending stress on concave surface.

13.7 Discussion of numerical results

A number of important observations can be made from the numerical results presented in Figures 13.2 to 13.37. These observations fall naturally into 3 categories.

(1) Observations concerning panel boundary conditions.

(2) Observations concerning material properties.

(3) Observations concerning panel geometry.

Each of these has implications for the design of sonar panels and is discussed in turn.

13.7.1 Boundary conditions

It may be seen from Figures 13.2 and 13.3 that the radial displacement of the panel (w) is much greater for the simply supported (SS) condition than for either the hinged (CS) or fully clamped (CC) conditions. Further the nature of the variation of the radial displacement across the panel in the transverse direction is quite different in form in the case of the SS condition compared with the CS and CC conditions. It may also be seen from these figures that the magnitude and variation of displacement for the CS and CC conditions are very similar.

From Figures 13.4 to 13.7 it may be seen that the bending stresses σ_x^b and σ_ϕ^b, for the SS condition, are large over most of the central region of the shell, and change in sense between the centre and the edge. In contrast to the CS and CC conditions where these bending stresses are confined to a narrow zone near the edge of the shell. Further it may be seen from these figures that the direct membrane stresses σ_x^d and σ_ϕ^d are almost constant over the whole shell for the CS and CC conditions whilst showing

considerable variation from the centre to the edge for the SS condition.

Overall from Figure 13.2 to 13.7 it may be observed that, except near the edges for stresses, there is little difference in the variation of either displacement or stresses, between the fully clamped and the hinged boundary condition cases. This indicates that the behaviour of the shell is strongly influenced by the membrane boundary conditions, which are the same for the two cases. Since for these two types of boundary conditions the bending stresses in the central region of the panel are very small, it may be said that this region of the shell is predominantly in a state of membrane stress.

13.7.2 Material properties

Figures 13.8 to 13.22 show the variations in behaviour of a clamped panel with variations of material properties. Within the ranges considered for each parameter, these graphs require detailed interpretation for any particular case. Nevertheless, some general observations can be made.

Figures 13.8 to 13.12 show the effects on panel behaviour of changes in the ratio E_x/E_ϕ in the range 0.5 to 2.0 with the isotropic case for comparison. Over this range it can be seen that although there is some variation in the form of the displacement curve in the transverse direction, there are no gross changes in behaviour between the isotropic and the orthotropic panels.

Further it may be seen from Figure 13.11 that the transverse stress $\sigma_\phi{}^d$ is almost the same for the isotropic and orthotropic cases. This is to be expected since the membrane stresses are determined from equilibrium considerations and the material properties do not come into the picture. The values of E_x and E_ϕ do of course have influence on the bending stresses, which are predominant near the edges of the panel, and also on the displacement behaviour.

Figures 13.13 to 13.17 show the effects of changes in the parameter $G_{x\phi}/E_\phi$ and it can be seen that over the fairly wide range of values considered, this parameter has little influence on panel behaviour. It is doubtful, therefore, whether effort expended on the accurate determination of shear modulus is worthwhile.

The other independent parameter, Poisson's ratio, clearly does have a significant influence on the membrane stress $\sigma_x{}^d$ as well as some influence on displacement (Figures 13.18 to 13.22).

13.7.3 Panel geometry

The effects of independent variation of the two geometry parameters α and R/L are shown in Figures 13.23 to 13.27 and 13.28 to 13.32 respectively. Both of these parameters are fixed for the cylindrical panels of this study, and the figures are included here for completeness, and to assist in the design of panels of different geometries.

The parameter R/h is of more direct interest here because this is in effect the thickness parameter. Figures 13.33 to 13.37 show the effects of independent variation of this.

It can be seen from these figures that bending effects become more predominant as the shell becomes thinner (R/h increasing) and this bending behaviour is reflected in the displacement behaviour of the panel. It is interesting to compare the displacement of the thinner panel (R/h = 400) with the behaviour of the simply supported panel considered earlier. In both cases bending action makes a significant contribution to the panel behaviour.

13.8 Implications for design of sonar panels

Overall recommendations for the future design of GRP sonar panels are made in Chapter 15 of this thesis, but it is possible, from the results of this parametric study alone, to draw some early conclusions.

13.8.1 Panel boundary conditions

Sonar panels have traditionally been attached to hull structures with bolted joints. These joints have been designed to be as rigid as possible, on the assumption that this would result in minimum deflection of the panels under load and much effort has been expended therefore in attempts to provide both lateral and rotational restraint at panel edges, ie to approach the fully clamped (CC) condition. It is clear from this parametric study that, at least for the case of cylindrical panels, some of this effort has been wasted.

From the point of view of minimising panel deflection Figure 13.2 indicates that there would seem to be no advantage in adopting the fully clamped edge condition (CC), over the membrane clamped or hinged condition (CS).

In fact the CS condition results in the distinct advantage of reduced bending stresses near the edges of the panel. Clearly, since the simply supported (SS) boundary condition results in very large deflections and very large bending stresses, panel edges must be restrained laterally, (any relaxation of lateral restraint will bring the edge condition nearer to the SS case) but rotational restraint of the edges is less important, and may even be undesirable because of the high bending stresses which result (see Figure 13.5).

13.8.2 Material properties

Whilst it is essential for accurate prediction of displacements and stresses, that material elastic properties be accurately known, the overall behaviour of a loaded panel is not strongly influenced by the relative values of the Young's Moduli in the two principal panel and material directions. Thus, within the range of values considered here (E_x/E_ϕ = 0.5 to 2.0), the displacement and stress distribution curves for the orthotropic and isotropic cases are broadly similar in shape (Figures 13.8 and 13.12).

It can be observed however that the predominant membrane stresses, for the geometry of panel considered here, are in the ϕ direction. If it were possible to redesign the panel material so that it were no longer approximately square symmetric, then some structural advantage might be gained by ensuring that a majority of fibres lie in this direction. This would correspond to the case $E_x/E_\phi = 0.5$ in Figures 13.8 to 13.12. Such a basic redesign of the laminate would, of course, be outside the scope of this work and might have other impli-

cations for sonar performance.

13.8.3 Panel geometry

Panel geometry parameters are determined in the main by the dimensions of the sonar array and by the ship's hull configuration. For any particular case these will normally be fixed prior to any structural design of the panel. The panels considered in this study are similarly of fixed basic geometry, with the only dimensional parameter that is not fixed being the panel thickness. The need to minimise panel thickness whilst maintaining structural stiffness and strength provides of course, one of the main reasons for this work.

It is observed from the parametric study that as the panel becomes thinner, bending behaviour predominates. This suggests again the possibility that some redesign of the laminate, if acceptable from an acoustic point of view, could be beneficial. The aim of such a redesign would be to increase the bending stiffness of the material without introducing either more glass or more resin into the laminate. In principle this might be achieved by redistribution of the fibres away from the centre laminae and towards the outer facings, perhaps allowing the central layers of the laminate to become slightly resin rich.

13.9 Concluding remarks on the Parametric Study

The curves presented in this chapter represent the behaviour of uniform perfect cylindrical panels, with idealised boundary conditions, subject to uniform pressure loading. Neither the uniformity of the panels, nor the ideal boundary conditions are achievable in practice and it is unlikely that

any real panels will behave exactly as predicted here. Nevertheless, these curves do give bounds for the behaviour of real panels with real boundary conditions and may be used for preliminary design purposes. In each case the range of parameters considered, though obviously incomplete, is sufficient to show the development of significant trends in behaviour. Additional data may be readily obtained, if required, by use of the programs given in Appendix F.

In the following chapter it will be shown that the results given here show good agreement both with finite element analysis and, in most cases, with the experimental results from the sonar panel testing. The given curves may therefore be used with some confidence.

CHAPTER 14

FINITE ELEMENT ANALYSIS AND COMPARISON OF EXPERIMENTAL AND ANALYTICAL RESULTS

14.1 Introduction

The numerical Galerkin procedure, detailed in Chapter 12 and 13, proves very convenient for the analysis of the cylindrical GRP panels of this study. Changes of parameters can be readily investigated and useful design information can be quickly obtained. Unfortunately the method is not suitable for the analysis of sonar domes in general. The most important deficiency of the method in this respect is that it may only be applied to shells of simple geometry; cylindrical, hyperbolic, parabolic, and so on, for which governing differential equations exist or can be formulated, and then only for relatively straightforward boundary conditions. Many sonar domes, and other shells, are of completely general form. For these cases finite element modelling offers the most practical method of analysis.

Since it is the historical failure to obtain good agreement between PAFEC finite element analysis of sonar domes and experimental observations of dome behaviour, which provides the main reason for this work, and since finite element modelling must remain the primary design tool, there is clearly a need to demonstrate the agreement or otherwise between finite element results and the numerical Galerkin solution on the one hand, and between both of these and the experimental observations on the other. If good agreement can be demonstrated between the finite element and Galerkin results for those cases to which both are applicable then more confidence can be placed in both methods.

It is clearly essential that confidence be established in the finite element method if it is to be applied to cases for which an alternative numerical solution is not available.

In this chapter PAFEC finite element results are presented for the pressure loaded cylindrical panels of this study. Results are presented first for those isotropic cases previously examined using the Galerkin procedure. Good agreement is shown in these cases. Further finite element results are then presented to show the effects of some additional variations in the panel boundary conditions, again for the isotropic case. Finally finite element results are presented for each of the GRP sonar panels using the experimentally determined orthotropic properties. These results are compared with both the Galerkin solution results for the fully clamped case, and with the experimental results from the panel testing.

In order to be consistent, all graphical results presented in this chapter are presented in the same format and use the same non-dimensional parameters as used previously.

14.2 Finite element modelling of cylindrical panels

A cylindrical shell panel is very easy to model with rectangular facet elements or rectangular planform curved shell elements, mesh generation presents few problems, and the mesh generation aids provided in the PAFEC suite including PAFBLOCKS and PIGS were not needed in this application.

For all of the cylindrical shell analysis reported here, principal node co-ordinates and element topology were entered manually with only the twin PAFEC facilities ARC-NODES and LINE-NODES (equally distributed nodes on a pre set arc or line) being used to position intermediate nodes. The ARC-NODES facility was

particularly useful here in that its use minimised the risk of any inaccuracy in the cylindrical form of the model, which might have resulted from rounding errors in manually calculated nodal co-ordinates.

Since the cylindrical shell shape has two planes of symmetry, it is in principle sufficient to model only $\frac{1}{4}$ of the panel (see Figure 14.1). This is provided of course that suitable restraints are provided along the axes of symmetry. These restraints are easily provided in the PAFEC data file, but as a check on the validity of this approach, one initial PAFEC run was undertaken with the complete panel modelled (4 quadrants). The results of this were then compared with the results obtained with a single quadrant panel model of identical mesh arrangement. Stress and displacement results for the two PAFEC runs were found to be identical. All subsequent analysis, except the investigation of asymmetric behaviour, was carried out using the single quadrant model.

14.3 Convergence of the Finite element model

14.3.1 Facet Element

The isoparametric facet shell elements 44210 and 44215 perform best when their aspect ratios are approximately unity. Since the aspect ratio of each of the cylindrical panels of this study is also approximately unity it is clear that a quadrant of a panel can be best modelled with a square array of approximately square elements.

Using the parameters and properties of the aluminium panel AL1, successive runs of the PAFEC program were made with the quadrant of the panel

modelled with 2 × 2, 4 × 4, 8 × 8 and 16 × 16 facet elements. Corresponding to 47, 232, 896 and 3712 degrees of freedom (DOF) for the fully clamped case. Values of displacements and stresses were examined for each run and the results for representative nodes are summarised in Figure 14.2. Stress output from the PAFEC program is given in the form of principal stresses and principal stress directions, on each face of the shell, and at the shell mid-surface for each node position. To be consistent with the approach adopted for the Galerkin solution, these stresses were separated into membrane and bending components (the element 44210 is in effect a combined plane stress and plate bending element). Using this approach it is clear from Figure 14.2 that whilst displacements and membrane stresses show quite rapid convergence with this element, bending stresses are much slower to converge. At the 896 DOF level (8 × 8 element mesh) the displacements and membrane stresses are fully converged and also show good agreement with the Galerkin solution (Figures 14.3 and 14.4), bending stresses however, show very poor agreement at the 896 DOF level, and only fair agreement at the 3712 DOF level. Agreement for the simply supported case was rather better Figures 14.5 and 14.6). In an attempt to obtain satisfactory convergence of bending stresses using this element, one further run was made using a 32 × 32 element mesh, corresponding to 15104 DOF. Figure 14.4 shows that using this model, bending stresses now give

good agreement with those obtained using the Galerkin solution, and appear to be converging. The clear indication here is that further mesh refinement would improve the agreement still further. However, since the 15104 DOF model required nearly 22 hours of CPU time to run, this was felt to be impractical. A more efficient element was therefore sought.

14.3.2 Semi-Loof Element

The remainder of the analysis was carried out using the semi-Loof elements 43210 (isotropic) and 43215 (orthotropic). These elements proved very much more efficient than the facet elements in this application, giving very rapid convergence in all cases.

The relative performance of the facet and semi-Loof elements, in this respect, is illustrated clearly in Figures 14.7 and 14.8. It can be seen that the two elements show almost perfect agreement for displacements and for membrane stresses, and that an 8×8 mesh of semi-Loof elements, corresponding to 784 DOF, gives results for bending stresses comparable with those obtained using the facet element at 15104 DOF, again giving almost perfect agreement with the Galerkin solution.

Although the remainder of the finite element analysis was carried out using semi-Loof elements, it should be said in defence of the facet elements, that they provide a very convenient and simple means of obtaining both panel displacements and membrane stresses, and that the deficiency with respect to bending stresses

is one of slow convergence only. Mesh generation and control of boundary conditions are more complicated where semi-Loof elements are used.

14.4 Further investigation of panel boundary conditions using the finite element model

14.4.1 Sensitivity to lateral edge displacements

Using the finite element model it is possible to examine further the effects of specific boundary condition changes on panel behaviour.

In the parametric study in Chapter 13 it was shown that panel boundary conditions and particularly the membrane boundary conditions strongly influence the radial deflection behaviour of the panel. It was shown that the provision or otherwise of rotational edge restraint had comparatively little influence on panel deflection. However, since the boundary conditions considered in Chapter 13 were applied in each case uniformly to all four panel edges, it was not possible to infer from this alone whether the membrane boundary conditions along the longitudinal (straight) on the transverse (curved) panel edges, had the greatest influence. The finite element model allows this to be examined.

Figure 14.9 shows the effect on the radial deflection behaviour of the aluminium panel AL1, of various combinations of boundary conditions.

The cases of 'all edges clamped' and 'all edges simply supported' are self explanatory and represent the two extreme cases possible for the panel.

The case of 'straight edges clamped' corresponds to a lateral freedom of movement allowed at the curved edges of the panel, all other edge freedoms being disallowed. Similarly, the case of 'curved edges clamped' allows the corresponding lateral freedom only, at the straight edges of the panel.

The figure shows clearly that it is the lateral freedom or restraint of the longitudinal edges of the panel which has the predominant effect on panel deflection, other freedoms or restraints at the other panel edges have a very much lesser influence. This confirms the experimental observations made in Chapter 11 that the radial deflection behaviour of the test panels was found to be very sensitive to lateral displacements of the longitudinal panel edges but less sensitive to displacements of the transverse edges.

The experimental result obtained for the aluminium test panel (from test No 35) is shown in Figure 14.9 for comparison. It can be seen that this result is totally consistent with the case of imperfect lateral restraint of the longitudinal panel edges.

To further illustrate and confirm this point Figure 14.10 shows the radial deflection behaviour prediction for the aluminium panel based on prescribed displacements at the panel longitudinal edges. These prescribed displacements are

the actual measured displacements of the longitudinal edges taken during the testing of this panel (taken from Figure 11.4).

Agreement here between the finite element predicted radial displacement and the experimental result is quite good. The small remaining difference being readily attributable to small departures from the ideal full clamping, in the other, less significant boundary conditions.

It should be noted that the lateral displacement required at the mid point of the longitudinal panel edges to achieve the result shown in Figure 14.10 (prescribed displacement curve) for the aluminium panel AL1 at a pressure of 50 kPa (maximum test pressure) is 0.07 mm. To put this displacement into perspective it is approximately 1% of the panel thickness and approximately 0.01% of the panel semi-span in the direction of the displacement. This very small lateral displacement results in predicted panel radial displacements more than double those predicted when this displacement is disallowed. Thus, the sensitivity of the panel radial displacement behaviour, to the degree of lateral restraint of the panel longitudinal edges, is firmly established.

14.4.2 Asymmetry of panel behaviour

This sensitivity of panel behaviour to small lateral displacements at the longitudinal panel edges has implications not only for the overall panel deflection behaviour, as illustrated in Figure 14.10, but also for the symmetry of that behaviour.

The longitudinal edges of the test panels, were supported in the test rig, and the edges of real panels are supported in the hull or casing of the ship or submarine, by what are in effect steel edge beams. If these edge beams are of even slightly differing stiffness (as is almost certain to be the case with such fabricated structures) then the boundary conditions achieved at the two longitudinal panel edges will differ slightly.

In the experimental work reported earlier it was observed that all of the test panels exhibited some degree of asymmetry in behaviour. It was suggested in Chapter 11 that this asymmetry might be due to asymmetry of boundary conditions along the panel longitudinal edges, as well as to non-uniformity of panel thickness; particularly since the asymmetry was also observed with the aluminium panel, which was of course of very uniform thickness.

By making use of the finite element model, this hypothesis can now be supported. Using the model for the full panel with prescribed displacements in the ϕ direction at the longitudinal edges, asymmetry similar

to that observed in the experimental work can be produced. Figure 14.11 shows the effect of applying the total measured edge displacements for the aluminium panel AL1 distributed 40%/60% between the two longitudinal edges. (This arbitrary distribution could not be confirmed experimentally, due to the difficulties of measuring very small displacements of a fabricated structure, but it seems a fairly conservative estimate of the likely asymmetry in the test rig). It can be seen that considerable asymmetry, of a form totally consistent with the experimental work, is predicted by this model. It can also be observed from this figure that variation of panel thickness, as might be expected, has an influence on asymmetry (middle line of the three graphs) but that this effect is rather less pronounced for thickness variations that are within practical limits. This line of the graph represents a finite element model of the aluminium panel where the material one side of the longitudinal centreline is increased to 6.8 mm thickness and the other side decreased to 6 mm thickness, this is a fairly gross non-uniformity of thickness, unlikely to be exceeded in practice, even with a hand lay up GRP panel.

Clearly in any real situation either or both of these asymmetry producing mechanisms might operate, and they might either cancel their effect, or be cumulative. However, it is clear from the

above that small variations in panel thickness, such as might reasonably be achieved in practice with well controlled hand lay up procedures, will not result in serious asymmetry in panel behaviour and that the most significant cause of such asymmetry will be variation in the panel boundary conditions.

14.5 Comparison of predicted and experimental panel behaviour

14.5.1 Displacement Behaviour

Very good agreement has been demonstrated between the displacement predictions obtained from the Galerkin and finite element methods for the isotropic panel case (aluminium panel AL1) with fully clamped boundary conditions. The experimental results obtained from the testing of this panel have also been shown to agree closely with finite element predictions when imperfect boundary conditions at the longitudinal panel edges are included in the finite element model.

For the orthotropic cases corresponding to the three GRP panels the comparisons between finite element predictions, Galerkin method predictions, and experimental results for displacements are given in Figures 14.12, 14.13 and 14.14. These are for panels GRP1, GRP2 and GRP3 respectively. Because edge displacements encountered during the testing of these panels were too small to be measured, the fully clamped case is assumed for both analytical models.

It may be seen from these figures that excellent agreement exists between the finite element and Galerkin prediction in all three cases. For panels GRP2 and GRP3 agreement with the experimental results is also extremely good. Agreement between predicted and experimental displacement behaviour for the panel GRP1 is less good but still acceptable. It may be noted that the panel GRP1 was the thinest GRP panel and showed most variation in its elastic properties during material testing, also because it was the thinest panel it might reasonably be expected to show most sensitivity to any small unmeasured edge displacements.

14.5.2 Stress Behaviour

Since near perfect agreement has been demonstrated between the Galerkin and the finite element predictions, the experimentally determined stresses are compared here only with the former. Also, since only a limited number of strain gauges were employed in the experimental work, no attempt is made to plot the experimentally determined stresses; instead, stress values obtained at the discrete strain gauge rosette positions are superimposed on the Galerkin stress plots (fully clamped case) for each panel.

Figures 14.15 and 14.16 show this superimposition for the panel AL1 and Figures 14.17 to 14.22 for the panels GRP1, 2 and 3. In the case of

Figures 14.15 and 14.16, the Galerkin prediction for the simply supported case is also shown for comparison.

It may be seen from these figures that for the case of the aluminium panel, agreement between experiment and prediction is quite good at all measured points. The small discrepancies here are generally consistent with a slight relaxation of the fully clamped boundary conditions ie the experimental points tend to err in the direction of the simply supported case.

For the GRP panels it may be seen that agreement between experimental and predicted stresses is less good. This was of course to be expected since it was anticipated that strain gauge readings taken on the GRP material would be less reliable than those taken on the aluminium panels. It will be noted, particularly with respect to the membrane stress components, that the experimental stress values are lower than the predicted values. This is consistent with the results which would be expected if local stiffening of the test panels by the gauges was taking place (see Appendix B). Nevertheless, the clear similarities between the experimental and predicted stress values are quite evident from these figures and the results from all three GRP panels are consistent.

14.6 Concluding Remarks

For the case of an isotropic or orthotropic cylindrical shell panel, excellent agreement has been demonstrated between the Galerkin solution, presented earlier and a suitably refined finite element model using a semi-Loof type element. This agreement is both for panel deflection behaviour, and for stresses.

Good agreement has been shown in all cases between the experimentally measured deflection behaviour of the test panels, and the predicted behaviour. This agreement is particularly good when allowance is made for measured imperfections of the test panel boundary conditions. Sensitivity of deflection behaviour to control of the membrane boundary conditions at the panel longitudinal edges (lateral panel displacements at these edges) has also been demonstrated.

Good agreement, for the isotropic case, and fair agreement for the orthotropic cases has been obtained between predicted and experimental membrane and bending stresses. With hindsight it is felt that improved agreement for stresses could have been obtained, if the selected strain gauge type been specifically calibrated for use on the GRP material. However this is not considered a serious shortcoming of these results.

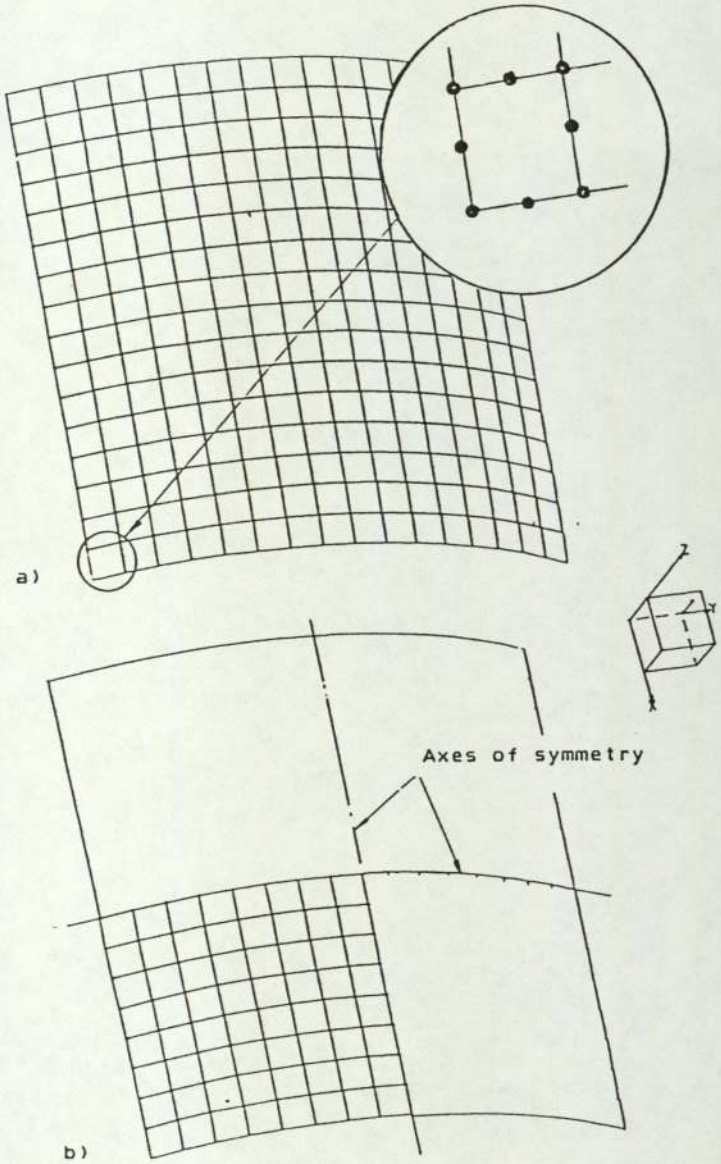

Fig. 14.1 Finite Element Model of Cylindrical Panel
a) Full panel model (16 x 16 elements)
b) Quarter panel model (8 x 8 elements)

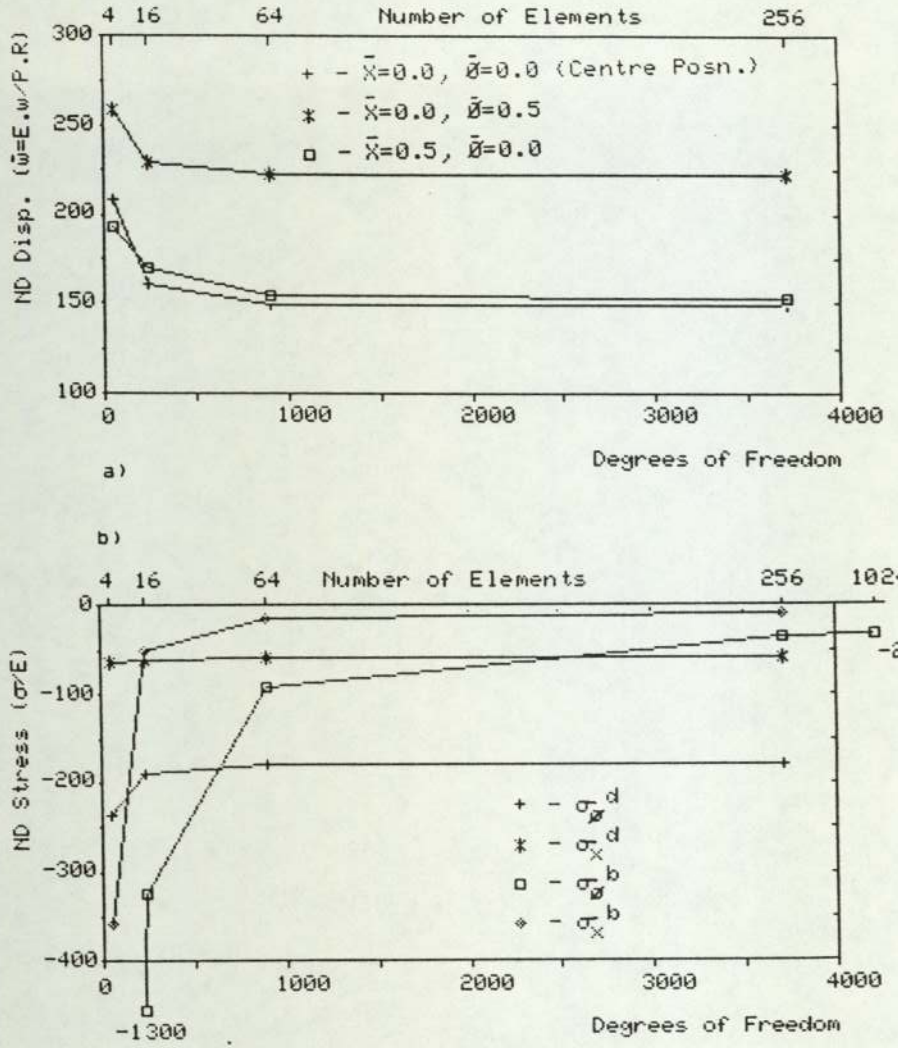

Fig. 14.2 Finite Element results for AL1 (using facet element 44210) showing convergence with increasing number of elements or dof.

a) Displacements at selected panel positions
b) Bending & Membrane stresses at centre

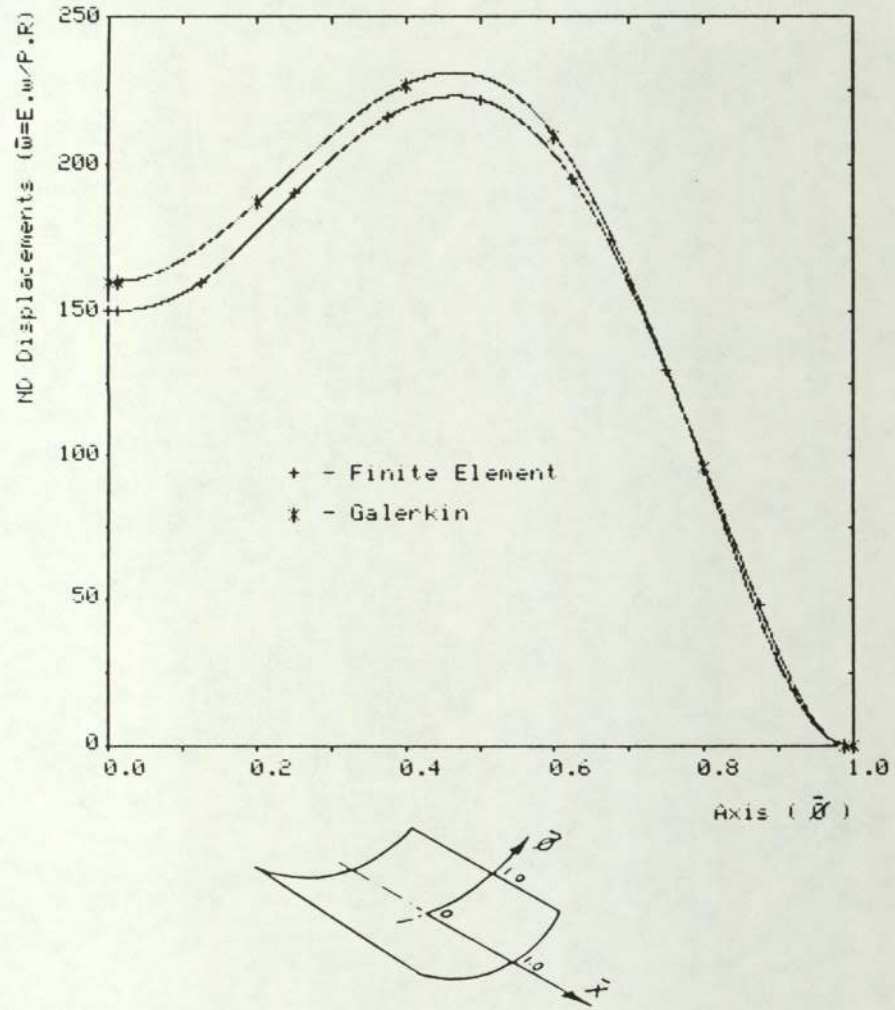

Fig. 14.3 Comparison of predicted displacements for AL1 from Finite Element (44210 - 896dof) and Galerkin methods. (Fully clamped case)

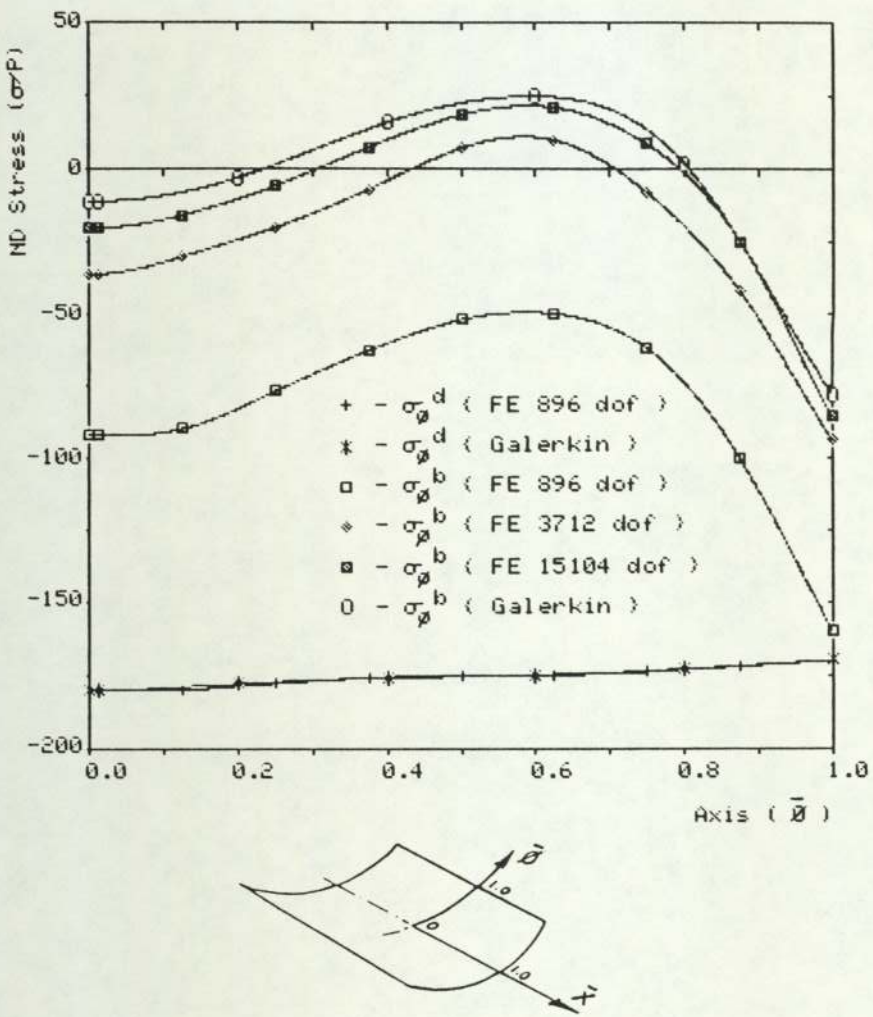

Fig. 14.4 Comparison of predicted bending & membrane stresses for AL1 from Finite Element (44210) and Galerkin methods. (Fully clamped case)

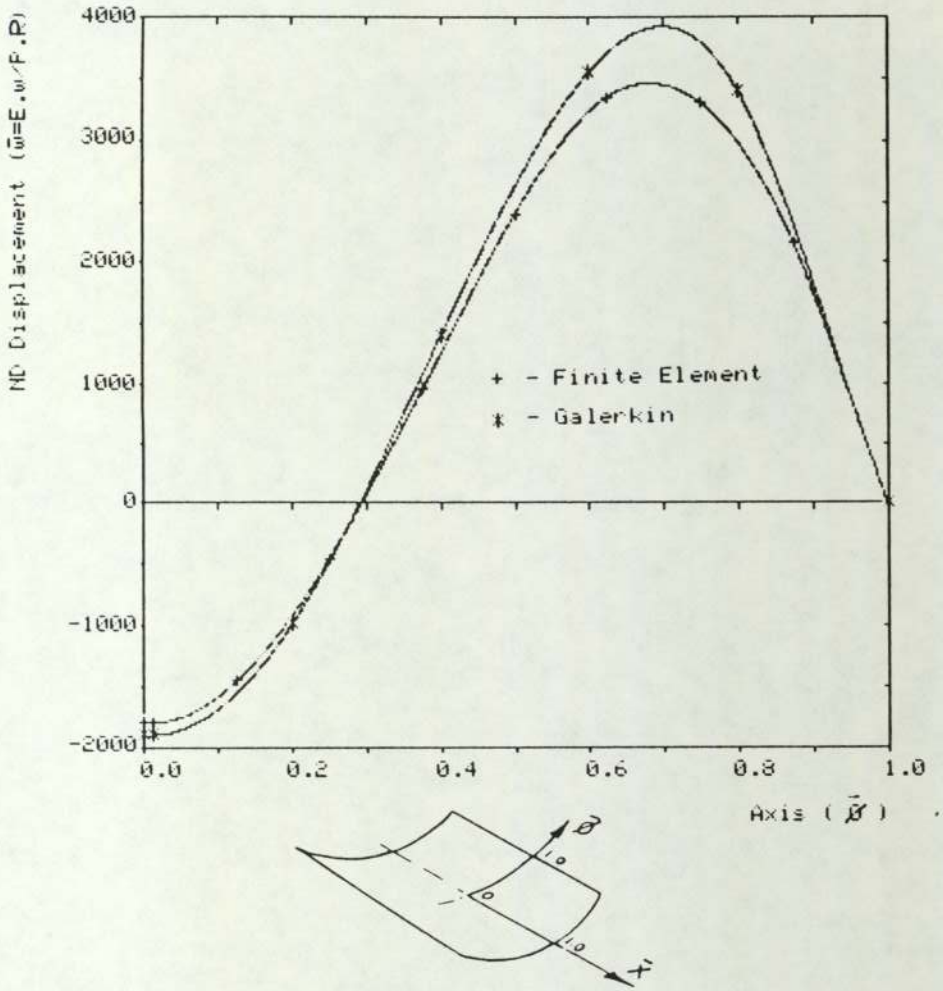

Fig. 14.5 Comparison of predicted displacements for AL1 from Finite Element (44210 - 896dof) and Galerkin methods. (Simply supported case)

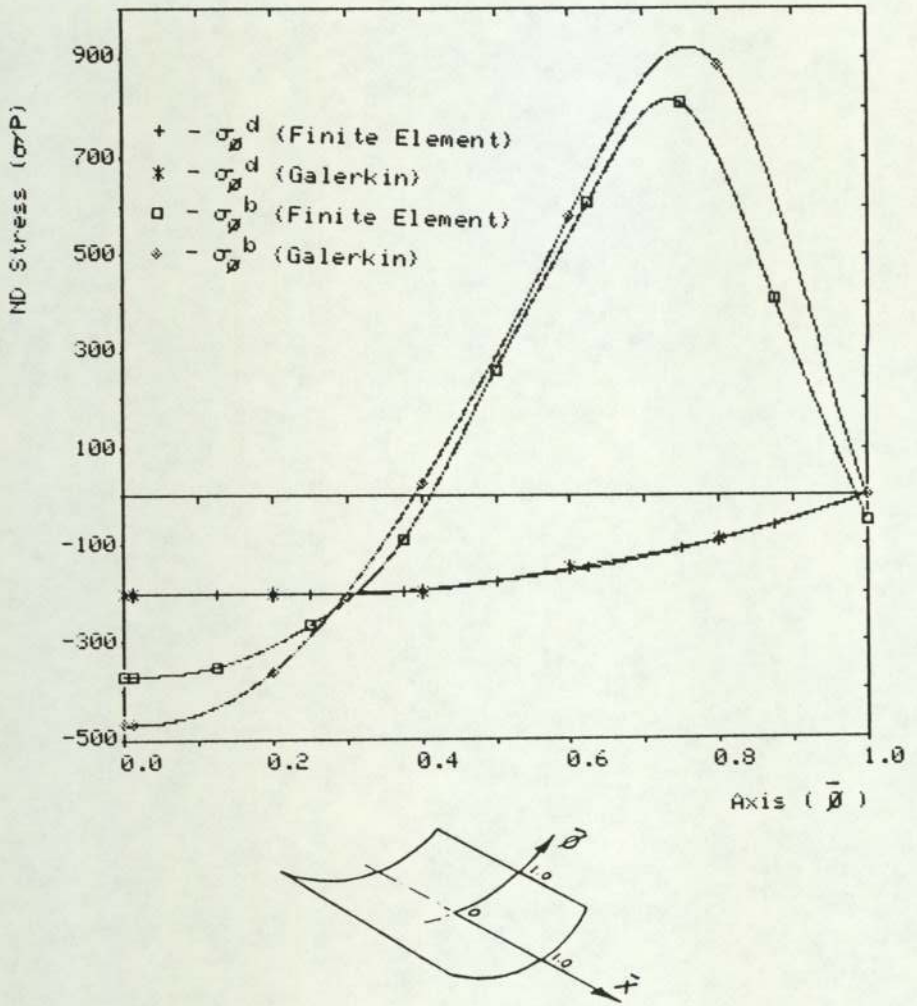

Fig. 14.6 Comparison of predicted bending & membrane stresses for AL1 from Finite Element (44210 - 896dof) and Galerkin methods. (Simply supported case)

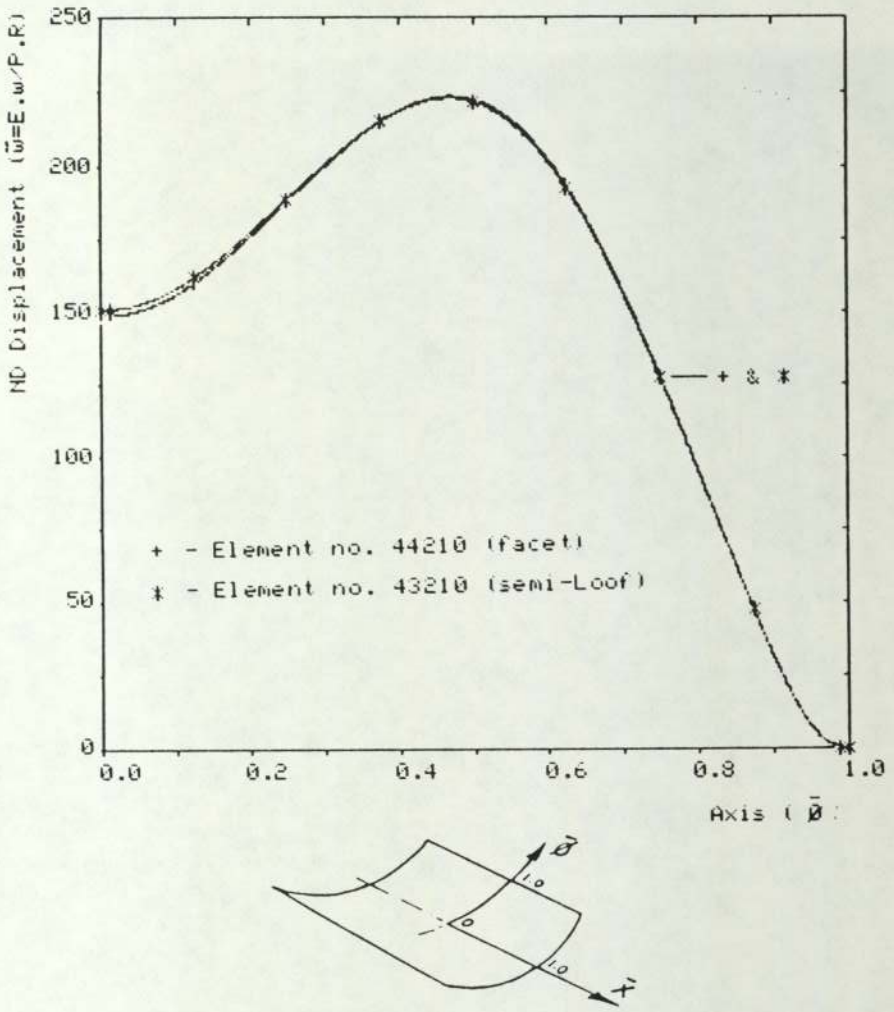

Fig. 14.7 Comparison of predicted displacements for AL1 from Finite Element analysis using facet (44210) and semi-Loof (43210) elements.

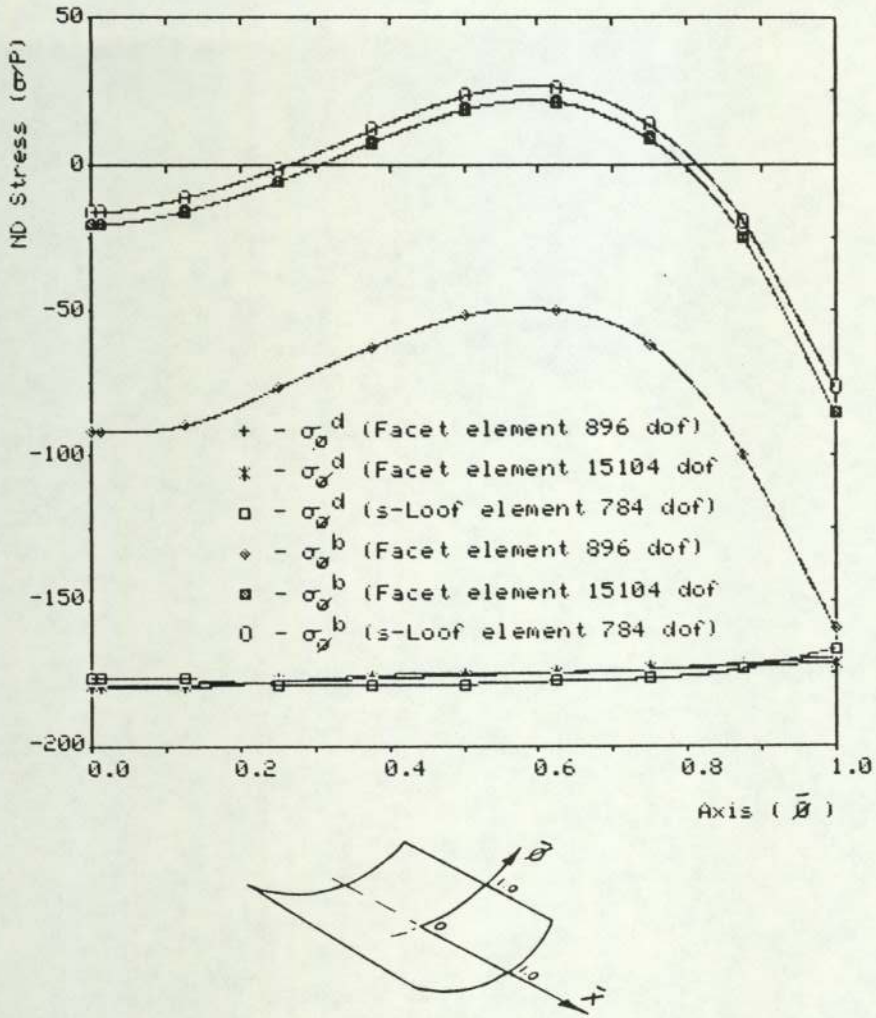

Fig. 14.8 Comparison of predicted bending & membrane stresses for AL1 from Finite Element analysis using facet (44210) and semi-Loof (43210) elements.

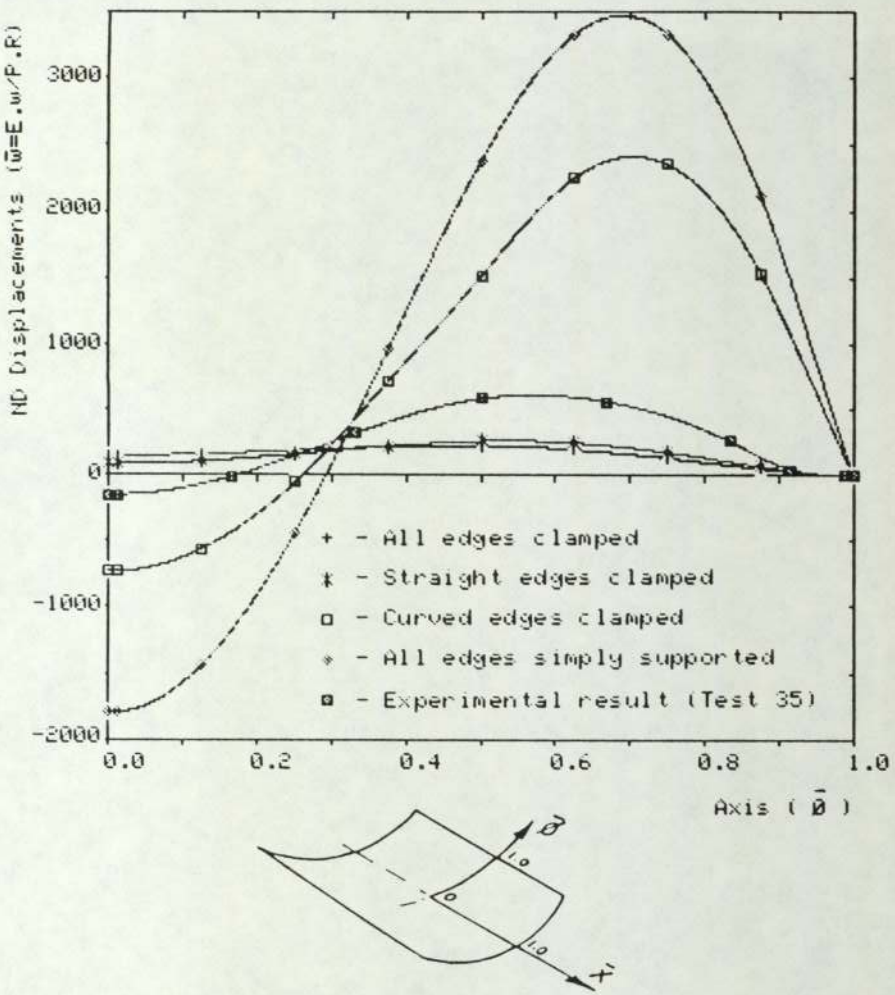

Fig. 14.9 Comparison of predicted displacements for AL1 from Finite Element analysis for various combinations of edge restraint. (Experimental result for AL1 included for comparision)

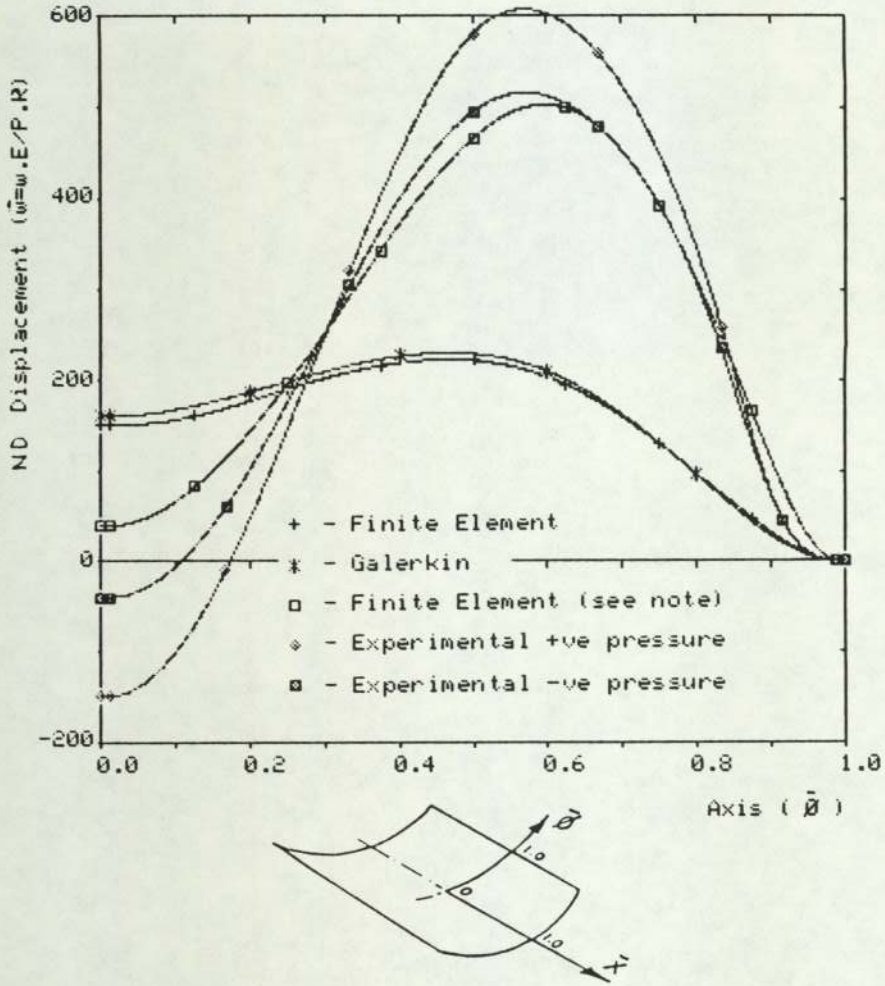

Fig. 14.10 Comparision of predicted and experimental displacements for panel AL1.

(Note: This prediction based on prescribed displacements from Figure 11.4)

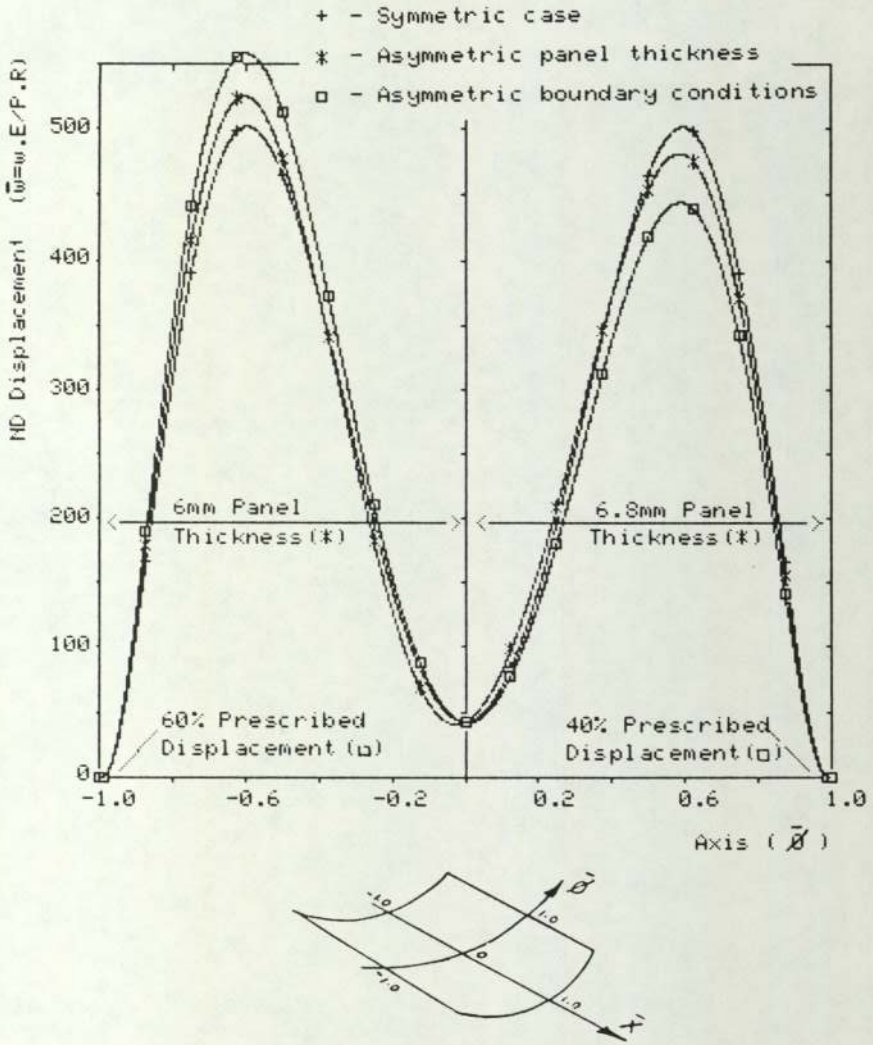

Fig. 14.11 Effect on symmetry of panel behaviour of asymmetric boundary conditions and asymmetric panel thickness.

(Note: Finite Element predictions for aluminium panel AL1.)

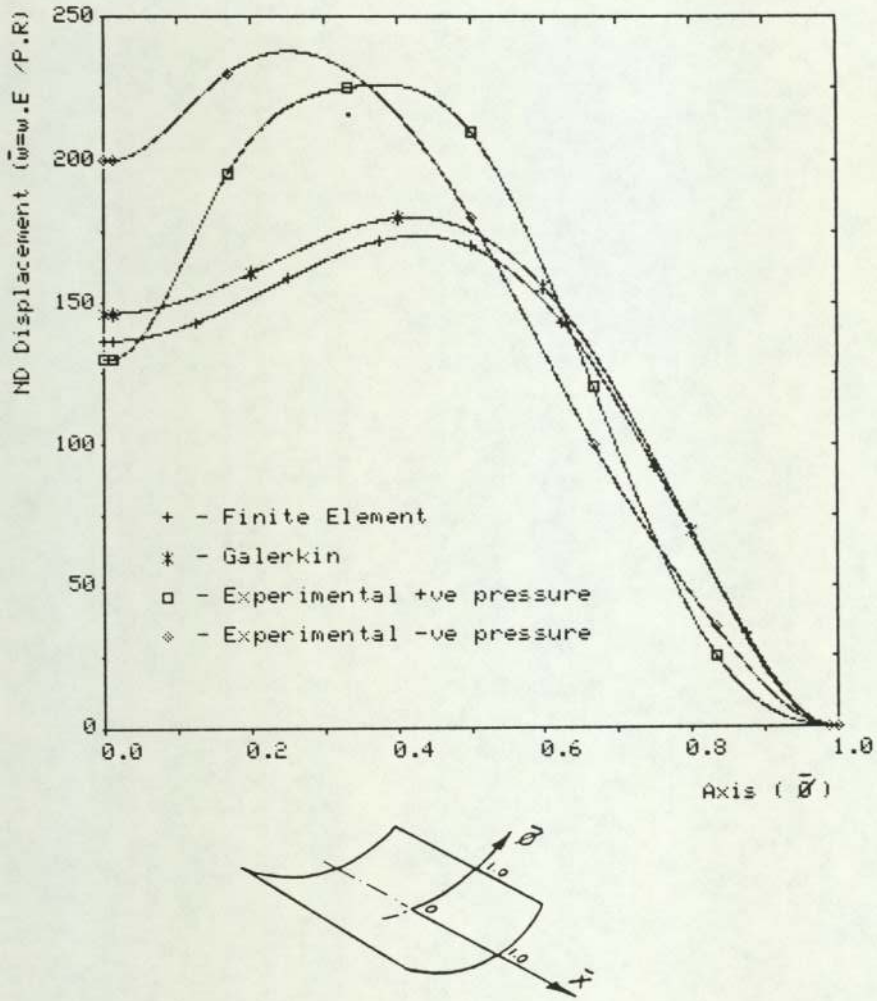

Fig. 14.12 Comparision of predicted and experimental displacements for panel GRP1.

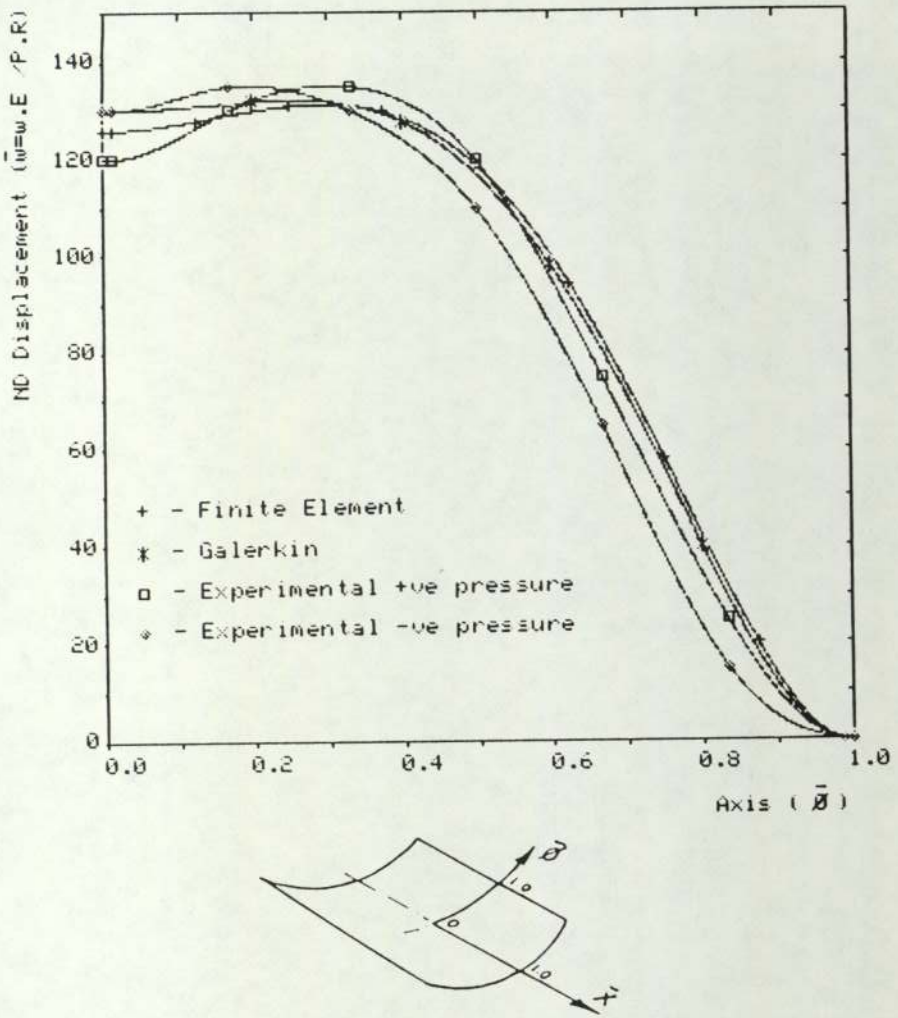

Fig. 14.13 Comparision of predicted and experimental displacements for panel GRP2.

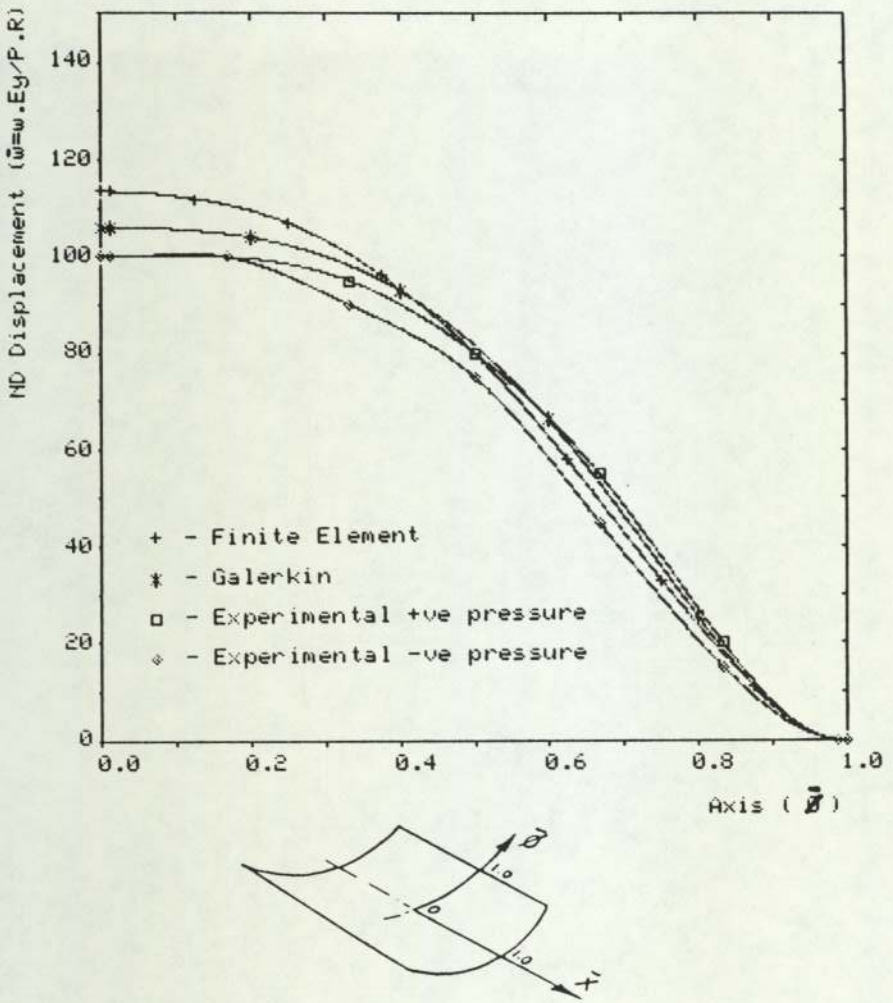

Fig. 14.14 Comparision of predicted and experimental displacements for panel GRP3.

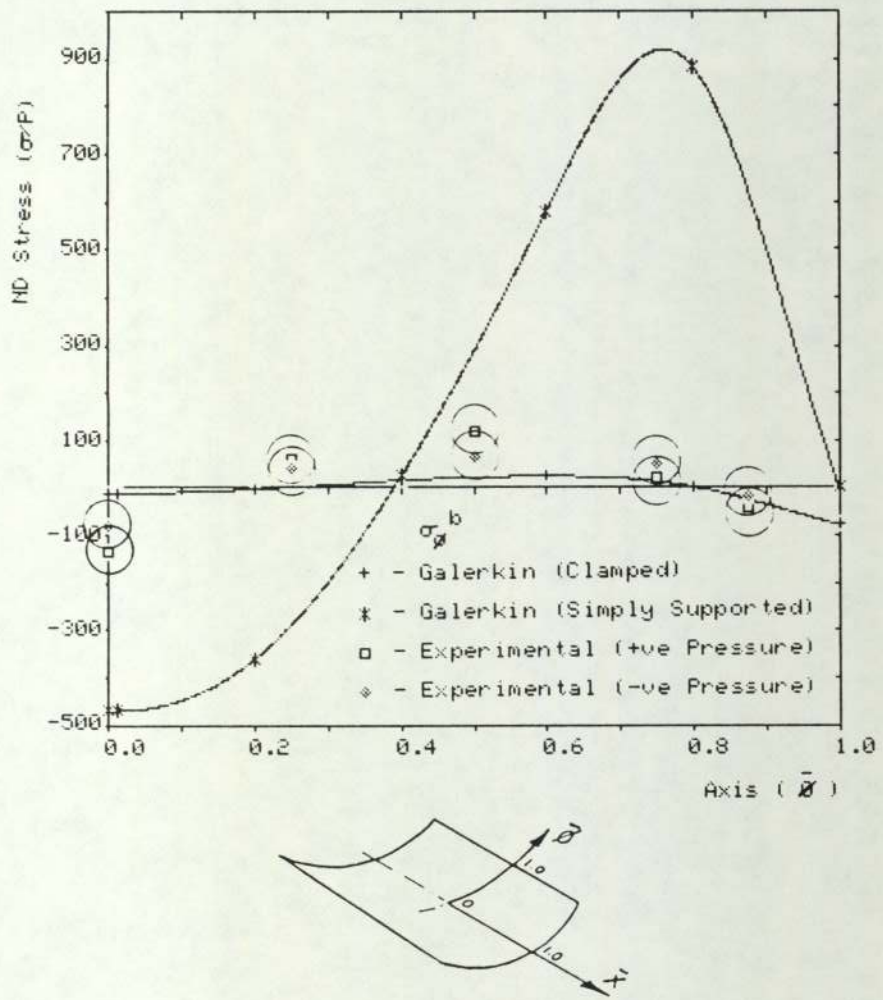

Fig. 14.15 Comparision of predicted and experimental bending stresses in ø direction for panel AL1.

(Note: Experimental stress values shown ringed for clarity.)

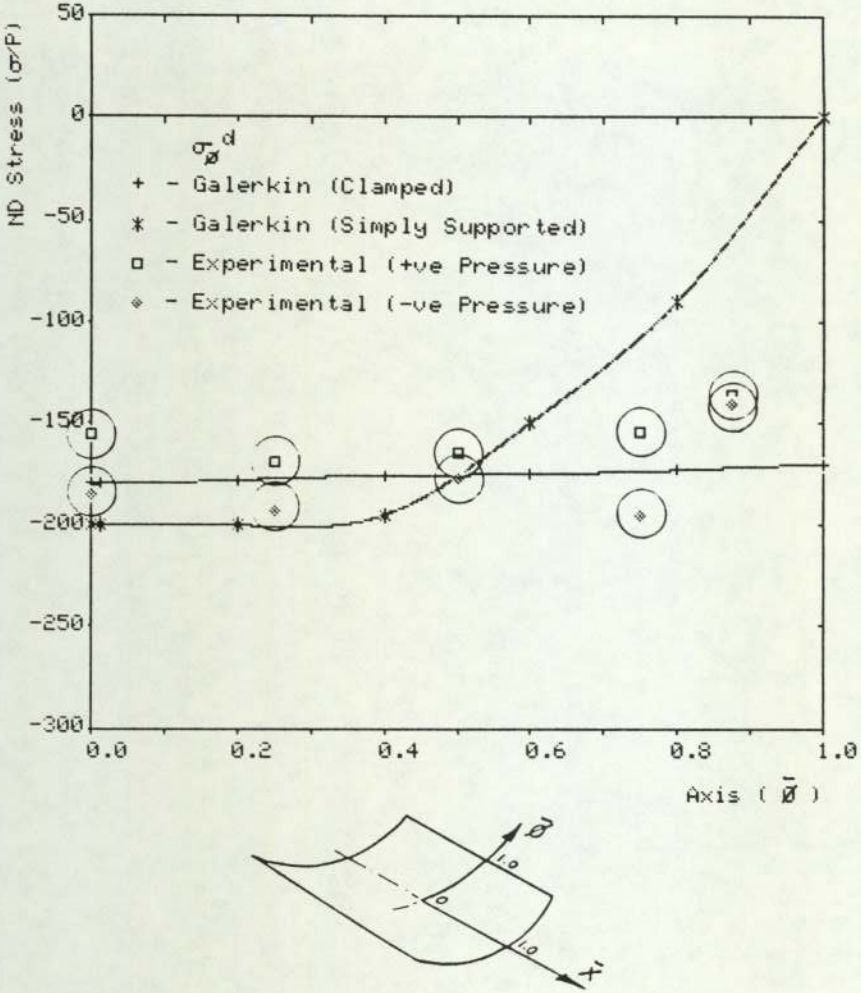

Fig. 14.16 Comparision of predicted and experimental membrane stresses in ø direction for panel AL1.

(Note: Experimental stress values shown ringed for clarity.)

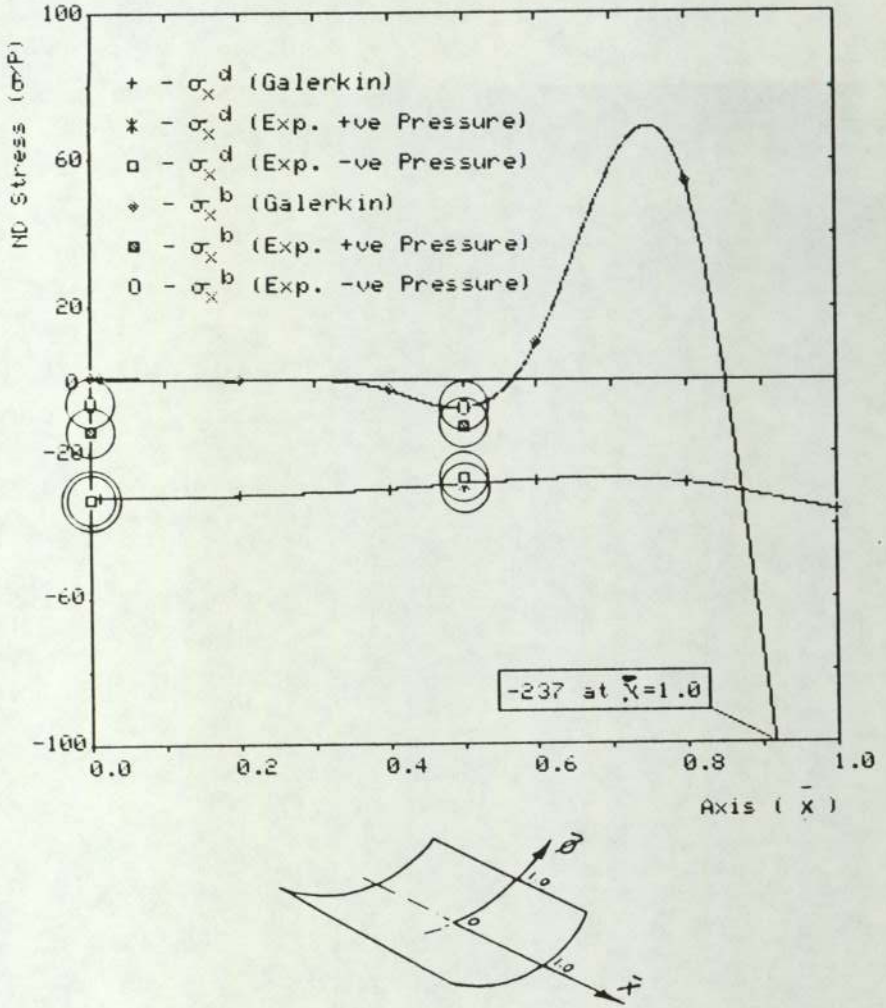

Fig. 14.17 Comparision of predicted and experimental bending & membrane stresses in x direction for panel GRP1.

(Note: Experimental stress values shown ringed for clarity.)

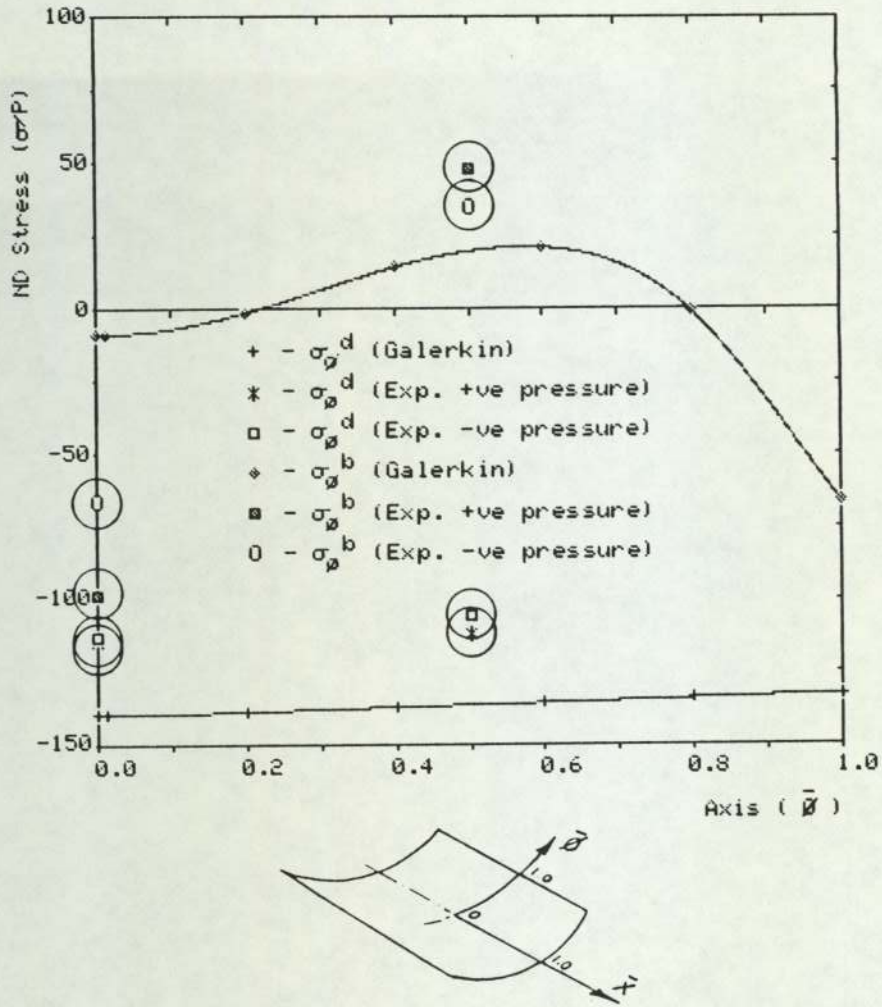

Fig. 14.18 Comparision of predicted and experimental bending & membrane stresses in ϕ direction for panel GRP1.

(Note: Experimental stress values shown ringed for clarity.)

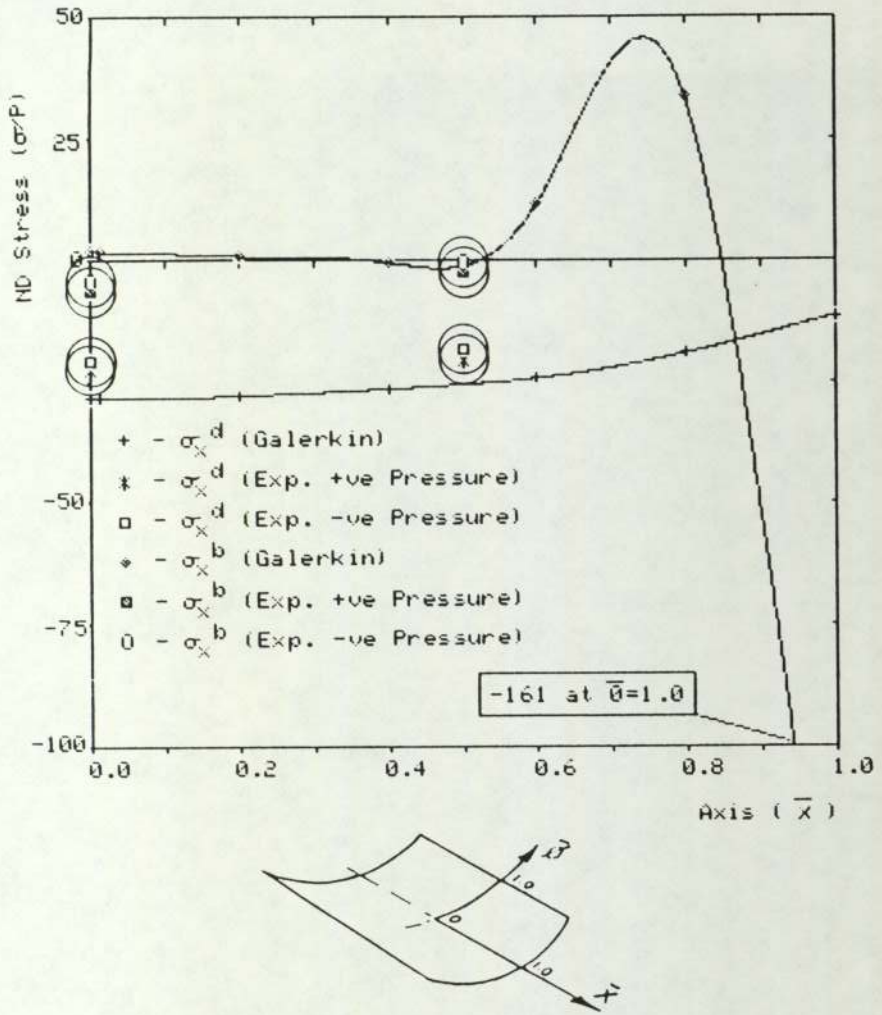

Fig. 14.19 Comparision of predicted and experimental bending & membrane stresses in x direction for panel GRP2.

(Note: Experimental stress values shown ringed for clarity.)

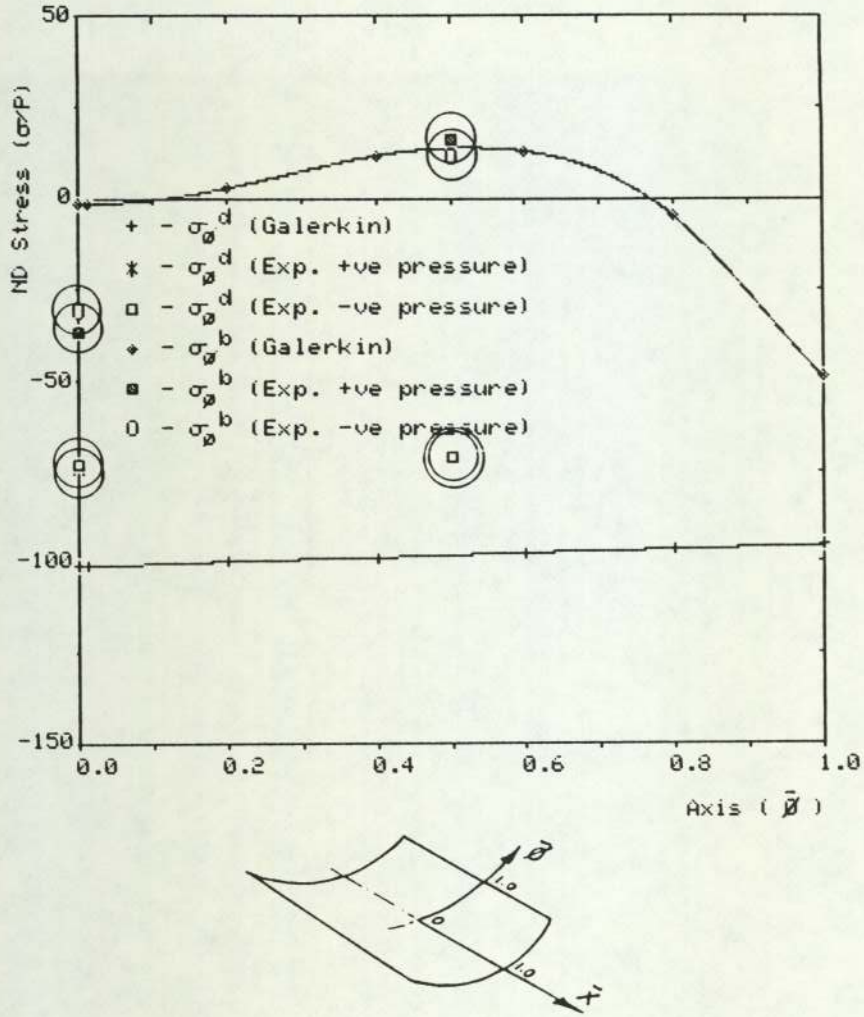

Fig. 14.20 Comparision of predicted and experimental bending & membrane stresses in ø direction for panel GRP2.

(Note: Experimental stress values shown ringed for clarity.)

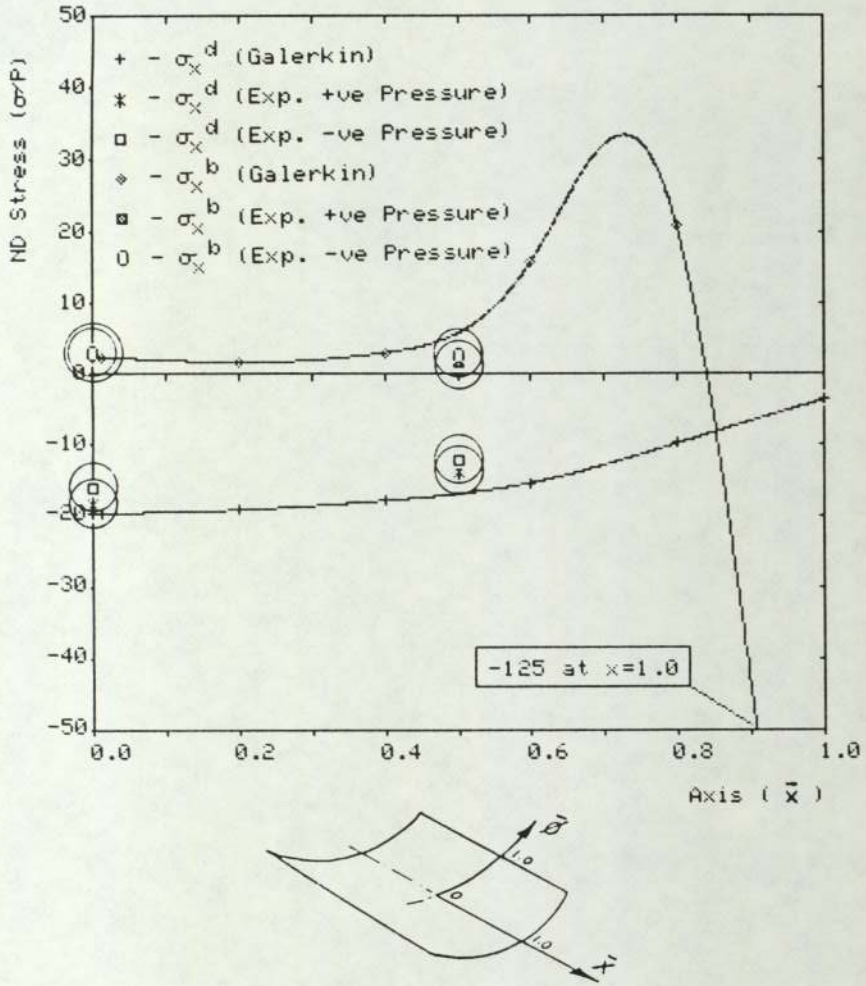

Fig. 14.21 Comparision of predicted and experimental bending & membrane stresses in x direction for panel GRP3.

(Note: Experimental stress values shown ringed for clarity.)

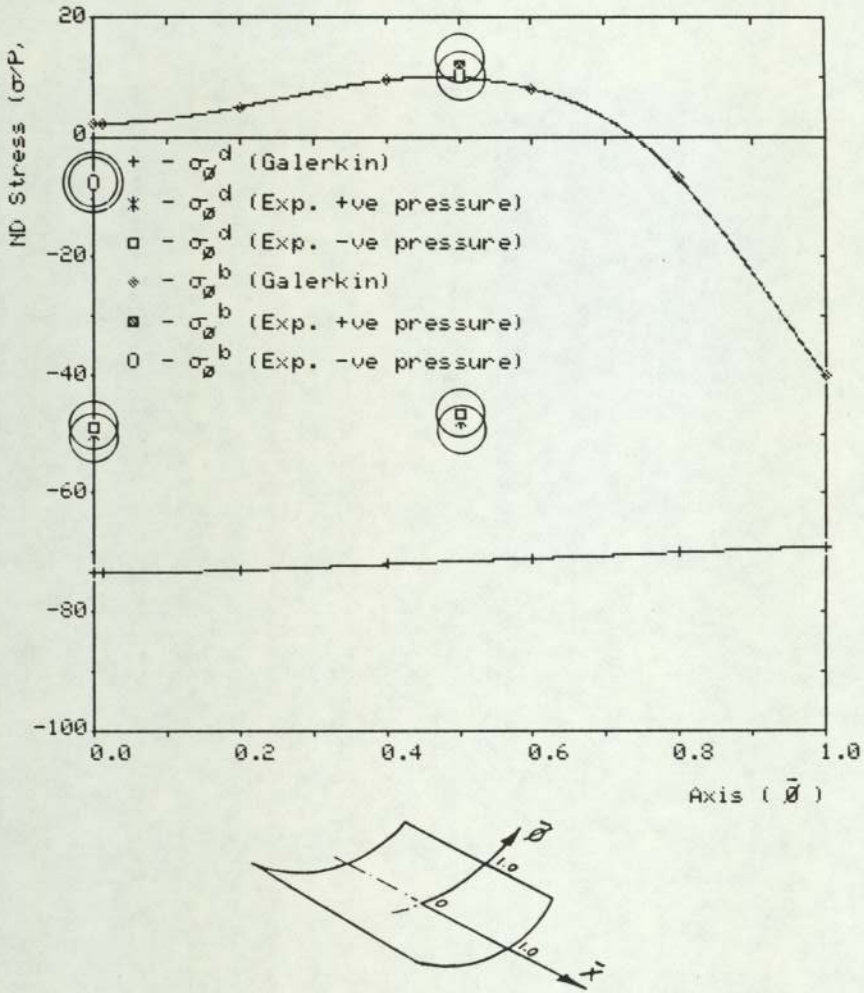

Fig. 14.22 Comparision of predicted and experimental bending & membrane stresses in ø direction for panel GRP3.

(Note: Experimental stress values shown ringed for clarity.)

CHAPTER 15

CONCLUSIONS AND DESIGN RECOMMENDATIONS

15.1 Aims of this Thesis

The aims of this thesis were threefold:

(1) To examine the behaviour of a cylindrical GRP panel with all of its edges mechanically clamped and subject to a uniform pressure loading on its convex surface. This panel to be of a construction and geometry representative of a GRP sonar panel.

(2) To determine if possible the reasons for the historical failure to achieve agreement between finite element analysis of sonar panels on the one hand, and experimental scale model panels on the other.

(3) To make recommendations leading to the more efficient design of sonar domes and panels, for use in the ships and submarines of the Royal Navy.

The first two of these aims are of course closely related, and the current work has sought an understanding of the behaviour of these cylindrical panels by a combination of experimental testing of panels, experimental determination of material elastic properties, and numerical analysis of panel behaviour. The numerical analysis has involved both finite element methods and a Galerkin solution of the cylindrical shell equations.

It has been shown in the previous chapters that panel behaviour is dependent upon material elastic properties, mechanical boundary conditions, and panel geometry. From the work reported here a number of important conclusions can be drawn regarding the behaviour under load of cylindrical sonar panels, not only of the behaviour of ideal geometrically perfect panels of uniform elastic properties and idealised boundary conditions, but also of real panels

of non-uniform composition and properties, and subject to non-ideal, but nevertheless practically realisable boundary conditions.

In the light of this work a number of recommendations can be made regarding:

(1) Methods of improving production techniques so that a more nearly uniform and consequently a more predictable product may be produced.

(2) Improving the analysis procedures so that more realistic predictions of panel behaviour become available; and by which those factors which have been identified as influencing panel behaviour may be quantified.

(3) Possible improvements in panel design and mounting so that maximum benefit may be obtained from the unique structural properties of the composite material.

15.2 Cylindrical Panel Behaviour

Detailed predictions of panel behaviour and the results of the experimental testing are given in the earlier chapters. However, a number of general observations are worth restating here.

15.2.1 Deflection Behaviour

From the work reported in the previous chapters it may be observed that a fully clamped cylindrical panel subject to a uniform pressure load on its convex side will deflect in the direction of the load. The precise pattern of the deflection will depend upon the geometry of the panel but the maximum deflection will not generally occur in the centre. For the geometry range considered in this study a double lobed deflection pattern may be expected. This deflection pattern will become more pronounced as the panel becomes thinner ($R/_h$ increasing).

If the bending boundary conditions are relaxed, so that the edges of the panel are free to rotate (hinged or pinned rather than fully clamped), then the effect on panel deflection will be only slight. (Maximum deflection will be increased by less than 10% for the panels considered here and the lobed deflection pattern will become only slightly more pronounced). However, if the membrane boundary conditions are relaxed, particularly along the longitudinal edges of the panel, so that lateral displacements in the ϕ direction are permitted at these edges, then the double lobed pattern will become much more pronounced. In this case, for some panel geometries, a central deflection in the opposite direction to the load may result. This deflection pattern is similar in form to that predicted for the simply supported case and involves deflections of magnitude several times greater than those predicted for the fully clamped case.

The sensitivity to membrane edge condition that this implies, results, for the case of real panels with imperfectly clamped edges, in a certain degree of asymmetry of deflection behaviour. This asymmetry, caused by asymmetry of the membrane boundary conditions at the two longitudinal edges of the panel, is manifest as an asymmetry of the lobed deflection pattern. A similar asymmetry of the deflection pattern may also be produced by non-uniformity of the panel itself about its longitudinal axis of symmetry; possibly due to variations in panel thickness or in quality of lay up. However, within the practical limits of lamination practice, this effect is considered a less significant cause of asymmetic behaviour. It may of course have a

contributary effect in any particular case.

15.2.2 Stress Behaviour

For a fully clamped cylindrical panel the predominant stress in the central portion of the panel is the membrane stress; only near the edges of the panel do bending stresses become significant.

This membrane state of stress in the central region of the panel can be determined very simply by membrane shell analysis. For example, the membrane hoop stress in an externally pressure loaded cylinder can be obtained as:

$$\frac{\sigma_\phi}{p} = - \frac{R}{2h}$$

For the dimensions of the panel AL1 (R/h = 355.3) this gives:

$$\frac{\sigma_\phi}{p} = - 177.65$$

This compares very favourably with the result obtained from the Galerkin solution for this panel of:

$$\frac{\sigma_\phi}{p} = - 179.2$$

Furthermore since the strain in the longitudinal direction is prevented, membrane analysis indicates that the stress in the longitudinal direction should be:

$$\frac{\sigma_x}{p} = \nu \frac{\sigma_\phi}{p} = - 55.07$$

(ν = 0.31)

compared with the result obtained from the Galerkin solution of:

$$\frac{\sigma_x}{p} = - 52.05$$

Thus, very close agreement with membrane theory is demonstrated for the fully clamped case.

Near the edges of the clamped panel, although the membrane stresses remain largely unchanged, the bending stresses become more significant. Of particular interest is the bending stress σ_x^b at the curved edges of the panel. For the fully clamped case this longitudinal bending stress is the greatest stress occurring anywhere in the material. Thus it is at this point, the curved clamped edge, that failure of an overloaded fully clamped panel would be expected.

Relaxation of the edge restraints has a number of interesting effects on the panel stress behaviour.

If the bending edge restraints are relaxed resulting in the hinged or pinned boundary condition as before, then the bending stresses at the panel edges are of course reduced to zero. Bending stresses now make a significant contribution to total stresses only near, but not at, the panel edges, and peak values of bending stresses are very much reduced. These bending stresses are again superimposed upon the fairly uniform state of membrane stress existing over the whole panel. The penalty for this reduction in bending stress, and consequently in total stress, is the slight increase in panel deflection discussed in the previous section.

If, additionally, the membrane boundary conditions are relaxed, so that the panel becomes simply supported, then the result is firstly, a small increase in membrane stresses in the centre of the panel, with of course zero membrane stresses at the edges, and secondly a complete

change in the bending stress distribution so that bending stresses now predominate over the whole panel. These bending stresses are of significantly greater magnitude than the membrane stresses and for the geometries of panel considered in this study exhibit a change of sign between the centre and edges of the panel. A panel with this boundary condition would be expected to fail due to bending (away from the panel edges) at a loading significantly less than that which either the fully clamped or the hinged panel might be expected to safely sustain.

15.3 Comparison of Predicted and Experimental Results

In this work good agreement has been shown between the observed behaviour of the experimental test panels and analysis of the panels using both a Galerkin solution of the governing differential equations and finite element methods.

This agreement has been obtained using analysis based upon carefully measured material elastic properties and carefully defined panel boundary condition.

In view of the difficulties that have been experienced in attaining this level of agreement it is reasonable to suppose that the failure to achieve reliable results in previous testing programs was due to:

(1) Failure to obtain reliable material elastic properties. The measured values used in this study were obtained separately for each panel and considerable variation was found between panels. Use of global properties, taken from the material specification, is not satisfactory.

(2) Failure to properly define panel boundary conditions. It is clear from this work that a bolted panel connection cannot be assumed to give a fully clamped edge condition and that small departures from the fully clamped condition may result in gross changes in panel behaviour.

(3) Unsophisticated finite element models based on facet type elements may be very slow to converge particularly for bending stresses. This effect may be obscured if total stress values are taken from the finite element model without separation into bending and membrane components.

15.4 Recommendations

Recommendations for design improvements for future sonar domes and panels may be considered under three headings:

(1) Manufacture and material specification.

(2) Design and analysis strategy.

(3) Boundary conditions.

15.4.1 Manufacture and Material Specification

As has been stated earlier, the good agreement achieved in this study between analysis of panels and experimental results, has been obtained using material properties determined from experimental testing. Clearly for the design of a working sonar dome or panel it is necessary to predict behaviour before the dome is constructed; testing of material samples may give useful confirmation that material specifications have been met, but these results cannot be used retrospectively for analysis.

The existing material specifications and manufacturing practices are unsatisfactory for the following reasons:

(1) The specification of material properties is too loosely drawn. Appendix A gives the current specification. Only material strength and minimum fibre fraction are specified. Elastic properties are not specified.

(2) The specified material properties are difficult to achieve using the current hand lay-up practice. More closely specified properties would be more difficult to achieve.

(3) Once a dome is completed it is not generally possible to check the material properties by non-destructive means. Properties of separately laid up specimens may be different.

Clearly there are two possible approaches to improving the quality and uniformity of the sonar dome material. Either the specification must be revised to include details of elastic properties and laminate thicknesses, with specified limits and suitable quality control procedures, or else the manufacturing technique must be modified to give a more uniform product. It is considered doubtful whether tightening of the specifications, without some modifications to the manufacturing practice, could be made to result in anything more than a marginal improvement in product quality. The most promising approach is therefore to seek improved methods of manufacture.

A number of techniques are available for manufacture of large GRP structures of consistent quality and properties. The most successful of these is the

'Resin Injection' method widely used in the aircraft industry for the production of radomes. This method requires the use of a double mould, usually of steel to withstand the pressure of the injection process and the temperature of curing. Dry reinforcing fibres are placed in the cavity between the male and female moulds. allowing very precise control over both quantity of reinforcement and fibre direction. Resin, usually low viscosity epoxy, is then injected under pressure into the mould. The mould is electrically heated to cure the resin, and finally split to remove the dome. This results in a dome of very high quality, uniform thickness, and predictable mechanical properties. Unfortunately the cost of the process is high. Marine sonar domes are usually very much larger than aircraft radomes and production runs are usually one or possibly two off. Very long production runs are normally required to justify the cost of resin injection for even relatively small components. The method is not considered suitable for sonar domes.

Three other techniques offer the prospect of improved sonar dome manufacture. Ln order of additional cost and probably performance over the current practice, they are:

(1) Improved hand lay up using unidirectional reinforcements in place of woven rovings and chopped strand mat.

(2) Fabrication of large domes from small dome elements. These might be produced by

'improved' hand lay up techniques or by any of the more advanced techniques including resin injection.

(3) Vacuum assisted injection techniques using low cost GRP moulds.

Improvements in the hand lay up technique could be made at relatively low cost by replacing the present lay up of woven rovings and chopped strand mat with unidirectional reinforcements. Clearly since this would involve a change in the laminate composition the acoustic properties of the material would need further investigation but with suitable selection of lamina stacking sequence it ought to be possible to produce a satisfactory laminate in this way. This is a low cost option for achieving some improvement over the current practice.

One of the difficulties of achieving uniform material properties by hand lay up is that large structures cannot be laid up with the same control as can small structures. However, techniques for producing bonded joints in composite materials are now well established and properly designed joints can have mechanical properties very similar to those of the parent material. There would seem to be no practical reason why a large sonar panel should not be fabricated from a large number of small elements. Since these elements would be of relatively simple form, possibly flat facets, stringent quality control could be applied to their production. A proper program of material testing could be undertaken for element samples, and sub standard elements could be rejected before fabri-

cation. It would of course be necessary to evaluate fully the proposed jointing techniques and acoustic properties of this form of dome construction before it could be adopted for full size domes. Nevertheless, it is considered worthy of further investigation.

The third technique of vacuum assisted resin injection is a newly developed technique pioneered by the Dutch boatbuilder Le Comte Holland BV. Most of the details of the technique are Commercial-in-Confidence but the principles are straightforward. A double mould is used as in conventional resin injection, and the reinforcement is laid dry. However, because of the lower pressures involved in the process these moulds may be made of GRP and are consequently much cheaper than steel moulds. Resin is injected by a combination of vacuum assistance applied to the moulds, and static head pressure created by suspending the resin barrels several metres above the structure. Multiple resin inlets are provided and slow curing resins are employed so that the injection process may take several days to complete. Because the moulds are of transparent GRP the progress of the injection can be monitored visually. Once gelation of the resin has begun the mould can be split and curing can continue with the structure supported from one side only.

Le Comte have used this technique to produce landing craft up to 22 m in length and now believe that they have developed the method sufficiently for it to be of use for larger structures. The quality of

laminate produced by vacuum assisted resin injection is not as good as that produced by conventional high pressure resin injection, and the attainable fibre fractions are not so high. Nevertheless, the use of a double mould and the ability to lay reinforcements in the dry state, means that excellent dimensional control and fibre direction control can be achieved. Le Comte claim that the laminate produced by this method is structurally superior to hand lay up in terms of 'strength to weight ratio'. If this is true then the method should be quite suitable for production of sonar domes and would seem to offer a very useful production option for all but the largest domes. Since two moulds are required, and both are more complex than a single hand lay up mould, the cost of the process would clearly be greater than that of hand lay up for production runs of one or two off. This extra cost would be offset to some extent however by reduced labour costs. Hand lay up is a very labour intensive process.

15.4.2 Design and Analysis Strategy

Provided that a uniform laminate of known material elastic properties can be produced, and provided also that realistic boundary conditions are incorporated into the model, it has been shown here that shell structures of GRP sonar dome laminate can be successfully modelled using a single layer orthotropic semi-Loof shell element. It has been shown that, for the specific case of a cylindrical sonar panel, the membrane boundary conditions are the most significant boundary conditions for overall

displacement behaviour, and it seems reasonable to assume that this will also be the case for a large class of other shell forms.

Due to slow convergence, the use of facet elements for the analysis of sonar domes is not recommended, particularly if bending stresses are required. Facet elements will however give good results for displacement behaviour and may be useful for preliminary analysis.

The method used here to incorporate realistic membrane boundary conditions into the finite element model, ie setting prescribed displacements at the panel edges, suffers from the disadvantage of being specific to particular panel properties and to a particular load. A better strategy for design purposes might be to incorporate an array of spring elements around the panel edges. If this method is used, spring stiffnesses must of course be determined from some knowledge of the surrounding structure. Panel membrane edge reactions can be reliably estimated from a simple preliminary membrane analysis.

The work also indicated that it is unnecessary to include in the finite element modelling, either transverse shear effects or material non-linearities.

15.4.3 Boundary Conditions

Detailed design of the bolted joint between a sonar panel and the hull or casing of the ship or submarine to which it is fixed, is outside the scope of this work. Nevertheless in the light of the results obtained in this study the following observations can be made.

If the deflections of a sonar panel are to be minimised when the panel is subject to external pressure then this will be best achieved if all of the panel boundaries are fully clamped. That is, if both rotational (bending) and lateral (membrane) restraint is provided at all of the panel edges.

Notwithstanding the above some considerable advantage may be gained if the rotational restraint condition is relaxed. It has been shown that the penalty, in terms of displacements, for allowing some rotational edge freedom, is very small, whilst at the same time bending stresses at and near the panel edges are considerably reduced. Consequently there would seem to be little advantage in providing this rotational restraint.

In contrast to rotational edge restraint, which has little influence on panel displacement, membrane restraint, particularly of the longitudinal edges of a cylindrical panel, has a very significant influence on panel displacement behaviour. It is vital that this restraint be imposed if panel deflections are to be controlled. It is clear that allowance must be made at the design stage for any anticipated flexibility of the supporting structure in this respect.

Since cylindrical sonar panels in particular show great sensitivity to the membrane edge condition along their longitudinal edges, it may be

possible in particular cases to provide additional membrane restraint for panels of this type. Possibly by the provision of tie members across the chord of the panel to make the structures self reacting.

For sonar domes of any shape the membrane boundary conditions are likely to be important, even in those cases where the dome is not as sensitive in this respect as a cylindrical panel; it is essential therefore that the bolted joints be designed so that no slip can occur. Slipping of a joint is a relaxation of the membrane edge condition irrespective of the inherent stiffness of the surrounding structure. Consideration should be given to providing additional means of preventing joint slip, possibly by the doweling of joints in addition to bolting. One method of achieving this might be to laminate steel inserts into the edges of the panels so that fitted dowels could be added after assembly.

Since the main requirement of the bolted joints is to provide membrane clamping rather than bending clamping it might be considered that a larger number of smaller diameter bolts, arranged in a single row, would be preferable for future panel fixing, to the double row arrangement of large bolts used on the current test rig.

15.5 Concluding Remarks

This work has examined the behaviour of a pressure loaded cylindrical GRP sonar panel by a combination of experimental testing and numerical analysis. By incorporating into the modelling, realistic

boundary conditions and accurate material properties, good agreement between predicted behaviour, and experimental results, has been demonstrated. A number of suggestions have also been made for improving the current design and manufacturing practice, for GRP sonar domes in the Royal Navy.

In the next few years new developments and improvements in the field of advanced composite materials will no doubt influence the performance of future sonar domes. Likewise, advances in sonar technology will doubtless influence the sizes, shapes and acoustic requirements for future domes. In some cases, the development of new sonar techniques, such as towed array, may remove the need for sonar domes entirely.

The results presented in this thesis are in the main applicable to a wide range of orthotropic and isotropic materials as well as to GRP. Similarly the general observations made concerning panel and dome behaviour are applicable not only to sonar panels, but to many other engineering situations both inside and outside of the marine environment.

APPENDIX A. SPECIFICATION FOR POLYESTER RESIN/GLASS FIBRE REINFORCED LAMINATE

(Extracted from ARE specification UD 62571)

Introduction

This specification is intended to cover the manufacture of acoustically transparent polyester resin/glass fibre laminates produced by cold curing hand lay up techniques.

Glass Fibre Reinforcement

A list of approved materials is published separately. The weight of reinforcement and the number of laminations required will be specified on the production drawings of the article to be manufactured.

All the above materials should be kept in a dry store to avoid inferior laminates due to damp glass filament.

Resins

A list of approved resins and ancillary materials is published separately.

To avoid the use of stale resin, it is recommended that a minimum, stock say for a 2 months production should be ordered and replenishment made as required.

These materials should be kept in a store which is well ventilated, dry and most important of all, cool.

Resin Mix

The constituent materials are to be prepared at room temperature (approximately 20°C) in accordance with the resin manufacturer's instructions.

It is preferred that the resin and accelerator be mixed overnight so as to allow any entrapped air to be released before adding the catalyst and proceeding with lay up.

The mixing process is to be available for inspection by the Inspecting Authority.

Whilst the manufacturer may vary the mix to suit his own conditions of working, suitable mixes when using Uralam 8008 resin have been found to be as follows:

Uralam 8008	-	100 parts by weight
Catalyst (50% HCH)	-	¾-2 parts by weight
Accelerator (6% Cobalt)	-	⅓-1¼ parts by weight
Aerosil	-	4½ parts by weight
Styrene	-	22 parts by weight (see below)

The total Styrene content of this lay-up mix must not exceed 45%. This means that to the Uralam 8001 Resin, which has 33% Styrene Monomer added by manufacturer, the maximum amount of Styrene which may be added to 100 parts of resin is 23 parts. Similarly with Uralam 8008 the maximum additional Styrene permitted is 28 parts.

The amounts and type of catalyst and accelerator used may be varied to suit the manufacturer, but the respective directions supplied with each must be strictly adhered to.

Particular attention should be paid to avoiding the following defects during lay-up.

a. Entrapped air voids.

b. Incomplete wetting of the glass resulting in dry areas.

c. Resin rich areas, especially at corners.

d. Resin starved areas.

e. De-lamination.

Post Cure

The laminate, after gelation is complete, is to be post cured. At least 4 hours must elapse after gelation before post curing is commenced.

Curing may be carried out in a hot room or oven at uniform temperature, or as an alternative infra-red heaters may be used with care.

At 40°C, duration of cure must be 8 hours and at 80°C duration must be 4 hours. Temperatures between these may be used for corresponding times.

For large items a post cure temperature of 55°F minimum may be used for a minimum period of 14 days before testing.

Tests

Generally, there are two types of laminates used:

Type A - comprising chopped strand mat only which should contain 30-40% glass, and

Type B - comprising alternate layers of chopped strand mat and woven rovings which should contain 35-45% glass.

The physical properties of a completely cured laminate when tested in accordance with BS 2782 Part 3 must not be less than:

Tensile Strength (Method 301C - Min 3 Specimens)

	Type A		Type B	
Minimum:	93 MPa	(13,500 psi)	103 MPa	(15,000 psi)
Average:	110 MPa	(16,000 psi)	124 MPa	(18,000 psi)

Flexural Strength (Method 304B - Wide Specs, Min 5 Specimens)

	Type A		Type B	
Minimum:	128 MPa	(18,500 psi)	165 MPa	(24,000 psi)
Average:	159 MPa	(23,000 psi)	207 MPa	(30,000 psi)

Tests should be carried out, to the satisfaction of the inspection authority at least once during a manufacturing run of any component.

The test specimens must be laid up during the laying up of the component in question, using the same materials.

Remarks

When manufacturing acoustically transparent moulding, the following points are extremely important:

a. All flow surfaces (Gelcoat surfaces normally) require a finish of high quality and no rough areas or undulations can be tolerated.

b. Particular attention is to be paid to effectively removing all traces of release agent by means of a suitable solvent. In the case of a PVA release agent, hot detergent may be used.

c. No filler materials are permitted.

APPENDIX B USE OF ELECTRICAL RESISTANCE STRAIN GAUGES ON GRP

The purpose of this Appendix is to highlight the major problems associated with the use of strain gauges on composite materials and to indicate how these problems may be reduced or overcome in practice.

There are two basic questions which should be asked before strain gauges are considered for use on composite materials. These are:

1. Will the techniques to be employed, result in accurate measurement of surface strains?

2. What significance do values of surface strain have for the performance of the composite structure?

The strain gauge analysis of a typical metal component normally involves four sequential steps, performed at each point of interest on the component.

1. Measurement of surface strains at the selected point.

2. Transformation of the measured strains into the significant strains (normally the principal strains).

3. Conversion of the principal strains into principal stresses through appropriate stress/strain relationships.

4. Comparison of the principal stresses with the material strength via an assumed failure criterion for the material.

For composite materials such as GRP which are not ordinarily isotropic and homogeneous, but anisotropic and heterogeneous, the above procedure can no longer be regarded as directly applicable.

Even for the simple case of a single lamina considered at the macroscopic level, the principal stress directions do not necessarily coincide with the principal strain directions. Thus, there is in general, no direct means to convert principal strains to principal stresses. For a built up composite laminate consisting of several layers with different fibre orientations, the correspondence between principal strains and principal stresses is still more remote. Laminate behaviour is also complicated by variations of stress from layer to layer and by the presence of interlaminar shear stresses.

Even where reliable stresses in a particular layer of a laminate can be reliably measured or computed, the significance of these stresses may not always be clear; failure criteria for composites are themselves complex.

It is clear from the above that the interpretation of the significance of measured surface strains for a particular composite material requires a detailed knowledge of the material and of the structure of the composite. Nevertheless, if the discussion is limited to consideration of a single orthotropic layer, then much useful information may still be gained from measurement of surface strain. It may be noted for example that the first detectable damage to the sonar dome laminate of this study occurs at a strain of approximately 1%. This damage is due to matrix cracking, and occurs quite independently of stress values in any particular lamina. However, using the macroscopic material elastic properties this 'damaging strain' can be interpreted as a mean laminate stress in a particular direction. The stress transformation and strain transformation relationships can then be applied as for any conventional engineering material.

The adoption of this practical simplification however, presupposes that the surface strains on the GRP material can be accurately and reliably measured. It is here that practical difficulties arise. Strain gauges on composite materials present a number of unique problems not encountered with metals. If strain gauges are used on composites without consideration of these problems then very inaccurate results will be obtained. If adequate precautions are taken then most of these problems can be overcome.

The major problems encountered using strain gauges on fibre composites can be listed as follows:

1. Selection of suitable gauge length. The gauge length must be large with respect to the significant reinforcement dimensions (maximum fibre diameter and/or spacing). At the same time, the gauge length should not be so great as to prevent measuring peak strains in the presence of macroscopic strain gradients.

2. Reinforcement of the composite by the gauge. Because composites are generally very much less stiff than metals the bonding of strain gauges to the composite can result in significant local stiffening, resulting in low strain readings.

3. Gauge heating. Because composite materials generally have low thermal conductivity, local heating of the gauge is likely unless precautions are taken to prevent it. This gauge heating can have a number of effects. Firstly the gauge will give a high apparent strain reading because it is heated, second the hot gauge may adversely effect the bond between the gauge and its backing, and between the backing and the component, and third, local heating may effect the properties of the composite in the region of the gauge.

Gauge length selection will depend upon the particular composite, and on the size of the component. In practice this is unlikely to present too great a difficulty unless the component is very small. For the GRP sonar dome laminate gauge lengths between 3 and 9 have been found to be quite satisfactory, THOMPSON, HARTSHORN and SUMMERSCALES [93].

Reinforcement of the composite by the strain gauge is unavoidable to some extent and there is currently no generalised procedure which can be used to correct for this. In practice however, the errors from this source may be no more significant than the variation in material properties from one sample to the next, and can be reduced by careful gauge selection. Planar rosettes are to be preferred to stacked rosettes in this respect, and have the additional advantage of being less prone to self heating effects.

The third problem, that of gauge heating, is the one that is most difficult to quantify, but is also the one for which the most satisfactory solution exists. The Compulog system of gauge excitation used in the current work ensures that a particular gauge is only energised for sufficient time for it to be interrogated. Since this is less than 0.1 seconds for each interrogation, gauge heating and all of the associated problems, are virtually eliminated.

In the absence of such a system as this, gauge resistance should be selected to minimise self-heating effects. For any bridge excitation voltage, the power dissipation varies inversely with the gauge resistance; thus, higher resistances are normally advantageous. With most generally available gauge types available in 120 Ω and 350 Ω versions, the latter are obviously preferable and will reduce heat generation by a factor of about 3. Higher gauge resistances of 500 Ω or 1000 Ω can be considered, but these are usually available in only limited ranges. Reduction of bridge excitation voltage can produce a similar effect and should also be considered. The above argument only applies of course, when bridge voltage is controlled. If a constant current bridge circuit is employed, as is common practice with many commercial strain gauge systems, then the reverse argument applies and lower resistance gauges should be selected to give the lower heating effect.

It should be noted at the gauge selection stage that composites often possess the potential for extreme principal strain ratios. If this is likely to be the case then consideration should be given to making correction for transverse sensitivity of the gauges. The need for this correction will depend of course on the type of composite and the characteristics of the selected gauges.

Finally some attention should be given to the practice to be adopted in fixing the gauges to the composite specimens. Selection of a suitable adhesive should take into account the curing temperature, which must obviously be within the range allowed for the composite, and also the elongation capability of the adhesive since large strains are often encountered with these materials. For use on GRP, cyanoacrylate adhesives are generally suitable provided no moisture is present in the material.

Surface preparation prior to bonding should follow normal practice (clean and grease free) but it is worth noting that composites are often contaminated with silicone release agents left over from moulding. These may be very difficult to remove and care should be taken that they do not contaminate the gauge bonding facilities.

In the usual practice of installing gauges on metal objects, the lead wires are soldered to the gauges after the gauges have been bonded in place. It is well worthwhile reversing this procedure with composites. The low thermal conductivity of typical composites results in a risk of heat damage to the gauge (or even to the composite surface) if this practice is followed. If the leadwires are soldered to the gauge before it is bonded in place then this danger is avoided.

With the present "state of the art" in the experimental stress analysis of composites the attainable accuracy of strain measurements on these materials is likely to be somewhat lower than for the common structural metals. Since composites vary so widely in their constituents and properties, the selection of gauge type, adhesive and procedure in any particular case will always be conditioned by the idiosyncracies of the material involved. Nevertheless, with reasonable care and an appreciation of the problems likely to be encountered, strain gauges can still provide a useful tool for the stress analysis of composites.

APPENDIX C TEST RIG MANUFACTURING DRAWINGS

Main Assembly Drawing

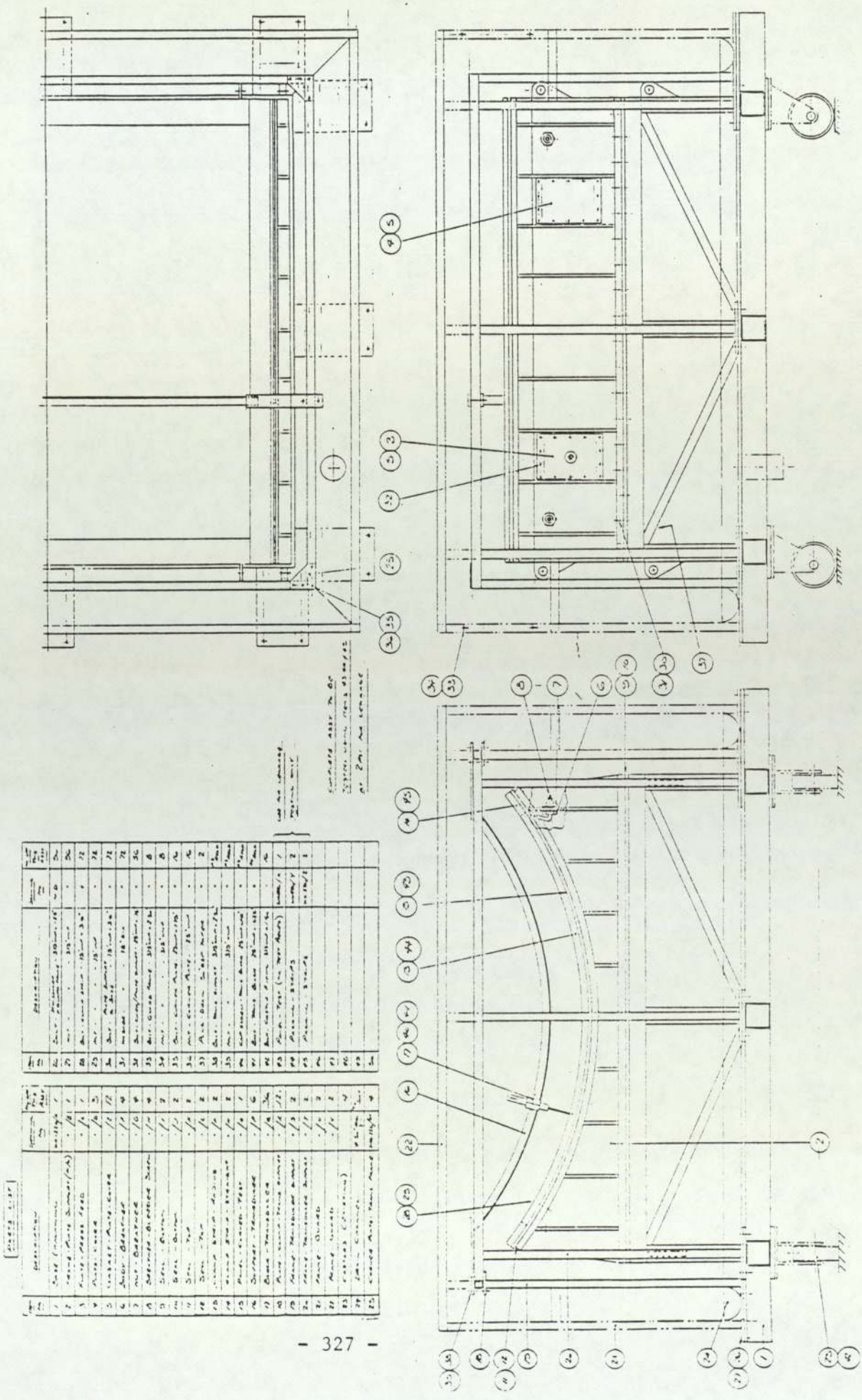

Base Section Machining Drawing

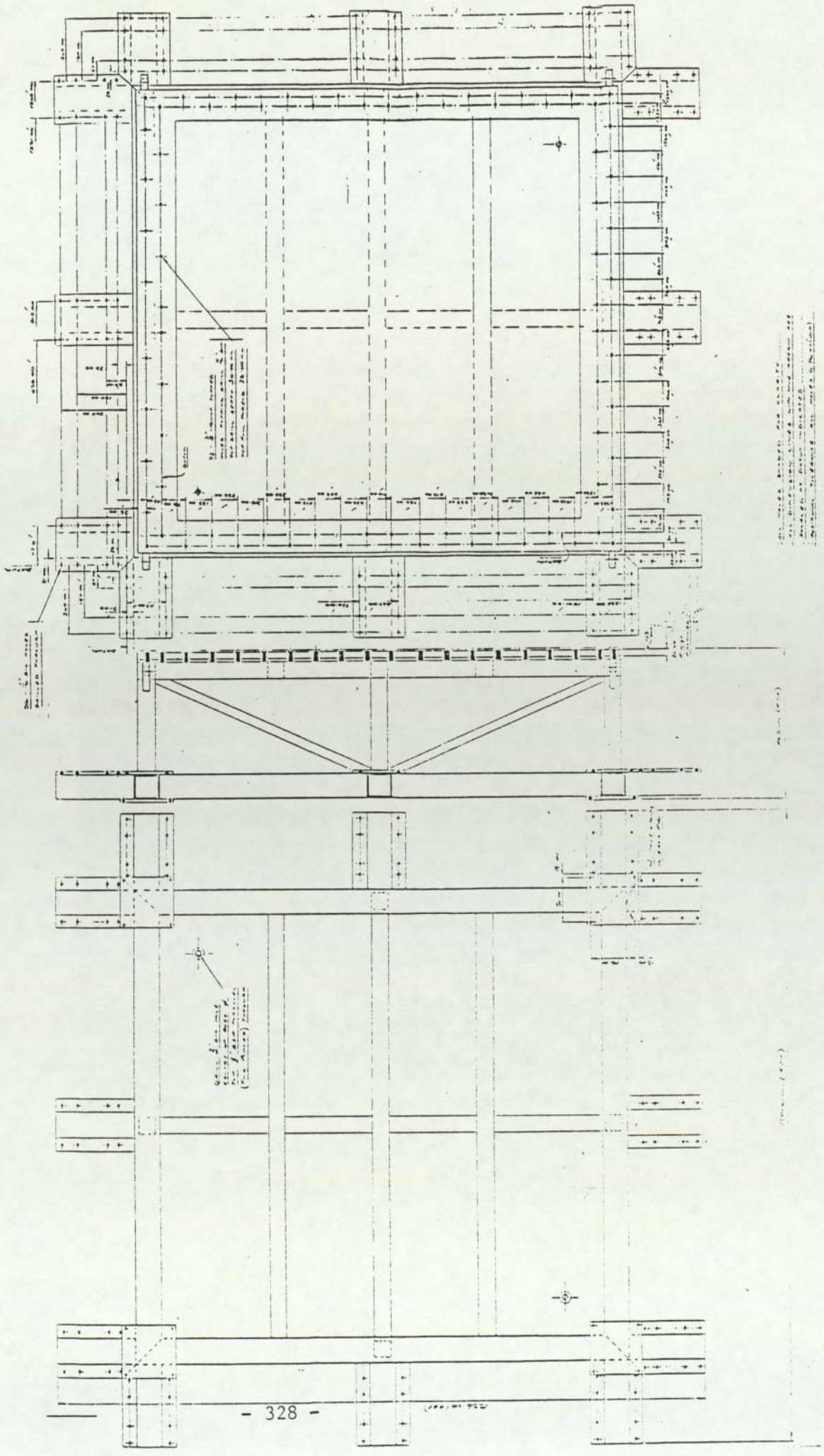

Panel Fixture Machining Drawing

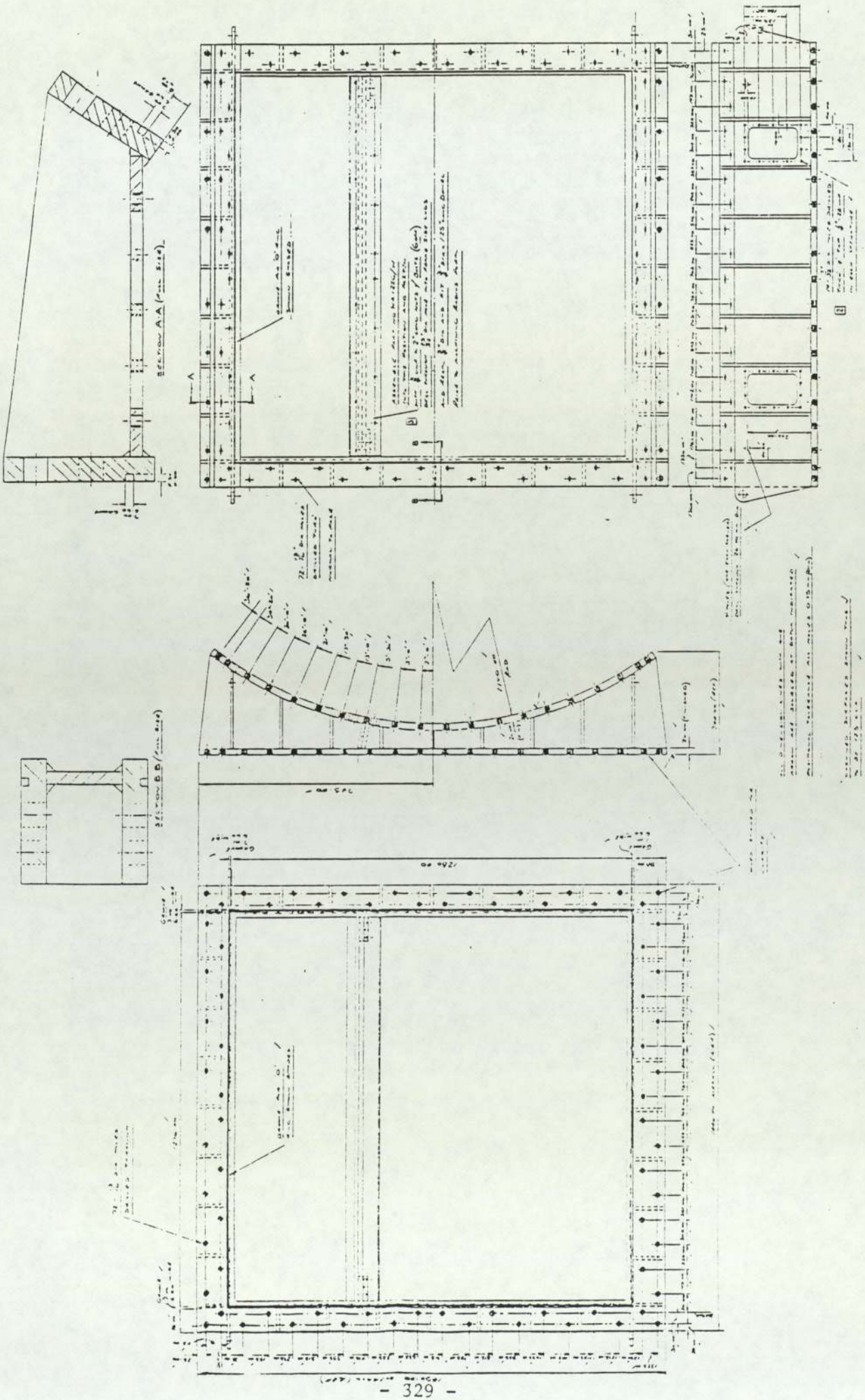

APPENDIX D. PRINCIPLE OF THE GALERKIN METHOD

This method for the approximate solution of boundary-value problems was proposed by B G GALERKIN in 1915. The method is closely related to the Raleigh-Ritz technique and indeed in solid mechanics problems the two methods are often exactly equivalent. The Galerkin method however, is generally more straightforward to apply. Whereas the Raleigh-Ritz method requires the use of a functional, the Galerkin method makes direct use of the differential equation, involves no consideration of any variational problem, and can be applied even in situations where no functional exists.

The basis of the method is straightforward. Suppose it is required to solve a linear differential equation:

$$L(u) = 0 \qquad \text{in some two dimension domain 'A'}$$

subject to some linear homogeneous boundary conditions.
(Note: The method can also be applied to non-linear problems).
Suppose the exact solution is:

$$u(x, y)$$

We can seek an approximate solution of the problem in the form:

$$u_n(x, y) = \sum_{j=1}^{n} a_j \phi_j(x, y)$$

where ϕ_j are suitable co-ordinate functions selected to satisfy the same boundary conditions as the exact solution and a_j are undetermined constants. It is the selection of these 'trial' functions which is the critical step in the method and which determines the suitability of the method in any particular case. As well as exactly satisfying all of the problem boundary conditions the set $\{\phi_j\}$ should be complete in the sense that any continuous function $f(x, y)$ in the domain A can be approximated

to any degree of accuracy by the sum $\sum_{j=1}^{N} c_j \phi_j$

in such a way that $\delta_N = \iint_A (f - \sum_{j=1}^{N} c_j \phi_j)^2 dx\, dy$

can be made as small as is required. The finite sum $u_n(x, y)$ will not normally satisfy the differential equation and the substitution will give:

$$L(u_n) = \varepsilon_n(x, y), \quad \varepsilon_n(x, y) \neq 0 \quad \text{in the domain } A$$

$\varepsilon_n(x, y)$ can be viewed as an error function. If max $\varepsilon_n(x, y)$ is small then clearly $u_n(x, y)$ can be considered a satisfactory approximation to $u(x, y)$ the task is therefore to select the undetermined constants a_j so as to minimise $\varepsilon_n(x, y)$ If $u(x, y)$ is represented by:

$$u(x, y) = \sum_{i=1}^{\infty} a_i \phi_i$$

then considering the nth partial sum

$$u_n = \sum_{i=1}^{n} a_i \phi_i$$

then

$$\iint_A L(u_n)\phi_i(x, y)\,dx\,dy = 0 \qquad \text{as } n \to \infty$$

is equivalent to $L(u) = 0$

The Galerkin method imposes on the error function $L(u_n)$ a set of orthogonality conditions

$$\iint_A L(u_n)\phi_i(x, y)\,dx\,dy = 0 \qquad (i = 1, 2, 3 \ldots\ldots n)$$

yielding a set of n equations

$$\iint_A L\left(\sum_{j=1}^{n} a_j \phi_j\right)\phi_i\,dx\,dy = 0 \qquad (i = 1, 2, 3 \ldots\ldots n)$$

These equations can be solved for the n constants a_j in the approximate solution.

APPENDIX E CYLINDRICAL SHELL EQUATIONS

E.1 Governing Differential equations

Using the notation of this study and the shell element shown in Figure (E.1) Flügge gives the basic equilibrium equations for a cylindrical shell as:

$$N'_x + N^{\cdot}_{\phi x} + p_x R = 0 \tag{E.1}$$

$$RN^{\cdot}_{\phi} + RN'_{x\phi} - M^{\cdot}_{\phi} - M'_{x\phi} + p_{\phi} R^2 = 0 \tag{E.2}$$

$$M^{\cdot\cdot}_{\phi} + M'_{x\phi} + M'^{\cdot}_{\phi x} + M''_x + RN_{\phi} - p_r R^2 = 0 \tag{E.3}$$

$$RN_{x\phi} - RN_{\phi x} + M_{\phi x} = 0 \tag{E.4}$$

where $(\,)' = R \frac{\partial}{\partial x} (\,)$: $(\,)^{\cdot} = \frac{\partial}{\partial \phi} (\,)$

The strain-displacement relationships are:

$$\varepsilon_x = \frac{u'}{R} - z \frac{w''}{R^2} \tag{E.5}$$

$$\varepsilon_{\phi} = \frac{v^{\cdot}}{R} - \frac{z}{R} \frac{w^{\cdot\cdot}}{(R + z)} + \frac{w}{R + z} \tag{E.6}$$

$$\gamma_{x\phi} = \frac{u^{\cdot}}{R + z} + \frac{R + z}{R} v' - \frac{w'^{\cdot}}{R} \left[\frac{z}{R} + \frac{z}{R + z} \right] \tag{E.7}$$

For the orthotropic case the stress-strain relationships are:

$$\sigma_x = E_1 \varepsilon_x + E_{\nu} \varepsilon_{\phi} \tag{E.8}$$

$$\sigma_{\phi} = E_{\nu} \varepsilon_x + E_2 \varepsilon_{\phi} \tag{E.9}$$

$$\tau_{x\phi} = G_{x\phi} \gamma_{x\phi} \tag{E.10}$$

where $E_1 = \frac{E_x}{1 - \nu_x \nu_{\phi}}$; $E_2 = \frac{E_{\phi}}{1 - \nu_x \nu_{\phi}}$; $E_{\nu} = \frac{E_x \nu_x}{1 - \nu_x \nu_{\phi}} = \frac{E_{\phi} \nu_{\phi}}{1 - \nu_x \nu_{\phi}}$

The various rigidities may be expressed as:

a. $D_x = E_1 t$
$D_{\phi} = E_2 t$
$D_{\nu} = E_{\nu} t$
) extensional rigidities

b. $D_{x\phi} = G_{x\phi} t$ shear rigidity

c. $K_x = \frac{E_1 t^3}{12}$)
$K_\phi = \frac{E_2 t^3}{12}$) bending rigidities
$K_\nu = \frac{E_\nu t^3}{12}$)

d. $K_{x\phi} = \frac{G_{x\phi} t^3}{12}$ twisting rigidity

Then, the force-displacement relationships may be expressed as:

$$N_\phi = \frac{D_\phi}{R}(v\cdot + w) + \frac{D_\nu}{R} u' + \frac{K_x}{R^3}(w + w'') \qquad (E.11)$$

$$N_x = \frac{D_x}{R} u' + \frac{D_\nu}{R}(v\cdot + w) - \frac{K_x}{R^3} w'' \qquad (E.12)$$

$$N_{x\phi} = \frac{D_{x\phi}}{R}(u\cdot + v') + \frac{K_{x\phi}}{R^3}(v' - w'\cdot) \qquad (E.13)$$

$$N_{\phi x} = \frac{D_{x\phi}}{R}(u\cdot + v') + \frac{K_{x\phi}}{R^3}(u\cdot + w'\cdot) \qquad (E.14)$$

$$M_\phi = \frac{K_\phi}{R^2}(w + w'') + \frac{K_\nu}{R^2} w'' \qquad (E.15)$$

$$M_x = \frac{K_x}{R^2}(w'' + u') + \frac{K_\nu}{R^2}(w'' - v\cdot) \qquad (E.16)$$

$$M_{\phi x} = K_{x\phi}(2w'\cdot + u\cdot - v') \qquad (E.17)$$

$$M_{x\phi} = \frac{2K_{x\phi}}{R^2}(w'\cdot - v') \qquad (E.18)$$

Substituting these force-displacement relationships and their derivatives into the equilibrium equations gives the governing differential equations for the cylindrical shell.

$$R\frac{\partial N_x}{\partial x} + \frac{\partial N_{\phi x}}{\partial \phi} + P_x R = 0 \quad \text{(1st equilibrium eqn)} \qquad (E.1)$$

$$N_x = D_x \frac{\partial u}{\partial x} + \frac{D_\nu}{R}\left(\frac{\partial v}{\partial \phi} + w\right) - \frac{K_x}{R}\frac{\partial^2 w}{\partial x^2}$$

$$\therefore \frac{\partial N_x}{\partial x} = D_x R \frac{\partial^2 u}{\partial x^2} + D_\nu \left(\frac{\partial^2 v}{\partial \phi \partial x} + \frac{\partial w}{\partial x} \right) - K_x \frac{\partial^3 w}{\partial x^3}$$

$$N'_x = \frac{D_x}{R} u'' + \frac{D_\nu}{R} (v'\cdot + w') - \frac{K_x}{R^3} w'''$$

$$N_{\phi x} = D_{x\phi} \left(\frac{\partial u}{R \partial \phi} + \frac{\partial v}{\partial x} \right) + K_{x\phi} \left(\frac{\partial u}{R^3 \partial \phi} + \frac{\partial^2 w}{R^2 \partial x \partial \phi} \right)$$

$$\frac{\partial N_{\phi x}}{\partial \phi} = D_{x\phi} \left(\frac{\partial^2 u}{R \partial \phi^2} + \frac{\partial^2 v}{\partial x \partial \phi} \right) + K_{x\phi} \left(\frac{\partial^2 u}{R^3 \partial \phi^2} + \frac{\partial^3 w}{R^2 \partial x \partial \phi^2} \right)$$

$$= \frac{D_{x\phi}}{R} (u'' + v'\cdot) + \frac{K_{x\phi}}{R^3} (u'' + w'''')$$

Substituting

$$\frac{D_x u''}{R} + \frac{D_\nu}{R} (v'\cdot + w') - \frac{K_x w'''}{R^3} + \frac{D_{x\phi}}{R} (u'' + v'\cdot)$$

$$+ \frac{K_{x\phi}}{R^3} (u'' + w'''') + p_x R = 0$$

or

$$D_x u'' + D_{x\phi} u'' + (D_\nu + D_{x\phi}) v'\cdot + D_\nu w' + \frac{1}{R^2} \{K_{x\phi} u'' - K_x w''' + K_{x\phi} w''''\} + p_x R^2 = 0 \qquad \text{(E.19)}$$

$$RN'_\phi + RN'_{x\phi} - M'_\phi - M'_{x\phi} + p_\phi R^2 = 0 \text{ (2nd equilibrium eqn)} \qquad \text{(E.2)}$$

$$N_\phi = \frac{D_\phi}{R} (v'' + w\cdot) + \frac{D_\nu}{R} u'\cdot + \frac{K_\phi}{R^3} (w\cdot + w'''')$$

$$RN'_\phi = D_\phi (v'' + w\cdot) + D_\nu u'\cdot + \frac{K_\phi}{R^2} (w\cdot + w'''')$$

$$N'_{x\phi} = \frac{D_{x\phi}}{R} (u'\cdot + v'') + \frac{K_{x\phi}}{R^3} (v'' - w''\cdot)$$

$$RN'_{x\phi} = D_{x\phi} (u'\cdot + v'') + \frac{K_{x\phi}}{R^2} (v'' - w''\cdot)$$

$$M_{\phi}^{\cdot} = \frac{K_{\phi}}{R^2}(w^{\cdot} + w^{\cdot\cdot\cdot}) + \frac{K_{\nu}}{R^2} w^{''\cdot}$$

$$M'_{x\phi} = \frac{2K_{x\phi}}{R^2}(w^{''\cdot} - v'')$$

Substituting

$$D_{\phi}(v^{\cdot\cdot} + w^{\cdot}) + D_{\nu}u^{'\cdot} + \frac{K_{\phi}}{R^2}(w^{\cdot} + w^{\cdot\cdot\cdot}) + D_{x\phi}(u^{'\cdot} + v'')$$

$$+ \frac{K_{x\phi}}{R^2}(v'' - w^{''\cdot}) - \frac{K_{\phi}}{R^2}(w^{\cdot} + w^{\cdot\cdot\cdot}) - \frac{K_{\nu}}{R^2} w^{''\cdot} - \frac{2K_{x\phi}}{R^2}(w^{''\cdot} - v'') + p_{\phi}R^2 = 0$$

or

$$\boxed{(D_{x\phi} + D_{\nu})u^{'\cdot} + D_{\phi}v^{\cdot\cdot} + D_{x\phi}v'' + \frac{1}{R^2}\left[3K_{x\phi}(v'' - w^{''\cdot}) - \frac{K_{\nu}}{R^2} w^{''\cdot}\right] + p_{\phi}R^2 = 0} \qquad (E.20)$$

$$M_{\phi}^{\cdot\cdot} + M'_{x\phi} + M'_{\phi x} + M''_{x} + RN_{\phi} - p_r R^2 = 0 \text{ (3rd equilibrium eqn)} \qquad (E.3)$$

$$M_{\phi}^{\cdot\cdot} = \frac{K_{\phi}}{R^2}(w^{\cdot\cdot} + w^{\cdot\cdot\cdot\cdot}) + \frac{K_{\nu}}{R^2} w^{''\cdot\cdot}$$

$$M'^{\cdot}_{x\phi} = \frac{2K_{x\phi}}{R^2}(w^{''\cdot\cdot} - v^{''\cdot})$$

$$M'^{\cdot}_{\phi x} = \frac{K_{x\phi}}{R^2}(2w^{''\cdot\cdot} + u^{'\cdot\cdot} - v^{'''\cdot})$$

$$M''_{x} = \frac{K_{x}}{R^2}(w'''' - u''') + \frac{K_{\nu}}{R^2}(w^{''\cdot\cdot} - v^{''\cdot})$$

Substituting and re-arranging:

$$D_{\phi}(v^{\cdot} + w) + D_{\nu}u' + \frac{K_{\phi}}{R^2}(w + w^{\cdot\cdot}) + \frac{K_{\phi}}{R^2}(w^{\cdot\cdot} + w^{\cdot\cdot\cdot\cdot})$$

$$+ \frac{K_{\nu}}{R^2} w^{''\cdot\cdot} + \frac{2K_{x\phi}}{R^2}(w^{''\cdot\cdot} - v^{'''\cdot}) + \frac{K_{x\phi}}{R^2}(2w^{''\cdot\cdot} + u^{'\cdot\cdot} - v^{''\cdot})$$

$$+ \frac{K_{x}}{R^2}(w'''' - u''') + \frac{K_{\nu}}{R^2}(w^{''\cdot\cdot} - v^{'''\cdot}) - p_r R^2 = 0$$

or

$$D_\phi(v\cdot + w) + D_\nu u' + \frac{1}{R^2}\left[K_{x\phi}u'\cdot\cdot - K_x u''' - (3K_{x\phi} + K_\nu)v''\cdot + K_x w'''' + (4K_{x\phi} + 2K_\nu)\, w''\cdot\cdot + K_\phi w\cdot\cdot\cdot\cdot + 2K_\phi w\cdot\cdot + K_\phi w\right] - p_r R^2 = 0 \tag{E.21}$$

E.2 Approximate differential equations

Greatly simplified governing differential equations can be formed if the 2nd equilibrium equation, presented earlier, is modified to eliminate the effect of transverse shear Q_ϕ. The force-displacement relationships can also be reduced if higher order terms of t/R are neglected.

$$N_x' + N_{\phi x}\cdot + p_x R = 0 \tag{E.22}$$

$$RN_\phi\cdot + RN_{x\phi}' + p_\phi R^2 = 0 \tag{E.23}$$

$$M_\phi\cdot\cdot + M_x'' + 2M_{x\phi}'\cdot + RN_\phi - p_r R^2 = 0 \tag{E.24}$$

Force-displacement relationships:

$$N_\phi = \frac{D_\phi}{R}(v\cdot + w) + \frac{D_\nu}{R}u' \tag{E.25}$$

$$N_x = \frac{D_x}{R}u' + D_\nu(v\cdot + w) \tag{E.26}$$

$$N_{x\phi} = N_{\phi x} = \frac{D_{x\phi}}{R}(u\cdot + v') \tag{E.27}$$

$$M_\phi = \frac{K_\phi}{R^2}w\cdot\cdot + \frac{K_\nu}{R^2}w'' \tag{E.28}$$

$$M_x = \frac{K_x}{R^2}w'' + \frac{K_\nu}{R^2}w\cdot\cdot \tag{E.29}$$

$$M_{x\phi} = M_{\phi x} = \frac{2K_{x\phi}}{R^2}w'\cdot \tag{E.30}$$

Substituting these force displacement relationships and their derivatives into the equilibrium equation as before:

$$N_x' + N_{x\phi}^{\cdot} + p_x R = 0 \quad \text{(1st equilibrium equation)} \qquad \text{(E.22)}$$

Substituting

$$\frac{D_x}{R} u'' + \frac{D_\nu}{R} (v'^{\cdot} + w') + \frac{D_{x\phi}}{R} (u^{\cdot\cdot} + v'^{\cdot}) + p_x R = 0$$

or
$$\boxed{D_x u'' + D_{x\phi} u^{\cdot\cdot} + (D_{x\phi} + D_u)\, v'^{\cdot} + D_\nu w' + p_x R^2 = 0} \qquad \text{(E.31)}$$

$$RN_\phi^{\cdot} + N_x' + p_\phi R^2 = 0 \quad \text{(2nd equilibrium equation)} \qquad \text{(E.23)}$$

Substituting

$$D_\phi (v^{\cdot\cdot} + w^{\cdot}) + D_\nu u'^{\cdot} + D_{x\phi} (u'^{\cdot} + v'') + p_\phi R^2 = 0$$

or
$$\boxed{(D_\nu + D_{x\phi})\, u'^{\cdot} + D_\phi v^{\cdot\cdot} + D_{x\phi} v'' + D_\phi w^{\cdot} + p_\phi R^2 = 0} \qquad \text{(E.32)}$$

$$M_\phi^{\cdot\cdot} + M_x'' + 2M_{x\phi}'^{\cdot} + RN_\phi - p_r R^2 = 0 \quad \text{(3rd equilibrium equation)} \qquad \text{(E.24)}$$

Substituting

$$\frac{K_\phi}{R^2} w^{\cdot\cdot\cdot\cdot} + \frac{K_\nu}{R^2} w''^{\cdot\cdot} + \frac{K_x}{R^2} w'''' + \frac{K_\nu}{R^2} w''^{\cdot\cdot} + \frac{4K_{x\phi}}{R^2} w''^{\cdot\cdot}$$

$$+ D_\phi (v^{\cdot} + w) + D_\nu u' - p_r R^2 = 0$$

or
$$\boxed{D_\nu u' + D_\phi (v^{\cdot} + w) + \frac{1}{R^2}\left[K_x w'''' + (2K_\nu + 4K_{x\phi}) w''^{\cdot\cdot} + K_\phi w^{\cdot\cdot\cdot\cdot}\right] - p_r R^2 = 0} \qquad \text{(E.33)}$$

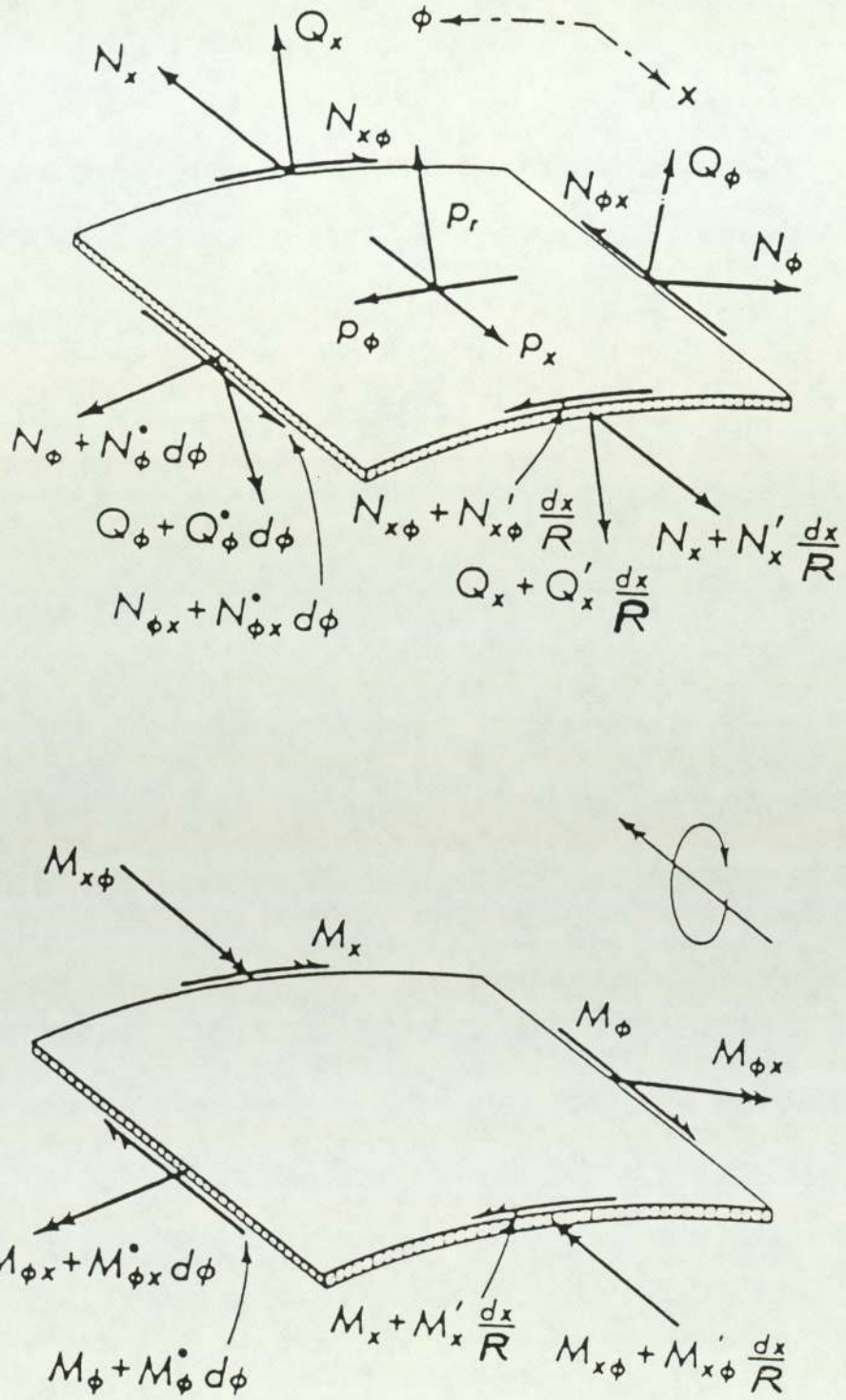

Fig. E.1 Forces and moments on a cylindrical shell element.
Forces (above) and moments (below) shown separately for clarity.

APPENDIX F FORTRAN PROGRAMS FOR GALERKIN SOLUTION

C
C Fully Clamped Case
C
C

```
      IMPLICIT REAL(L),INTEGER(X,Y,F)
      DIMENSION A(300,300),VV(300),V(300),B1(300),B2(300)
      DIMENSION AA(300,300),WKS1(300),WKS2(300)
      DIMENSION BNX(125),BNY(125),BNXY(125),BMX(125),BMY(125),BMXY(125)
      DIMENSION BQX(125),BQY(125),BW(125),BU(125),BV(125)
      DIMENSION SXDR(125),SYDR(125),SXBN(125),SYBN(125)
      CALL CREV('STAERR','STATUS',1,1,1,'LOCAL')
      CALL SCLCMD('DETF $LOCAL.TAPE199 STATUS=STAERR')
      CALL SCLCMD('ATTF $USER.TAPE199')
      OPEN (UNIT=101,FILE='$INPUT')
      OPEN (UNIT=102,FILE='$OUTPUT')
      OPEN (UNIT=198,FILE='RSLTORT')
    1 READ(199,FMT=*) NDATAIP,NDATAOP,NDATTOP,NOPTOP,NOPTIP,NCOEFOP,NSOL
     CNOP,NRSLTOP
      WRITE(NDATTOP,4)
      WRITE(NDATTOP,FMT=*)'DATA INPUT-TYPE 1 NO. AT A TIME AS REQUESTED'
      WRITE(NDATTOP,FMT=*) '**********'
      WRITE(NDATTOP,300)
  300 FORMAT(//)
  301 FORMAT(/)
      WRITE(NDATTOP,FMT=*) 'NU-X (POISSON RATIO IN X-DIRECTION)'
      READ(NDATAIP,FMT=*) VX
      WRITE(NDATTOP,301)
      WRITE(NDATTOP,FMT=*) 'NU-Y (POISSON RATIO IN Y-DIRECTION)'
      READ(NDATAIP,FMT=*) VY
      WRITE(NDATTOP,301)
      WRITE(NDATTOP,FMT=*) 'ALPHA (SEMI-CENTRAL ANGLE IN DEGREES)'
      READ(NDATAIP,FMT=*) ALPHA
      WRITE(NDATTOP,301)
      WRITE(NDATTOP,FMT=*) 'R/L (RADIUS TO HALF THE LENGTH RATIO)'
      READ(NDATAIP,FMT=*) RQL
      WRITE(NDATTOP,301)
      WRITE(NDATTOP,FMT=*) 'R/H (RADIUS TO HALF THE THICKNESS RATIO)'
      READ(NDATAIP,FMT=*) RQH
      WRITE(NDATTOP,301)
      WRITE(NDATTOP,FMT=*) 'EX/EY (ELASTICITY MODULI RATIO)'
      READ(NDATAIP,FMT=*) EQ
      WRITE(NDATTOP,301)
      WRITE(NDATTOP,FMT=*) 'G/EX (SHEAR TO ELASTICITY MODULI RATIO)'
      READ(NDATAIP,FMT=*) GQ
      WRITE(NDATTOP,301)
      WRITE(NDATTOP,FMT=*) 'K (NUMBER OF TERMS, MAX.=10)'
      READ(NDATAIP,FMT=*) K
      WRITE(NDATTOP,300)
      WRITE(NDATTOP,FMT=*) 'LOWER LIMIT OF YBAR'
      READ(NDATAIP,FMT=*) BYMN
      WRITE(NDATTOP,FMT=*) 'UPPER LIMIT OF YBAR'
      READ(NDATAIP,FMT=*) BYMX
      WRITE(NDATTOP,FMT=*) 'STEP SIZE FOR YBAR'
      READ(NDATAIP,FMT=*) DY
      WRITE(NDATTOP,301)
      WRITE(NDATTOP,FMT=*) 'LOWER LIMIT OF XBAR'
      READ(NDATAIP,FMT=*) BXMN
      WRITE(NDATTOP,FMT=*) 'UPPER LIMIT OF XBAR'
      READ(NDATAIP,FMT=*) BXMX
      WRITE(NDATTOP,FMT=*) 'STEP SIZE FOR XBAR'

      READ(NDATAIP,FMT=*) DX
      WRITE(NDATTOP,300)
      WRITE(NDATAOP,4)
    4 FORMAT(//////////,' TITLE: ANALYSIS OF AN ALLROUND CLAMPED CIRCULAR
     C CYLINDRICAL SHELL (ORTHOTROPIC)',/,' -----',/////)
      WRITE(NDATAOP,5) VX,VY,ALPHA,RQL,RQH,EQ,GQ
    5 FORMAT('DATA',/,'****',///,' NU-X  (POISSON RATIO IN X-DIRECTION)',
     C17X,'=',F8.3,/,' NU-Y  (POISSON RATIO IN Y-DIRECTION)',17X,'=',F8.
     C3,/,' ALPHA (SEMI-CENTRAL ANGLE)',27X,'=',F8.3,' DEGREES',/,' R/L
     C  (RADIUS TO HALF THE LENGTH RATIO)',14X,'=',F8.3,/,' R/H   (RADIU
     CS TO HALF THE THICKNESS RATIO)',11X,'=',F8.3,/,' EX/EY (RATIO OF E
     CLASTICITY MODULI IN X AND Y DIRNS.) =',F8.3,/,' G/EX  (RATIO OF SH
     CEAR TO ELASTICITY(X) MODULI)',7X,'=',F8.3)
      CONTINUE
   11 WRITE(NDATAOP,12) K
   12 FORMAT(' K     (NUMBER OF TERMS)',30X,'=',I4,/)
      IF (K.LE.10) GO TO 17
      WRITE(NDATAOP,FMT=*) '10 TERMS MAXIMUM ON THIS VERSION AT PRESENT'
      K=10
      GO TO 11
```

```
   17 PI=3.1415926536
      PI2=PI*PI
      PI4=PI2*PI2
      AL=ALPHA*PI/180.0
   18 SNAL=SIN(AL)
      CSAL=COS(AL)
      AL2=AL*AL
      AL4=AL2*AL2
      K2=K*K
   19 RQL2=RQL*RQL
      RQL4=RQL2*RQL2
      HQR2=1/(RQH*RQH)
      HQL2=RQL2*HQR2
      GV=GQ*(1-VX*VY)
      GEV=GV*EQ
C
C
C
   20 X=1
   21 DO 85 M=1,K
   22 M1=2*M-1
      M2=M*M
      M4=M2*M2
      M12=M1*M1
      M14=M12*M12
   23 LM=2.365C4
      IF (M.GT.1) LM=0.25*(4*M-1)*PI
   24 LM2=LM*LM
      LM4=LM2*LM2
      THLM=TANH(LM)
   25 DO 84 N=1,K
   26 N1=2*N-1
      N2=N*N
      N4=N2*N2
      N12=N1*N1
      N14=N12*N12
   27 LN=2.365C4
      IF (N.GT.1) LN=0.25*(4*N-1)*PI
   28 LN2=LN*LN
      LN4=LN2*LN2
      THLN=TANH(LN)
   29 NGMN=(-1)**(M+N)
   30 Y=1
   31 DO 81 I=1,K
   32 I1=2*I-1
      I2=I*I
      I4=I2*I2
      I12=I1*I1
      I14=I12*I12
   33 LI=2.365C4
      IF (I.GT.1) LI=0.25*(4*I-1)*PI
   34 LI2=LI*LI
      LI4=LI2*LI2
      THLI=TANH(LI)
   35 DO 80 J=1,K
   36 J1=2*J-1
      J2=J*J
      J4=J2*J2
      J12=J1*J1
      J14=J12*J12
   37 LJ=2.365C4
      IF (J.GT.1) LJ=0.25*(4*J-1)*PI
   38 LJ2=LJ*LJ
      LJ4=LJ2*LJ2
      THLJ=TANH(LJ)
   39 NGIJ=(-1)**(I+J)
      NGMNIJ=(-1)**(M+N+I+J)
C
  391 A(X,Y)=B1(X)=B2(X)=999.999999
C
C
   40 IF(X-K2)41,41,52
   41 IF(Y-K2)42,42,45
   42 IF (M.EQ.I.AND.N.EQ.J) GO TO 44
   43 A(X,Y)=0.0
      GO TO 79
   44 A(X,Y)=-PI2*(0.25*GV*N12+RQL2*AL2*M2)
      GO TO 79
   45 IF (Y-2*K2)46,46,48
   46 TOP=-16*(GV+VX)*RQL2*AL2*I1*J*NGMNIJ*M*N1
   47 A(X,Y)=TOP/((4*M2-I12)*(4*J2-N12))
      GO TO 79
```

```
   48 IF (Y-3*K2)49,49,51
   49 TOP=128*PI2*VX*RQL2*AL2*LI*LI2*LJ2*NGMN*M*N1*THLI
   50 A(X,Y)=TOP/((M4*PI4-LI4)*(N14*PI4-16*LJ4))
      GO TO 79
   51 B1(X)=B2(X)=0.0
      GO TO 83
   52 IF (X-2*K2)53,53,65
   53 IF (Y-K2)54,54,56
   54 TOP=-16*(GEV+VY)*I*J1*NGMNIJ*N*M1
   55 A(X,Y)=TOP/((4*I2-M12)*(4*N2-J12))
      GO TO 79
   56 IF (Y-2*K2)57,57,60
   57 IF (M.EQ.I.AND.N.EQ.J) GO TO 59
   58 A(X,Y)=0.0
      GO TO 79
   59 A(X,Y)=-PI2*(0.25*GEV*M12*RQL2*AL2+N2)
      GO TO 79
   60 IF (Y-3*K2)61,61,63
   61 TOP=128*PI2*LI2*LJ2*LJ*NGMN*N*M1*THLJ
   62 A(X,Y)=TOP/((M14*PI4-16*LI4)*(N4*PI4-LJ4))
      GO TO 79
   63 B1(X)=8*NGMN*N*AL*SNAL/(M1*(AL2-N2*PI2))
   64 B2(X)=0.0
      GO TO 83
   65 IF (Y-K2)66,66,68
   66 TOP=32*PI2*VY*NGIJ*LM*LM2*LN2*I*J1*THLM
   67 A(X,Y)=TOP/((LM4-I4*PI4)*(J14*PI4-16*LN4))
      GO TO 79
   68 IF (Y-2*K2)69,69,71
   69 TOP=32*PI2*NGIJ*LM2*LN2*LN*J*I1*THLN
   70 A(X,Y)=TOP/((I14*PI4-16*LM4)*(LN4-J4*PI4))
      GO TO 79
   71 IF (Y-3*K2)72,72,77
   72 IF (M.EQ.I.AND.N.EQ.J) GO TO 75
   73 TOP=32*HQL2*LM2*LN2*LI2*LJ2*(LM*THLM-LI*THLI)*(LN*THLN-LJ*THLJ)
      TOP=TOP*(VY+2*GEV)
      BOT=3*AL2*(LM4-LI4)*(LN4-LJ4)
      IF (BOT)74,741,74
   74 A(X,Y)=TOP/BOT
      GO TO 79
  741 A(X,Y)=0.0
      GO TO 79
   75 C=2*HQL2*LM*LN*THLM*THLN*(1-LM*THLM)*(1-LN*THLN)/(3*AL2)
      C=C*(VY+2*GEV)
   76 A(X,Y)=C+1.0+HQR2*(RQL4*EQ*LM4+LN4/AL4)/3
      GO TO 79
   77 B1(X)=4*LN2*THLM*(LN*CSAL*THLN+AL*SNAL)/(LM*(AL4-LN4))
   78 B2(X)=4*THLM*TAN(LN)/(LM*LN)
      GO TO 83
C
C
C
   79 Y=Y+1
   80 CONTINUE
   81 CONTINUE
   82 IF (Y-3*K2)31,31,391
   83 X=X+1
   84 CONTINUE
   85 CONTINUE
   86 IF (X-3*K2)21,21,87
   87 CONTINUE
   88 WRITE(NOPTOP,FMT=*) 'IS PRINTOUT OF CO-EFFICIENT MATRIX REQUIRED?'
   89 WRITE(NOPTOP,FMT=*) 'TYPE -1 FOR NO, 1 FOR YES'
   90 READ(NOPTIP,FMT=*) FOPT1
   91 IF (FOPT1)104,92,92
   92 DO 103 X=1,3*K2
   93 WRITE(NCOEFOP,94) X
   94 FORMAT(///,'CO-EFFICIENT MATRIX*ROW',I3,/)
   95 DO 98 Y=1,3*K2
   96 WRITE(NCOEFOP,97) A(X,Y)
   97 FORMAT(F16.6)
   98 CONTINUE
   99 WRITE(NCOEFOP,100) B1(X)
  100 FORMAT(/,F16.6,'  R.H.S.CASE 1 -DEAD LOAD')
  101 WRITE(NCOEFOP,102) B2(X)
  102 FORMAT(F16.6,'  R.H.S.CASE 2 -PRESSURE LOAD')
  103 CONTINUE
  104 WRITE(NOPTOP,300)
  105 WRITE(NOPTOP,FMT=*)'IS RUN TO BE FOR DEAD,PRESSURE LOAD OR BOTH?'
  106 WRITE(NOPTOP,FMT=*)'TYPE 1 FOR DEAD, 2 FOR PRESSURE, 3 FOR BOTH'
  107 READ(NOPTIP,FMT=*) FOPT2
      WRITE(NOPTOP,300)
```

```
  108 IF (FOPT2-2)109,110,111
  109 F1=F2=1
      GO TO 116
  110 F1=F2=2
      GO TO 116
  111 F1=1
      F2=2
C
C
C
  116 DO 232 NCASE=F1,F2
  122 IF (NCASE-1)123,123,127
  123 DO 125 X=1,3*K2
  124 VV(X)=B1(X)
  125 CONTINUE
  126 GO TO 130
  127 DO 129 X=1,3*K2
  128 VV(X)=B2(X)
  129 CONTINUE
C
C
C
  130 KK=3*K2
      IA=IAA=300
      JJ=0
      CALL F04ATF(A,IA,VV,KK,V,AA,IAA,WKS1,WKS2,JJ)
  321 IF (NCASE-1)322,322,325
  322 WRITE(NOPTOP,FMT=*)'IS PRINTOUT OF THE SIMULT.EQN. SOLUTION WITH'
  323 WRITE(NOPTOP,FMT=*)'RESIDUALS REQUIRED FOR THE DEAD LOAD, CASE 1?'
  324 GO TO 327
  325 WRITE(NOPTOP,FMT=*)'IS PRINTOUT OF THE SIMULT.EQN. SOLUTION WITH'
  326 WRITE(NOPTOP,FMT=*)'RESIDUALS REQUIRED FOR PRESSURE LOAD, CASE 2?'
  327 WRITE(NOPTOP,FMT=*)'TYPE -1 FOR NO, 1 FOR YES'
  328 READ(NOPTIP,FMT=*) FOPT3
      WRITE(NOPTOP,300)
  329 IF (FOPT3)343,343,330
  330 WRITE(NSOLNOP,331) NCASE
  331 FORMAT(////////,6X,'SOLUTION VECTOR  RESIDUALS VECTOR -CASE',I2)
  332 DO 342 X=1,3*K2
  333 SUM=0.0
  334 DO 336 Y=1,3*K2
  335 SUM=SUM+A(X,Y)*V(Y)
  336 CONTINUE
  337 IF (NCASE-1)338,338,339
  338 RESD=SUM-B1(X)
      GO TO 340
  339 RESD=SUM-B2(X)
  340 WRITE(NSOLNOP,341) X,V(X),RESD
  341 FORMAT('ROW',I3,2(F16.6))
  342 CONTINUE
  343 IF (JJ.EQ.1) WRITE(NSOLNOP,344)
  344 FORMAT(///,'EQUATIONS WERE SINGULAR',//)
C
C
C
C
  138 DO 141 J=1,125
  139 BNX(J)=BNY(J)=BNXY(J)=BMX(J)=BMY(J)=BMXY(J)=0.0
  140 BQX(J)=BQY(J)=BW(J)=BU(J)=BV(J)=0.0
      SXDR(J)=SYDR(J)=SXBN(J)=SYBN(J)=0.0
  141 CONTINUE
  142 J=1
  143 DO 187 BY=BYMN,BYMX,DY
  144 DO 186 BX=BXMN,BXMX,DX
  145 I=1
  146 DO 184 M=1,K
  147 IF (M.EQ.1) LM=2.36504
  148 IF (M.GT.1) LM=0.25*(4*M-1)*PI
  149 LM2=LM*LM
      LM3=LM*LM2
  150 CHLMX=COSH(LM*BX)
      CHLM=COSH(LM)
      CSLMX=COS(LM*BX)
      CSLM=COS(LM)
  151 SHLMX=SINH(LM*BX)
      SNLMX=SIN(LM*BX)
  152 CSMX=COS(M*PI*BX)
      CSM1X=COS((M-0.5)*PI*BX)
  153 SNMX=SIN(M*PI*BX)
      SNM1X=SIN((M-0.5)*PI*BX)
  154 DO 183 N=1,K
  155 IF (N.EQ.1) LN=2.36504
  156 IF (N.GT.1) LN=0.25*(4*N-1)*PI
```

```
  157 LN2=LN*LN
      LN3=LN*LN2
  158 CHLNY=COSH(LN*BY)
      CHLN=COSH(LN)
      CSLNY=COS(LN*BY)
      CSLN=COS(LN)
  159 SHLNY=SINH(LN*BY)
      SNLNY=SIN(LN*BY)
  160 CSNY=COS(N*PI*BY)
      CSN1Y=COS((N-0.5)*PI*BY)
  161 SNNY=SIN(N*PI*BY)
      SNN1Y=SIN((N-0.5)*PI*BY)
  162 Q1=CHLMX/CHLM
      Q2=CSLMX/CSLM
      Q3=SHLMX/CHLM
      Q4=SNLMX/CSLM
  163 Q5=CHLNY/CHLN
      Q6=CSLNY/CSLN
      Q7=SHLNY/CHLN
      Q8=SNLNY/CSLN
  164 P1=(Q1-Q2)*(Q5-Q6)
      P2=(Q1+Q2)*(Q5-Q6)
      P3=(Q1-Q2)*(Q5+Q6)
  165 P4=(Q3+Q4)*(Q7+Q8)
      P5=(Q3-Q4)*(Q5-Q6)
      P6=(Q3+Q4)*(Q5+Q6)
  166 P7=(Q1-Q2)*(Q7-Q8)
      P8=(Q1+Q2)*(Q7+Q8)
  167 DBNX=EQ*V(I)*M*PI*CSMX*CSN1Y
      DBNX=DBNX+VY*V(I+K2)*N*PI*CSM1X*CSNY+VY*V(I+2*K2)*P1
  168 DBNY=VY*V(I)*M*PI*CSMX*CSN1Y+V(I+K2)*N*PI*CSM1X*CSNY+V(I+2*K2)*P1
  169 DBNXY=V(I)*(N-0.5)*PI*SNMX*SNN1Y/(RQL*AL)
  170 DBNXY=DBNXY+RQL*AL*V(I+K2)*(M-0.5)*PI*SNM1X*SNNY
  171 DBMX=V(I+2*K2)*(RQL2*LM2*P2*EQ+VY/AL2*LN2*P3)
  172 DBMY=V(I+2*K2)*(LN2/AL2*P3+VY*RQL2*LM2*P2)
  173 DBMXY=V(I+2*K2)*LM*LN*P4
  174 DBQX=RQL*HQL2*EQ*LM3*P5+(VY+2*GEV)*HQL2/(RQL*AL2)*LM*LN2*P6
      DBQX=DBQX*V(I+2*K2)
  175 DBQY=V(I+2*K2)*(HQR2/(AL*AL2)*LN3*P7+(VY+2*GEV)*HQL2/AL*LM2*LN*P8)
  176 DBW=V(I+2*K2)*P1
      DBU=V(I)*SNMX*CSN1Y
      DBV=V(I+K2)*CSM1X*SNNY
  177 BNX(J)=BNX(J)+DBNX
      BNY(J)=BNY(J)+DBNY
      BNXY(J)=BNXY(J)-GEV*DBNXY
  178 BMX(J)=BMX(J)+HQR2/3*DBMX
      BMY(J)=BMY(J)+HQR2/3*DBMY
  179 BMXY(J)=BMXY(J)+2*GEV*HQR2/3*RQL/AL*DBMXY
  180 BQX(J)=BQX(J)+DBQX/3
      BQY(J)=BQY(J)+DBQY/3
  181 BW(J)=BW(J)+RQH*(1-VX*VY)*DBW/2
      BU(J)=BU(J)+RQH*(1-VX*VY)*DBU/(2*RQL)
      BV(J)=BV(J)+RQH*AL*(1-VX*VY)*DBV/2
  182 I=I+1
  183 CONTINUE
  184 CONTINUE
      SXDR(J)=BNX(J)*RQH/2
      SYDR(J)=BNY(J)*RQH/2
      SXBN(J)=BMX(J)*3/(2*HQR2)
      SYBN(J)=BMY(J)*3/(2*HQR2)
  185 J=J+1
  186 CONTINUE
  187 CONTINUE
C
  350 IF (NCASE-1)351,351,353
  351 WRITE(NOPTOP,FMT=*)'IS PRINTOUT OF RESULTS FOR THE DEAD LOAD CASE'
  352 GO TO 354
  353 WRITE(NOPTOP,FMT=*)'IS PRINTOUT OF RESULTS FOR PRESSURE LOAD CASE'
  354 WRITE(NOPTOP,FMT=*)'REQUIRED IN THE FORM OF STRESS RESULTANTS AND'
  355 WRITE(NOPTOP,FMT=*)'DISPLACEMENTS OR STRESSES AND RADIAL'
      WRITE(NOPTOP,FMT=*)'DISPLACEMENT OR BOTH?'
  356 WRITE(NOPTOP,FMT=*)'TYPE 1 FOR STRESS RESULTANTS AND DISPLACEMENT'
  357 WRITE(NOPTOP,FMT=*)'TYPE 2 FOR STRESSES AND RADIAL DISPLACEMENT'
  358 WRITE(NOPTOP,FMT=*)'TYPE 3 FOR BOTH'
  360 READ(NOPTIP,FMT=*) FOPT4
      WRITE(NOPTOP,300)
  361 IF (FOPT4-2)188,215,188
C
  188 FLAG=-1
  189 IF (NCASE-1)1891,1891,1892
 1891 WRITE(NRSLTOP,1893)
      GO TO 1895
```

```
1892 WRITE(NRSLTOP,1894)
1893 FORMAT(///,'CASE 1 - DEAD LOAD',//,'******')
1894 FORMAT(///,'CASE 2 - PRESSURE LOAD',//,'******')
1895 IF (FLAG)1896,1896,1898
1896 WRITE(NRSLTOP,1897)
      GO TO 191
1897 FORMAT(//,4X,'_',6X,'_',9X,'_',13X,'_',13X,'_')
1898 WRITE(NRSLTOP,190)
 190 FORMAT(//,4X,'_',6X,'_',9X,'_',13X,'_',13X,'_',13X,'_',13X,'_')
 191 IF (FLAG)192,193,194
 192 WRITE(NRSLTOP,195)
     GO TO 198
 193 WRITE(NRSLTOP,196)
     GO TO 198
 194 WRITE(NRSLTOP,197)
     GO TO 198
 195 FORMAT(4X,'Y',6X,'X',9X,'NX',12X,'NY',12X,'NXY',/)
 196 FORMAT(4X,'Y',6X,'X',9X,'MX',12X,'MY',12X,'MXY',/)
 197 FORMAT(4X,'Y',6X,'X',9X,'QX',12X,'QY',12X,'W',13X,'U',13X,'V',/)
 198 I=1
 199 DO 208 BY=BYMN,BYMX,DY
 200 DO 207 BX=BXMN,BXMX,DX
 201 IF (FLAG)202,203,204
 202 WRITE(NRSLTOP,205) BY,BX,BNX(I),BNY(I),BNXY(I)
     GO TO 206
 203 WRITE(NRSLTOP,205) BY,BX,BMX(I),BMY(I),BMXY(I)
     GO TO 206
 204 WRITE(NRSLTOP,212) BY,BX,BQX(I),BQY(I),BW(I),BU(I),BV(I)
 205 FORMAT(2(F7.2),3(F14.6))
 206 I=I+1
 207 CONTINUE
     WRITE(NRSLTOP,301)
 208 CONTINUE
 209 FLAG=FLAG+1
 210 IF (FLAG-1)189,189,211
 211 CONTINUE
 212 FORMAT(2(F7.2),5(F14.6))
 213 WRITE(NRSLTOP,214)
 214 FORMAT(//,'NOTE: FORCES',8X,'ARE NON-DIMENSIONAL WITH RESPECT TO (
    CPR)',/,6X,'MOMENTS',7X,'ARE NON-DIMENSIONAL WITH RESPECT TO (PR.R)
    C',/,6X,'DISPLACEMENTS ARE NON-DIMENSIONAL WITH RESPECT TO (EY/PR)'
    C,///,6X,'_',9X,'_',/,6X,'X=X/L AND Y=PHI/ALPHA, P - INTENSITY OF LO
    CAD')
      IF (FOPT4-2)232,232,215
 215 IF (NCASE-1)216,216,217
 216 WRITE(NRSLTOP,1893)
     GO TO 218
 217 WRITE(NRSLTOP,1894)
 218 WRITE(NRSLTOP,219)
 219 FORMAT(//,4X,'_',6X,'_',65X,'-')
 220 WRITE(NRSLTOP,221)
 221 FORMAT(4X,'Y',6X,'X',6X,'SX(DIRECT)    SY(DIRECT)    SX(BENDING)
    C SY(BENDING)',6X,'W',/)
 222 I=1
 223 DO 229 BY=BYMN,BYMX,DY
 224 DO 228 BX=BXMN,BXMX,DX
 225 WRITE(NRSLTOP,226) BY,BX,SXDR(I),SYDR(I),SXBN(I),SYBN(I),BW(I)
 226 FORMAT(2(F7.2),5(F14.6))
 227 I=I+1
 228 CONTINUE
     WRITE(NRSLTOP,301)
 229 CONTINUE
 230 WRITE(NRSLTOP,231)
 231 FORMAT(//,'NOTE: THE STRESSES ARE NON-DIMENSIONAL WITH RESPECT TO
    CTHE LOAD',/,6X,'SX(DIRECT)=(SX/P) ETC. WBAR=(EY.W/PR)',//,6X,'_',9
    CX,'_',/,6X,'X=X/L AND Y=PHI/ALPHA, P - INTENSITY OF LOAD',//,6X,'P
    COSITIVE STRESS - TENSILE,  NEGATIVE STRESS - COMPRESSIVE,  BENDING
    C STRESS IS AT INNER SURFACE (R-H)')
 232 CONTINUE
 233 WRITE(NOPTOP,234)
 234 FORMAT(//,' THE RESULTS ARE STORED IN A FILE CALLED RSLTORT',//,' T
    CO PRINT THEM TYPE THE FOLLOWING COMMAND IN RESPONSE TO THE PROMPT'
    C,//,' PRIF RSLTORT',//,' NOTE: WHEN THE PROGRAM IS RUN AGAIN WITH
    CNEW DATA THE EXISTING RESULTS',/,7X,'IN FILE RSLTORT ARE OVERWRITT
    CEN BY THE NEW ONES GENERATED SO IT IS',/,7X,'NECESSARY TO ENSURE T
    CHAT THE ABOVE COMMAND IS GIVEN TO SEND THE',/,7X,'RESULTS TO THE L
    CINE PRINTER BEFORE ANOTHER RUN IS INITIATED')
 235 CALL DELV('STAERR')
 236 CLOSE (UNIT=198,STATUS='KEEP')
 237 CALL SCLCMD('COPF $LOCAL.RSLTORT $USER.RSLTORT')
 238 END
```

Hinged Case (membrane clamped)

```
C
C
C
      IMPLICIT REAL(L),INTEGER(X,Y,F)
      DIMENSION A(300,300),VV(300),V(300),B1(300),B2(300)
      DIMENSION AA(300,300),WKS1(300),WKS2(300)
      DIMENSION BNX(125),BNY(125),BNXY(125),BMX(125),BMY(125),BMXY(125)
      DIMENSION BQX(125),BQY(125),BW(125),BU(125),BV(125)
      DIMENSION SXDR(125),SYDR(125),SXBN(125),SYBN(125)
      CALL CREV('STAERR','STATUS',1,1,1,'LOCAL')
      CALL SCLCMD('DETF $LOCAL.TAPE199 STATUS=STAERR')
      CALL SCLCMD('ATTF $USER.TAPE199')
      OPEN (UNIT=101,FILE='$INPUT')
      OPEN (UNIT=102,FILE='$OUTPUT')
      OPEN (UNIT=198,FILE='RSLTHNG')
    1 READ(199,FMT=*) NDATAI',NDATAOP,NDATTOP,NOPTOP,NOPTIP,NCOEFOP,NSOL
     CNOP,NRSLTOP
      WRITE(NDATTOP,2222)
      WRITE(NDATTOP,FMT=*)'DATA INPUT-TYPE 1 NO. AT A TIME AS REQUESTED'
      WRITE(NDATTOP,FMT=*) '**********'
      WRITE(NDATTOP,300)
  300 FORMAT(//)
  301 FORMAT(/)
      WRITE(NDATTOP,FMT=*) 'MU (POISSON RATIO)'
      READ(NDATAIP,FMT=*) U
      WRITE(NDATTOP,301)
      WRITE(NDATTOP,FMT=*) 'ALPHA (SEMI-CENTRAL ANGLE IN DEGREES)'
      READ(NDATAIP,FMT=*) ALPHA
      WRITE(NDATTOP,301)
      WRITE(NDATTOP,FMT=*) 'R/L (RADIUS TO HALF THE LENGTH RATIO)'
      READ(NDATAIP,FMT=*) RQL
      WRITE(NDATTOP,301)
      WRITE(NDATTOP,FMT=*) 'R/H (RADIUS TO HALF THE THICKNESS RATIO)'
      READ(NDATAIP,FMT=*) RQH
      WRITE(NDATTOP,301)
      WRITE(NDATTOP,FMT=*) 'K (NUMBER OF TERMS, MAX.=10)'
      READ(NDATAIP,FMT=*) K
      WRITE(NDATTOP,300)
      WRITE(NDATTOP,FMT=*) 'LOWER LIMIT OF YBAR'
      READ(NDATAIP,FMT=*) BYMN
      WRITE(NDATTOP,FMT=*) 'UPPER LIMIT OF YBAR'
      READ(NDATAIP,FMT=*) BYMX
      WRITE(NDATTOP,FMT=*) 'STEP SIZE FOR YBAR'
      READ(NDATAIP,FMT=*) DY
      WRITE(NDATTOP,301)
      WRITE(NDATTOP,FMT=*) 'LOWER LIMIT OF XBAR'
      READ(NDATAIP,FMT=*) BXMN
      WRITE(NDATTOP,FMT=*) 'UPPER LIMIT OF XBAR'
      READ(NDATAIP,FMT=*) BXMX
      WRITE(NDATTOP,FMT=*) 'STEP SIZE FOR XBAR'
      READ(NDATAIP,FMT=*) DX
      WRITE(NDATTOP,300)
      WRITE(NDATAOP,2222)
 2222 FORMAT(//,' TITLE: ANALYSIS OF AN ALLROUND HINGED CIRCULAR CYLINDR
     CICAL SHELL (ISOTROPIC)',//,' -----',////)
    3 WRITE(NDATAOP,4) U
    4 FORMAT('DATA',/,'****',//,' MU    (POISSON RATIO)',12X,'=',F7.2)
    5 WRITE(NDATAOP,6) ALPHA
    6 FORMAT(' ALPHA (SEMI-CENTRAL ANGLE)',7X,'=',F7.2,' DEGREES')
    7 WRITE(NDATAOP,8) RQL
    8 FORMAT(' R/L   (RADIUS TO LENGTH RATIO)   =',F7.2)
    9 WRITE(NDATAOP,10) RQH
   10 FORMAT(' R/H   (RADIUS TO THICKNESS RATIO)=',F7.2)
   11 WRITE(NDATAOP,12) K
   12 FORMAT(' K     (NUMBER OF TERMS)',10X,'=',I4,/)
      IF (K.LE.10) GO TO 17
      WRITE(NDATAOP,FMT=*) '10 TERMS MAXIMUM ON THIS VERSION AT PRESENT'
      K=10
      GO TO 11
   17 PI=3.1415926536
      PI2=PI*PI
      PI4=PI2*PI2
      AL=ALPHA*PI/180.0
   18 SNAL=SIN(AL)
      CSAL=COS(AL)
      AL2=AL*AL
      AL4=AL2*AL2
      K2=K*K
   19 RQL2=RQL*RQL
      RQL4=RQL2*RQL2
      HQR2=1/(RQH*RQH)
      HQL2=RQL2*HQR2
```

```
   20 X=1
   21 DO 85 M=1,K
   22 M1=2*M-1
      M2=M*M
      M4=M2*M2
      M12=M1*M1
      M14=M12*M12
   25 DO 84 N=1,K
   26 N1=2*N-1
      N2=N*N
      N4=N2*N2
      N12=N1*N1
      N14=N12*N12
   29 NGMN=(-1)**(M+N)
   30 Y=1
   31 DO 81 I=1,K
   32 I1=2*I-1
      I2=I*I
      I4=I2*I2
      I12=I1*I1
      I14=I12*I12
   35 DO 80 J=1,K
   36 J1=2*J-1
      J2=J*J
      J4=J2*J2
      J12=J1*J1
      J14=J12*J12
   39 NGIJ=(-1)**(I+J)
      NGMNIJ=(-1)**(M+N+I+J)
      NGMI=(-1)**(M+I)
      NGNJ=(-1)**(N+J)
  391 A(X,Y)=B1(X)=B2(X)=999.999999
C
C
   40 IF(X-K2)41,41,52
   41 IF(Y-K2)42,42,45
   42 IF (M.EQ.I.AND.N.EQ.J) GO TO 44
   43 A(X,Y)=0.0
      GO TO 79
   44 A(X,Y)=PI2*(0.125*(U-1)*N12-RQL2*AL2*M2)
      GO TO 79
   45 IF (Y-2*K2)46,46,48
   46 TOP=-8*(U+1)*RQL2*AL2*I1*J*NGMNIJ*M*N1
   47 A(X,Y)=TOP/((4*M2-I12)*(4*J2-N12))
      GO TO 79
   48 IF (Y-3*K2)49,49,51
   49 IF (N.EQ.J) GO TO 50
      A(X,Y)=0.0
      GO TO 79
   50 A(X,Y)=-4*U*RQL2*AL2*I1*M*NGMI/(4*M2-I12)
      GO TO 79
   51 B1(X)=B2(X)=0.0
      GO TO 83
   52 IF (X-2*K2)53,53,65
   53 IF (Y-K2)54,54,56
   54 TOP=-8*(1+U)*I*J1*NGMNIJ*N*M1
   55 A(X,Y)=TOP/((4*I2-M12)*(4*N2-J12))
      GO TO 79
   56 IF (Y-2*K2)57,57,60
   57 IF (M.EQ.I.AND.N.EQ.J) GO TO 59
   58 A(X,Y)=0.0
      GO TO 79
   59 A(X,Y)=PI2*(0.125*(U-1)*M12*RQL2*AL2-N2)
      GO TO 79
   60 IF (Y-3*K2)61,61,63
   61 IF (M.EQ.I) GO TO 62
      A(X,Y)=0.0
      GO TO 79
   62 A(X,Y)=-4.0*J1*N*NGNJ/(4.0*N2-J12)
      GO TO 79
   63 B1(X)=0.0
   64 B2(X)=0.0
      GO TO 83
   65 IF (Y-K2)66,66,68
   66 IF (N.EQ.J) GO TO 67
      A(X,Y)=0.0
      GO TO 79
   67 A(X,Y)=4*U*I*M1*NGMI/(4*I2-M12)
      GO TO 79
   68 IF (Y-2*K2)69,69,71
   69 IF (M.EQ.I) GO TO 70
      A(X,Y)=0.0
      GO TO 79
   70 A(X,Y)=4.0*J*N1*NGNJ/(4.0*J2-N12)
      GO TO 79
```

```
   71 IF (Y-3*K2)72,72,77
   72 IF (M.EQ.I.AND.N.EQ.J) GO TO 75
   73 A(X,Y)=0.0
   74 GO TO 79
   75 A(X,Y)=1+HQR2*PI4/48*(RQL2*M12+N12/AL2)**2
   76 GO TO 79
   77 B1(X)=-16*NGMN/(M1*N1*PI2)
   78 B2(X)=-16*NGMN/(M1*N1*PI2)
      GO TO 83
   79 Y=Y+1
   80 CONTINUE
   81 CONTINUE
   82 IF (Y-3*K2)31,31,391
   83 X=X+1
   84 CONTINUE
   85 CONTINUE
   86 IF (X-3*K2)21,21,87
   87 CONTINUE
   88 WRITE(NOPTOP,FMT=*) 'IS PRINTOUT OF CO-EFFICIENT MATRIX REQUIRED?'
   89 WRITE(NOPTOP,FMT=*) 'TYPE -1 FOR NO, 1 FOR YES'
   90 READ(NOPTIP,FMT=*) FOPT1
   91 IF (FOPT1)104,92,92
   92 DO 103 X=1,3*K2
   93 WRITE(NCOEFOP,94) X
   94 FORMAT(///,'CO-EFFICIENT MATRIX*ROW',I3,/)
   95 DO 98 Y=1,3*K2
   96 WRITE(NCOEFOP,97) A(X,Y)
   97 FORMAT(F16.6)
   98 CONTINUE
   99 WRITE(NCOEFOP,100) B1(X)
  100 FORMAT(/,F16.6,'  R.H.S.')
  103 CONTINUE
  104 WRITE(NOPTOP,300)
  109 F1=F2=1
      GO TO 116
  110 F1=F2=2
      GO TO 116
  111 F1=1
      F2=2
  116 DO 232 NCASE=F1,F2
  122 IF (NCASE-1)123,123,127
  123 DO 125 X=1,3*K2
  124 VV(X)=B1(X)
  125 CONTINUE
  126 GO TO 130
  127 DO 129 X=1,3*K2
  128 VV(X)=B2(X)
  129 CONTINUE
  130 KK=3*K2
      IA=IAA=300
      JJ=0
      CALL F04ATF(A,IA,VV,KK,V,AA,IAA,WKS1,WKS2,JJ)
  321 IF (NCASE-1)322,322,325
  322 WRITE(NOPTOP,FMT=*)'IS PRINTOUT OF THE SIMULT.EQN. SOLUTION WITH'
  323 WRITE(NOPTOP,FMT=*)'RESIDUALS REQUIRED?'
  324 GO TO 327
  325 WRITE(NOPTOP,FMT=*)'IS PRINTOUT OF THE SIMULT.EQN. SOLUTION WITH'
  326 WRITE(NOPTOP,FMT=*)'RESIDUALS REQUIRED FOR PRESSURE LOAD, CASE 2?'
  327 WRITE(NOPTOP,FMT=*)'TYPE -1 FOR NO, 1 FOR YES'
  328 READ(NOPTIP,FMT=*) FOPT3
      WRITE(NOPTOP,300)
  329 IF (FOPT3)343,343,330
  330 WRITE(NSOLNOP,331)
  331 FORMAT(////////,6X,'SOLUTION VECTOR   RESIDUALS VECTOR')
  332 DO 342 X=1,3*K2
  333 SUM=0.0
  334 DO 336 Y=1,3*K2
  335 SUM=SUM+A(X,Y)*V(Y)
  336 CONTINUE
  337 IF (NCASE-1)338,338,339
  338 RESD=SUM-B1(X)
      GO TO 340
  339 RESD=SUM-B2(X)
  340 WRITE(NSOLNOP,341) X,V(X),RESD
  341 FORMAT('ROW',I3,2(F16.6))
  342 CONTINUE
  343 IF (JJ.EQ.1) WRITE(NSOLNOP,344)
  344 FORMAT(///,'EQUATIONS WERE SINGULAR',//)
C
  138 DO 141 J=1,125
  139 BNX(J)=BNY(J)=BNXY(J)=BMX(J)=BMY(J)=BMXY(J)=0.0
  140 BQX(J)=BQY(J)=BW(J)=BU(J)=BV(J)=0.0
  141 CONTINUE
```

```
  142 J=1
  143 DO 187 BY=BYMN,BYMX,DY
  144 DO 186 BX=BXMN,BXMX,DX
  145 I=1
  146 DO 184 M=1,K
  147 M1=2*M-1
      M12=M1*M1
  152 CSMX=COS(M*PI*BX)
      CSM1X=COS((M-0.5)*PI*BX)
  153 SNMX=SIN(M*PI*BX)
      SNM1X=SIN((M-0.5)*PI*BX)
  154 DO 183 N=1,K
  155 N1=2*N-1
      N12=N1*N1
  160 CSNY=COS(N*PI*BY)
      CSN1Y=COS((N-0.5)*PI*BY)
  161 SNNY=SIN(N*PI*BY)
      SNN1Y=SIN((N-0.5)*PI*BY)
C
C
  166 P1=CSM1X*CSN1Y
  167 DBNX=V(I)*M*PI*CSMX*CSN1Y+U*V(I+K2)*N*PI*CSM1X*CSNY+U*V(I+2*K2)*P1
  168 DBNY=U*V(I)*M*PI*CSMX*CSN1Y+V(I+K2)*N*PI*CSM1X*CSNY+V(I+2*K2)*P1
  169 DBNXY=V(I)*(N-0.5)*PI*SNMX*SNN1Y/(RQL*AL)
  170 DBNXY=DBNXY+RQL*AL*V(I+K2)*(M-0.5)*PI*SNM1X*SNNY
  171 DBMX=-PI2/4*V(I+2*K2)*P1*(RQL2*M12+U*N12/AL2)
  172 DBMY=-PI2/4*V(I+2*K2)*P1*(U*RQL2*M12+N12/AL2)
  173 DBMXY=PI2/4*V(I+2*K2)*M1*N1*SNM1X*SNN1Y
  176 DBW=V(I+2*K2)*P1
      DBU=V(I)*SNMX*CSN1Y
      DBV=V(I+K2)*CSM1X*SNNY
  177 BNX(J)=BNX(J)+DBNX
      BNY(J)=BNY(J)+DBNY
      BNXY(J)=BNXY(J)+0.5*(U-1)*DBNXY
  178 BMX(J)=BMX(J)+HQR2/3*DBMX
      BMY(J)=BMY(J)+HQR2/3*DBMY
  179 BMXY(J)=BMXY(J)+(1-U)*HQR2/3*RQL/AL*DBMXY
  181 BW(J)=BW(J)+RQH*(1-U*U)*DBW/2
      BU(J)=BU(J)+RQH*(1-U*U)*DBU/(2*RQL)
      BV(J)=BV(J)+RQH*AL*(1-U*U)*DBV/2
  182 I=I+1
  183 CONTINUE
  184 CONTINUE
      SXDR(J)=BNX(J)*RQH/2
      SYDR(J)=BNY(J)*RQH/2
      SXBN(J)=BMX(J)*3/(2*HQR2)
      SYBN(J)=BMY(J)*3/(2*HQR2)
  185 J=J+1
  186 CONTINUE
  187 CONTINUE
C
C
C
C
  350 IF (NCASE-1)351,351,353
  351 WRITE(NOPTOP,FMT=*)'IS PRINTOUT OF RESULTS'
  352 GO TO 354
  353 WRITE(NOPTOP,FMT=*)'IS PRINTOUT OF RESULTS FOR PRESSURE LOAD CASE'
  354 WRITE(NOPTOP,FMT=*)'REQUIRED IN THE FORM OF STRESS RESULTANTS AND'
  355 WRITE(NOPTOP,FMT=*)'DISPLACEMENTS OR STRESSES AND RADIAL'
      WRITE(NOPTOP,FMT=*)'DISPLACEMENT OR BOTH?'
  356 WRITE(NOPTOP,FMT=*)'TYPE 1 FOR STRESS RESULTANTS AND DISPLACEMENT'
  357 WRITE(NOPTOP,FMT=*)'TYPE 2 FOR STRESSES AND RADIAL DISPLACEMENT'
  358 WRITE(NOPTOP,FMT=*)'TYPE 3 FOR BOTH'
  360 READ(NOPTIP,FMT=*) FOPT4
      WRITE(NOPTOP,300)
  361 IF (FOPT4-2)188,215,188
C
  188 FLAG=-1
  189 IF (NCASE-1)1891,1891,1892
 1891 GO TO 1895
 1892 WRITE(NRSLTOP,1894)
 1893 FORMAT(///,'CASE 1 - DEAD LOAD',/,'******')
 1894 FORMAT(///,'CASE 2 - PRESSURE LOAD',/,'******')
 1895 IF (FLAG)1896,1896,1898
 1896 WRITE(NRSLTOP,1897)
      GO TO 191
 1897 FORMAT(//,4X,'_',6X,'_',9X,'_',13X,'_',13X,'_')
 1898 WRITE(NRSLTOP,1897)
  190 FORMAT(//,4X,'_',6X,'_',9X,'_',13X,'_',13X,'_',13X,'_',13X,'_')
  191 IF (FLAG)192,193,194
  192 WRITE(NRSLTOP,195)
      GO TO 198
```

```
193 WRITE(NRSLTOP,196)
    GO TO 198
194 WRITE(NRSLTOP,197)
    GO TO 198
195 FORMAT(4X,'Y',6X,'X',9X,'NX',12X,'NY',12X,'NXY',/)
196 FORMAT(4X,'Y',6X,'X',9X,'MX',12X,'MY',12X,'MXY',/)
197 FORMAT(4X,'Y',6X,'X',9X,'W',13X,'U',13X,'V',/)
198 I=1
199 DO 208 BY=BYMN,BYMX,DY
200 DO 207 BX=BXMN,BXMX,DX
201 IF (FLAG)202,203,204
202 WRITE(NRSLTOP,205) BY,BX,BNX(I),BNY(I),BNXY(I)
    GO TO 206
203 WRITE(NRSLTOP,205) BY,BX,BMX(I),BMY(I),BMXY(I)
    GO TO 206
204 WRITE(NRSLTOP,212) BY,BX,BW(I),BU(I),BV(I)
205 FORMAT(2(F7.2),3(F14.6))
206 I=I+1
207 CONTINUE
    WRITE(NRSLTOP,301)
208 CONTINUE
209 FLAG=FLAG+1
210 IF (FLAG-1)189,189,211
211 CONTINUE
212 FORMAT(2(F7.2),5(F14.6))
213 WRITE(NRSLTOP,214)
214 FORMAT(//,'NOTE: FORCES',8X,'ARE NON-DIMENSIONAL WITH RESPECT TO (
   CPR)',/,6X,'MOMENTS',7X,'ARE NON-DIMENSIONAL WITH RESPECT TO (PR.R)
   C',/,6X,'DISPLACEMENTS ARE NON-DIMENSIONAL WITH RESPECT TO (EY/PR)'
   C,//,6X,'_',9X,'_',/,6X,'X=X/L AND Y=PHI/ALPHA, P - INTENSITY OF LO
   CAD')
    IF (FOPT4-2)232,232,215
215 IF (NCASE-1)216,216,217
216 GO TO 218
217 WRITE(NRSLTOP,1894)
218 WRITE(NRSLTOP,219)
219 FORMAT(//,4X,'_',6X,'_',65X,'-')
220 WRITE(NRSLTOP,221)
221 FORMAT(4X,'Y',6X,'X',6X,'SX(DIRECT)    SY(DIRECT)    SX(BENDING)
   C SY(BENDING)',6X,'W',/)
222 I=1
223 DO 229 BY=BYMN,BYMX,DY
224 DO 228 BX=BXMN,BXMX,DX
225 WRITE(NRSLTOP,226) BY,BX,SXDR(I),SYDR(I),SXBN(I),SYBN(I),BW(I)
226 FORMAT(2(F7.2),5(F14.6))
227 I=I+1
228 CONTINUE
    WRITE(NRSLTOP,301)
229 CONTINUE
230 WRITE(NRSLTOP,231)
231 FORMAT(//,'NOTE: THE STRESSES ARE NON-DIMENSIONAL WITH RESPECT TO
   CTHE LOAD',/,6X,'SX(DIRECT)=(SX/P) ETC. WBAR=(EY.W/PR)',//,6X,'_',9
   CX,'_',/,6X,'X=X/L AND Y=PHI/ALPHA, P - INTENSITY OF LOAD',//,6X,'P
   COSITIVE STRESS - TENSILE,  NEGATIVE STRESS - COMPRESSIVE,  BENDING
   C STRESS IS AT INNER SURFACE (R-H)')
232 CONTINUE
233 WRITE(NOPTOP,234)
234 FORMAT(//,' THE RESULTS ARE STORED IN A FILE CALLED RSLTHNG',/,' T
   CO PRINT THEM TYPE THE FOLLOWING COMMAND IN RESPONSE TO THE PROMPT
   C',//,' PRIF RSLTHNG           ',//,' NOTE: WHEN THE PROGRAM IS RUN
   C AGAIN WITH NEW DATA THE EXISTING RESULTS',/,7X,'IN FILE RSLTHNG A
   CRE OVERWRITTEN BY THE NEW ONES GENERATED SO IT IS',/,7X,'NECESSARY
   C TO ENSURE THAT THE ABOVE COMMAND IS GIVEN TO SEND THE',/,7X,'RESU
   CLTS TO THE LINE PRINTER BEFORE ANOTHER RUN IS INITIATED')
235 CALL DELV('STAERR')
236 CLOSE (UNIT=198,STATUS='KEEP')


237 CALL SCLCMD('COPF $LOCAL.RSLTHNG $USER.RSLTHNG')
238 END
```

Simply Supported Case

```
C
C
C
C
      DIMENSION BNX(125),BNY(125),BNXY(125)
      DIMENSION BMX(125),BMY(125),BMXY(125),BW(125)
      DIMENSION SXDR(125),SYDR(125),SXBN(125),SYBN(125)
      CALL CREV('STAERR','STATUS',1,1,1,'LOCAL')
      CALL SCLCMD('DETF $LOCAL.TAPE299 STATUS=STAERR')
      CALL SCLCMD('ATTF $USER.TAPE299')
      OPEN (UNIT=101,FILE='$INPUT')
      OPEN (UNIT=102,FILE='$OUTPUT')
      OPEN (UNIT=298,FILE='RSLTSS')
    1 READ(299,FMT=*) NDATAIP,NDATAOP,NDATTOP,NOPTOP,NOPTIP,NRSLTOP
      WRITE(NDATTOP,4)
      WRITE(NDATTOP,FMT=*)'DATA INPUT-TYPE 1 NO. AT A TIME AS REQUESTED'
      WRITE(NDATTOP,FMT=*) '**********'
      WRITE(NDATTOP,300)
  300 FORMAT(//)
  301 FORMAT(/)
      WRITE(NDATTOP,FMT=*) 'NU-X (POISSON RATIO IN X-DIRECTION)'
      READ(NDATAIP,FMT=*) VX
      WRITE(NDATTOP,301)
      WRITE(NDATTOP,FMT=*) 'NU-Y (POISSON RATIO IN Y-DIRECTION)'
      READ(NDATAIP,FMT=*) VY
      WRITE(NDATTOP,301)
      WRITE(NDATTOP,FMT=*) 'ALPHA (SEMI-CENTRAL ANGLE IN DEGREES)'
      READ(NDATAIP,FMT=*) ALPHA
      WRITE(NDATTOP,301)
      WRITE(NDATTOP,FMT=*) 'R/L (RADIUS TO HALF THE LENGTH RATIO)'
      READ(NDATAIP,FMT=*) AQL
      WRITE(NDATTOP,301)
      WRITE(NDATTOP,FMT=*) 'R/H (RADIUS TO HALF THE THICKNESS RATIO)'
      READ(NDATAIP,FMT=*) AQH
      WRITE(NDATTOP,301)
      WRITE(NDATTOP,FMT=*) 'EX/EY (ELASTICITY MODULI RATIO)'
      READ(NDATAIP,FMT=*) EQ
      WRITE(NDATTOP,301)
      WRITE(NDATTOP,FMT=*) 'G/EX (SHEAR TO ELASTICITY MODULI RATIO)'
      READ(NDATAIP,FMT=*) GQ
      WRITE(NDATTOP,301)
      WRITE(NDATTOP,FMT=*) 'K (NUMBER OF TERMS)'
      READ(NDATAIP,FMT=*) K
      WRITE(NDATTOP,300)
      WRITE(NDATTOP,FMT=*) 'LOWER LIMIT OF YBAR'
      READ(NDATAIP,FMT=*) BYMN
      WRITE(NDATTOP,FMT=*) 'UPPER LIMIT OF YBAR'
      READ(NDATAIP,FMT=*) BYMX
      WRITE(NDATTOP,FMT=*) 'STEP SIZE FOR YBAR'
      READ(NDATAIP,FMT=*) DY
      WRITE(NDATTOP,301)
      WRITE(NDATTOP,FMT=*) 'LOWER LIMIT OF XBAR'
      READ(NDATAIP,FMT=*) BXMN
      WRITE(NDATTOP,FMT=*) 'UPPER LIMIT OF XBAR'
      READ(NDATAIP,FMT=*) BXMX
      WRITE(NDATTOP,FMT=*) 'STEP SIZE FOR XBAR'
      READ(NDATAIP,FMT=*) DX
      WRITE(NDATTOP,300)
      WRITE(NDATAOP,4)
    4 FORMAT(//,' TITLE: ANALYSIS OF AN ALLROUND SIMPLY SUPPORTED CIRCUL
     CAR CYLINDRICAL SHELL (ORTHOTROPIC)',/,' -----',/////)
      WRITE(NDATAOP,5) VX,VY,ALPHA,AQL,AQH,EQ,GQ
    5 FORMAT('DATA',/,'****',//,' NU-X  (POISSON RATIO IN X-DIRECTION)',
     C17X,'=',F8.3,/,' NU-Y  (POISSON RATIO IN Y-DIRECTION)',17X,'=',F8.
     C3,/,' ALPHA (SEMI-CENTRAL ANGLE)',27X,'=',F8.3,' DEGREES',/,' R/L
     C  (RADIUS TO HALF THE LENGTH RATIO)',14X,'=',F8.3,/,' R/H   (RADIU
     CS TO HALF THE THICKNESS RATIO)',11X,'=',F8.3,/,' EX/EY (RATIO OF E
     CLASTICITY MODULI IN X AND Y DIRNS.) =',F8.3,/,' G/EX  (RATIO OF SH
     CEAR TO ELASTICITY(X) MODULI)',7X,'=',F8.3)
      CONTINUE
      WRITE(NDATAOP,6) K
    6 FORMAT(' K      (NUMBER OF TERMS)',30X,'=',I4,/)
C
C
    9 PI=3.1415926536
      PI2=PI*PI
      PI4=PI2*PI2
      AL=ALPHA*PI/180.0
   10 AQL2=AQL*AQL
      AQH2=AQH*AQH
   11 GX=GQ*(1-VX*VY)
      GY=EQ*GX
```

```
   12 GXY=GX+1/GY-1/GX*(GX+VX)**2
      VGX=2*(VX+2*GX)
   13 A1=VGX+GXY
      A2=2/EQ+VGX*GXY
      A3=(VGX+GXY)/EQ
   14 A4=(1/EQ)**2
      A5=(1/EQ-VX*VX)*3*AQH2
C
C
C
   15 DO 18 J=1,125
   16 BNX(J)=0.0
      BNY(J)=0.0
      BNXY(J)=0.0
   17 BMX(J)=0.0
      BMY(J)=0.0
      BMXY(J)=0.0
      BW(J)=0.0
   18 CONTINUE
   19 J=1
   20 DO 50 BY=BYMN,BYMX,DY
   21 DO 49 BX=BXMN,BXMX,DX
   22 DO 47 M=1,K,2
   23 B=M*AQL
      B2=B*B
      B4=B2*B2
      B6=B2*B4
      B8=B4*B4
   24 P=B*PI/2
      P2=P*P
      P4=P2*P2
   25 CSX=COS(M*PI/2*BX)
      SNX=SIN(M*PI/2*BX)
   26 DO 46 N=1,K,2
   27 D=N/AL
      D2=D*D
      D4=D2*D2
      D6=D2*D4
      D8=D4*D4
   28 Q=D*PI/2
      Q2=Q*Q
      Q4=Q2*Q2
   29 CSY=COS(Q*AL*BY)
      SNY=SIN(Q*AL*BY)
   30 CMN=-16/(M*N*PI2)*(-1)**((M+N-2)/2)
   31 TOP=CMN*(B4+B2*D2*GXY+D4/EQ)
   32 AMN=TOP/(PI4/16*(B8+A1*B6*D2+A2*B4*D4+A3*B2*D6+A4*D8)+A5*B4)
   33 QP=Q4/EQ+VGX*P2*Q2+P4
   34 DBNX=Q2/P2*CSX*CSY*(AMN*QP-CMN)
   35 DBNY=DBNX*P2/Q2
   36 DBNXY=Q/P*SNX*SNY*(AMN*QP-CMN)
   37 DBMX=AMN*(P2+VX*Q2)*CSX*CSY
   38 DBMY=AMN*(Q2/EQ+VX*P2)*CSX*CSY
   39 DBMXY=AMN*P*Q*SNX*SNY
   40 DBW=AMN*CSX*CSY
   41 BNX(J)=BNX(J)-DBNX
      BNY(J)=BNY(J)-DBNY
   42 BNXY(J)=BNXY(J)-DBNXY
   43 BMX(J)=BMX(J)-DBMX
      BMY(J)=BMY(J)-DBMY
   44 BMXY(J)=BMXY(J)+2*GX*DBMXY
   45 BW(J)=BW(J)+3*AQH2*AQH*(1-VX*VY)*DBW/2
   46 CONTINUE
   47 CONTINUE
      SXDR(J)=BNX(J)*AQH/2
      SYDR(J)=BNY(J)*AQH/2
      SXBN(J)=BMX(J)*3*AQH2/2
      SYBN(J)=BMY(J)*3*AQH2/2
   48 J=J+1
   49 CONTINUE
   50 CONTINUE
  350 WRITE(NOPTOP,FMT=*) 'IS PRINTOUT OF RESULTS'
  354 WRITE(NOPTOP,FMT=*) 'REQUIRED IN THE FORM OF STRESS RESULTANTS'
  355 WRITE(NOPTOP,FMT=*) 'AND DISPLACEMENTS OR STRESSES AND RADIAL'
      WRITE(NOPTOP,FMT=*) 'DISPLACEMENT OR BOTH?'
  356 WRITE(NOPTOP,FMT=*)'TYPE 1 FOR STRESS RESULTANTS AND DISPLACEMENT'
  357 WRITE(NOPTOP,FMT=*)'TYPE 2 FOR STRESSES AND RADIAL DISPLACEMENT'
  358 WRITE(NOPTOP,FMT=*)'TYPE 3 FOR BOTH'
  360 READ(NOPTIP,FMT=*) FOPT4
      WRITE(NOPTOP,300)
  361 IF (FOPT4-2)188,215,188
```

```
 188 FLAG=-1
 189 IF (FLAG)1896,1896,1898
1896 WRITE(NRSLTOP,1897)
     GO TO 191
1897 FORMAT(//,4X,'_',6X,'_',9X,'_',13X,'_',13X,'_')
1898 WRITE(NRSLTOP,190)
 190 FORMAT(//,4X,'_',6X,'_',9X,'_')
 191 IF (FLAG)192,193,194
 192 WRITE(NRSLTOP,195)
     GO TO 198
 193 WRITE(NRSLTOP,196)
     GO TO 198
 194 WRITE(NRSLTOP,197)
     GO TO 198
 195 FORMAT(4X,'Y',6X,'X',9X,'NX',12X,'NY',12X,'NXY',/)
 196 FORMAT(4X,'Y',6X,'X',9X,'MX',12X,'MY',12X,'MXY',/)
 197 FORMAT(4X,'Y',6X,'X',9X,'W',/)
 198 I=1
 199 DO 208 BY=BYMN,BYMX,DY
 200 DO 207 BX=BXMN,BXMX,DX
 201 IF (FLAG)202,203,204
 202 WRITE(NRSLTOP,205) BY,BX,BNX(I),BNY(I),BNXY(I)
     GO TO 206
 203 WRITE(NRSLTOP,205) BY,BX,BMX(I),BMY(I),BMXY(I)
     GO TO 206
 204 WRITE(NRSLTOP,212) BY,BX,BW(I)
 205 FORMAT(2(F7.2),3(F14.6))
 206 I=I+1
 207 CONTINUE
     WRITE(NRSLTOP,301)
 208 CONTINUE
 209 FLAG=FLAG+1
 210 IF (FLAG-1)189,189,211
 211 CONTINUE
 212 FORMAT(2(F7.2),F14.6)
 213 WRITE(NRSLTOP,214)
 214 FORMAT(//,'NOTE: FORCES',8X,'ARE NON-DIMENSIONAL WITH RESPECT TO (
    CPR)',/,6X,'MOMENTS',7X,'ARE NON-DIMENSIONAL WITH RESPECT TO (PR.R)
    C',/,6X,'DISPLACEMENTS ARE NON-DIMENSIONAL WITH RESPECT TO (EY/PR)'
    C,///,6X,'_',9X,'_',/,6X,'X=X/L AND Y=PHI/ALPHA, P - INTENSITY OF LO
    CAD')
     IF (FOPT4-2)232,232,215
 215 CONTINUE
 218 WRITE(NRSLTOP,219)
 219 FORMAT(//,4X,'_',6X,'_',65X,'-')
 220 WRITE(NRSLTOP,221)
 221 FORMAT(4X,'Y',6X,'X',6X,'SX(DIRECT)    SY(DIRECT)    SX(BENDING)
    C SY(BENDING)',6X,'W',/)
 222 I=1
 223 DO 229 BY=BYMN,BYMX,DY
 224 DO 228 BX=BXMN,BXMX,DX
 225 WRITE(NRSLTOP,226)BY,BX,SXDR(I),SYDR(I),SXBN(I),SYBN(I),BW(I)
 226 FORMAT(2(F7.2),5(F14.6))
 227 I=I+1
 228 CONTINUE
     WRITE(NRSLTOP,301)
 229 CONTINUE
 230 WRITE(NRSLTOP,231)
 231 FORMAT(//,'NOTE: THE STRESSES ARE NON-DIMENSIONAL WITH RESPECT TO
    CTHE LOAD',/,6X,'SX(DIRECT)=(SX/P) ETC. WBAR=(EY.W/PR)',//,6X,'_',9
    CX,'_',/,6X,'X=X/L AND Y=PHI/ALPHA, P - INTENSITY OF LOAD',//,6X,'P
    COSITIVE STRESS - TENSILE,  NEGATIVE STRESS - COMPRESSIVE,  BENDING
    C STRESS IS AT INNER SURFACE (R-H)')
 232 CONTINUE
 233 WRITE(NOPTOP,234)
 234 FORMAT(//,' THE RESULTS ARE STORED IN A FILE CALLED RSLTSS',/,' TO
    C PRINT THEM TYPE THE FOLLOWING COMMAND IN RESPONSE TO THE PROMPT:
    C',//,' PRIF RSLTSS              ',//,' NOTE: WHEN THE PROGRAM IS RUN
    C AGAIN WITH NEW DATA THE EXISTING RESULTS',/,7X,'IN FILE RSLTSS  A
    CRE OVERWRITTEN BY THE NEW ONES GENERATED SO IT IS',/,7X,'NECESSARY
    C TO ENSURE THAT THE ABOVE COMMANDS ARE GIVEN TO SEND THE',/,7X,'RE
    CSULTS TO THE LINE PRINTER BEFORE ANOTHER RUN IS INITIATED')
 235 CALL DELV('STAERR')
 236 CLOSE (UNIT=298,STATUS='KEEP')
 237 CALL SCLCMD('COPF $LOCAL.RSLTSS $USER.RSLTSS')
 238 END
```

REFERENCES

1. KIRCHOFF G "Uber Das Gleichgewicht und die Bewegung Eine Elastischen Scheibe". Journal fur reine und angewandte Mathematik, Vol 40 (1850).

2. LOVE A E H "On the Small Free Vibrations and Deformations of the Elastic Shells". Phil Trans Royal Soc (London), Ser A, 17, pp 491-546, (1888).

3. TIMOSHENKO S "On the Transverse Vibration of Bars of Uniform Cross-Section". Philosophical Magazine Series 6, Vol 43, pp 125-131, (1922).

4. REISSNER E "The Effect of Transverse Shear Deformation on the Bending of Elastic Plates". Journal of Applied Mechanics, Trans, ASME Vol 12, p 64 (1945).

5. GOODIER J N "Discussion of 4. above". Journal of Applied Mechanics, Trans, ASME Vol 13, p A251 (1946).

6. REISSNER E "On the Bending of Elastic Plates". Quarterly of Applied Mathematics, Vol 5, pp 55-68 (1947).

7. MINDLIN R D "Influence of Rotary Inertia and Shear on Flexural Motions of Isotropic Elastic Plates". Journal of Applied Mechanics, Trans, ASME Vol 18, pp 31-38, (1951).

8. NAGHDI P M "On the Theory of Thin Elastic Shells". Quarterly of Applied Mathematics, Vol 14, pp 369-380, (1957).

9. ESSENBURG F "On the Significance of the Inclusion of the Effect of Transverse Normal Strain in Problems involving Beams with Surface Constraints". Journal of Applied Mechanics, Trans, ASME Vol 97, Ser E, pp 127-132, (1975).

10. WHITNEY J M and SUN C T "A Higher Theory for Extensional Motion of Laminated Composites". Journal of Sound and Vibration, Vol 30, pp 85-97, (1973).

11. WHITNEY J M and SUN C T "A Refined Theory for Laminated, Anisotropic Cylindrical Shells". Journal of Applied Mechanics, Trans, ASME Vol 41, No 2, pp 471-476, June (1974).

12. NELSON R B and LORCH D R "A Refined Theory of Laminated Orthotropic Plates". Journal of Applied Mechanics, Trans, ASME Vol 41, pp 177-183, March (1974).

13. REISSNER E "On Transverse Bending of Plates, Including Effects of Transverse Shear Deformation". Int Journal of Solids and Structures, Vol 11, pp 569-573, (1975).

14. LO K H, CHRISTENSEN R M and WU E M "A High Order Theory of Plate Deformation, Part I: Homogeneous Plates". Journal of Applied Mechanics, Trans, ASME, Vol 44, pp 633-668 Dec (1977).

15. LO K H, CHRISTENSEN R M and WU E M "A High Order Theory of Plate Deformation, Part 2: Laminated Plates". Journal of Applied Mechanics, Trans, ASME, Vol 44, pp 669-676, Dec (1977).

16. STARSKY Y "On the Theory of Symmetrically Heterogeneous Plates Having the Same Thickness Variation of Elastic Moduli". Topics in Applied Mechanics, (Abir D, Ollendorff and Reiner M Eds), Americal Elserier, (1965).

17. YANG P C, NORRIS C H and STARSKY Y "Elastic Wave Propagation in Meterogeneous Plates". Int Journal Solids and Structures, Vol 2, pp 665-684, (1966).

18. PAGANO N J "Elastic Behaviour of Multilayer Bidirectional Composites". AIAA Journal, 10, pp 931-933, (1972).

19. WHITNEY J M "The Effect of Transverse Shear Deformation on the Bending of Laminated Plates". Journal of Composite Materials, 3 (3), pp 534-547, (1969).

20. MAU S T "A Refined Laminated Plate Theory". Journal of Applied Mechanics, Trans, ASME, 37, pp 1031-1036, (1970).

21. KULKANNI S V and PAGANO N J "Dynamic Characteristics of Composite Laminates". Journal of Sound and Vibration, Vol 23, pp 127-143, (1972).

22. CHOW T S "On the Propagation of Flexural Waves in an Orthotropic Laminated Plate and its Response to an Impulsive Load". Journal of Composite Materials, Vol 5, No 3, pp 306-319, July (1971).

23. WHITNEY J M "Shear Correction Factors for Orthotropic Laminates Under Static Load". Journal of Applied Mechanics, Trans, ASME, Vol 40, p 302, (1973).

24. BERT C W and GORDANINEJAD F "Transverse Shear Effects in Bimodular Composite Laminates". Journal of Composite Materials, Vol 17, No 4, pp 282-298, July (1983).

25. COHEN G A "Transverse Shear Stiffness of Laminated Anisotropic Shells". Comp Methods in Applied Mechanics and Engineering, 13, pp 205-220, (1978).

26. MURTHY M V V "An Improved Transverse Shear Deformation Theory for Laminated Anisotropic Plates". (NASA-TP-1903), 39, Nov (1981).

27. SECHLER E E "Thin Shell Structures - Theory Experiment and Design". Ed Y C Fung, E E Sechler, Prentice Hall, ISBM Q-13-918193-8, (1974).

28. BERT C W "Structure Design and Analysis, Part 1". Ed C C Chamis, New York; Academic Press, pp 207-258, (1975).

29. LORENZ R "Die Nichtachsensymmetrische Knickung Dunnwanger Howlzylinder". Phys Z, Vol 13, pp 241-260, (1911).

30. SOUTHWELL R V "On the Collapse of Tubes by External Pressure". Phil Mag Vol 25, pp 687-698, (1913).

31. VON MISES R "Der Kritische Ausendruck Zylindrischer Rohre". Z Ver Duetsch Ing, Vol 58, pp 750-755, (1914).

32. DONNEL L H "Stability of Thin Walled Tubes Under Torsion". NACA Rep 479, (1933).

33. VON KARMAN T and TSIEN H S "The Buckling of Thin Cylindrical Shells Under Axial Compression and Bending". J Aeronaut Sci, Vol 8, pp 303-312, August (1941).

34. FLUGGE W "Stresses in Shells". Springer-Verlag, ISEN 0-387-05322-0, (1960) and (1973).

35. LUNDGREN H "Cylindrical Shells Vol 1". The Institution of Danish Civil Eng. The Danish Technical Press, Copenhagen, (1949).

36. RAMASWAMY G S, RAMAIAH M, and TAMHANKAR H G "Approximate Analysis of Cylindrical Shells as Folded Plates". Proc Colloquium on Simplified Calculation Methods of Shell Structures. Brussels 1961, North-Holland Pub Co, (1962).

37. MORICE P B "An Approximate Solution to the Problem of Longitudinally Continuous Shells". Magazine of Concrete Research, 9, pp 95-104, (1957).

38. SCHORER H "Line Load Action on Thin Cylindrical Shells". Proceedings of the American Society of Civil Eng, Vol 61, No 3, pp 281-316, (1935).

39. SINGER J, MEER A and BARUCH M "Buckling of Cylindrical Panels Under Lateral Pressure". Technion Israel Inst of Tech, Haifa, Israel, TAE Report No 85, March (1968).

40. ALMROTH B O, BROZAN F A "Bifurication Buckling as an Approximation of the Collapse Load for General Shells". AIAA Journal, Vol 10, pp 463-467, April (1972).

41. RUSHTON K R "Large Deflexion of Plates with Initial Curvature". Int J Mech Sci, Vol 12, pp 1037-1051, (1970).

42. RUSHTON K R "Buckling of Laterally Loaded Plates Having Initial Curvature". Int J Mech Sci, Vol 14, pp 667-680, (1972).

43. HUDSON J "The Non-Linear Behaviour of Thin Curved Panels". PhD Thesis, University of Strathclyde, (1971).

44. MARSHALL I H "The Non-Linear Behaviour of Thin Initially Curved Orthotropic Plates". PhD Thesis, University of Strathclyde, (1976).

45. MARSHALL I H, RHODES J and BANKS W M "The Non-Linear of Thin Orthotropic Curved Panels Under Lateral Loading". J Mech Eng Sci, 19, No 1, pp 30-37, Feb (1977).

46. MARSHALL I H, RHODES J and BANKS W M "Experimental Snap-Bockling Behaviour of Thin GRP Curved Panels Under Lateral Loading". Composites, pp 81-86, April (1977).

47. MARSHALL I H, THODES J and BANKS W M "General Investigation of Snap-Through Buckling of Shallow Orthotropic Shells". Acta Technica Academiae Scientiarum Hungaricae, 87, pp 69-86 (1978).

48. RHODES J, MARSHALL I H "Unsummetrical Buckling of Laterally Loaded Reinforced Plastic Shells". Proceedings ICCM/2, Toranto, 303-315, (1978).

49. MARSHALL I H "Unsymmetrical Buckling of Laterally Loaded, Thin, Initially Imperfect, Orthotropic Plates". Proceedings 1st Int Conf on Comp Structures, pp 352-365, September (1981).

50. CHU KUANG-HAN and TURULA P "Buckling of Open Cylindrical Shells Under Lateral Load". Journal of Engineering Mechanics Division, ASCE, 96, (EM6), Paper 7736, December (1970).

51. YANG T H and GURALNICK S A "An Experimental Study of the Buckling of Open Cylindrical Shells". Experimental Mechanics Vol 15, No 4, pp 121-7, April (1975).

52. & 53. PICKET G and GOPALACHUYULU S "Clamped Cylindrical Shell Panel (by Fourier Procedure), Also (by Energy Method)". 2 Papers Proceedings of Seminar on Shell Structures, Bengal Eng College, Shibpur, India. Oxford Book & Stationery Co, Calcutta Vol 5, No 3, Papers 7 & 8, January (1962).

54. DE G, ALLEN D N and HOLMAN J M L. "Mathematical Analysis of the Stress Distribution in Cylindrical Concrete Shell Roofs". Proceedings of the Institution of Civil Eng (London), Vol 22, pp 405-418, (1962).

55. CHANDRASHEKHARA K, CHANDRASHEKHARA S "Analysis of Clamped Circular Cylindrical Shells Using Basic Functions". Bulletin of Int Assoc for Shell and Spacial Structures, Vol 49, pp 43-57, June (1972).

56. CHANDRASHEKHARA K, CHANDRASHEKHARA S "Analysis of Clamped Cylindrical Shell Panels". Acta Technica Academiae Scientiarum Hungaricae, Vol 74, Part 4-5, pp 337-361, (1973).

57. TURNER M J, CLOUGH R W, MARTIN H C, TOPP L J "Stiffness and Deflection Analysis of Complex Structures". J Aero Science, Vol 23, No 9, pp 805-823, (1953).

58. MELOSH R J "A Stiffness Matrix for the Analysis of Thin Plates in Bending". J Aeron Science, Vol 28, No 1, pp 34-42, Jan (1961).

59. ADINI A, CLOUGH R W "Analysis of Plate Bending by the Finite Element Method". Report to National Science Foundation Grant G7337 (1961).

60. TOCHER J L "Analysis of Plate Bending Using Triangular Elements". PhD Thesis, Civil Eng Dept, University of California (1962).

61. MELOSH R J "Basis for Derivation of Matrices for the Direct Stiffness Method". J Am Inst Aero Astron, Vol 1, No 7, pp 1631-37, July (1963).

62. FRAEIJS DE VEUBEKE B "Upper and Lower Bounds in Matrix Structural Analysis" in "Matrix Methods in Structural Analysis". AGARD Vol 72, pp 165-201 (1964).

63. ZIENKIEWICZ O C, CHEUNG Y K "The Finite Element Method in Structural and Continuum Mechanics". McGraw-Hill, New York (1967).

64. ROBINSON J, BLACKHAM S "An Evaluation of Plate Bending Elements - MSc/NASTRAN, ASAS, PAFEC, ANSYS and SAP4". Robinson Ford Associates, Cranborne, Dorset, (1981).

65. ROBINSON J, BLACKHAM S "An Evaluation of Membrane Elements - MSc/NASTRAN, ASAS, PAFEC, ANSYS and SAP4". Robinson Ford Associates, Cranborne, Dorset, (1981).

66. HENSHELL R D PAFEC Theory Manual, 1984. Update of PAFEC 75 Theory and Results Manual Dec 75.

67. CHAMIS C C and SENDECKYJ "Critique on Theories Predicting Thermoelastic Properties of Fibrous Composites, J Composite Materials". July (1968), pp 332-358.

68. TSAI S W In "Experimental Mechanics". Proc Ann Symp., 11th, Albuquerque, New Mexico, February 11-12 (1971), pp 1-8.

69. STURGEON J B "Specimens and Test Methods for Carbon Fibre Reinforced Plastics". Recommendations by Government Laboratories. Royal Aircraft Establishment Technical Report 71026, February (1971).

70. HUBER M T "The Theory of Crosswise Reinforced Ferroconcrete Slabs and its application to various important constructional problems involving Rectangular Slabs.

71. HENNESSEY J M, WHITNEY J M and RILEY M B "Experimental Methods for Determining Shear Modulus of Fibre Reinforced Composite Materials". Air Force Materials Laboratory AFML-TR-65-42, AD623316 (1965).

72. HADCOCK R N and WHITESIDE J B In "Composite Materials: Testing and Design". Amer. Soc. Testing Materials, Spec Tech Publ 460, pp 27-36 (1969).

73. BALABAN M M and JACKSON W T "Experimental Mechanics". Vol 11, p 224 (1971).

74. WHITNEY J M, STANSBARGER D L and HOWELL H B "Analysis of the Rail Shear Test - Applications and Limitations. Journal of Composite Materials, January 1971, 5(1), pp 24-34.

75. GARCIA R, WEISSHAAR T A and McWITHEY R R "An Experimental and Analytical Investigation of the Rail Shear Test Method as applied to Composite Materials". Experimental Mechanics, August 1980, 20(8), pp 273-279.

76. SIMMS D F "In-Plane Shear Stress-Strain Response of Unidirectional Composite Materials". Journal of Composite Materials, January, (1973), 7(1), pp 124-128.

77. XINGHUA P "Measuring In-Plane Shear Properties of Glass Fibre/Epoxy Laminates". Composite Technology Review, Spring (1980), 2(2), pp 3-13.

78. NADAI A "Die Elastischen Platten" Verlag J Springer, 1925.

79. TSAI S W "Experimental Determination of the Elastic Behaviour of Orthotropic Plates". J Eng Ind, Vol 87(3), pp 315-318 (1965).

80. BECKETT R E, DOHRMANN R J and IVES K D "Discussion of ref [79] J Eng Ind, Vol 87(3), pp 317-318 (1965).

81. FOYE R L "Deflection Limits on the Plate Twisting Test". J Comp Matls, Vol 1(2), pp 194-198 (1967).

82. PURSLOW D "The Shear Properties of Unidirectional Carbon Fibre Reinforced Plastics" and their experimental determination Aeronautical Research Council Current Paper ARC-CP-1381, July (1976).

83. HARTSHORN R T, SMITH M D, SUMMERSCALES J "Determination of the Through-Plane Shear Modulus for Glass Reinforced Plastic". First International Conference on Testing Evaluation and Quality Control of Composites (TEQCCI) Butterworth Scientific, Guildford, Surrey, 13-14 September (1983).

84. CARGEN M R "Anticlastic Bending Test for Determination of the In-plane Shear Modulus of GRP Laminates". Project Report Royal Naval Engineering College, Manadon, Plymouth, April (1984).

85. CARGEN M R, HARTSHORN R T, SUMMERSCALES J "The Effect of Short Term Continuous Sea Water Exposure on the Shear Properties of a Marine Laminate". Transaction of the Institute of Marine Engineers, November (1985), Series C, Vol 97, Paper 21, pp 131-134, ISBN 0-927206-14-X.

86. CARPENTER "Testing of a curved GRP Plate", RNEC Structural Testing Facility Experimental Test Nos 58 to 67, Oct (1980).

87. CARPENTER "Testing of a Curved Aluminium Plate', RNEC Structural Testing Facility Experimental Test Nos 68 to 75, Nov (1980).

88. KANTOROVICH L V and KRYLOV V I "Approximate Methods of Higher Analysis". Interscience Publishers Inc, New York (1964).

89. RICHARDS T H, "Energy Methods in Stress Analysis". Ellis Horwood Series in Engineering Science, ISBN 85312-048-X (1977).

90. YOUNG D and FELGAR, "Tables of Characteristic functions for the normal modes of vibration of a beam", University of Texas Publication No 4913 (1949).

91. YOUNG D and FELGAR, "Formulas for Integrals containing characteristic functions of a Vibrating Beam", University of Texas circular No 14 (1950).

92. MIKHLIN S G, "On the convergence of Galerkin's method" (Russian) DAN SSSR 61 2:197-199 (1948).

93. THOMPSON S J, HARTSHORN R T and SUMMERSCALES J. "Strain Gauges on Glass Reinforced Polyester Laminates", the 3rd International Conference on Composite Structures PAISLEY Paper 53 pp 748-759 Sep (1985).

BIBLIOGRAPHY

References 94 onwards are not referred to directly in the text.

Sonar Domes and Marine application of Composite Materials

94. Jane's Fighting Ships, Maritime Defence Journal and Navy International Journal.

95. FRIED N and GRANER W R 'Durability of reinforced structural materials in Marine Service', Marine Technology, Vol 3(3), pp 321-327 (1966).

96. HUNTER W F 'An Introduction to Acoustic Exploration' In STEPHENS (Ed) 'Underwater Acoustics', Wiley-Interscience, London 1970, p 121.

97. ROSS D 'Mechanics of Underwater Noise', Pergamon Press, New York, 1976, ISBN-0-08-021182-8.

98. 'Reinforced Plastic Sonar Dome Material Investigation; Volume I: Panel construction'. Lunn Laminates report 45250-I, 1968 AD A060 289.

99. 'Reinforced Plastic Sonar Dome Material Investigation, Volume II: Physical Test'. Lunn Laminates report 45250-II, 1968 AD A044 039.

100. 'Sonar Domes - The Merits of GRP'. Maritime Defence, May 1984, 9(5) 192-195.

101. KALLAS D H 'Development of Rubber-plastic composites for Sonar Domes'. NASL-9300-7-TM-1, 17 Jun 1964, AD A060 193.

Composite Materials

102. JONES R M 'Mechanics of Composite Materials' McGraw Hill (1975) ISBN 0-07-032790-4.

103. PIGGOTT M R 'Load Bearing Fibre Composites', Pergamon Int. Lib of Science and Tech. 1980, ISBN 0-08-024230-8.

104. CALCOTE L R 'The Analysis of Laminated Composite Structures' Van Nostrand Reinhold Co 1969, LCCCN 79-97167.

105. DIETZ A G H (Ed) 'Composite Engineering Laminates The MIT Press 1969, LCCCN 68-18234.

106. BUNSELL A R and KELLY A (Eds) 'Composite Materials: A Directory of European Research'. Butterworth & Co 1985, ISBN 0-408-221-658.

Plates and Shells

107. CALLADINE C R 'Theory of Shell Structures', Cambridge University Press 1983, ISBN 0-521-23835-8.

108. NARAYANAN R (Ed) 'Shell Structures: Stability and Strength'.
Elsevier Applied Science Publishers (1985), ISBN 0-85334-343-8.

109. FUNG Y C and SECHLER E E (Ed) 'Thin-Shell Structures: Theory, Experiment and Design'.
Prentice-Hall Inc (1974), ISBN 0-13-918193-8.

110. KRAUS H 'Thin Elastic Shells'
John Wiley & Sons Inc NY, 1967, LCCCN 67-23328.

111. TURNER C E 'Introduction to Plate and Shell Theory'
Longmans (1965).

112. YAMAKI N 'Elastic Stability of Circular Cylindrical Shells', North Holland Ser. in App. Maths and Mechanics (1984), ISBN 0-444-86857-7.

113. RICHARDS T H and STANLEY P (Eds) 'Stability Problems in Engineering Structures and Components'. Applied Science Publishers (1979), ISBN 0-85334-836-7.

114. KOLLAR L and DULACSKA 'Buckling of Shells for Engineers'.
John Wiley & Sons (1984), ISBN 0-471-90328-0.

115. BRUSH D O and ALMROTH B O 'Buckling of Bars, Plates and Shells'.
McGraw-Hill Book Co (1975), ISBN 0-07-008593-5.

116. TIMOSHENKO S and WOINOWSKY-KRIEGER S 'Theory of Plates and Shells'.
McGraw Hill Book Co (1959), LCCCN 58-59675.

Solid Mechanics

117. LEIPHOLZ H 'Theory of Elasticity', Noordhoff International Publishing (1974), ISBN 90-286-0193-7.

118. WASHIZU K 'Variational Methods in Elasticity and Plasticity'.
Pergamon Press (1975), ISBN 0-08-017653-4.

119. LANDAU L D and LIFSHITZ E M 'Theory of Elasticity'
Pergamon Press (1959 and 1970), LCCCN 77-91701.

120. WANG CHI-TEH 'Applied Elasticity', McGraw Hill Book Co (1953), LCCCN 53-5178.

121. SOKOLNIKOFF I S 'Mathematical Theory of Elasticity'
McGraw Hill Book Co (1956), LCCCN 55-9554.

122. DYM C L and SHAMES I H 'Solid Mechanics: A Variational Approach'.
McGraw Hill (1973), ISBN 0-07-018556-5.

123. TIMOSHENKO S and GOODIER J N 'Theory of Elasticity'
McGraw Hill Book Co, Engineering Soc. Monographs (1951).

Numerical Analysis including Finite Element Systems.

124. REDDY J N 'An Introduction to the Finite Element Method'.
McGraw Hill Book Co (1984), ISBN 0-07-051346-5.

125. DAWE D J 'Matrix and Finite Element Displacement Analysis of
Oxford Engineering Science Series (1984), ISBN 0-19-856211-X.

126. BREBBIA C A (Ed) 'Finite Element Systems: A Handbook'.
Springer-Verlag, Computational Mechanics 1985,
ISBN 0-905451-31-7.

127. CRANDALL S H 'Engineering Analysis: A Survey of Numerical Procedures'.
McGraw Hill Book Co, Engineering Soc. Monographs (1956)
LCCCN 56-6952.

128. KANTOROVICH L V and KRYLOV V I 'Approximate Methods of Higher Analysis', translated by BENSTER C D.
Inter-science Pub, P Noordoff Ltd (1964).